

PROMISE: Preconditioned Stochastic Optimization Methods by Incorporating Scalable Curvature Estimates

Zachary Frangella*
Stanford University

ZFRAN@STANFORD.EDU

Pratik Rathore*
Stanford University

PRATIKR@STANFORD.EDU

Shipu Zhao
Cornell University

SZ533@CORNELL.EDU

Madeleine Udell
Stanford University

UDELL@STANFORD.EDU

Editor:

Abstract

This paper introduces PROMISE (**P**reconditioned **S**tochastic **O**ptimization **M**ethods by **I**ncorporating **S**calable **C**urvature **E**stimates), a suite of sketching-based preconditioned stochastic gradient algorithms for solving large-scale convex optimization problems arising in machine learning. PROMISE includes preconditioned versions of SVRG, SAGA, and Katyusha; each algorithm comes with a strong theoretical analysis and effective default hyperparameter values. In contrast, traditional stochastic gradient methods require careful hyperparameter tuning to succeed, and degrade in the presence of ill-conditioning, a ubiquitous phenomenon in machine learning. Empirically, we verify the superiority of the proposed algorithms by showing that, using default hyperparameter values, they outperform or match popular *tuned* stochastic gradient optimizers on a test bed of 51 ridge and logistic regression problems assembled from benchmark machine learning repositories. On the theoretical side, this paper introduces the notion of *quadratic regularity* in order to establish linear convergence of all proposed methods even when the preconditioner is updated infrequently. The speed of linear convergence is determined by the *quadratic regularity ratio*, which often provides a tighter bound on the convergence rate compared to the condition number, both in theory and in practice, and explains the fast global linear convergence of the proposed methods.

Keywords: Stochastic optimization, quasi-Newton, preconditioning, randomized low-rank approximation

*. Equal contribution

Table of Contents

1	Introduction	5
1.1	PROMISE	7
1.2	Roadmap	9
1.3	Notation	9
2	Scalable preconditioning techniques	10
2.1	Mathematical and algorithmic formulation	11
2.1.1	Subsampled Newton (SSN)	11
2.1.2	Nyström Subsampled Newton (NYSSN)	14
2.1.3	Sketch-and-Solve Subsampled Newton (SASSN)	17
2.1.4	Diagonal Subsampled Newton (DIAGSSN)	18
2.2	Preconditioner defaults and comparisons	18
2.3	Quality of the preconditioners	19
2.3.1	Preliminaries on sampling	20
2.3.2	Subsampled Newton	23
2.3.3	Nyström Subsampled Newton	23
2.3.4	Sketch-and-solve Subsampled Newton	24
3	Algorithms	24
3.1	Notation in algorithms	25
3.2	SketchySGD	25
3.3	SketchySVRG	26
3.4	SketchySAGA	28
3.5	SketchyKatyusha	29
3.6	Algorithm recommendations	30
4	Related work	31
4.1	Stochastic second-order and preconditioned stochastic gradient methods	31
4.2	Lazy updating and Newton’s method.	36
4.3	Fast global convergence in theory?	37
5	Theory	38
5.1	A subtlety in notation	39
5.2	Assumptions	39
5.3	Technical preliminaries	40
5.3.1	Quadratic regularity	40
5.3.2	ζ -spectral approximation and quadratic regularity in action: a simple example	42
5.3.3	Hessian dissimilarity	46
5.3.4	Preconditioner stability	47
5.3.5	Controlling the smoothness of the preconditioned stochastic gradient	48
5.3.6	Weighted quadratic regularity ratio	49
5.4	SketchySVRG	49
5.5	SketchySVRG: Fast local convergence	51

5.6	SketchySAGA	52
5.7	SketchyKatyusha	53
5.8	Convergence proof of SketchySVRG	54
5.8.1	Notation	54
5.8.2	Preliminary lemmas	54
5.8.3	SketchySVRG convergence: Proof of Theorem 24	56
6	Numerical experiments	56
6.1	Performance experiments	57
6.1.1	Ridge regression	58
6.1.2	l^2 -regularized logistic regression	58
6.2	Suboptimality experiments	60
6.3	Showcase experiments	61
6.4	Streaming experiments	63
6.5	Sensitivity study	64
6.5.1	Effects of changing the rank	66
6.5.2	Effects of changing the update frequency	67
6.6	Regularity study: Why PROMISE methods exhibit fast global convergence	68
7	Conclusion	69
8	Acknowledgements	70
A	Additional preconditioner details	71
A.1	SASSN preconditioner	71
A.2	DIAGSSN preconditioner	73
B	General lemmas	74
C	Proofs of main results	76
C.1	Proof of Lemma 7	76
C.2	Proofs of sampling and low-rank approximation bounds	76
C.2.1	Preliminaries	76
C.2.2	Proof of Proposition 9	77
C.2.3	Proof of Proposition 10	78
C.2.4	Proof of ζ -spectral approximation for SASSN	79
C.3	Proofs for quadratic regularity	81
C.3.1	Proof of Proposition 12	81
C.3.2	Proof of Proposition 13	82
C.4	Proofs of Hessian dissimilarity bounds	84
C.4.1	Proof of Lemma 19	84
C.4.2	Proof of Proposition 20	84
C.5	Proof of Proposition 21	85
C.6	Proof of Proposition 22	85
C.7	SketchySVRG: Fast local convergence	87
C.7.1	Notation	87

C.7.2	Preliminary lemmas	87
C.7.3	Proof of Theorem 26	95
C.8	SketchySAGA	95
C.8.1	Notation	96
C.8.2	Preliminary lemmas	96
C.8.3	SketchySAGA convergence: Proof of Theorem 28	102
C.9	SketchyKatyusha	102
C.9.1	Notation	103
C.9.2	Preliminary lemmas	103
C.9.3	SketchyKatyusha convergence: Proof of Theorem 30	107
D	Experimental details	108
D.1	Computational resources	108
D.2	Optimizer details	108
D.3	Performance experiments (additional)	109
D.3.1	Datasets and preprocessing	109
D.3.2	Performance plots for $\nu = 10^{-1}/n_{\text{tr}}$	110
D.3.3	Comparison of SSN and NYSSN on sparse/dense logistic regression	112
D.3.4	DIAGSSN vs. SSN/NYSSN/SASSN-C/SASSN-R	112
D.4	Suboptimality experiments (additional)	113
D.4.1	SketchySGD vs. SketchySVRG/SketchySAGA/SketchyKatyusha	113
D.5	Showcase experiments (additional)	113
D.6	Streaming experiments (additional)	115
D.6.1	Datasets and preprocessing	115
D.6.2	Comparison to SAGA with default hyperparameters	115
D.7	Gradient batchsize relative to dataset size	115
D.8	Sensitivity study (additional)	116
D.8.1	Additional sensitivity plots	116
D.9	Regularity study (additional)	117

1. Introduction

Modern machine learning (ML) poses significant challenges for optimization, owing to the sheer scale of the problems. Modern datasets are both enormous and high-dimensional, often with millions of datapoints and features. As a consequence, classic methods such as gradient descent and L-BFGS, which make a full pass through the data at each iteration, are prohibitively expensive. In this context, stochastic gradient descent (SGD) and its variants, which operate on only a small mini-batch of data at each iteration, have become the dominant optimization methods for modern ML.

When the problem is well-conditioned, SGD quickly finds models that are nearly optimal. Further, although classic SGD converges to a ball around the optimum (with fixed learning rate) or sublinearly (with decaying learning rate) (Moulines and Bach, 2011; Gower et al., 2019b), *variance reduction* techniques like SVRG, SAGA, Katyusha, and L-Katyusha significantly improve performance on convex problems, and linearly converge to the optimum for strongly convex problems (Johnson and Zhang, 2013; Defazio et al., 2014; Allen-Zhu, 2018; Kovalev et al., 2020).

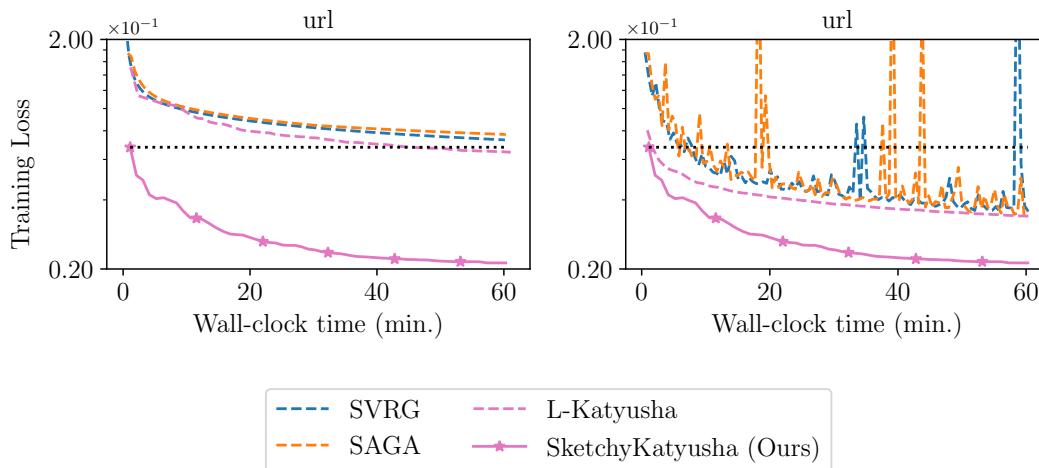


Figure 1: SketchyKatyusha (an algorithm in the PROMISE suite, see Algorithm 8) with its default hyperparameters outperforms standard stochastic gradient optimizers with both default (left) and tuned (right) hyperparameters. The loss curves start after a single epoch of training has been completed; the black dotted line indicates the training loss attained by SketchyKatyusha after a single epoch. Each optimizer is allotted 1 hour of runtime.

Unfortunately SGD and related algorithms are difficult to tune and converge slowly when the data is poorly conditioned. Parameters like the learning rate are difficult to choose and important to get right: slow convergence or divergence loom on either side of the best parameter choice (Nemirovski et al., 2009). Even with the best learning rate, variance-reduced stochastic gradient methods require at least $\mathcal{O}(n + \sqrt{n\kappa} \log(1/\epsilon))$ stochastic gradient evaluations to reach ϵ accuracy (Woodworth and Srebro, 2016), which is problematic as the condition number for many ML problems is typically on the order of 10^4 to 10^8 (see Fig. 15). Hence the convergence of stochastic gradient methods can be excruciatingly slow

(see Fig. 1) and popular stochastic optimizers often provide only low-quality solutions even with generous computational budgets.

How should the challenges of ill-conditioning and sensitivity to the learning rate be addressed? Classical optimization wisdom suggests using second-order information based on the Hessian. Second-order methods converge locally at super-linear rates under mild assumptions and exhibit superior performance to first-order methods in practice (Nocedal and Wright, 1999; Boyd and Vandenberghe, 2004), but they are difficult to adapt to use stochastic gradients and Hessians. As noted in Kovalev et al. (2019); Frangella et al. (2023a), many preexisting methods in the literature require exponentially increasing gradient batchsizes and Hessian batchsizes depending upon the condition number to achieve linear convergence. Worse, most of these methods are difficult to deploy in real-world ML pipelines, as they introduce new hyperparameters without practical guidelines for choosing them.

Another difficulty with many preexisting second-order methods (Bollapragada et al., 2018; Roosta-Khorasani and Mahoney, 2019; Na et al., 2022) is that they require reestimating the Hessian at every iteration. Reestimating the Hessian at each iteration leads to a noticeable slowdown in wall-clock time, particularly on large problem instances. Consequently, stochastic second-order methods must update the Hessian approximation infrequently to remain competitive with popular first-order methods on large-scale problems.

In this work, we introduce PROMISE, a suite of preconditioned stochastic gradient methods which use scalable curvature estimates to directly address the theoretical and algorithmic issues that plague existing stochastic first- and second-order methods in the literature. The methods we propose avoid difficulties with hyperparameter selection and ill-conditioning by estimating second-order information from minibatch data (i.e., stochastic Hessians), and they use infrequent (“lazy”) updating to remain competitive with first-order methods. The resulting algorithms, such as SketchyKatyusha (Algorithm 8), converge quickly even on ill-conditioned problems and require minimal or no hyperparameter tuning.

Figure 1 illustrates the benefits of PROMISE by applying SketchyKatyusha to a malicious link detection task using the url dataset ($n = 2,396,130$, $p = 3,231,961$), which yields a large l^2 -regularized logistic regression problem. The performance of popular stochastic optimizers using the default learning rates is quite poor. In contrast, with default hyperparameters, the proposed method SketchyKatyusha achieves a loss three times smaller than the best competing method after an hour of training! In fact, even after an hour of training, the other optimizers barely match the training loss that SketchyKatyusha achieves after a single epoch (pass through the data). Even with extensive hyperparameter tuning (which, in practice, increases the cost of optimization by orders of magnitude), the other first-order methods cannot match the performance of SketchyKatyusha with its default hyperparameters.

PROMISE also improves upon preexisting theory for stochastic second-order methods. In contrast to prior approaches, PROMISE methods achieve linear convergence with lazy updates to the preconditioner and without large batchsizes for the gradient and Hessian. Significantly, PROMISE methods come with default hyperparameters (including the learning rate) that enable them to work out-of-the-box and outperform or match popular stochastic optimizers *tuned* to achieve their best performance. We rigorously verify this claim with numerical experiments on a test bed of 51 ridge and logistic-regression problems. Hence

our methods avoid the usual theory-practice gap: our theoretical advances really do yield practical algorithms.

In order to show linear convergence under lazy updates, our analysis introduces a new analytic quantity we call the *quadratic regularity ratio* that controls the convergence rate of all PROMISE methods. The quadratic regularity ratio provides a natural generalization of the condition number to the Hessian norm. Unlike the condition number, the quadratic regularity ratio is equal to one for quadratic objectives, and approaches one as the iterate approaches the optimum for general objectives with Lipschitz Hessians. Hence the quadratic regularity ratio often gives tighter convergence rates than the condition number and is capable of explaining why the proposed methods empirically exhibit fast global linear convergence and outperform the competition.

1.1 PROMISE

The methods in PROMISE solve convex empirical risk minimization problems of the form

$$\underset{w \in \mathbb{R}^p}{\text{minimize}} F(w) := \frac{1}{n} \sum_{i=1}^n f_i(w) + \frac{\nu}{2} \|w\|^2, \quad (1)$$

where each f_i is real-valued, smooth, and convex, and $\nu > 0$.

We provide a high-level overview of the PROMISE methods in the Meta-algorithm and Table 1. Each iteration consists of two phases: (lazy) preconditioner updates and parameter updates. In the preconditioner update phase, our methods determine whether the preconditioner should be updated (generally, updates occur at a fixed frequency). If so, the preconditioner P is updated using a stochastic Hessian estimate at the current iterate w_k , and the learning rate is recomputed to adapt to the new preconditioner. In the parameter update phase, our methods compute a stochastic gradient g_k and preconditioned direction $v_k = P^{-1}g_k$. Our methods then use a parameter update subroutine \mathcal{S} to compute the next iterate w_{k+1} . The $*$ in the call to \mathcal{S} denotes additional arguments to perform variance reduction and acceleration.

Input	Description
w_0	Initial iterate, typically set to 0.
\mathcal{O}_g	Computes a stochastic gradient.
\mathcal{O}_H	Used for computing a stochastic/subsampled Hessian. Does not compute the entire subsampled Hessian in practice.
b_g, b_H	Batchsizes for computing stochastic gradients and Hessians. Used as inputs to \mathcal{O}_g and \mathcal{O}_H .
\mathcal{P}	Preconditioner object. Examples provided in Section 2.1.
\mathcal{U}	Times at which to update the preconditioner.
\mathcal{S}	Subroutine that updates the iterate. May include calculations related to variance reduction and acceleration.

Table 1: Inputs to the Meta-algorithm.

The finite sum structure of the objective (1) makes it easy to construct unbiased estimators of the gradient $\nabla F(w)$ and the Hessian $\nabla^2 F(w)$. Given batchsizes b_g and b_H , we

Meta-algorithm: PROMISE

Require: initial iterate w_0 , stochastic gradient oracle \mathcal{O}_g , stochastic Hessian oracle \mathcal{O}_H , gradient and Hessian batchsizes b_g and b_H , preconditioner object \mathcal{P} , preconditioner update times $\mathcal{U} \subseteq \mathbb{N}$, parameter update subroutine \mathcal{S}

```

for  $k = 0, 1, \dots$  do
  # Preconditioner update
  if  $k \in \mathcal{U}$  then
     $\mathcal{P}.\text{update}(\mathcal{O}_H(w_k, b_H))$            ▷ Update preconditioner  $P$  via stochastic Hessian
     $\eta = \mathcal{P}.\text{get\_learning\_rate}()$        ▷ Compute learning rate based on  $P$ 
  end if

  # Parameter update
   $g_k = \mathcal{O}_g(w_k, b_g)$                    ▷ Compute stochastic gradient
   $v_k = \mathcal{P}.\text{direction}(g_k)$            ▷ Compute  $v_k = P^{-1}g_k$ 
   $w_{k+1} = \mathcal{S}(w_k, g_k, v_k, *)$        ▷ Compute next iterate
end for

```

have unbiased estimators for the gradient and Hessian:

$$\widehat{\nabla}F(w) = \frac{1}{b_g} \sum_{i \in \mathcal{B}_g} \nabla f_i(w) + \nu w, \quad \widehat{\nabla}^2 F(w) = \frac{1}{b_H} \sum_{i \in \mathcal{B}_H} \nabla^2 f_i(w) + \nu I,$$

where \mathcal{B}_g and \mathcal{B}_H are two subsets of size b_g and b_H respectively, sampled independently and uniformly from $\{1, \dots, n\}$. As a concrete example, consider a generalized linear model (GLM) with $f_i(w) = \phi_i(a_i^T w)$, so

$$\nabla f_i(w) = \phi'_i(a_i^T w) a_i, \quad \nabla^2 f_i(w) = \phi''_i(a_i^T w) a_i a_i^T.$$

The stochastic Hessian as written is a $p \times p$ matrix: rather large! But none of the methods we discuss instantiate such a matrix. Instead, they take advantage of the low-rank structure of the preconditioner to compute the approximate Newton direction $P^{-1}g_k$ efficiently using the Woodbury formula (see Table 7).

Contributions. We summarize the contributions of this work as follows:

1. We propose preconditioned versions of SVRG, SAGA, and Katyusha, which we title SketchySVRG, SketchySAGA, and SketchyKatyusha. These methods use stochastic approximations to the Hessian to perform preconditioning.
2. We formally describe a wide array of preconditioners that are compatible with our methods. We show that any preconditioner that approximates the Hessian sufficiently well is compatible with our theoretical convergence results.
3. We define the quadratic regularity ratio, which generalizes the condition number to support global analysis, and use this ratio to prove our methods converge linearly to the optimum despite lazy updates to the preconditioner.

4. We show global linear convergence, independent of the condition number, for SketchySVRG, SketchySAGA, and SketchyKatyusha applied to ridge regression. We also show local linear convergence, independent of the condition number, for SketchySVRG on any strongly convex finite-sum problem with Lipschitz Hessians.
5. We provide default hyperparameters and a heuristic to automatically compute a good learning rate for our proposed methods.
6. We present extensive experiments demonstrating that SketchySVRG, SketchySAGA, and SketchyKatyusha, equipped with their default hyperparameters and learning rate heuristic, outperform popular stochastic optimizers for GLMs.

1.2 Roadmap

Section 2 introduces several scalable preconditioning techniques that are compatible with the PROMISE framework; we provide both implementation details and theoretical results for these preconditioners. Section 3 presents the algorithms that comprise the PROMISE framework, along with default hyperparameters and algorithmic recommendations for various GLMs. Section 4 reviews the literature on preconditioning and stochastic second-order methods and places PROMISE in the context of these existing works. Section 5 establishes linear convergence of all of the proposed methods for strongly convex machine learning problems. Section 6 demonstrates the superior performance of the algorithms in PROMISE over popular *tuned* stochastic optimizers through extensive numerical experiments.

1.3 Notation

We define $[n] := \{1, \dots, n\}$. Throughout the paper \mathcal{B}_k and \mathcal{S}_k denote subsets of $[n]$ that are sampled independently and uniformly without replacement. The corresponding minibatch gradient and Hessian are given by

$$\begin{aligned}\widehat{\nabla} f(w) &= \frac{1}{b_{g_k}} \sum_{i \in \mathcal{B}_k} \nabla f_i(w), \\ \widehat{\nabla}^2 f(w) &= \frac{1}{b_{h_k}} \sum_{i \in \mathcal{S}_k} \nabla^2 f_i(w),\end{aligned}$$

where $b_{g_k} := |\mathcal{B}_k|$, $b_{h_k} := |\mathcal{S}_k|$. We abbreviate positive-semidefinite as psd. We use $\mathbb{S}_p^+(\mathbb{R})$ to denote the convex cone of psd matrices in $\mathbb{R}^{p \times p}$. We denote the Loewner order on the convex cone of psd matrices by \preceq , where $A \preceq B$ means $B - A$ is psd. Given a psd matrix $A \in \mathbb{R}^{p \times p}$, we enumerate its eigenvalues in decreasing order, $\lambda_1(A) \geq \lambda_2(A) \geq \dots \geq \lambda_p(A)$. We define $B(w, r)$ to be the closed Euclidean norm ball of radius r , centered at w .

Throughout the remainder of this paper, we assume we have access to some GLM \mathcal{M} . We note our theoretical convergence results do not require the objective to be GLM, however our SASSN preconditioner (Section 2.1) result requires this structure. Moreover, most convex machine learning problems arising in practice are GLMs, so we specialize our implementation to GLMs. Given that F is a GLM, we assume access to oracles for obtaining the regularization parameter ν , row subsamples of the data matrix $A \in \mathbb{R}^{n \times p}$, the diagonal of the stochastic Hessian of F (excluding the regularization ν), stochastic gradients of F ,

and full gradients of F . We present the names, inputs, and outputs of these oracles in Table 2.

The oracles `get_data` and `get_hessian_diagonal` output $A_{\mathcal{B}}w$ and $\Phi''(A_{\mathcal{B}}w)$, respectively, for minibatch $\mathcal{B} = \{i_1, i_2, \dots, i_{|\mathcal{B}|}\} \subseteq [n]$, where

$$A_{\mathcal{B}} := \begin{pmatrix} a_{i_1}^T \\ a_{i_2}^T \\ \vdots \\ a_{i_{|\mathcal{B}|}}^T \end{pmatrix}, \quad \Phi''(A_{\mathcal{B}}w) := \text{diag} \left(\begin{pmatrix} \phi''_{i_1}(a_{i_1}^T w) \\ \phi''_{i_2}(a_{i_2}^T w) \\ \vdots \\ \phi''_{i_{|\mathcal{B}|}}(a_{i_{|\mathcal{B}|}}^T w) \end{pmatrix} \right).$$

The oracles `get_reg`, `get_data` and `get_hessian_diagonal` are used in the preconditioners described in Section 2.1, while the oracles `get_stoch_grad` and `get_full_grad` are used in the optimization algorithms in Section 3. In practice, `get_hessian_diagonal` returns the diagonal as a vector, not a matrix.

Oracle	Output
<code>M.get_reg()</code>	ν
<code>M.get_data(\mathcal{B})</code>	$A_{\mathcal{B}}$
<code>M.get_hessian_diagonal(\mathcal{B}, w)</code>	$\Phi''(A_{\mathcal{B}}w)$
<code>M.get_stoch_grad(\mathcal{B}, w)</code>	$\frac{1}{ \mathcal{B} } \sum_{i \in \mathcal{B}} \nabla f_i(w) + \nu w$
<code>M.get_full_grad(w)</code>	$\nabla F(w)$

Table 2: Oracles associated with the GLM \mathcal{M} . $\mathcal{B} \subseteq [n]$ is a batch of indices and $w \in \mathbb{R}^p$.

2. Scalable preconditioning techniques

We present four scalable preconditioning techniques: Subsampled Newton (SSN), Nyström Subsampled Newton (NYSSN), Sketch-and-Solve Subsampled Newton (SASSN), and Diagonal Subsampled Newton (DIAGSSN), all of which are based on stochastic approximations of the Hessian. The key driver behind the scalability of these methods is that subsampling and randomized low-rank approximation provide cheap, reliable estimates of the curvature.

For general convex, finite-sum objectives, the SSN, NYSSN, and DIAGSSN preconditioners require access to a stochastic Hessian, while the SASSN preconditioner requires access to the square root of the stochastic Hessian. Fortunately, the stochastic Hessian in GLMs, $\frac{1}{b_H} A_{\mathcal{B}}^T \Phi''(A_{\mathcal{B}}w) A_{\mathcal{B}}$, has a structure that allows us to compute all of these preconditioners using its square root, $\frac{1}{\sqrt{b_H}} [\Phi''(A_{\mathcal{B}}w)]^{1/2} A_{\mathcal{B}}$. An overview of the proposed preconditioners is provided in Table 3.

Preconditioner	Key ideas	Oracle requirements
SSN (Section 2.1.1)	Subsampling	Stochastic Hessian
N _Y SSN (Section 2.1.2)	Subsampling, randomized low-rank approximation, randomized Nyström approximation	Stochastic Hessian
SASSN (Section 2.1.3)	Subsampling, randomized low-rank approximation, sparse embedding, Newton sketch	Square root of stochastic Hessian
DIAGSSN (Section 2.1.4)	Subsampling, diagonal approximation	Stochastic Hessian

Table 3: Overview of proposed preconditioners.

We present mathematical and algorithmic formulations of the four preconditioning techniques in Table 3 in Section 2.1. We then compare the computational costs associated with each preconditioner and provide preconditioner recommendations for various problem regimes in Section 2.2. Finally, we analyze the approximation quality of the proposed preconditioners (with the exception of DIAGSSN) in Section 2.3.

2.1 Mathematical and algorithmic formulation

Here we provide both mathematical formulations and pseudocode of the preconditioners in Table 3. Throughout, we assume that we are working in the GLM setting. The pseudocode for each preconditioning technique is presented in an object-oriented framework. All of the preconditioners have two key methods: `update` and `direction`. The `update` method constructs the preconditioner and updates an estimate of the preconditioned smoothness constant (effectively combining the `update` and `get_learning_rate` methods in the Meta-algorithm), while the `direction` method computes a preconditioned stochastic gradient (similar to `direction` in the Meta-algorithm). These preconditioner objects play a critical role in the optimization algorithms presented in Section 3.

2.1.1 SUBSAMPLED NEWTON (SSN)

The first preconditioning method we present is SSN (Erdogdu and Montanari, 2015; Roosta-Khorasani and Mahoney, 2019). SSN forms a preconditioner using the Hessian of a random subsample of the terms in the finite-sum objective of Eq. (1). Given a point $w \in \mathbb{R}^p$, SSN constructs the preconditioner

$$P = \frac{1}{b_H} \sum_{i \in \mathcal{B}} \nabla^2 f_i(w) + \rho I, \quad (2)$$

where $\rho \geq \nu$ and \mathcal{B} consists of b_H elements sampled uniformly at random from $[n]$. In the GLM setting $f_i = \phi_i(a_i^T w)$, so Eq. (2) simplifies to

$$P = \frac{1}{b_H} \sum_{i \in \mathcal{B}} \phi_i''(a_i^T w) a_i a_i^T + \rho I = \frac{1}{b_H} A_{\mathcal{B}}^T \Phi''(A_{\mathcal{B}} w) A_{\mathcal{B}} + \rho I. \quad (3)$$

If $b_H \geq p$, we may form and factor P (via Cholesky) in $\mathcal{O}(b_H p^2 + p^3)$ time and compute $P^{-1}v$ for $v \in \mathbb{R}^p$ in $\mathcal{O}(p^2)$ time via triangular solves. When $b_H \leq p$ (the typical setting of interest), we compute the Cholesky factorization $LL^T = \Phi''(A_{\mathcal{B}}w)^{1/2} A_{\mathcal{B}} A_{\mathcal{B}}^T \Phi''(A_{\mathcal{B}}w)^{1/2} + \rho I$ and $P^{-1}v = (v - A_{\mathcal{B}}^T \Phi''(A_{\mathcal{B}}w)^{1/2} L^{-T} L^{-1} \Phi''(A_{\mathcal{B}}w)^{1/2} A_{\mathcal{B}} v) / \rho$ via the Woodbury formula (Higham, 2002). We summarize the costs of these operations in Lemma 1.

Lemma 1 *Let $v \in \mathbb{R}^p$ and let P be as in (3). If $b_H \leq p$, then the Cholesky factorization can be constructed in $\mathcal{O}(b_H^2 p + b_H^3)$ time and $P^{-1}v$ can be computed in $\mathcal{O}(b_H p)$ time. Furthermore, if the data matrix A is row-sparse with sparsity parameter s , the computational cost of $P^{-1}v$ can be reduced to $\mathcal{O}(b_H s)$ time.*

An implementation of the SSN preconditioner is provided in the \mathcal{P}_{ssn} class (Table 4 and Algorithms 1 and 2). The attributes of the \mathcal{P}_{ssn} class are given in Table 4, and pseudocode for the `update` and `direction` methods is provided in Algorithms 1 and 2, respectively.

Attribute	Description
ρ	Regularization for preconditioner
b	Size of Hessian batch used for preconditioner construction
X	Square root of subsampled Hessian (excluding l^2 -regularization)
L	Lower-triangular Cholesky factor for storing preconditioner
$\lambda_{\mathcal{P}}$	Estimate of preconditioned smoothness constant

Table 4: Attributes of the \mathcal{P}_{ssn} class.

The `update` method takes a GLM \mathcal{M} , Hessian batches $\mathcal{B}_1, \mathcal{B}_2$, and vector $w \in \mathbb{R}^p$ as input.

Algorithm 1 Update \mathcal{P}_{ssn} preconditioner and preconditioned smoothness constant

Require: \mathcal{P}_{ssn} object with attributes $\rho, b, X, L, \lambda_{\mathcal{P}}$
function $\mathcal{P}_{\text{ssn}}.\text{update}(\mathcal{M}, \mathcal{B}_1, \mathcal{B}_2, w)$
 $\rho \leftarrow \mathcal{P}_{\text{ssn}}.\rho$ ▷ Get attributes

Phase 1: Update preconditioner

 $A_{\text{sub}} \leftarrow \mathcal{M}.\text{get_data}(\mathcal{B}_1)$
 $d_{\text{sub}} \leftarrow \mathcal{M}.\text{get_hessian_diagonal}(\mathcal{B}_1, w)$
 $X \leftarrow \text{diag}(\sqrt{d_{\text{sub}}})A_{\text{sub}}$
▷ Square root of subsampled Hessian
if $|\mathcal{B}_1| \geq p$ **then**
 $L \leftarrow \text{cholesky}(X^T X + \rho I)$
else
 $L \leftarrow \text{cholesky}(X X^T + \rho I)$
end if

Phase 2: Update estimated preconditioned smoothness constant

 $A_{\text{sub}} \leftarrow \mathcal{M}.\text{get_data}(\mathcal{B}_2)$
 $d_{\text{sub}} \leftarrow \mathcal{M}.\text{get_hessian_diagonal}(\mathcal{B}_2, w)$
 $Z \leftarrow A_{\text{sub}}^T \text{diag}(d_{\text{sub}})A_{\text{sub}} + \mathcal{M}.\text{get_reg}()I$
▷ Subsampled Hessian
 $\lambda_{\mathcal{P}} \leftarrow \text{eig}(Z(X^T X + \rho I)^{-1}, k = 1)$
▷ Compute largest eigenvalue
 $\mathcal{P}_{\text{ssn}}.b \leftarrow |\mathcal{B}_1|, \mathcal{P}_{\text{ssn}}.X \leftarrow X, \mathcal{P}_{\text{ssn}}.L \leftarrow L, \mathcal{P}_{\text{ssn}}.\lambda_{\mathcal{P}} \leftarrow \lambda_{\mathcal{P}}$
▷ Set attributes

In the first phase, this method constructs the SSN preconditioner P at w by computing the square root of the subsampled Hessian, followed by an appropriate Cholesky factorization. The matrix used in the Cholesky factorization changes depending on the Hessian batchsize in order to obtain the computational costs in Lemma 1. In the second phase, this method estimates the preconditioned smoothness constant by computing $\lambda_1(P^{-1/2}\widehat{\nabla}^2 F(w)P^{-1/2}) = \lambda_1(\widehat{\nabla}^2 F(w)P^{-1})$. We never instantiate the subsampled Hessian to perform this calculation. Instead, we define matrix-vector products with the subsampled Hessian and inverse preconditioner and compute the largest eigenvalue via powering (our implementation uses `scipy.sparse.linalg.eigs`).

The `direction` method takes a vector $g \in \mathbb{R}^p$ (typically a stochastic gradient) as input.

Algorithm 2 Compute \mathcal{P}_{ssn} direction

Require: \mathcal{P}_{ssn} object with attributes $\rho, b, X, L, \lambda_{\mathcal{P}}$

```

function  $\mathcal{P}_{\text{ssn}}.\text{direction}(g)$ 
   $b \leftarrow \mathcal{P}_{\text{ssn}}.b, L \leftarrow \mathcal{P}_{\text{ssn}}.L, X \leftarrow \mathcal{P}_{\text{ssn}}.X$  ▷ Get attributes
  if  $b \geq p$  then
     $v \leftarrow L^{-1}g$  ▷ Triangular solve
     $v \leftarrow L^{-T}v$  ▷ Triangular solve
    return  $v$ 
  else
     $v \leftarrow Xg$ 
     $v \leftarrow L^{-1}v$  ▷ Triangular solve
     $v \leftarrow L^{-T}v$  ▷ Triangular solve
     $v \leftarrow X^T v$ 
    return  $(g - v)/\rho$ 
  end if

```

This method then computes $P^{-1}g$ using the Cholesky factor L and the square root of the subsampled Hessian X (as necessary). The reason for having two cases is to achieve the computational complexity in Lemma 1 by taking advantage of the Woodbury formula.

2.1.2 NYSTRÖM SUBSAMPLED NEWTON (NYSSN)

NYSSN combines the SSN preconditioner with randomized low-rank approximation, specifically the randomized Nyström approximation (Williams and Seeger, 2000; Gittens and Mahoney, 2016; Tropp et al., 2017). It was previously developed by the authors in Frangella et al. (2023a) to precondition stochastic gradient descent. Given a symmetric psd matrix $H \in \mathbb{R}^{p \times p}$, the randomized Nyström approximation with respect to a random test matrix $\Omega \in \mathbb{R}^{p \times r}$ is given by

$$\hat{H} = (H\Omega) (\Omega^T H\Omega)^\dagger (H\Omega)^T. \quad (4)$$

Common choices for Ω include standard normal random matrices, subsampled randomized Hadamard transforms, and sparse sign embeddings (Tropp et al., 2017). The benefit of the latter two test matrices is that computation of the sketch $H\Omega$ becomes cheaper.

For a minibatch \mathcal{B} ($|\mathcal{B}| = b_H$) and query point $w \in \mathbb{R}^p$, NYSSN takes $H = \frac{1}{b_H} A_{\mathcal{B}}^T \Phi''(A_{\mathcal{B}}w) A_{\mathcal{B}}$ in (4), and produces a randomized low-rank approximation \hat{H} of (the un-regularized portion of) the subsampled Hessian.

A practical algorithm (Algorithm 3) for constructing the randomized low-rank approximation outputs \hat{H} in the factored form $U\hat{\Lambda}U^T$, where $U \in \mathbb{R}^{p \times r}$ is an orthogonal matrix containing approximate eigenvectors and $\hat{\Lambda} \in \mathbb{R}^{r \times r}$ is a diagonal matrix containing approximate eigenvalues. We emphasize that this algorithm never forms $\frac{1}{b_H} A_{\mathcal{B}}^T \Phi''(A_{\mathcal{B}}w) A_{\mathcal{B}}$ explicitly. The resulting preconditioner is

$$P = \hat{H} + \rho I = U\hat{\Lambda}U^T + \rho I. \quad (5)$$

The dominant costs in the (practical) construction of P are computing the sketch $H\Omega$ and a SVD of a $p \times r$ matrix. Furthermore, we can compute $P^{-1}v$ via the Woodbury

formula, which yields

$$P^{-1}v = U \left(\hat{\Lambda} + \rho I \right)^{-1} U^T v + \frac{1}{\rho} (v - UU^T v).$$

We summarize the costs of these operations in Lemma 2.

Lemma 2 *Let $v \in \mathbb{R}^p$ and let P be as in (5). Then P can be constructed in $\mathcal{O}(b_H r p + r^2 p)$ time and $P^{-1}v$ can be computed in $\mathcal{O}(r p)$ time. For GLMs, $b_H \geq r$, so the construction cost is reduced to $\mathcal{O}(b_H r p)$.*

The main advantage of NYSSN over SSN is in the setting where the data matrix A is dense and has rapid spectral decay. When A has rapid spectral decay, we can use a relatively small value of r ($r \leq 10$) to construct the NYSSN preconditioner. With this small value of r , the $\mathcal{O}(r p)$ cost of applying the NYSSN preconditioner to a vector is usually cheaper than the $\mathcal{O}(b_H p)$ cost of applying the SSN preconditioner. On the other hand, when A is row-sparse with sparsity parameter s , the cost of applying the SSN preconditioner to a vector is reduced to $\mathcal{O}(b_H s)$, which negates the speedups provided by the NYSSN preconditioner.

An implementation of the NYSSN preconditioner is provided in the $\mathcal{P}_{\text{nyssn}}$ class (Table 5 and Algorithms 3 and 4). The attributes of the $\mathcal{P}_{\text{nyssn}}$ class are given in Table 5, and pseudocode for the `update` and `direction` methods is provided in Algorithms 3 and 4, respectively.

Attribute	Description
r	Rank for constructing preconditioner
ρ	Regularization for preconditioner
d	Approximate eigenvalues in Nyström approximation
U	Approximate eigenvectors in Nyström approximation
$\lambda_{\mathcal{P}}$	Estimate of preconditioned smoothness constant

Table 5: Attributes of the $\mathcal{P}_{\text{nyssn}}$ class.

The `update` method takes a GLM \mathcal{M} , Hessian batches $\mathcal{B}_1, \mathcal{B}_2$, and vector $w \in \mathbb{R}^p$ as input.

Algorithm 3 Update $\mathcal{P}_{\text{nyssn}}$ preconditioner and preconditioned smoothness constant

Require: $\mathcal{P}_{\text{nyssn}}$ object with attributes $r, \rho, d, U, \lambda_{\mathcal{P}}$ **function** $\mathcal{P}_{\text{nyssn}}.\text{update}(\mathcal{M}, \mathcal{B}_1, \mathcal{B}_2, w)$ $r \leftarrow \mathcal{P}_{\text{nyssn}}.r, \rho \leftarrow \mathcal{P}_{\text{nyssn}}.\rho$ ▷ Get attributes

Phase 1: Update preconditioner

 $A_{\text{sub}} \leftarrow \mathcal{M}.\text{get_data}(\mathcal{B}_1)$ $d_{\text{sub}} \leftarrow \mathcal{M}.\text{get_hessian_diagonal}(\mathcal{B}_1, w)$ $X \leftarrow \text{diag}(\sqrt{d_{\text{sub}}})A_{\text{sub}}$ ▷ Square root of subsampled Hessian $\Omega \leftarrow \text{randn}(p, r)$ ▷ Generate random Gaussian embedding $\Omega \leftarrow \text{qr_econ}(\Omega)$ ▷ Improves numerical stability $Y \leftarrow X^T(X\Omega)$ ▷ Sketch of subsampled Hessian $\delta \leftarrow \sqrt{\text{peps}(\text{norm}(Y))}$ ▷ Compute shift for stability $Y_{\delta} \leftarrow Y + \delta\Omega$ ▷ Shifted sketch $C \leftarrow \text{cholesky}(\Omega^T Y_{\delta})$ ▷ Lower triangular Cholesky factor $S \leftarrow Y_{\delta} C^{-1}$ ▷ Triangular solve $(U, \Sigma, \sim) \leftarrow \text{svd}(S)$ ▷ Thin SVD $d \leftarrow \max(\Sigma^2 - \delta, 0)$ ▷ Remove shift, compute eigenvalues

Phase 2: Update estimated preconditioned smoothness constant

 $A_{\text{sub}} \leftarrow \mathcal{M}.\text{get_data}(\mathcal{B}_2)$ $d_{\text{sub}} \leftarrow \mathcal{M}.\text{get_hessian_diagonal}(\mathcal{B}_2, w)$ $Z \leftarrow A_{\text{sub}}^T \text{diag}(d_{\text{sub}})A_{\text{sub}} + \mathcal{M}.\text{get_reg}()I$ ▷ Subsampled Hessian $\lambda_{\mathcal{P}} \leftarrow \text{eig}(Z(U(\text{diag}(d) + \rho I)^{-1}U^T + \frac{1}{\rho}(I - UU^T))), k = 1)$ ▷ Compute largest eigenvalue $\mathcal{P}_{\text{nyssn}}.d \leftarrow d, \mathcal{P}_{\text{nyssn}}.U \leftarrow U, \mathcal{P}_{\text{nyssn}}.\lambda_{\mathcal{P}} \leftarrow \lambda_{\mathcal{P}}$ ▷ Set attributes

In the first phase, this method constructs a randomized-low rank approximation \hat{H} to the subsampled Hessian at w ; updating this low-rank approximation is equivalent to updating the preconditioner since $P = \hat{H} + \rho I$. The first phase starts by computing the square root of the subsampled Hessian, X . From this point forward, we follow the stabilized procedure in Tropp et al. (2017) to compute U and d , which leads to a factored form of the randomized low-rank approximation, $\hat{H} = U\text{diag}(d)U^T$. In the second phase, this method estimates the preconditioned smoothness constant by taking a similar approach to the \mathcal{P}_{ssn} class.

The `direction` method takes a vector $g \in \mathbb{R}^p$ (typically a stochastic gradient) as input.

Algorithm 4 Compute preconditioned $\mathcal{P}_{\text{nyssn}}$ direction

Require: $\mathcal{P}_{\text{nyssn}}$ object with attributes $r, \rho, d, U, \lambda_{\mathcal{P}}$ **function** $\mathcal{P}_{\text{nyssn}}.\text{direction}(g)$ $U \leftarrow \mathcal{P}_{\text{nyssn}}.U, d \leftarrow \mathcal{P}_{\text{nyssn}}.d, \rho \leftarrow \mathcal{P}_{\text{nyssn}}.\rho$ ▷ Get attributes $v \leftarrow U^T g$ $v \leftarrow (1/(d + \rho) - 1/\rho)v$ ▷ Elementwise division, subtraction, and multiplication**return** $g/\rho + Uv$

The method then computes $P^{-1}g$ using the Woodbury formula with the preconditioner factors d and U ; this computation has complexity $\mathcal{O}(rp)$.

2.1.3 SKETCH-AND-SOLVE SUBSAMPLED NEWTON (SASSN)

The next preconditioning technique we discuss is SASSN. Similar to NYSSN, the fundamental goal of SASSN is to reduce the cost of the SSN preconditioner by replacing it with a randomized low-rank approximation. However, instead of using the randomized Nyström approximation, SASSN computes an approximation in the style of the Newton Sketch (Pilanci and Wainwright, 2017; Lacotte et al., 2021). To start, observe that the subsampled Hessian $\widehat{\nabla}^2 F(w)$ has the form

$$\widehat{\nabla}^2 f(w) + \nu I = R^T R + \nu I,$$

where $R = \Phi''(A_{\mathcal{B}}w)^{1/2}A_{\mathcal{B}}$. Hence, given a test matrix $\Omega \in \mathbb{R}^{r \times b_H}$, we construct the preconditioner

$$P = R^T \Omega^T \Omega R + \rho I. \quad (6)$$

The dominant costs in the construction of P are computing the sketch ΩR and a Cholesky factorization of $\Omega R(\Omega R)^T + \rho I$. Taking Ω to be a column-sparse or row-sparse (LESS-uniform) embedding (Derezinski et al., 2021), ΩR can be computed in $\mathcal{O}(b_H p)$ time. A preconditioner generated by a column-sparse embedding is referred to as SASSN-C, while a preconditioner generated by a row-sparse embedding is referred to as SASSN-R. SASSN-R tends to be better than SASSN-C because it is cheaper to apply to vectors when the data matrix A is row-sparse. Similar to the NYSSN preconditioner, we can compute $P^{-1}v$ via the Woodbury Formula, which yields

$$P^{-1}v = \frac{1}{\rho} \left(v - (\Omega R)^T (\Omega R(\Omega R)^T + \rho I)^{-1} (\Omega R)v \right).$$

We summarize the costs of these operations in Lemma 3.

Lemma 3 *Let $v \in \mathbb{R}^p$ and let P be as in (6). Then P can be constructed in $\mathcal{O}(b_H p + r^2 p + r^3)$ time and P^{-1} may be applied to vectors in $\mathcal{O}(rp)$ time. Furthermore, if the data matrix A is row-sparse with sparsity parameter s , the computational cost of $P^{-1}v$ for SASSN-R can be reduced to $\mathcal{O}(rs)$ time.*

Similar to NYSSN, the costs of constructing and applying the SASSN preconditioner are lower than the costs incurred by SSN. A potential advantage of SASSN over NYSSN is that SASSN requires $\mathcal{O}(b_H p + r^2 p + r^3)$ time to construct the preconditioner, whereas NYSSN requires $\mathcal{O}(b_H r p)$. Furthermore, the SASSN-R preconditioner takes $\mathcal{O}(rs)$ time to apply when the data matrix A is row-sparse, whereas NYSSN takes $\mathcal{O}(rp)$.

However, our experiments (Section 6) suggest that the SASSN preconditioner tends to be of lower quality than the NYSSN preconditioner (i.e., it does not reduce the condition number as much), and the theoretical complexity advantage of SASSN is not always realized as the computations in NYSSN benefit from (embarassing) parallelism. Concrete comparisons and recommendations between SSN, NYSSN, SASSN-C, and SASSN-R are given in Tables 7 and 8 below. An implementation of the SASSN-C/SASSN-R preconditioners is provided in Appendix A.1.

2.1.4 DIAGONAL SUBSAMPLED NEWTON (DIAGSSN)

The final preconditioning technique we discuss is DIAGSSN. DIAGSSN does exactly what its name suggests: it computes the diagonal of the subsampled Hessian (excluding regularization) $\widehat{\nabla}^2 f(w) = \frac{1}{b_H} A_B^T \Phi''(A_B w) A_B$, and constructs the preconditioner

$$P = \text{diag}(\widehat{\nabla}^2 f(w) + \rho I).$$

The resulting preconditioner can be applied to vectors in $\mathcal{O}(p)$ time. DIAGSSN is a stochastic generalization of Jacobi preconditioning, a classical preconditioning strategy in optimization (Nocedal and Wright, 1999; Jambulapati et al., 2020; Qu et al., 2022). It serves as a baseline in this work to illustrate that low-rank approximation is much more powerful than diagonal approximation for the subsampled Hessian: DIAGSSN can be computed quickly but its performance is poor in practice. The experiments in Section 6 show that the performance of our PROMISE methods using DIAGSSN is worse than with any of the other preconditioners. An implementation of the DIAGSSN preconditioner is provided in Appendix A.2.

2.2 Preconditioner defaults and comparisons

We provide default values for rank r and regularization ρ for each preconditioner in Table 6; we use these defaults for r and ρ in the experiments in Section 6. We also summarize the costs to construct and apply each preconditioner in Table 7. These costs assume that the Hessian batchsize $b_H = \lfloor \sqrt{n} \rfloor$ in the PROMISE algorithms; we provide motivation for this selection in Section 2.3 and use this selection in our experiments in Section 6. We also provide guidelines for which preconditioner to use as the problem size varies in Table 8. We do not recommend using DIAGSSN or SASSN-C in practice and so we omit them from Table 8.

Preconditioner	r	ρ
SSN (Algorithms 1 and 2)	N/A	10^{-3}
NySSN (Algorithms 3 and 4)	10	10^{-3}
SASSN-C (Algorithms 9, 11 and 12)	10	10^{-3}
SASSN-R (Algorithms 10 to 12)	10	10^{-3}
DIAGSSN (Algorithms 13 and 14)	N/A	10^{-3}

Table 6: Default values of r and ρ for each preconditioner. The default for ρ assumes that $\nu \leq 10^{-3}$, which is common in practice and is always the case in our experiments; if $\nu > 10^{-3}$, this default for ρ should be increased.

Preconditioner	Construction cost	Cost to apply	Cost to apply (sparse)
SSN (Algorithms 1 and 2)	$\mathcal{O}(np + n^{3/2})$	$\mathcal{O}(\sqrt{np})$	$\mathcal{O}(\sqrt{ns})$
NYSSN (Algorithms 3 and 4)	$\mathcal{O}(\sqrt{nrp})$	$\mathcal{O}(rp)$	$\mathcal{O}(rp)$
SASSN-C (Algorithms 9, 11 and 12)	$\mathcal{O}(\sqrt{np})$	$\mathcal{O}(rp)$	$\mathcal{O}(rp)$
SASSN-R (Algorithms 10 to 12)	$\mathcal{O}(\sqrt{np})$	$\mathcal{O}(rp)$	$\mathcal{O}(rs)$
DIAGSSN (Algorithms 13 and 14)	$\mathcal{O}(\sqrt{np})$	$\mathcal{O}(p)$	$\mathcal{O}(p)$

Table 7: Summary of costs of proposed preconditioners. s denotes the row sparsity of the data matrix A .

Regime	SSN	NYSSN	SASSN-R
$n \gg p$ (dense)	2	1	3
$n \gg p$ (sparse)	1	2	3
$n \sim p$ (dense)	3	1	2
$n \sim p$ (sparse)	1	3	2
$n \ll p$ (sparse)	1	3	2

Table 8: Guidelines for selecting a preconditioner. The best preconditioner for each regime is assigned a rank of 1. NYSSN is effective for dense problems, but for sparse problems SSN generally works better as it preserves the sparsity of the data in the preconditioner.

2.3 Quality of the preconditioners

We now analyze the quality of the SSN, NYSSN, and SASSN preconditioners that were introduced in Section 2.1. Our goal is to show that these preconditioners satisfy the following *good-spectral approximation property* with high probability.

Definition 4 (ζ -spectral approximation) *Let $w \in \mathbb{R}^p$, $\zeta \in (0, 1)$. Then we say P is a ζ -spectral approximation of $\nabla^2 F(w)$ if the following relation holds:*

$$(1 - \zeta)P \preceq \nabla^2 F(w) \preceq (1 + \zeta)P. \quad (7)$$

If P satisfies Definition 4, then

$$\kappa_2(P^{-1/2}\nabla^2 F(w)P^{-1/2}) \leq \frac{1 + \zeta}{1 - \zeta}.$$

Hence preconditioning $\nabla^2 F(w)$ by P results in a good (small) condition number for moderate ζ (e.g., $\zeta \leq .9$). Moreover, as $P^{-1/2}\nabla^2 F(w)P^{-1/2}$ is nearly the identity, P^{-1} is close to

$\nabla^2 F(w)^{-1}$, which ensures the approximate Newton direction computed with P^{-1} is close to the true Newton direction. As a consequence of this last observation, essentially all works on approximate Newton methods require the Hessian approximation to satisfy the conditions of Definition 4 (Pilanci and Wainwright, 2017; Roosta-Khorasani and Mahoney, 2019; Marteau-Ferey et al., 2019a; Ye et al., 2021).

2.3.1 PRELIMINARIES ON SAMPLING

To establish the ζ -approximation property for the preconditioners, we require some fundamental concepts from matrix approximation via random sampling, which we now review. We start with the definition of ridge leverage scores (Cohen et al., 2017; Li et al., 2020).

Definition 5 (Ridge leverage scores) *Let $\nu \geq 0$ and $i \in [n]$. Then the i th ridge leverage score of a matrix $A \in \mathbb{R}^{n \times p}$ is given by*

$$l_i^\nu(A) := a_i^T (A^T A + n\nu I)^\dagger a_i.$$

where a_i^T is the i th row of A and the maximum ridge leverage score is $l_\infty^\nu(A) = \max_{1 \leq i \leq n} l_i^\nu(A)$.

The i th ridge leverage score measures the importance of row i in the matrix A . These scores play a crucial role in determining how well the matrix $\frac{1}{n}A^T A + \nu I$ may be approximated via uniform sampling. To understand this relation, we recall the notions of effective dimension and ridge leverage incoherence.

Definition 6 (Effective dimension and ridge leverage coherence) *Given $A \in \mathbb{R}^{n \times p}$ and $\nu \geq 0$, the effective dimension of A is given by*

$$d_{\text{eff}}^\nu(A) := \sum_{i=1}^n l_i^\nu(A) = \sum_{j=1}^p \frac{\sigma_j^2(A)}{\sigma_j^2(A) + n\nu} = \sum_{j=1}^p \frac{\lambda_j(A^T A)}{\lambda_j(A^T A) + n\nu}. \quad (8)$$

If $H \in \mathbb{S}_p^+(\mathbb{R})$ with $H = A^T A$, then we overload notation and define $d_{\text{eff}}^\nu(H) := d_{\text{eff}}^\nu(A)$. The ridge leverage coherence is given by

$$\chi^\nu(A) := \frac{n}{d_{\text{eff}}^\nu(A)} l_\infty^\nu(A). \quad (9)$$

Similarly, if $H \in \mathbb{S}_p^+(\mathbb{R})$ with $H = A^T A$, we overload notation and define $\chi^\nu(H) := \chi^\nu(A)$.

Effective dimension: discussion. The effective dimension $d_{\text{eff}}^\nu(A)$ has an intuitive interpretation: it provides a smoothed count of the eigenvalues greater than or equal to the regularization ν . In the regularized setting, only directions associated with eigenvalues larger than ν matter, so $d_{\text{eff}}^\nu(A)$ rather than p is the relevant measure of degrees of freedom for the problem. As many data matrices have fast spectral decay (Derezinski et al., 2020), or obtain it through some algorithmic transformation, such as the celebrated random features method of (Rahimi and Recht, 2007), $d_{\text{eff}}^\nu(A)$ is often much smaller than $\min\{n, p\}$. Hence the effective dimension appears in the analysis of non-parametric learning, RandNLA, and statistical learning (Caponnetto and De Vito, 2007; Hsu et al., 2014; Marteau-Ferey et al., 2019b).

When the loss function f belongs to the GLM family and A has polynomial spectral decay, the following lemma demonstrates that the effective dimension of the Hessian, $A^T \Phi''(Aw)A$, is much smaller than the ambient dimension p . Various results of this form are well known in the literature, see for instance Caponnetto and De Vito (2007); Bach (2013); Marteau-Ferey et al. (2019a). Nevertheless, we provide a proof of Lemma 7, as we are unable to provide a reference with an identical result.

Lemma 7 (Effective dimension under polynomial decay) *Let f be a GLM loss satisfying $\sup_{w \in \mathbb{R}^p} \phi''(w) \leq B$, with data matrix $A \in \mathbb{R}^{n \times p}$ and regularization ν . Suppose the matrix A has polynomial (or faster) spectral decay:*

$$\sigma_j(A) = \mathcal{O}(j^{-\beta}) \quad (1 \leq j \leq p),$$

for some $\beta \in \mathbb{Z}_+$ satisfying $\beta \geq 1$. Then for any $w \in \mathbb{R}^p$,

$$d_{\text{eff}}^\nu(A^T \Phi''(Aw)A) \leq \frac{\pi/(2\beta)}{\sin(\pi/(2\beta))} \left(\frac{C}{n\nu} \right)^{1/2\beta}.$$

Hence, if $\nu = \mathcal{O}(\frac{1}{n})$ we have

$$d_{\text{eff}}^\nu(A^T \Phi''(Aw)A) = \mathcal{O}(\sqrt{n}),$$

The proof is given in Appendix C.1. Given mild hypotheses, Lemma 7 shows that the effective dimension of the Hessian for GLMs is no larger than $\mathcal{O}(\sqrt{n})$. Thus, we generally expect the effective dimension of the Hessian, $d_{\text{eff}}^\nu(A^T \Phi''(Aw)A)$, to be significantly smaller than the ambient dimension of the problem, p . The ‘‘smallness’’ of the effective dimension has been exploited in numerous works to develop fast algorithms for solving a variety of machine learning problems (Bach, 2013; Alaoui and Mahoney, 2015; Rudi et al., 2017; Marteau-Ferey et al., 2019a; Lacotte et al., 2021; Zhao et al., 2022; Frangella et al., 2023b). Similar to these prior works, we will also exploit the small effective dimension of the Hessian to develop effective preconditioners that can be constructed at negligible cost.

Ridge leverage coherence: discussion. When $\nu = 0$, the ridge leverage coherence $\chi^\nu(A)$ is equivalent to the coherence parameter from compressed sensing and matrix completion (Candes and Romberg, 2007; Candes and Recht, 2012), and its formulation in Definition 6 is the proper generalization to the regularized setting. The ridge leverage coherence measures the uniformity of ridge leverage scores, which determines how challenging it is to approximate $(1/n)A^T A + \nu I$ through row sampling from A . When $\chi^\nu(A) = \mathcal{O}(1)$, the ridge leverage scores are uniform, with each row contributing relatively equally to $d_{\text{eff}}^\nu(A)$. As a result, A has no distinguished rows carrying more weight than the rest, so uniform sampling will perform well. A classic family of matrices that have small ridge-leverage coherence are matrices whose left singular vectors are uniformly distributed on the Stiefel manifold $\mathcal{S}_p(\mathbb{R}^n)$ (the set of all p -dimensional orthonormal frames in \mathbb{R}^n (Milman and Schechtman, 2009)). Concretely, let $A \in \mathbb{R}^{n \times p}$ with SVD $A = U\Sigma V^T$, $U \in \mathbb{R}^{n \times p}$, $\Sigma, V \in \mathbb{R}^{p \times p}$, and suppose U is uniformly distributed on $\mathcal{S}_p(\mathbb{R}^n)$. Then with high probability, $\chi^\nu(A) = \tilde{\mathcal{O}}(1)$. When $\nu = 0$, in which case the ridge-leverage coherence is simply the coherence, this result was

established Candes and Recht (2012). We now give a sketch of the argument for $\nu > 0$. To this end, first observe that a routine calculation reveals

$$l_i^\nu(A) = u_i^T (\Sigma^2 (\Sigma^2 + n\nu I)^{-1}) u_i,$$

where u_i is the i th row of U . From this relation we find

$$\mathbb{E}[l_i^\nu(A)] = \mathbb{E}[u_i^T (\Sigma^2 (\Sigma^2 + n\nu I)^{-1}) u_i] = \frac{1}{n} \text{trace}(\Sigma^2 (\Sigma^2 + n\nu I)^{-1}) = \frac{1}{n} d_{\text{eff}}^\nu(A).$$

To control the deviation of $l_i^\nu(A)$ from its expectation, we may apply the Hanson-Wright inequality (Rudelson and Vershynin, 2013) to find $|l_i^\nu(A) - d_{\text{eff}}^\nu(A)/n| = \tilde{\mathcal{O}}(d_{\text{eff}}^\nu(A)/n)$ with high probability. Applying a union bound, we conclude $l_\infty^\nu(A) = \tilde{\mathcal{O}}(d_{\text{eff}}^\nu(A)/n)$, which immediately implies $\chi^\nu(A) = \tilde{\mathcal{O}}(1)$. Hence matrices whose left-singular vectors are uniformly distributed on the Stiefel manifold are ridge-leverage incoherent with high probability.

In contrast, when $\chi^\nu(A) = \Omega(n)$, a small number of rows significantly contribute to $d_{\text{eff}}^\nu(A)$, leading to highly non-uniform ridge leverage scores. In this setting, uniform sampling is unlikely to yield satisfactory results, as it may fail to sample the important rows. As an example, consider the family of matrices $A \in \mathbb{R}^{n \times p}$ whose rows satisfy

$$a_1 = nu, \quad a_j = u, \quad \text{for all } 2 \leq j \leq n, \quad \text{and } \|u\|_2 = 1.$$

Note for any n , A is rank-1 matrix with $\lambda_1(A^T A) = n^2 + n - 1$, and that the first row is a heavy-hitter. Suppose $\nu = \frac{1}{n}$, then direct calculation shows

$$l_\infty^\nu(A) = \frac{n^2}{n^2 + n}, \quad d_{\text{eff}}^\nu(A) = \frac{n^2 + n - 1}{n^2 + n}.$$

Hence, by the definition of ridge leverage coherence,

$$\chi^\nu(A) = \frac{n}{1 + n^{-1} + n^{-2}}.$$

Thus, even though the matrix is rank-1, uniform sampling must effectively sample every row of A to obtain a good approximation. This example shows only one outlier row is needed to make uniform sampling ineffective.

The preceding observations are made rigorous in the following lemma, which is well-known in the literature (Alaoui and Mahoney, 2015; Cohen et al., 2017; Li et al., 2020).

Lemma 8 (Uniform sampling: spectral approximation) *Let $A \in \mathbb{R}^{n \times p}$. Suppose we sample the rows of A according to the set \mathcal{J} , where $\mathcal{J} \subseteq [n]$ is drawn uniformly at random*

and $|\mathcal{J}| = \Omega\left(\frac{\chi^\nu(A) d_{\text{eff}}^\nu(A) \log\left(\frac{d_{\text{eff}}^\nu(A)}{\delta}\right)}{\zeta^2}\right)$. Then with probability at least $1 - \delta$

$$(1 - \zeta) \left(\frac{1}{|\mathcal{J}|} A_{\mathcal{J}}^T A_{\mathcal{J}} + \nu I \right) \preceq \left(\frac{1}{n} A^T A + \nu I \right) \preceq (1 + \zeta) \left(\frac{1}{|\mathcal{J}|} A_{\mathcal{J}}^T A_{\mathcal{J}} + \nu I \right). \quad (10)$$

Lemma 8 shows that for an incoherent matrix with $\chi^\nu(A) = \mathcal{O}(1)$, it only takes $\tilde{\mathcal{O}}(d_{\text{eff}}^\nu(A))$ rows to obtain a good spectral approximation to $(1/n)A^T A + \nu I$. In contrast, for a coherent matrix with $\chi^\nu(A) = \mathcal{O}(n)$, as many as $\mathcal{O}(n)$ rows may be needed to obtain a good spectral approximation. Thus, when the coherence is large, uniform sampling cannot exploit low effective dimensionality. The sample complexity for coherent matrices can be reduced using approximate leverage score sampling (ALS) procedures such as BLESS (Rudi et al., 2018), which sample rows according to their importance. However, since uniform sampling performs very well in our experiments, we omitted ALS procedures, as ALS increases algorithmic complexity and computational overhead.

We now establish that the various preconditioning methods introduced in Section 2.1 possess the ζ -spectral approximation property with high probability.

2.3.2 SUBSAMPLED NEWTON

The following proposition shows that SSN yields a ζ -spectral approximation for GLMs with high probability.

Proposition 9 *Let $w \in \mathbb{R}^p$, $\zeta_0 \in (0, 1)$, and suppose f is a GLM. Construct the subsampled Hessian with batchsize $b_H = \Omega\left(\frac{\chi^\rho(\nabla^2 f(w))d_{\text{eff}}^\rho(\nabla^2 f(w))\log\left(\frac{d_{\text{eff}}^\rho(\nabla^2 f(w))}{\delta}\right)}{\zeta_0^2}\right)$. Then with probability at least $1 - \delta$,*

$$(1 - \zeta)(\widehat{\nabla}^2 f(w) + \rho I) \preceq \nabla^2 f(w) + \nu I \preceq (1 + \zeta)(\widehat{\nabla}^2 f(w) + \rho I), \quad (11)$$

where $\zeta = 1 - (1 - \zeta_0)\nu/\rho$.

Proposition 9 is well-known in the literature (Li et al., 2020); however, as the proof is immediate given Lemma 8, we provide the proof in Appendix C.2 for completeness. Proposition 9 shows that when $\chi^\rho(\nabla^2 f(w)) = \mathcal{O}(1)$, a batchsize of $b_H = \tilde{\mathcal{O}}(d_{\text{eff}}^\rho(\nabla^2 f(w)))$ is sufficient to ensure that the subsampled Hessian is a ζ -spectral approximation. Furthermore, when the data matrix exhibits polynomial spectral decay, applying Lemma 7 reduces this requirement to $b_H = \tilde{\mathcal{O}}(\sqrt{n})$. This reduced requirement motivates our default hyperparameter setting $b_H = \lfloor \sqrt{n} \rfloor$ for the PROMISE algorithms in Section 3.

2.3.3 NYSTRÖM SUBSAMPLED NEWTON

The following proposition shows that NYSSN yields a ζ -spectral approximation with high probability.

Proposition 10 *Let $w \in \mathbb{R}^p$, $\zeta_0 \in (0, 1)$, and suppose f is a GLM. Construct the subsampled Hessian with batchsize $b_H = \Omega\left(\frac{\chi^\nu(\nabla^2 f(w))d_{\text{eff}}^\nu(\nabla^2 f(w))\log\left(\frac{d_{\text{eff}}^\nu(\nabla^2 f(w))}{\delta}\right)}{\zeta_0^2}\right)$. Further, assume either:*

1. Ω is a Gaussian random matrix with $r = \Omega\left(\frac{d_{\text{eff}}^\rho(\widehat{\nabla}^2 f(w)) + \log(\frac{1}{\delta})}{\zeta_0^2}\right)$ columns.

2. Ω is an SRHT matrix with $r = \Omega \left(\frac{d_{\text{eff}}^\rho(\widehat{\nabla}^2 f(w)) + \log(\frac{1}{\zeta_0 \delta}) \log\left(\frac{d_{\text{eff}}^\rho(\widehat{\nabla}^2 f(w))}{\delta}\right)}{\zeta_0^2} \right)$ columns.

3. Ω is an sparse sign embedding with sparsity $s = \Omega \left(\frac{\log\left(\frac{d_{\text{eff}}^\rho(\widehat{\nabla}^2 f(w))}{\delta}\right)}{\zeta_0} \right)$ and $r = \Omega \left(\frac{d_{\text{eff}}^\rho(\widehat{\nabla}^2 f(w)) \log\left(\frac{d_{\text{eff}}^\rho(\widehat{\nabla}^2 f(w))}{\delta}\right)}{\zeta_0^2} \right)$ columns.

Then with probability at least $1 - \delta$

$$(1 - \zeta)(\hat{H} + \rho I) \preceq \nabla^2 f(w) + \nu I \preceq (1 + \zeta)(\hat{H} + \rho I), \quad (12)$$

where $\zeta = 1 - (1 - \zeta_0)\nu/\rho$.

The proof is given in Appendix C.2. The regularization parameter ρ controls how much we may truncate the rank parameter r . As ρ increases, $d_{\text{eff}}^\rho(\widehat{\nabla}^2 f(w))$ decreases, so we can use a smaller value of r to construct the preconditioner; conversely, as ρ approaches ν , we must use a larger value of r . This leads to a trade-off, in that a smaller rank parameter leads to faster computation and storage, but potentially leads to a less effective preconditioner. On the other hand, a larger rank parameter leads to slower computation and more storage, but yields a more effective preconditioner, which can lead to fewer required iterations achieve convergence. In practice, this tradeoff is not as dramatic as the theory might suggest, and we find a rank of $r = 10$ yields excellent performance (Section 6).

2.3.4 SKETCH-AND-SOLVE SUBSAMPLED NEWTON

An analogous result for the SASSN preconditioners can be found in Appendix C.2.

3. Algorithms

In this section, we introduce the PROMISE algorithms SketchySGD (Section 3.2), SketchySVRG (Section 3.3), SketchySAGA (Section 3.4), and SketchyKatyusha (Section 3.5). SketchySGD was first proposed in Frangella et al. (2023a); the other algorithms are new. A summary of these algorithms is provided in Table 9. Each algorithm is compatible with all five preconditioning methods (SSN, NYSSN, SASSN-C, SASSN-R, DIAGSSN) described in Section 2.1. Each algorithm comes with default hyperparameters, which we use in the empirical evaluation in Section 6. In particular, we describe how to automatically compute the learning rate for each algorithm using the estimated preconditioned smoothness constant. The learning rate is hard to tune in stochastic optimization, and it is remarkable that this automated selection works across a wide range of problems (Section 6). Finally, we recommend the best algorithm to use for two important applications, ridge and l^2 -regularized logistic regression (Section 3.6).

Algorithm	Base Algorithm	Variance reduction	Acceleration	Stochastic gradients only?
SketchySGD (Algorithm 5)	SGD	✗	✗	✓
SketchySVRG (Algorithm 6)	SVRG (Johnson and Zhang, 2013)	✓	✗	✗
SketchySAGA (Algorithm 7)	b-nice SAGA (Gazagnadou et al., 2019)	✓	✗	✓
SketchyKatyusha (Algorithm 8)	Loopless Katyusha (Kovalev et al., 2020)	✓	✓	✗

Table 9: Summary of algorithms in PROMISE. **Ticks** are pros while **crosses** are cons. SVRG and Katyusha require some full gradients rather than stochastic gradients only.

3.1 Notation in algorithms

Throughout this section, \mathcal{M} denotes a GLM with the oracles defined in Table 2. We use P to denote a preconditioner object, which is a member of one of the five preconditioner classes ($\mathcal{P}_{\text{ssn}}, \mathcal{P}_{\text{nyssn}}, \mathcal{P}_{\text{sassn-c}}, \mathcal{P}_{\text{sassn-r}}, \mathcal{P}_{\text{diagssn}}$). $\mathcal{U} \subseteq \mathbb{N}$ denotes a (possibly infinite) set of times that indicate when to update the preconditioner. We also use the index j to track the time when the preconditioner is constructed: every time the preconditioner is updated, the index j is updated to the most recently used element of \mathcal{U} . This index does not have to be tracked in the implementations of these algorithms, but it plays a key role in the theoretical analysis of the proposed algorithms (Section 5).

3.2 SketchySGD

We present SketchySGD in Algorithm 5.

Algorithm 5 SketchySGD

Require: initialization w_0 , gradient and Hessian batchsizes b_g and b_H , preconditioner object P , model \mathcal{M} , preconditioner update times \mathcal{U} , learning rate multiplier α

```

for  $k = 0, 1, \dots$  do
  if  $k \in \mathcal{U}$  then
    Sample independent batches  $\mathcal{S}_k^1, \mathcal{S}_k^2$ 
     $P.\text{update}(\mathcal{M}, \mathcal{S}_k^1, \mathcal{S}_k^2, w_k)$ 
     $\eta \leftarrow \alpha / P.\lambda_{\mathcal{P}}$ 
    end if
    Sample batch  $\mathcal{B}_k$ 
     $g_k \leftarrow \mathcal{M}.\text{get\_stoch\_grad}(\mathcal{B}_k, w_k)$ 
     $v_k \leftarrow P.\text{direction}(g_k)$ 
     $w_{k+1} \leftarrow w_k - \eta v_k$ 
  end for

```

\triangleright Update preconditioner & learning rate
 $\triangleright |\mathcal{S}_k^1| = |\mathcal{S}_k^2| = b_H$
 \triangleright Compute preconditioner P_j at w_k & update $P.\lambda_{\mathcal{P}}$
 \triangleright Update learning rate
 $\triangleright |\mathcal{B}_k| = b_g$
 \triangleright Get approx. Newton step $P_j^{-1}g_k$
 \triangleright Update parameters

Explanation of algorithm SketchySGD is a preconditioned version of SGD that was originally proposed in Frangella et al. (2023a). Whenever the number of iterations $k \in \mathcal{U}$, both the preconditioner and learning rate are updated. SketchySGD uses a preconditioned stochastic gradient v_k to update the parameters rather than performing an SGD step at every iteration using g_k .

Default hyperparameters The main hyperparameters in SketchySGD are the gradient and Hessian batchsizes b_g and b_H , preconditioner update times \mathcal{U} , and learning rate multiplier α . The gradient batchsize b_g can be set to a wide range of values (our experiments on medium-scale datasets use $b_g = 256$, while our experiments on large-scale datasets use $b_g = 4096$); we recommend setting the Hessian batchsize $b_H = \lfloor \sqrt{n} \rfloor$. The selection $b_H = \lfloor \sqrt{n} \rfloor$ is motivated by the discussion in Section 2.3. We recommend setting \mathcal{U} according to a constant update frequency u , i.e., $\mathcal{U} = \{0, u, 2u, 3u, \dots\}$. For least squares/ridge regression, which has a constant Hessian, we recommend setting $u = \infty$, which results in the preconditioner being computed exactly once and held constant for the remainder of the optimization. For problems with a non-constant Hessian, such as logistic regression, we recommend setting $u = \lceil n/b_g \rceil$, which is equivalent to updating the preconditioner after each pass through the training set. Based on numerical experiments, we recommend setting the multiplier $\alpha = 1/2$.

3.3 SketchySVRG

We formally introduce SketchySVRG in Algorithm 6.

Explanation of algorithm SketchySVRG is a preconditioned version of SVRG (Johnson and Zhang, 2013). Similar to SVRG, SketchySVRG consists of an “outer” and “inner” loop indexed by s and k , respectively.

The algorithm starts in the outer loop by computing a full gradient \bar{g} at the snapshot \hat{w} , which is critical for performing variance reduction. The algorithm then sets the first iterate in the inner loop, w_0 , equal to \hat{w} .

The inner loop of the algorithm updates the parameters with a preconditioned, variance-reduced stochastic gradient, v_k . Similar to SketchySGD, SketchySVRG uses the preconditioner update times \mathcal{U} to determine when the preconditioner and learning rate should be updated.

After m iterations of the inner loop, the algorithm returns to the outer loop and updates the snapshot \hat{w} by either using the final inner-iterate w_m (Option I) or sampling the previous m iterates uniformly randomly (Option II). In practice, we use Option I, but the theoretical analysis is conducted using Option II (Section 5.4). This discrepancy also appears in the original SVRG analysis (Johnson and Zhang, 2013) and is therefore not a drawback of the analysis in this paper.

Default hyperparameters The main hyperparameters in SketchySVRG are the gradient and Hessian batchsizes b_g and b_H , preconditioner update times \mathcal{U} , learning rate multiplier α , and snapshot update frequency m . We recommend setting b_g , b_H , and \mathcal{U} similar to SketchySGD. We recommend setting $\alpha \in [1/3, 1/2]$; our practical implementation uses the SAGA-inspired update rule $\eta \leftarrow \max\{1/(2(\nu n + P \cdot \lambda_{\mathcal{P}})), 1/(3P \cdot \lambda_{\mathcal{P}})\}$. We recommend computing a full gradient every one or two passes through the dataset, i.e., setting $m \in$

Algorithm 6 SketchySVRG

Require: initialization \hat{w}_0 , gradient and Hessian batchsizes b_g and b_H , preconditioner object P , model \mathcal{M} , preconditioner update times \mathcal{U} , learning rate multiplier α , snapshot update frequency m

Initialize: snapshot $\hat{w} \leftarrow \hat{w}_0$

```

for  $s = 0, 1, \dots$  do                                     ▷ Outer loop
     $\bar{g} \leftarrow \mathcal{M}.\text{get\_full\_grad}(\hat{w})$              ▷ Full gradient at snapshot
     $w_0 \leftarrow \hat{w}$ 
    for  $k = 0, 1, \dots, m - 1$  do                             ▷ Inner loop
        if  $ms + k \in \mathcal{U}$  then                               ▷ Update preconditioner & learning rate
            Sample independent batches  $\mathcal{S}_k^1, \mathcal{S}_k^2$            ▷  $|\mathcal{S}_k^1| = |\mathcal{S}_k^2| = b_H$ 
             $P.\text{update}(\mathcal{M}, \mathcal{S}_k^1, \mathcal{S}_k^2, w_k)$  ▷ Compute preconditioner  $P_j$  at  $w_k$  & update  $P.\lambda_{\mathcal{P}}$ 
             $\eta \leftarrow \alpha / P.\lambda_{\mathcal{P}}$                  ▷ Update learning rate
        end if
        Sample batch  $\mathcal{B}_k$                                      ▷  $|\mathcal{B}_k| = b_g$ 
         $\widehat{\nabla}f(w_k) \leftarrow \mathcal{M}.\text{get\_stoch\_grad}(\mathcal{B}_k, w_k)$ 
         $\widehat{\nabla}f(\hat{w}) \leftarrow \mathcal{M}.\text{get\_stoch\_grad}(\mathcal{B}_k, \hat{w})$ 
         $g_k \leftarrow \widehat{\nabla}f(w_k) - \widehat{\nabla}f(\hat{w}) + \bar{g}$            ▷ Unbiased estimate of  $\nabla f(w_k)$ 
         $v_k \leftarrow P.\text{direction}(g_k)$                    ▷ Get approx. Newton step  $P_j^{-1}g_k$ 
         $w_{k+1} \leftarrow w_k - \eta v_k$                        ▷ Update parameters
    end for
    Option I:  $\hat{w} \leftarrow w_m$                              ▷ Update snapshot to final inner-iterate
    Option II:  $\hat{w} \leftarrow w_t$  for  $t \sim \text{Unif}(\{0, 1, \dots, m - 1\})$  ▷ Update snapshot randomly
end for
    
```

$\lceil n/b_g, 2n/b_g \rceil$ or so. Our experiments use $m = \lceil n/b_g \rceil$, which corresponds to computing a full gradient every pass through the training set.

3.4 SketchySAGA

We formally introduce SketchySAGA in Algorithm 7.

Algorithm 7 SketchySAGA

Require: initialization w_0 , gradient and Hessian batchsizes b_g and b_H , preconditioner object P , model \mathcal{M} , preconditioner update times \mathcal{U} , learning rate multiplier α

Initialize: gradient table $\psi_0 \leftarrow 0 \in \mathbb{R}^{p \times n}$, table avg. $x_0 \leftarrow \frac{1}{n}\psi_0 \mathbf{1}_n \in \mathbb{R}^p$

```

for  $k = 0, 1, \dots$  do
  if  $k \in \mathcal{U}$  then
    Sample independent batches  $\mathcal{S}_k^1, \mathcal{S}_k^2$ 
     $P.\text{update}(\mathcal{M}, \mathcal{S}_k^1, \mathcal{S}_k^2, w_k)$ 
     $\eta \leftarrow \alpha/P.\lambda_{\mathcal{P}}$ 
     $\triangleright$  Update preconditioner & learning rate
     $\triangleright |\mathcal{S}_k^1| = |\mathcal{S}_k^2| = b_H$ 
     $\triangleright$  Compute preconditioner  $P_j$  at  $w_k$  & update  $P.\lambda_{\mathcal{P}}$ 
     $\triangleright$  Update learning rate
  end if
  Sample batch  $\mathcal{B}_k$ 
   $\text{aux} \leftarrow \sum_{i \in \mathcal{B}_k} (\mathcal{M}.\text{get\_stoch\_grad}(i, w_k) - \psi_k^i)$ 
   $g_k \leftarrow x_k + \frac{1}{|\mathcal{B}_k|} \text{aux}$ 
   $x_{k+1} \leftarrow x_k + \frac{1}{n} \text{aux}$ 
   $\psi_{k+1}^i \leftarrow \begin{cases} \psi_k^i, & i \notin \mathcal{B}_k \\ \mathcal{M}.\text{get\_stoch\_grad}(i, w_k), & i \in \mathcal{B}_k \end{cases}$ 
   $v_k \leftarrow P.\text{direction}(g_k)$ 
   $w_{k+1} \leftarrow w_k - \eta v_k$ 
   $\triangleright |\mathcal{B}_k| = b_g$ 
   $\triangleright$  Unbiased estimate of  $\nabla f(w_k)$ 
   $\triangleright$  Update table average
   $\triangleright$  Update table columns for all  $i \in [n]$ 
   $\triangleright$  Get approx. Newton step  $P_j^{-1} g_k$ 
   $\triangleright$  Update parameters
end for

```

Explanation of algorithm SketchySAGA is a preconditioned version of a minibatch variant of SAGA (Gazagnadou et al., 2019).

Similar to SketchySGD, SketchySAGA updates the preconditioner and learning rate at each preconditioner update time in \mathcal{U} . At each iteration, the algorithm computes the stochastic gradient at every index in the batch \mathcal{B}_k . These stochastic gradients are used to update aux , an auxiliary vector used to reduce computation.

The auxiliary vector is then used to update the variance-reduced stochastic gradient g_k and table average x_{k+1} . The gradient table ψ is then updated: if i is in the batch, then the corresponding row of ψ is updated with the appropriate stochastic gradient; otherwise it is left unchanged. This update to ψ is a critical step for variance reduction.

After updating the table, SketchySAGA computes the preconditioned version of the variance-reduced stochastic gradient, v_k , and uses this quantity to update the parameters. Note that SketchySAGA does not require full gradient computations, making this algorithm well-suited for large-scale GLMs.

The memory requirement of SketchySAGA is dominated by the gradient table ψ , which requires $\mathcal{O}(np)$ storage in a naive implementation. Similar to Defazio et al. (2014), the storage of ψ can be reduced to $\mathcal{O}(n)$ for GLMs, since $\nabla f_i(w)$ is a multiple of a_i . For

example, in least squares regression, $\nabla f_i(w) = \nabla (a_i^T w_i - b_i)^2 / 2 = (a_i^T w_i - b_i) a_i$, so we can simply store $a_i^T w_i - b_i$ in place of $(a_i^T w_i - b_i) a_i$. Fully modifying the algorithm to reduce the storage of ψ requires fairly simple changes to the updates of aux and ψ , while also taking care to decouple the regularization-induced term νw from the stochastic gradient calculation. We use this improved version of the algorithm in our experiments.

Default hyperparameters The main hyperparameters in SketchySAGA are the gradient and Hessian batchsizes b_g and b_H , preconditioner update times \mathcal{U} , and learning rate multiplier α . We recommend setting b_g , b_H , and \mathcal{U} similar to SketchySGD. Similar to SketchySVRG, we recommend setting $\alpha \in [1/3, 1/2]$, although our practical implementation again uses $\eta \leftarrow \max\{1/(2(\nu n + P.\lambda p)), 1/(3P.\lambda p)\}$.

3.5 SketchyKatyusha

We formally introduce SketchyKatyusha in Algorithm 8.

Algorithm 8 SketchyKatyusha

Require: initialization w_0 , gradient and Hessian batchsizes b_g and b_H , preconditioner object P , model \mathcal{M} , preconditioner update times \mathcal{U} , momentum multiplier α , momentum parameter θ_2 , snapshot update probability π , strong convexity parameter μ

Initialize: snapshot $y \leftarrow w_0$, $z_0 \leftarrow w_0$, full gradient $\bar{g} \leftarrow \mathcal{M}.\text{get_full_grad}(w_0)$

```

for  $k = 0, 1, \dots$  do
  if  $k \in \mathcal{U}$  then
    Sample independent batches  $\mathcal{S}_k^1, \mathcal{S}_k^2$  ▷  $|\mathcal{S}_k^1| = |\mathcal{S}_k^2| = b_H$ 
     $P.\text{update}(\mathcal{M}, \mathcal{S}_k^1, \mathcal{S}_k^2, w_k)$  ▷ Compute preconditioner  $P_j$  at  $w_k$  & update  $P.\lambda p$ 
     $L \leftarrow P.\lambda p$ 
     $\sigma \leftarrow \mu / L$  ▷ Estimate of inverse condition number
     $\theta_1 \leftarrow \min(\sqrt{\alpha n \sigma}, 1/2)$  ▷ Update momentum parameter
     $\eta \leftarrow \frac{\theta_2}{(1+\theta_2)\theta_1}$  ▷ Update learning rate
  end if
   $x_k \leftarrow \theta_1 z_k + \theta_2 y + (1 - \theta_1 - \theta_2) w_k$  ▷ “Negative momentum” step
  Sample batch  $\mathcal{B}_k$  ▷  $|\mathcal{B}_k| = b_g$ 
   $\widehat{\nabla} f(x_k) \leftarrow \mathcal{M}.\text{get\_stoch\_grad}(\mathcal{B}_k, x_k)$ 
   $\widehat{\nabla} f(y) \leftarrow \mathcal{M}.\text{get\_stoch\_grad}(\mathcal{B}_k, y)$ 
   $g_k \leftarrow \widehat{\nabla} f(x_k) - \widehat{\nabla} f(y) + \bar{g}$  ▷ Unbiased estimate of  $\nabla f(x_k)$ 
   $v_k \leftarrow P.\text{direction}(g_k)$  ▷ Get approx. Newton step  $P_j^{-1} g_k$ 
   $z_{k+1} \leftarrow \frac{1}{1+\eta\sigma} (n\sigma x_k + z_k - \frac{\eta}{L} v_k)$ 
   $w_{k+1} \leftarrow x_k + \theta_1 (z_{k+1} - z_k)$  ▷ Update parameters
  Sample  $\mathcal{U} \sim \text{Unif}([0, 1])$ 
  if  $\mathcal{U} \leq \pi$  then ▷ Update snapshot & full gradient with probability  $\pi$ 
     $y \leftarrow w_k$ 
     $\bar{g} \leftarrow \mathcal{M}.\text{get\_full\_grad}(y)$ 
  end if
end for

```

Explanation of algorithm SketchyKatyusha is a preconditioned version of Loopless Katyusha (Kovalev et al., 2020). The following explanation of the algorithm is adapted from both Allen-Zhu (2018) and Kovalev et al. (2020).

Similar to SketchySGD, SketchyKatyusha uses the preconditioner update times \mathcal{U} to determine when the preconditioner and learning rate should be updated. However, the update to the learning rate no longer depends on just the learning rate multiplier and estimated preconditioned smoothness $P.\lambda_{\mathcal{P}}$. The learning rate for SketchyKatyusha is calculated by estimating the inverse condition number σ to determine momentum parameter θ_1 , which is followed by using the momentum parameters θ_1, θ_2 to determine η .

The vectors x_k and z_k are key to performing acceleration. At each iteration, SketchyKatyusha performs a “negative momentum” step, which computes x_k using a convex combination of z_k , the snapshot y , and current iterate w_k . This step counteracts the momentum provided by z_k by using the snapshot y as a “magnet” that prevents x_k from moving too far away from y . By using negative momentum, we are able to obtain the benefits of both variance reduction and acceleration at the same time.

After the negative momentum step, SketchyKatyusha computes the preconditioned version of the variance-reduced stochastic gradient, v_k . SketchyKatyusha then computes z_{k+1} , which is followed by a Nesterov momentum-like step to update the parameters w_{k+1} .

Finally, SketchyKatyusha randomly updates the snapshot y and full gradient \bar{g} with probability π . This random updating allows us to use just one loop in the implementation, unlike the original formulation of Katyusha (Allen-Zhu, 2018), which uses two loops.

Default hyperparameters The main hyperparameters in SketchyKatyusha are the gradient and Hessian batchsizes b_g and b_H , preconditioner update times \mathcal{U} , momentum multiplier α , momentum parameter θ_2 , snapshot update probability π , and strong convexity parameter μ . We recommend setting b_g, b_H , and \mathcal{U} similar to SketchySGD. We recommend setting $\alpha = 2/3$, $\theta_2 = 1/2$, $\pi = b_g/n$, and $\mu = \nu$, where ν is the regularization parameter in the GLM.

3.6 Algorithm recommendations

We present recommended algorithms for ridge regression and l^2 -regularized logistic regression in Tables 10 and 11, respectively.

Data Regime	Recommendation (full gradients)	Recommendation (streaming ≤ 10 epochs)	Recommendation (streaming > 10 epochs)	Preconditioner
Dense	SketchyKatyusha	SketchySGD	SketchySAGA	NySSN
Sparse	SketchyKatyusha	SketchySGD	SketchySAGA	SSN

Table 10: Recommended algorithms for ridge regression. We recommend SketchySGD for streaming settings with limited computation (≤ 10 epochs) as SketchySAGA offers no significant advantage over short durations.

Data Regime	Recommendation (full gradients)	Recommendation (streaming ≤ 10 epochs)	Recommendation (streaming > 10 epochs)	Preconditioner
Dense	SketchyKatyusha SketchySAGA	SketchySGD	SketchySAGA	NySSN
Sparse	SketchyKatyusha SketchySAGA	SketchySGD	SketchySAGA	SSN

Table 11: Recommended algorithms for l^2 -regularized logistic regression. We recommend SketchySGD for streaming settings with limited computation (≤ 10 epochs) as SketchySAGA offers no significant advantage over short durations.

4. Related work

We review the literature on stochastic second-order and preconditioned stochastic gradient methods for solving the finite sum optimization (1), with emphasis on work that assumes strongly convexity.

4.1 Stochastic second-order and preconditioned stochastic gradient methods

The deficiencies of the stochastic first-order methods presented in Section 1 are well-known within the optimization and machine learning communities. Indeed, in the past decade or so, the literature on stochastic second-order methods and stochastic preconditioning techniques for finite sum optimization has exploded. Roughly, these methods can be divided into three categories: 1) stochastic second-order methods that use full gradients, 2) stochastic second-order methods that use stochastic gradients, and 3) preconditioned stochastic gradient methods. The dividing line between stochastic second-order methods and preconditioned methods is not always clear, as many preconditioners use second-order information, including the PROMISE framework. We review the literature on these three approaches in detail below.

Stochastic second-order methods with full gradients. We begin with stochastic second-order methods that use full gradients and a stochastic approximation to the Hessian. To the authors’ knowledge, the earliest method of this form targeting the problem (1) is Byrd et al. (2011). Byrd et al. (2011) subsample the Hessian and use this stochastic approximation in conjunction with an L-BFGS style update. Erdogdu and Montanari (2015); Roosta-Khorasani and Mahoney (2019) independently investigated the application of Newton’s method to solve (1), where the Hessian is replaced with an approximation constructed through subsampling. The subsampled Newton method, as pioneered in these works, serves as the foundation for many subsequent developments in stochastic second-order methods.

In addition to introducing new algorithms, the works discussed above also provide analysis that lead to various convergence guarantees, which we now review. The earliest analysis of Byrd et al. (2011) is quite coarse, only showing their method converges to the global optimum, provided the objective is strongly convex and the subsampled Hessian is always positive definite. Byrd et al. (2011) provides neither a convergence rate nor a theoretical advantage over first-order methods. The analyses of Erdogdu and Montanari (2015) and Roosta-Khorasani and Mahoney (2019) yield considerably stronger results. Both works es-

establish linear convergence in the strongly convex setting. Furthermore, Roosta-Khorasani and Mahoney (2019) prove local superlinear convergence of Subsampled Newton, albeit under certain unattractive assumptions such as exponentially growing the Hessian batch-size b_H . Despite these assumptions, the results of Roosta-Khorasani and Mahoney (2019) point to potential benefits of stochastic second-order methods over first-order methods. We also note the analyses of these papers have been refined by Ye et al. (2021); Na et al. (2022). In particular, Na et al. (2022) propose a novel averaging scheme for the subsampled Hessian, which achieves local superlinear convergence without requiring a growing Hessian batchsize. Unfortunately, this approach is limited to settings where the dimension p of the feature vectors is modest, as it requires forming the subsampled Hessian for averaging, at a computational cost of $O(b_H p^2)$ and a storage cost of $O(p^2)$.

As an alternative to subsampling, some methods use sketching to construct a stochastic approximation to the full Hessian (Pilanci and Wainwright, 2017; Gower et al., 2019a; Lacotte et al., 2021). Sketching the Hessian has two main benefits over subsampling: (i) it generally produces higher-accuracy approximations to the Hessian (Martinsson and Tropp, 2020), and (ii) it is robust to the origins of the data. By robust, we mean that with an appropriate sketching matrix, the sketch size required to ensure the ζ -spectral approximation property is independent of the ridge leverage coherence. In detail, if the Hessian approximation is constructed from a sketching matrix belonging to an appropriate random ensemble, the sketch size required to ensure the ζ -spectral approximation property holds with high probability, is only $\tilde{O}(d_{\text{eff}}^\nu(A))$ (Lacotte et al., 2021). In contrast, the Hessian batchsize required by subsampling to ensure the ζ -good approximation property depends upon the ridge leverage coherence, which can be quite large when the data contains outliers.

However, sketching has several disadvantages relative to subsampling. A notable disadvantage of existing sketching-based methods is that they require a full pass through the data to approximate the Hessian, while subsampling methods do not. It is desirable to minimize full passes through the data when solving large-scale problems, which limits the usefulness of existing sketching-based methods in this setting. Another limitation of sketching-based methods, is that they may only be applicable to problems with certain structure. As a concrete example, the Newton Sketch (Pilanci and Wainwright, 2017; Lacotte et al., 2021) requires access to a matrix R such that $\nabla^2 f(w) = R^T R$. While such a matrix is always available when f is a GLM, this is not the case for more general losses. In contrast, subsampling can always be used to approximate the Hessian of a finite-sum objective, regardless of the form of the loss function. Last, we note that if f is a GLM, then the Newton Sketch with a row-sampling sketching matrix is equivalent to Subsampled Newton.

The analysis guarantees of sketching-based (approximate) second-order methods are similar to their subsampled counterparts. Pilanci and Wainwright (2017); Lacotte et al. (2021) focus on self-concordant functions for their global convergence analysis and show fast linear convergence independent of the condition number. Additionally, Pilanci and Wainwright (2017) show local superlinear convergence for smooth and strongly convex objectives with Lipschitz Hessians, but require a sketch size that depends on the condition number of the problem, which can be larger than n when the problem is ill-conditioned. However, in the setting where p is moderate in size, this issue may be resolved by using the Hessian averaging scheme of Na et al. (2022). Gower et al. (2019a) prove convergence for functions that are relatively smooth and relatively convex, a generalization of smoothness

and strong convexity to the local Hessian norm. They establish linear convergence with a rate that depends upon the *relative condition number* and the smallest non-zero eigenvalue of an expected projection matrix. When the objective is quadratic, the relative condition number equals 1, and so condition number-free linear convergence is achieved, which shows an improvement of over first-order methods.

Stochastic second-order methods with full gradients in the statistical setting.

In machine learning, the primary metric of interest is generalization error, i.e., the error made by the model on unseen data. Motivated by this, a line of work beginning with Rudi et al. (2017) and culminating with Marteau-Ferey et al. (2019a), has developed fast algorithms for l^2 -regularized kernel based methods for which low generalization error is the main goal. These approaches may be viewed as sketching based Newton methods to solve a reduced form of the objective. Rudi et al. (2017) develop the FALKON algorithm for fast approximate kernel ridge regression. By leveraging the smallness of the effective dimension of the kernel operator, they show the kernel matrix only has to be evaluated using $\mathcal{O}(d_{\text{eff}}^\nu)$ centers, instead of the usual n . This reduction leads to a highly overdetermined least-squares problem with an $n \times \mathcal{O}(d_{\text{eff}}^\nu)$ kernel matrix, which is then solved by using preconditioned conjugate gradient (PCG) with a randomized preconditioner that approximates the Hessian. The linear system solve may be viewed as preconditioned Newton Conjugate Gradient (Newton-CG). Rudi et al. (2017) proves that despite the various approximations, the FALKON algorithm achieves the minimax optimal statistical error rate for the kernel ridge regression problem. Moreover, under appropriate parameter settings, the work required to achieve optimal statistical error is only $\tilde{\mathcal{O}}(n^{3/2})$, a significant improvement over the $\mathcal{O}(n^3)$ cost of exact kernel ridge regression.

Marteau-Ferey et al. (2019a) extends the approach of Rudi et al. (2017) to loss functions that are generalized self-concordant, an idea first introduced in Bach (2010). Many popular losses in machine learning are generalized self-concordant, including the logistic loss, and more generally any GLMs with bounded second-derivatives. Similar to FALKON, the method of Marteau-Ferey et al. (2019a) reduces from working with the full $n \times n$ kernel matrix to an $n \times \mathcal{O}(d_{\text{eff}}^\nu)$ kernel matrix. However, unlike FALKON, the objective is no longer quadratic, and is highly ill-conditioned. To address this challenge, Marteau-Ferey et al. (2019a) propose a specialized approximate Newton-CG scheme to solve the problem. To handle the subproblem efficiently, Marteau-Ferey et al. (2019a) use sketch-and-precondition-style preconditioners (Rokhlin and Tygert, 2008; Martinsson and Tropp, 2020) with PCG to solve the Newton system fast at each iteration. Marteau-Ferey et al. (2019a) shows that their approximate Newton method achieves condition number-free convergence once the iterates enter an appropriate neighborhood of the optimum. However, Marteau-Ferey et al. (2019a) note the worst-case number of iterations required for Newton-CG to enter this neighborhood may be no better than accelerated gradient descent (AGD), whose convergence depends upon the condition number. To help alleviate this issue they propose a modified approximate Newton-CG scheme, whose required number of iterations to enter the neighborhood is bounded above by the product of norm of the solution and the generalized self-concordance constant. For many problems this leads to significant improvement over using AGD, but in the worst-case may fail to remove the dependence upon the condition

number. Similar to Rudi et al. (2017), Marteau-Ferey et al. (2019a) show their proposed approximate Newton scheme achieves optimal statistical rates.

The methods of Rudi et al. (2017) and Marteau-Ferey et al. (2019a) may both be viewed as second-order sketching-based Newton methods for solving a reduced problem. Indeed, the Newton Sketch directly solves an approximate Newton system with an approximate Hessian, while FALKON and the method of Marteau-Ferey et al. (2019a) solve the exact Newton system using PCG, with the approximate Hessian serving as a preconditioner. When statistical error is the primary metric of interest, FALKON and the approximate Newton method of Marteau-Ferey et al. (2019a) can deliver significant computational gains. The main deficit of these approaches is that it can be difficult to select the number of centers a priori, as the effective dimension is unknown. This can be problematic in practice, as if too few centers are chosen, the statistical performance will be much worse than that obtained by solving the exact problem. Moreover, Díaz et al. (2023) has shown empirically that the approximate solution produced by FALKON fails to match the statistical performance of the solution to the full kernel ridge regression problem, even when the number of centers chosen is $n/2$. Thus, even when statistical performance is the primary goal, there can be benefits to solving the original problem with the entire dataset.

Stochastic second-order methods with stochastic gradients for solving (1). In scenarios where both n and p are substantially large, the use of full gradients becomes prohibitively expensive. Consequently, a scalable second-order method must use both stochastic gradients and stochastic Hessian approximations. To address this challenge, many methods that employ fully stochastic first- and second-order information have been proposed for solving (1). A feature common to these proposals is that they all employ subsampling-based approximations to the Hessian (Byrd et al., 2016; Moritz et al., 2016; Gower et al., 2016; Bollapragada et al., 2018; Roosta-Khorasani and Mahoney, 2019; Bollapragada et al., 2019; Dereziński, 2022). These methods can be further categorized based on whether they directly compute the search direction by applying the inverse subsampled Hessian (Roosta-Khorasani and Mahoney, 2019; Bollapragada et al., 2019; Dereziński, 2022), or by combining the subsampled Hessian with an L-BFGS style update (Byrd et al., 2016; Moritz et al., 2016; Gower et al., 2016; Bollapragada et al., 2018). Hence most stochastic second-order methods that use stochastic gradients have their roots in the full-gradient methods of Byrd et al. (2011); Erdogdu and Montanari (2015); Roosta-Khorasani and Mahoney (2019).

The convergence guarantees of existing proposals vary greatly, often leaving much to be desired. Byrd et al. (2016) established an $\mathcal{O}(1/k)$ -rate for their stochastic L-BFGS method under strong convexity assumptions. However, their analysis relies on two restrictive assumptions: (i) bounded variance of stochastic gradients and (ii) strict positive definiteness of the subsampled Hessian. The first is known to be false for strongly convex functions, unless the iterates lie in a compact set, and the second fails in common applications such as GLMs, where the subsampled Hessian is singular unless $b_H \geq p$. Roosta-Khorasani and Mahoney (2019) present a range of convergence results for a variety of settings, including when F is strongly convex, for which they establish fast local linear convergence. Specifically, they show with high probability that after $\mathcal{O}(\kappa^2)$ iterations, the iterates enter a small neighborhood of the optimum, after which they converge linearly to the optimum at a condition-number independent rate. Hence the Subsampled Newton method enjoys the

fast local convergence of Newton’s method, albeit at a linear rather than quadratic rate. Nevertheless, the fast local convergence rate shows an advantage over stochastic first-order methods, whose convergence depends upon the condition number, regardless of how close the iterates are to the optimum. Unfortunately, in order to achieve their fast local convergence result, Roosta-Khorasani and Mahoney (2019) require the gradient batchsize to increase exponentially at each iteration, and that the batchsize for the subsampled Hessian satisfies $b_H = \tilde{\mathcal{O}}(\kappa/\epsilon^2)$, where $\epsilon \in (0, 1)$. Hence the theoretical analysis requires rapidly growing gradient batchsizes and large Hessian batchsizes, which is antithetical to the purpose of stochastic methods.

The first work to obtain a linear rate of convergence for (1) without requiring large/growing gradient and Hessian batchsizes was Moritz et al. (2016). Moritz et al. (2016) accomplished this by combining the stochastic L-BFGS method of Byrd et al. (2016) with SVRG, the latter of which removes the condition of growing the gradient batchsize. However, although Moritz et al. (2016) establish linear convergence, their result is only global, showing convergence after $\mathcal{O}(\kappa^2 \log(1/\epsilon))$ iterations. Fast local linear convergence is not established, and no theoretical benefit over stochastic first-order methods is demonstrated. Similar remarks hold for the stochastic L-BFGS methods of Gower et al. (2016); Bollapragada et al. (2018). In more recent work, Dereziński (2022) proposed Stochastic Variance Reduced Newton (SVRN), which combines Subsampled Newton with SVRG. Dereziński (2022) shows SVRN exhibits fast local linear convergence without increasing gradient batchsizes, which is no longer needed due to SVRN’s use of variance reduction. However, Dereziński (2022)’s analysis requires the gradient batchsize to satisfy $b_g = \tilde{\mathcal{O}}(\kappa)$, which is still very large, and can easily exceed n in the ill-conditioned setting.

Preconditioned stochastic gradient methods. Taking a general viewpoint, the stochastic second-order methods discussed above are all special cases of preconditioned stochastic gradient methods, where the current preconditioner P_k is based on an approximation to the Hessian matrix. Consequently, many proposals including PROMISE, refer to themselves as *preconditioned stochastic gradient methods*. One early notable proposal in this context, is the preconditioned SVRG algorithm of Gonen et al. (2016), which is specialized to ridge regression. Gonen et al. (2016) construct a preconditioner via low-rank approximation to the Hessian computed using the randomized block Krylov method of Musco and Musco (2015). While Gonen et al. (2016)’s analysis does exhibit improvements over SVRG, it suffers from a major deficiency, which is how the preconditioner is constructed. Forming the preconditioner requires multiple full passes through the data matrix, due to the use of a block Krylov method. Such a requirement does not pair well with larger problems where methods like SVRG are used, as the goal in this setting is to minimize the number of passes through the entire dataset as much as possible. Another low-rank preconditioning approach is the SVRG2 method of Gower et al. (2018), which combines SVRG with a preconditioner based on a randomized Nyström approximation to the Hessian. However, this method exhibits a similar deficit to the one of Gonen et al. (2016), in that every outer-iteration, a full pass through the data is required to construct the Hessian approximation, which is prohibitively expensive in the stochastic gradient regime. Another undesirable property of SVRG2 is that it does not employ lazy updating; it requires access to a fresh subsampled Hessian at every iteration. Last, we mention the work of Liu et al. (2019), which develop preconditioned

variants of SVRG and Katyusha. The preconditioners in Liu et al. (2019) use either the covariance matrix or a diagonal approximation to it. The former preconditioner costs $O(np^2)$ to form, making it impractical in the large-scale setting targeted by stochastic first-order methods. In contrast, the latter preconditioner is cheap to construct and scales very well, but it may perform quite poorly. Indeed, we find empirically that preconditioners based on diagonal approximation to the Hessian are ineffective, see Section 6 for details. Also, Liu et al. (2019) only consider a fixed preconditioner (i.e., the preconditioner never changes), which can result in worse performance for non-quadratic problems.

Relation to PROMISE. Among the many works discussed above, the most relevant methods in relation to PROMISE are Subsampled Newton (Roosta-Khorasani and Mahoney, 2019) and SVRN (Dereziński, 2022). When a PROMISE method uses the SSN preconditioner, it may be viewed as combining Subsampled Newton with the corresponding stochastic gradient algorithm. Variance reduction brings significant benefits and enables PROMISE to avoid exponentially growing gradient batchsizes, which vanilla Subsampled Newton (Roosta-Khorasani and Mahoney, 2019) requires to achieve linear convergence. As SVRN is simply Subsampled Newton combined with SVRG, it follows SketchySVRG equipped with the SSN preconditioner is equivalent to SVRN. However despite this equivalence, the aims of this work and those of Dereziński (2022) are quite different. Dereziński (2022) focuses on proving fast local linear convergence under the hypotheses of large gradient minibatches: their results require $b_g = \tilde{O}(\kappa)$. Moreover, Dereziński (2022) only suggests using SVRN to finish off the optimization, and that in the beginning, Subsampled Newton with full gradients should be used to get the iterates sufficiently close to the optimum. This stands in stark contrast to this work, which focuses on global linear convergence, allows for lazy updates, and considers variance reduction schemes beyond SVRG. Furthermore, we also prove fast local linear convergence of SketchySVRG, but without requiring the gradient batchsize to be on the order of the condition number, which is a significant theoretical and practical improvement.

To facilitate a straightforward comparison between PROMISE and prior work, we present Table 12. Table 12 compares the properties of various stochastic second-order methods for solving (1) when F is a GLM. We select SketchySVRG as a representative for PROMISE. Inspection of Table 12 shows SketchySVRG is the method that enjoys the best batchsize requirements, while still attaining fast local-linear convergence. Moreover, it is the only method in Table 12 whose theory accounts for lazy updates to the preconditioner, an essential property to ensure good practical performance.

4.2 Lazy updating and Newton’s method.

One of the major contributions of this work is to show linear convergence is still attainable even when the stochastic Hessian approximation is updated *infrequently*. In the literature, this is known as *lazy updating* or *lazy Hessians* (Doikov et al., 2023). Despite being of immense practical interest, lazy updating for Newton’s method in the *full gradient* setting has only recently been analyzed in Doikov et al. (2023), which proves an optimal update frequency of p iterations. Our setting is quite different from Doikov et al. (2023), as our focus is on solving the smooth convex ERM problem (1) with preconditioned stochastic gradient

methods based on stochastic Hessian approximations. Hence the analysis in Doikov et al. (2023) is incompatible with our problem class.

4.3 Fast global convergence in theory?

Of all the stochastic second-order methods with stochastic gradients we have discussed, none show a *global improvement* over stochastic first-order methods—at best they show improved local convergence. Moreover, for all the methods discussed, the worst-case global convergence rate scales as $\tilde{\mathcal{O}}(\kappa^2)$, which is a factor of κ worse than that of stochastic variance reduced first-order methods. This point has been noticed in the literature: Gower et al. (2020) discusses the disappointing convergence guarantees of existing second-order stochastic methods, noting that none of them have a better global convergence rate than that of SVRG. Thus, assuming F is given by (1), and is smooth, strongly convex, and has Lipschitz Hessians, it is natural to wonder whether or not such an improvement is possible. Unfortunately, we believe it is unlikely that stochastic second-order methods can significantly improve upon stochastic first-order methods in the worst-case. To see why, it helps to consider results for second-order methods in the full gradient setting. In a surprising result, Arjevani and Shamir (2017) show that if F satisfies the hypotheses listed above, then Newton’s method does not provide an improvement (up to logarithmic factors) over AGD in the worst-case. We say surprising, as in practice Newton’s method often converges in 10s of iterations on problems for which first-order methods converge slowly. If F does not have finite-sum structure, this “surprising” result is quite old, going back to the seminal work of Nemirovski and Yudin (1983), albeit without proof (Arjevani and Shamir, 2017). Hence, in the worst-case, no global improvement is possible from using second-order information. Arjevani and Shamir (2017)’s disappointing conclusion also applies to approximate schemes like Subsampled Newton methods (Erdogdu and Montanari, 2015; Roosta-Khorasani and Mahoney, 2019; Bollapragada et al., 2019). Thus, given the negative result of Arjevani and Shamir (2017) in the full gradient setting, we hypothesize that (without further assumptions) no stochastic second-order method can significantly improve upon the worst-case iteration complexity of $\mathcal{O}([n + \sqrt{n\kappa}] \log(1/\epsilon))$ for finite-sum optimization with stochastic first-order oracles (Woodworth and Srebro, 2016), which is achieved by the Katyusha algorithm with $b_g = 1$ (Allen-Zhu, 2018). It would be interesting to see if there is a stochastic second-order algorithm that achieves this complexity, while employing second-order information throughout the optimization. At present, when full gradients are used, the optimal second-order scheme (for appropriate values of problem parameters) in the smooth, strongly convex, Lipschitz Hessian setting is simply to run AGD until the iterates reach the region of quadratic convergence and then switch to Newton’s method (Arjevani et al., 2019). The latter scheme is essentially first-order and does not match how second-order methods are used in practice.

The previous paragraph is pessimistic in its conclusions, but it does not imply that stochastic second-order methods do not yield faster global convergence in practice—they clearly do. The purpose of the preceding discussion is to delineate what kind of convergence guarantees are reasonable to expect from stochastic second-order methods. If the class of functions considered is not further restricted by adding more assumptions, the previous discussion shows it is unreasonable to expect an improvement over the global convergence

Algorithm	b_g	$b_H /$ Sketch size	Lazy preconditioner updates	Fast local-linear convergence	Source
SketchySVRG (Algorithm 6)	τ_*^ν	$\tilde{O}(d_{\text{eff}}^\nu(A))$	✓	✓	This paper
Subsampled Newton	Exponentially increasing	$\tilde{O}(\kappa/\epsilon^2)$	✗	✓	Roosta- Khorasani and Mahoney (2019)
Newton Sketch	Full	$\tilde{O}(d_{\text{eff}}^\nu(A))$	✗	✓	Lacotte et al. (2021)
Stochastic Variance Reduced Newton	$\tilde{O}(\kappa)$	$\tilde{O}(\kappa/\epsilon^2)$	✗	✓	Dereziński (2022)
SLBFGS	Constant	Constant	✗	✗	Moritz et al. (2016)
Progressive Batching L-BFGS	Increasing	Increasing	✗	✗	Bollapragada et al. (2018)

Table 12: Comparison of preconditioned stochastic gradient methods for solving (1) when F is a GLM. Here b_g and b_H are gradient and Hessian batchsizes, κ is the condition number, and $d_{\text{eff}}^\nu(A)$ is the effective dimension of the data matrix. Of all the methods, SketchySVRG has the best required gradient and Hessian batchsizes, and is the only method whose theory accounts for lazy updates.

rate of stochastic first-order methods. Indeed, finding a (non-trivial) stochastic second-order scheme that matches Katyusha’s rate seems daunting, given how in the full gradient setting, the optimal scheme is essentially AGD for the vast majority of the optimization. Thus, in terms of theoretical guarantees, any reasonable stochastic second-order method should possess either (or both) of the following properties: (i) fast global linear convergence on quadratic objectives, (ii) fast condition number-free local convergence once the iterates are sufficiently close to the optimum. Improved convergence results beyond these two items seem very unlikely, unless further assumptions are imposed.

5. Theory

In this section we establish (global and local) linear convergence results for the PROMISE methods on smooth, strongly convex, finite-sum objectives (which does not restrict F to just being a GLM). This section begins with our assumptions and then introduces the key concepts of quadratic regularity and the quadratic regularity ratio, which generalize the notions of strong convexity, smoothness, and the condition number to the Hessian norm. We then provide a simple theoretical example illustrating why ζ -spectral approximations and quadratic regularity should improve convergence over vanilla gradient descent. We follow this by introducing Hessian dissimilarity, which plays a key role in analyzing PROMISE methods with stochastic gradients, and preconditioner stability, which is important for proving convergence under lazy updating. Finally, we state the convergence theorems for all of our PROMISE methods, provide a convergence proof for SketchySVRG which illustrates the techniques in our analysis, and show SketchySVRG achieves fast, condition number-free local convergence. Proofs not presented in the main text are in Appendix C.

Idea/result	Expression(s)	Reference
Quadratic regularity	$\gamma_u(\mathcal{C}), \gamma_\ell(\mathcal{C}), \mathfrak{q}(\mathcal{C})$	Definition 11
Hessian dissimilarity	$\tau_\star^\nu(\mathcal{C})$	Definition 18
Preconditioner stability	$\ w_j - w_\star\ _{P_{j+1}}^2 / \ w_j - w_\star\ _{P_j}^2,$ $\ w_j - w_\star\ _{P_{j-1}}^2 / \ w_j - w_\star\ _{P_j}^2$	Proposition 21
Expected preconditioned smoothness	$\mathbb{E}\ \widehat{\nabla}F(w) - \widehat{\nabla}F(w')\ _{P^{-1}}^2$	Proposition 22
SketchySVRG convergence	$F(w) - F(w_\star)$	Theorem 24
SketchySVRG fast local convergence	$F(w) - F(w_\star)$	Theorem 26
SketchySAGA convergence	$\ w - w_\star\ _{P_k}^2$	Theorem 28
SketchyKatyusha convergence	$F(w) - F(w_\star), F(y) - F(w_\star), \ z - w_\star\ _{P_k}^2$	Theorem 30

Table 13: A summary of the main ideas and theoretical results of this work.

As there are numerous ideas and results in this section, we provide Table 13, which lists the key ideas and results along with cross references to where they appear.

5.1 A subtlety in notation

We index the preconditioner in two different ways in this section; sometimes we denote the preconditioner by P_j , and other times we denote the preconditioner by P_k (or in the case of SketchySVRG, $P_k^{(s)}$). In this setting, j indexes the iterate where the preconditioner is constructed, while k (or $k^{(s)}$) indexes the current iterate in the algorithm.

There is a simple way to map a P_k to the corresponding P_j . If the preconditioner update indices $\mathcal{U} = \{u_1, u_2, \dots, u_m\}$, then a given P_k for $k \in \{u_i, u_i + 1, \dots, u_{i+1} - 1\}$ is the same as P_j for $j = u_i$. As a concrete example, suppose $\mathcal{U} = \{0, 4, 10\}$. Then, for $k \in \{0, 1, 2, 3\}$, P_k is the same as P_j where $j = 0$; for $k \in \{4, 5, 6, 7, 8, 9\}$, P_k is the same as P_j where $j = 4$; for $k \in \{10, 11, \dots\}$, P_k is the same as P_j where $j = 10$.

5.2 Assumptions

Here we provide assumptions that will be needed in the convergence analyses of all the PROMISE methods.

Assumption 1 (Smoothness and convexity) *For each $i \in [n]$, $f_i(w)$ is L_i -smooth and convex.*

The above assumption is standard in the analysis of stochastic gradient methods for solving (1).

Assumption 2 (ζ -spectral approximation) *If the preconditioner P_j was constructed at w_j , where $j \in \mathcal{U}$, then*

$$(1 - \zeta)P_j \preceq \nabla^2 f(w_j) + \nu I \preceq (1 + \zeta)P_j,$$

where $\zeta \in (0, 1)$.

Assumption 2 states each preconditioner constructed by the algorithm satisfies the ζ -spectral approximation property, which is reasonable as PROMISE preconditioners satisfy this property with high probability. Hence, Assumption 2 can be viewed as conditioning on the event that the preconditioners constructed by the algorithm satisfy the ζ -spectral approximation property, which holds with high probability via union bound. Moreover, if new preconditioning techniques are developed that lead to better preconditioners satisfying the ζ -spectral approximation property, Assumption 2 makes it easy to establish convergence of any PROMISE method equipped with this preconditioner.

Assumption 3 (Finite number of preconditioner updates) *Let P_k denote the preconditioner at iteration k . There exists $J \geq 0$, such that for all $k \geq J$ we have*

$$P_k = P_J.$$

This last assumption is somewhat technical in nature, and is needed only for SketchySAGA, and SketchyKatyusha. The need for Assumption 3 stems from the convergence analysis of SketchySAGA and SketchyKatyusha involving the metric $\|\cdot\|_{P_k}$, and having to compare it to the next (previous) metric $\|\cdot\|_{P_{k+1}}$, ($\|\cdot\|_{P_{k-1}}$). Consequently, if the number of preconditioner updates is not finite, we cannot guarantee that the quantities in \mathcal{E}_P and \mathcal{B}_P in Proposition 21 are finite, which prevents establishment of convergence. By instating Assumption 3, we remove this obstacle. From the viewpoint of theory, this assumption isn't very limiting, as once the iterates are close enough to the optimum, the benefit of updating the preconditioner becomes negligible. Nevertheless, we believe Assumption 3 is unnecessary in practice, and is an artifact of the analysis.

5.3 Technical preliminaries

5.3.1 QUADRATIC REGULARITY

We start by introducing the upper and lower quadratic regularity constants for a smooth, convex function $F : \mathcal{C} \mapsto \mathbb{R}$, where \mathcal{C} is a closed convex subset of \mathbb{R}^p . These ideas are crucial for establishing linear convergence under infrequent updating of the preconditioner.

Definition 11 *The upper quadratic regularity constant is defined by*

$$\gamma_u(\mathcal{C}) := \sup_{w_0 \in \mathcal{C}} \left(\sup_{w_1, w_2 \in \mathcal{C}, w_1 \neq w_2} \int_0^1 2(1-t) \frac{\|w_2 - w_1\|_{\nabla^2 F(w_1+t(w_2-w_1))}^2}{\|w_2 - w_1\|_{\nabla^2 F(w_0)}^2} dt \right). \quad (13)$$

Similarly, the lower quadratic regularity constant is defined by

$$\gamma_\ell(\mathcal{C}) := \inf_{w_0 \in \mathcal{C}} \left(\inf_{w_1, w_2 \in \mathcal{C}, w_1 \neq w_2} \int_0^1 2(1-t) \frac{\|w_2 - w_1\|_{\nabla^2 F(w_1+t(w_2-w_1))}^2}{\|w_2 - w_1\|_{\nabla^2 F(w_0)}^2} dt \right). \quad (14)$$

We say F is \mathcal{C} -quadratically regular if $0 < \gamma_\ell$ and $\gamma_u < \infty$. Further, if F is \mathcal{C} -quadratically regular, we define the quadratic regularity ratio to be

$$\mathfrak{q}(\mathcal{C}) := \frac{\gamma_u(\mathcal{C})}{\gamma_\ell(\mathcal{C})}.$$

Moreover, if $F(w) = \frac{1}{n} \sum_{i=1}^n F_i(w)$, and each F_i is \mathcal{C} -quadratically regular, we denote the corresponding quadratic regularity constants by $\gamma_{u_i}(\mathcal{C})$ and $\gamma_{\ell_i}(\mathcal{C})$, and we define

$$\gamma_u^{\max}(\mathcal{C}) := \max_{i \in [n]} \gamma_{u_i}, \quad \gamma_\ell^{\min}(\mathcal{C}) := \min_{i \in [n]} \gamma_{\ell_i}.$$

The terminology in Definition 11 is inspired by the following proposition, which shows that if F is quadratically regular in \mathcal{C} , then F can be upper- and lower-bounded in terms of the Hessian at any $w_0 \in \mathcal{C}$. Hence the upper and lower quadratic regularity constants may be viewed as generalizations of the smoothness and strong-convexity to the Hessian norm $\|\cdot\|_{\nabla^2 F(w)}$. Moreover, the quadratic regularity ratio \mathfrak{q} provides the generalization of the condition number κ to the Hessian norm.

Proposition 12 *Let F be \mathcal{C} -quadratically regular. Then for any $w_0, w_1, w_2 \in \mathcal{C}$,*

$$F(w_2) \leq F(w_1) + \langle \nabla F(w_1), w_2 - w_1 \rangle + \frac{\gamma_u(\mathcal{C})}{2} \|w_2 - w_1\|_{\nabla^2 F(w_0)}^2, \quad (15)$$

$$F(w_2) \geq F(w_1) + \langle \nabla F(w_1), w_2 - w_1 \rangle + \frac{\gamma_\ell(\mathcal{C})}{2} \|w_2 - w_1\|_{\nabla^2 F(w_0)}^2, \quad (16)$$

$$\|\nabla F(w_2) - \nabla F(w_1)\|_{\nabla^2 F(w_0)^{-1}} \leq \gamma_u(\mathcal{C}) \|w_2 - w_1\|_{\nabla^2 F(w_0)}. \quad (17)$$

The proof is given in Appendix C.3. Upper and lower quadratic regularity expand upon the ideas of Hessian stability from Karimireddy et al. (2018) and its refinements relative smoothness and relative convexity from Gower et al. (2019a). The relative smoothness and relative convexity parameters from Gower et al. (2019a) are defined similarly to the quadratic regularity constants, except they lack the outer supremum and infimum present in the definitions of γ_u and γ_ℓ , respectively. Unfortunately, relative smoothness and relative convexity are insufficient for our analysis, which incorporates infrequent updating. Under infrequent updating, the preconditioner is constructed at a point $w_0 \neq w_1, w_2$. Relative smoothness only provides bounds in terms of $\nabla^2 F(w_1)$, whereas our analysis requires bounds in terms of $\nabla^2 F(w_0)$, i.e., the Hessian at the iterate where the preconditioner is constructed, and these bounds are given in Proposition 12.

The additional power given by quadratic regularity could imply it only holds for a restrictive class of functions. However, the following proposition shows this is not the case, as quadratic regularity holds under many standard hypotheses, including smoothness and strong convexity.

Proposition 13 (Sufficient conditions for quadratic regularity) *The following conditions all imply F is \mathcal{C} -quadratically regular:*

1. The function F is L -smooth and μ -strongly convex over \mathcal{C} . Then F is \mathcal{C} -quadratically regular with

$$\frac{\mu}{L} \leq \gamma_\ell(\mathcal{C}) \leq \gamma_u(\mathcal{C}) \leq \frac{L}{\mu}.$$

2. The function F is μ -strongly convex and has a M -Lipschitz Hessian over \mathcal{C} , and \mathcal{C} is compact with diameter D . Then F is \mathcal{C} -quadratically regular with

$$\left(1 + \frac{MD}{\mu}\right)^{-1} \leq \gamma_\ell(\mathcal{C}) \leq \gamma_u(\mathcal{C}) \leq 1 + \frac{MD}{\mu}.$$

3. The function F is k -generalized self-concordant (Bach, 2010) over \mathcal{C} , and \mathcal{C} is compact with diameter D . Then F is \mathcal{C} -quadratically regular with

$$\exp(-kD) \leq \gamma_\ell(\mathcal{C}) \leq \gamma_u(\mathcal{C}) \leq \exp(kD).$$

4. The function $F(w) = \frac{1}{n} \sum_{i=1}^n \phi_i(a_i^T w) + \frac{\nu}{2} \|w\|^2$, that is F is a GLM. Then F is \mathcal{C} -quadratically regular with

$$\frac{\ell \lambda_1(\hat{\Sigma}) + \nu}{u \lambda_1(\hat{\Sigma}) + \nu} \leq \gamma_\ell(\mathcal{C}) \leq \gamma_u(\mathcal{C}) \leq \frac{u \lambda_1(\hat{\Sigma}) + \nu}{\ell \lambda_1(\hat{\Sigma}) + \nu},$$

where $\hat{\Sigma} = \frac{1}{n} A^T A$, $u = \sup_{1 \leq i \leq n} (\sup_{w \in \mathcal{C}} \phi_i''(a_i^T w))$, and $\ell = \inf_{1 \leq i \leq n} (\inf_{w \in \mathcal{C}} \phi_i''(a_i^T w))$.

The proof is given in Appendix C.3. Proposition 13 is similar to Theorem 1 in Karimireddy et al. (2018), which establishes analogous sufficient conditions for Hessian stability. Moreover, the bounds attained on the quadratic regularity constants are identical to those attained in Karimireddy et al. (2018). Hence, the bounds on the quadratic regularity constants are no worse than those of Karimireddy et al. (2018), even though they account for lazy updating, while Hessian stability does not.

To better understand quadratic regularity and its properties, it is instructive to compare the bounds in Proposition 13 and their implications. Notably, the bounds guaranteed by smoothness and strong convexity are looser than the bounds guaranteed by the other conditions. To see why, suppose F is an ill-conditioned quadratic. Clearly, $\gamma_\ell = \gamma_u = 1$, but the bound given by 1. in Proposition 13 is $\kappa^{-1} \leq \gamma_\ell \leq \gamma_u \leq \kappa$. In contrast, items 2–4. in Proposition 13 all yield $\gamma_\ell = \gamma_u = 1$. Thus, the bound given by 1. is pessimistic, which is unsurprising since the proof of 1. is based on simple worst-case norm conversion bounds.

5.3.2 ζ -SPECTRAL APPROXIMATION AND QUADRATIC REGULARITY IN ACTION: A SIMPLE EXAMPLE

Before presenting the convergence results for the PROMISE algorithms, we provide intuition for why ζ -spectral approximation and quadratic regularity lead to improved local convergence. To do so, we will compare the one-step improvement of an (approximate) lazy Newton method to that of gradient descent. The convergence proofs for PROMISE use stochastic gradients, which adds a layer of complexity to their analysis, while the analysis in this section uses full gradients. However, the ideas underlying the convergence proofs of PROMISE methods are similar to those in the following analysis.

We will assume the objective F is strongly convex and has M -Lipschitz Hessians. Furthermore, we will assume that the iterates are localized to a ball that contains the optimum. Under these assumptions, we show that an approximate, lazy version of Newton’s method has a better one-step improvement than gradient descent. This is accomplished with the following sequence of results:

1. Quadratic regularity leads to a “good” local model of F in a neighborhood of the iterate where the Hessian is computed (Lemma 14)
2. Newton’s method with lazy updates makes better progress compared to gradient descent (Corollary 15)
3. A ζ -spectral approximation in place of the Hessian still provides a “good” local model of F (Lemma 16)
4. Approximate Newton’s method with lazy updates still makes fast progress. (Corollary 17)

Lemma 14 (Lazy Hessians provide a good local model) *Let $w \in \mathbb{R}^p$, $\varepsilon \in (0, 1)$. Suppose F is strongly convex and has M -Lipschitz Hessians. Let $\mathcal{C} = B(w, \frac{\varepsilon\mu}{2M})$. Then*

$$\frac{1}{1 + \varepsilon} \leq \gamma_\ell(\mathcal{C}) \leq \gamma_u(\mathcal{C}) \leq 1 + \varepsilon,$$

so the quadratic regularity ratio is moderate:

$$\mathfrak{q}(\mathcal{C}) = \gamma_u/\gamma_\ell \leq (1 + \varepsilon)^2.$$

Furthermore, for any $w', w'' \in \mathcal{C}$,

$$\begin{aligned} F(w'') &\leq F(w') + \langle \nabla F(w'), w'' - w' \rangle + \frac{1 + \varepsilon}{2} \|w'' - w'\|_{\nabla^2 F(w)}^2, \\ F(w'') &\geq F(w') + \langle \nabla F(w'), w'' - w' \rangle + \frac{1}{2(1 + \varepsilon)} \|w'' - w'\|_{\nabla^2 F(w)}^2. \end{aligned}$$

Proof The result follows immediately by combining the definition of \mathcal{C} with item 2 in Proposition 13. ■

In Lemma 14, w is the iterate where the Hessian is computed, while w' and w'' are contained in a ball about w . Lemma 14 shows that within \mathcal{C} , F is well-conditioned (i.e., quadratic regularity provides a good local model) with respect to the $\nabla^2 F(w)$ norm, with condition number given by $\mathfrak{q}(\mathcal{C}) \leq (1 + \varepsilon)^2$.

Corollary 15 (One-step improvement for lazy Newton’s method) *Instate the hypotheses of Lemma 14. Set $w'' = w' - \frac{1}{1 + \varepsilon} \nabla^2 F(w)^{-1} \nabla F(w')$ and suppose $w', w'', w_\star \in B(w, \frac{\varepsilon\mu}{2M})$. Then*

$$F(w'') - F(w_\star) \leq \left[1 - \frac{1}{(1 + \varepsilon)^2} \right] (F(w') - F(w_\star)).$$

Proof The proof is similar to that of linear convergence of gradient descent for smooth, strongly convex functions.

Since $w', w'' \in B(w, \frac{\varepsilon\mu}{2M})$,

$$\begin{aligned} F(w'') &\leq F(w') + \langle \nabla F(w'), w'' - w' \rangle + \frac{1+\varepsilon}{2} \|w'' - w'\|_{\nabla^2 F(w)}^2 \\ &= F(w') + \left\langle \nabla F(w'), -\frac{1}{1+\varepsilon} \nabla^2 F(w)^{-1} \nabla F(w') \right\rangle + \frac{1+\varepsilon}{2} \left\| -\frac{1}{1+\varepsilon} \nabla^2 F(w)^{-1} \nabla F(w') \right\|_{\nabla^2 F(w)}^2 \\ &= F(w') - \frac{1}{2(1+\varepsilon)} \|\nabla F(w')\|_{\nabla^2 F(w)^{-1}}^2, \end{aligned}$$

where the inequality follows from upper quadratic regularity and the first equality follows from the definition of w'' .

To complete the proof, we use quadratic regularity to derive a lower bound on $\|\nabla F(w')\|_{\nabla^2 F(w)^{-1}}^2$ in terms of objective suboptimality. Since $w', w_* \in B(w, \frac{\varepsilon\mu}{2M})$,

$$\begin{aligned} F(w_*) &\geq F(w') + \langle \nabla F(w'), w_* - w' \rangle + \frac{1}{2(1+\varepsilon)} \|w_* - w'\|_{\nabla^2 F(w)}^2 \\ &\geq F(w') + \min_y \langle \nabla F(w'), y \rangle + \frac{1}{2(1+\varepsilon)} \|y\|_{\nabla^2 F(w)}^2 \\ &= F(w') - \frac{1+\varepsilon}{2} \|F(w')\|_{\nabla^2 F(w)^{-1}}^2, \end{aligned}$$

where the first inequality is due to lower quadratic regularity and the equality is due to minimizing the quadratic function with respect to y .

Rearranging the previous display yields

$$\frac{2}{1+\varepsilon} (F(w') - F(w_*)) \leq \|\nabla F(w')\|_{\nabla^2 F(w)^{-1}}^2,$$

which is precisely the lower bound we are seeking.

Therefore,

$$\begin{aligned} F(w'') &\leq F(w') - \frac{1}{2(1+\varepsilon)} \|\nabla F(w')\|_{\nabla^2 F(w)^{-1}}^2 \\ &\leq F(w') - \frac{1}{(1+\varepsilon)^2} (F(w') - F(w_*)). \end{aligned}$$

Adding $-F(w_*)$ to both sides of this display yields the claimed result. ■

We can compare the one-step improvement in Corollary 15 with that of a gradient descent update ($w'' = w' - \frac{1}{L} \nabla F(w')$), which has one-step improvement

$$F(w'') - F(w_*) \leq \left[1 - \frac{1}{\kappa} \right] (F(w') - F(w_*)).$$

This comparison suggests that Newton's method with lazy Hessian updates (locally) converges linearly at a rate independent of the condition number, unlike gradient descent, whose convergence rate depends on the condition number.

Lemma 16 (ζ -spectral approximations provide a good local model) *Suppose F is quadratically regular and P is a ζ -spectral approximation of $\nabla^2 F(w)$ and let $w', w'' \in \mathbb{R}^p$. Then*

$$F(w'') \leq F(w') + \langle \nabla F(w'), w'' - w' \rangle + \frac{(1 + \zeta)\gamma_u}{2} \|w'' - w'\|_P^2,$$

$$F(w'') \geq F(w') + \langle \nabla F(w'), w'' - w' \rangle + \frac{(1 - \zeta)\gamma_\ell}{2} \|w'' - w'\|_P^2.$$

Proof Since F is quadratically regular,

$$F(w'') \leq F(w') + \langle \nabla F(w'), w'' - w' \rangle + \frac{\gamma_u}{2} \|w'' - w'\|_{\nabla^2 F(w)}^2, \quad (18)$$

$$F(w'') \geq F(w') + \langle \nabla F(w'), w'' - w' \rangle + \frac{\gamma_\ell}{2} \|w'' - w'\|_{\nabla^2 F(w)}^2. \quad (19)$$

Since P is a ζ -spectral approximation of $\nabla^2 F(w)$, $(1 - \zeta)P \preceq \nabla^2 F(w) \preceq (1 + \zeta)P$, which implies

$$(1 - \zeta)\|w'' - w'\|_P^2 \leq \|w'' - w'\|_{\nabla^2 F(w)}^2 \leq (1 + \zeta)\|w'' - w'\|_P^2.$$

Substituting the previous display into Eqs. (18) and (19) yields the claimed result. \blacksquare

Quadratic regularity tells us that F has a condition number of $\gamma_u/\gamma_\ell = \mathfrak{q}$ in the $\nabla^2 F(w)$ norm. Lemma 16 shows that we pay a multiplicative factor of $\frac{1+\zeta}{1-\zeta}$ on the quadratic regularity ratio \mathfrak{q} to extend quadratic regularity to the P norm, where P is a ζ -spectral approximation of $\nabla^2 F(w)$. In other words, using a ζ -spectral approximation in place of the Hessian still provides a reliable local model for F .

A concrete example is given by ridge regression, for which $\mathfrak{q} = 1$. If P is a 0.9-spectral approximation of $\nabla^2 F(w)$, then $\frac{1+\zeta}{1-\zeta}\mathfrak{q} = 19$, which is better than the condition number κ for most ridge regression problems.

Corollary 17 (One-step improvement for approximate, lazy Newton's method) *Instate the hypotheses of the Lemmas 14 and 16. Set $w'' = w' - \frac{1}{(1+\zeta)(1+\varepsilon)}P^{-1}\nabla F(w')$ and suppose $w', w'', w_\star \in B(w, \frac{\varepsilon\mu}{2M})$. Then*

$$F(w'') - F(w_\star) \leq \left[1 - \frac{1 - \zeta}{1 + \zeta} \frac{1}{(1 + \varepsilon)^2} \right] (F(w') - F(w_\star)).$$

Proof Combining Lemmas 14 and 16, we have

$$F(w'') \leq F(w') + \langle \nabla F(w'), w'' - w' \rangle + \frac{(1 + \zeta)(1 + \varepsilon)}{2} \|w'' - w'\|_P^2, \quad (20)$$

$$F(w_\star) \geq F(w') + \langle \nabla F(w'), w_\star - w' \rangle + \frac{1 - \zeta}{2(1 + \varepsilon)} \|w'' - w'\|_P^2. \quad (21)$$

The remainder of the proof is analogous to that of Corollary 15—we use Eq. (20) to derive $F(w'') \leq F(w') - \frac{1}{2(1+\zeta)(1+\varepsilon)}\|\nabla F(w')\|_{P^{-1}}^2$ and Eq. (21) to derive $\frac{2(1-\zeta)}{1+\varepsilon}(F(w') - F(w_\star)) \leq \|\nabla F(w')\|_{P^{-1}}^2$. Combining these two bounds yields the claim. \blacksquare

Corollary 17, which analyzes the one-step improvement of approximate, lazy Newton’s method, is best understood by comparing with Corollary 15, which analyzes the one-step improvement of (exact) lazy Newton’s method. First, the stepsize in Corollary 17 is $1/[(1 + \zeta)(1 + \varepsilon)]$, while the stepsize in Corollary 15 is $1/(1 + \varepsilon)$. The ζ -spectral approximation multiplies the upper quadratic regularity constant by $1 + \zeta$ (Lemma 16), which explains the reduced stepsize. Furthermore, the multiplicative factor in Corollary 17 is $1 - [(1 - \zeta)/(1 + \zeta)]/(1 + \varepsilon)^2$, while the multiplicative factor in Corollary 15 is $1 - 1/(1 + \varepsilon)^2$. This is also consistent—Lemma 16 multiplies \mathbf{q} by $\frac{1+\zeta}{1-\zeta}$, so we would expect the multiplicative factor to be reduced from $1 - 1/\mathbf{q}$ to $1 - 1/[(1 + \zeta)/(1 - \zeta)\mathbf{q}] = 1 - [(1 - \zeta)/(1 + \zeta)]/\mathbf{q}$.

Despite this reduced improvement, we would expect approximate, lazy Newton’s method to perform better than gradient descent. For example, if $\zeta = \varepsilon = 0.5$, then $[(1 - \zeta)/(1 + \zeta)]/(1 + \varepsilon)^2 = 4/27$. Hence, if $\kappa \geq 7$ (which is common in ML problems), approximate, lazy Newton’s method would be expected to (locally) converge faster than gradient descent.

5.3.3 HESSIAN DISSIMILARITY

The next concept we shall need is the Hessian dissimilarity, which tells us how large the gradient batchsize must be to realize the benefits of preconditioning.

Definition 18 *Let \mathcal{C} be a closed convex subset of \mathbb{R}^p . Then the Hessian dissimilarity is given by*

$$\tau_\star^\nu(\mathcal{C}) := \sup_{w \in \mathcal{C}} \max_{1 \leq i \leq n} \lambda_1 \left((\nabla^2 f(w) + \nu I)^{-1/2} (\nabla^2 f_i(w) + \nu I) (\nabla^2 f(w) + \nu I)^{-1/2} \right).$$

The Hessian dissimilarity provides a uniform measure of how different $\nabla^2 F(w)$ is from each $\nabla^2 F_i(w)$. In many ways, Hessian dissimilarity is analogous to ridge leverage coherence in Section 2.3: it may be viewed as a generalization from measuring the uniformity of the rows of a matrix to measuring the uniformity of constituent psd Hessians of a finite-sum convex function $F(w)$. Furthermore, for GLMs, we will see that the Hessian dissimilarity is controlled by a uniform version of ridge leverage coherence.

The Hessian dissimilarity parameter τ_\star^ν is important for our analysis because it arises in our bound on the preconditioned smoothness constant (Proposition 22). In this bound, τ_\star^ν is a “price” incurred for sampling the gradients uniformly at random, as it controls the batchsize on the gradient required to ensure a “good” preconditioned smoothness constant. Plainly put, τ_\star^ν determines the worst-case gradient batchsize required to see the benefits of preconditioning.

The first important property of Hessian dissimilarity is that it never exceeds n , as shown by the following lemma.

Lemma 19 (Hessian dissimilarity never exceeds n) *The dissimilarity parameter satisfies*

$$1 \leq \tau_\star^\nu(\mathcal{C}) \leq \min \left\{ n, \frac{1}{2} + \frac{L_{\max}}{\nu} \right\}.$$

The proof is given in Appendix C.4. Lemma 19 guarantees that τ_\star^ν never exceeds n and that this quantity may be much smaller if the f_i ’s are well-conditioned. Unfortunately, this

bound on τ_\star^ν provides little comfort in the ill-conditioned setting, where the minimum is easily achieved by n . In practice, large gradient batchsizes are unnecessary, which suggests the bound in Lemma 19 is pessimistic. In particular, this bound fails to account for the structure of the objective. For GLMs, we can derive a more informative bound on the Hessian dissimilarity (see Proposition 20 below), which reveals a deeper connection to ridge leverage scores and ridge leverage coherence.

Proposition 20 (Hessian dissimilarity for GLMs) *Let F be a GLM, that is,*

$$F(w) = \frac{1}{n} \sum_{i=1}^n \phi_i(a_i^T w) + \frac{\nu}{2} \|w\|^2.$$

Further suppose that $\sup_{x \in \mathbb{R}} \phi_i''(x) \leq B$, for some $B > 0$. Then

$$\tau_\star^\nu \leq 1 + \chi_\star^\nu d_{\text{eff}}^{\nu/B}(A),$$

where $\chi_\star^\nu = \sup_{w \in \mathbb{R}^p} \chi^\nu(\Phi(Aw)^{1/2}A)$. In particular, for least squares and logistic regression, we have

$$\tau_\star^\nu \leq 1 + \chi_\star^\nu d_{\text{eff}}^\nu(A).$$

The proof is given in Appendix C.4. Proposition 20 shows that for GLMs, the Hessian dissimilarity is controlled by the global ridge leverage coherence of the Hessian, χ_\star^ν . When χ_\star^ν is small, the batchsize required to see the full effects of preconditioning is no larger than the effective dimension of the data matrix. As $d_{\text{eff}}^\nu(A)$ is much smaller than n under mild assumptions (recall Lemma 7), this implies we only need a small gradient batchsize to see the effects of preconditioning, which agrees with our empirical results. Conversely, when the data matrix has high coherence, Proposition 20 suggests that large gradient batchsizes may be necessary to realize the benefits of preconditioning.

5.3.4 PRECONDITIONER STABILITY

We also establish the following result that shows the preconditioners evolve in a stable fashion, which is needed for showing convergence of SketchySAGA and SketchyKatyusha.

Proposition 21 (Stable evolution of preconditioners) *Instate the hypotheses of Assumptions 1 to 3. Consider the sequences of random variables $\{X_j\}_{j \in [J]}$, $\{Y_j\}_{j \in [J]}$ defined by*

$$X_j := \max \left\{ \frac{\|w_j - w_\star\|_{P_{j+1}}^2}{\|w_j - w_\star\|_{P_j}^2}, 1 \right\}, \quad Y_j := \max \left\{ \frac{\|w_j - w_\star\|_{P_{j-1}}^2}{\|w_j - w_\star\|_{P_j}^2}, 1 \right\}$$

Then with probability 1, there exist constants ξ_j, β_j such that

$$X_j \leq \xi_j, \quad Y_j \leq \beta_j.$$

Hence with probability 1,

$$\prod_{j=1}^J X_j \leq \prod_{j=1}^J \xi_j := \mathcal{E}_P, \quad \prod_{j=1}^J Y_j \leq \prod_{j=1}^J \beta_j := B_P.$$

The proof is given in Appendix C.5.

5.3.5 CONTROLLING THE SMOOTHNESS OF THE PRECONDITIONED STOCHASTIC GRADIENT

Controlling the smoothness of the stochastic gradient is essential in the convergence analysis of stochastic gradient methods. Since we are working with preconditioned stochastic gradient methods, we must control the smoothness in the preconditioned norm ($\|\cdot\|_{P^{-1}}$) instead of the usual Euclidean norm ($\|\cdot\|_2$). The following proposition provides such control.

Proposition 22 (Preconditioned expected smoothness) *Let F be γ_u upper-quadratically regular and P be a ζ -spectral approximation. Instate Assumption 1 and Assumption 2. Then for any $w', w \in \mathbb{R}^p$,*

$$\mathbb{E}\|\widehat{\nabla}F(w) - \widehat{\nabla}F(w')\|_{P^{-1}}^2 \leq 2\mathcal{L}_P (F(w) - F(w') - \langle \nabla F(w'), w - w' \rangle),$$

where

$$\mathcal{L}_P = \left(\frac{n(b_g - 1)}{b_g(n - 1)}\gamma_u + \tau_\star^\nu \frac{n - b_g}{b_g(n - 1)}\gamma_u^{\max} \right) (1 + \zeta).$$

The proof is given in Appendix C.6. The constant \mathcal{L}_P in Proposition 22 provides the analogue of the preconditioned smoothness constant in the stochastic gradient setting. Indeed, if $n = b_g$, then $\mathcal{L}_P = (1 + \zeta)\gamma_u$, which is the smoothness constant of F with respect to the preconditioned norm $\|\cdot\|_P$ (Lemma 16). We have seen that when P provides a good quadratic model, that $\gamma_u \leq 1 + \varepsilon$, and so $\mathcal{L}_P \leq (1 + \varepsilon)(1 + \zeta)$. However, PROMISE operates in the setting $b_g \ll n$, in which case Proposition 22 yields a new phenomena not present when $b_g = n$; namely, that even if $\gamma_u^{\max} = 1$, so that P provides a perfect quadratic model, it is not guaranteed $\mathcal{L}_P = \mathcal{O}(1)$. To ensure $\mathcal{L}_P = \mathcal{O}(1)$, the gradient batchsize must satisfy $b_g = \mathcal{O}(\tau_\star^\nu)$. Hence to realize the benefits of preconditioning, the gradient batchsize cannot be arbitrary, it must be sufficiently large; how large the batchsize must be is determined by the Hessian dissimilarity. The dependence on τ_\star^ν is intuitive, and reflects the fact that the gradient batchsize must be large enough to ensure the minibatch Hessian is representative of the full Hessian. Indeed, if the batchsize for the stochastic gradient is too small, the corresponding minibatch Hessian will not resemble the true Hessian. Consequently, we should not expect a preconditioner built from a good approximation of the full Hessian to help, as the information it contains is unrelated to that of the stochastic gradient. Moreover, we have the natural conclusion that the more similar the $\nabla^2 F_i$ are, the smaller the required gradient batchsize, with the opposite holding true when the $\nabla^2 F_i$ are dissimilar.

To obtain a more concrete understanding of Proposition 22, let us consider the special case when F is a GLM. Proposition 20 shows the Hessian dissimilarity is bounded as $\tau_\star^\nu \leq 1 + \chi_\star^\nu d_{\text{eff}}^{\nu/B}(A)$, so the required gradient batchsize is no more than $\mathcal{O}\left(\chi_\star^\nu d_{\text{eff}}^{\nu/B}(A)\right)$, which is consistent with Proposition 9. However, this bound depends upon the global ridge leverage coherence χ_\star^ν instead of the ridge leverage coherence of the Hessian at w , which is in line with smoothness being a global quantity. When the global ridge leverage coherence is small, τ_\star^ν is no larger than the effective dimension, so the required gradient batchsize is small. Conversely, a large global ridge leverage coherence implies the required gradient batchsize may be large.

Overall, Proposition 22 shows that preconditioning is not a panacea. For problems with highly non-uniform data, convergence of PROMISE methods may be slow if the gradient

batchsize fails to satisfy $b_g = \mathcal{O}(\tau_\star^\nu)$. We emphasize this limitation is independent of any particular preconditioning technique, and would remain true even if PROMISE used the perfect preconditioner—the Hessian itself. The problem stems from the use of uniform sampling to construct the stochastic gradient. Evidently, given our extensive empirical results in Section 6, problem instances requiring large gradient batches seem to be uncommon. This is unsurprising, as the data in many ML problems is (approximately) i.i.d.; hence we have strong reasons to believe that data is relatively uniform due to statistical similarity. Nevertheless, it is worth being aware of worst-case problem instances.

To our knowledge, the analysis above is the first to demonstrate the necessity of a “kick-in” gradient batchsize to see the benefits of preconditioning. Previously, Dereziński (2022) realized at an intuitive level that least-squares with highly coherent data matrices necessitates large gradient batchsizes, and shows how leverage score sampling can remedy this situation. Nevertheless, this falls short of the full mathematical analysis we have provided in Proposition 22, which provides a simple explanation for this phenomena in a general setting.

5.3.6 WEIGHTED QUADRATIC REGULARITY RATIO

We have seen that \mathcal{L}_P is the analogue of the smoothness constant for PROMISE methods. As a consequence, the convergence rates of PROMISE methods will not depend on \mathfrak{q} , but on the *weighted* quadratic regularity ratio, $\bar{\mathfrak{q}}$, which we define below.

Definition 23 (Weighted quadratic regularity ratio) *Let $F : \mathbb{R}^p \mapsto \mathbb{R}$ be the quadratically regular, then the weighted quadratic regularity ratio is given by*

$$\begin{aligned} \bar{\mathfrak{q}} &:= \frac{\mathcal{L}_P}{\gamma_\ell} = \frac{\left(\frac{n(b_g-1)}{b_g(n-1)} \gamma_u + \tau_\star^\nu \frac{(n-b_g)}{b_g(n-1)} \gamma_u^{\max} \right) (1 + \zeta)}{\gamma_\ell} \\ &= \left(\frac{n(b_g-1)}{b_g(n-1)} \mathfrak{q} + \tau_\star^\nu \frac{(n-b_g)}{b_g(n-1)} \mathfrak{q}_{\max} \right) (1 + \zeta), \end{aligned}$$

where $\mathfrak{q}_{\max} := \frac{\gamma_u^{\max}}{\gamma_\ell}$.

5.4 SketchySVRG

For the variance reduced algorithms, we start with the global linear convergence of SketchySVRG (Theorem 24).

Theorem 24 (SketchySVRG convergence) *Instate the hypotheses of Assumption 1-Assumption 2. Run SketchySVRG with fixed learning rate $\eta = \frac{1}{8\mathcal{L}_P}$ and $m = \frac{19}{(1-\zeta)} \bar{\mathfrak{q}}$ inner-iterations. Then*

$$\mathbb{E}[F(\hat{w}^{(s)})] - F(w_\star) \leq \epsilon$$

after $s = 10 \log(1/\epsilon)$ outer-iterations. Hence, the total number of stochastic gradient queries to reach an ϵ -suboptimal point is bounded by

$$10 \left(n + \frac{19b_g}{(1-\zeta)} \bar{\mathfrak{q}} \right) \log \left(\frac{1}{\epsilon} \right).$$

The proof is given in Section 5.8. Theorem 24 shows that SketchySVRG converges linearly at rate controlled by the weighted quadratic regularity ratio \bar{q} . This should be contrasted with vanilla SVRG, whose rate is controlled by the condition number κ . As \bar{q} depends upon the quadratic regularity constants, it may be much smaller than κ for structured functions. Indeed, for quadratic objectives, with batchsize $b_g = \tau_\star^\nu$, $\bar{q} \leq 2(1 + \zeta)$, which is a significant improvement over κ . However, despite the explicit absence of κ in the convergence rate of Theorem 24, the overall guarantee provided by the theorem is pessimistic. The pessimism stems from the convergence rate's dependence upon the global value of \bar{q} , which Proposition 13 shows might be as large as κ^2 in the worst-case, which is a consequence of Theorem 24 failing to reflect that optimization trajectory is *localized*. Indeed, in practice SketchySVRG can take a large stepsize based on the good local model provided by the current preconditioner, and not the global one. Hence, the rate of convergence SketchySVRG achieves in practice is much faster than what Theorem 24 predicts, as it uses a much larger stepsize than the one required by Theorem 24, which is based on a pessimistic global constants. Moreover, the quality of the quadratic model provided by preconditioning improves as the iterates approach the optimum, as \bar{q} approaches a constant close to 1 provided $b_g = \mathcal{O}(\tau_\star^\nu)$. The analysis underlying Theorem 24 treats the entire optimization trajectory as if though it is always far from the optimum, and so is unable to exploit that \bar{q} ameliorates as the iterates near the optimum.

Unfortunately, while it is easy to identify the shortcomings of Theorem 24, it seems difficult to eliminate them, and obtain a theorem showing fast global convergence. Given the discussion in Section 4, this is unsurprising, as under our current hypotheses even Newton's method does not yield faster global convergence than first-order methods in the worst case; it can only guarantee fast local convergence. Thus, further assumptions beyond smoothness and strong convexity are likely required to show an improved global convergence rate. Nevertheless, we show in Theorem 26 that SketchySVRG achieves fast local convergence just like the classic Newton's method, albeit the rate is only linear instead of quadratic, as it uses stochastic gradients. So, SketchySVRG possesses the Newton-like property of fast local convergence, providing an advantage over stochastic first-order methods, which do not enjoy this property.

The exception to the preceding discussion on global convergence, is the case where F is quadratic, in which case the quadratic regularity constants equal 1, so we always obtain fast condition number-free global linear convergence (with appropriate gradient batchsize).

Corollary 25 (SketchySVRG: Fast ridge regression) *Instate the hypotheses of Theorem 24, and suppose F is quadratic. Run SketchySVRG with gradient batchsize $b_g = (1 + \chi^\nu(A)d_{\text{eff}}^\nu(A))$ and $m = 48\frac{1+\zeta}{1-\zeta}$ inner-iterations. Then*

$$\mathbb{E}[F(\hat{w}^{(s)})] - F(w_\star) \leq \epsilon$$

after $s = 10 \log\left(\frac{1}{\epsilon}\right)$ outer-iterations. Hence the total number of stochastic gradient evaluations to reach an ϵ -suboptimal point is bounded by

$$10 \left(n + 48 \frac{1+\zeta}{1-\zeta} [1 + \chi^\nu(A)d_{\text{eff}}^\nu(A)] \right) \log \left(\frac{1}{\epsilon} \right).$$

5.5 SketchySVRG: Fast local convergence

Here we establish local condition number-free linear convergence of SketchySVRG, which is analogous to the fast local convergence of Newton’s method in the full gradient setting. Convergence shall be established in the neighborhood

$$\mathcal{N}_{\varepsilon_0}(w_\star) = \left\{ w \in \mathbb{R}^P : \|w - w_\star\|_{\nabla^2 F(w_\star)} \leq \frac{\varepsilon_0 \nu^{3/2}}{2M} \right\},$$

where M is the uniform Lipschitz constant for each $\nabla^2 F_i$. With the neighborhood of local convergence specified, we have the following theorem.

Theorem 26 *Let $\varepsilon_0 \in (0, 1/6]$. Suppose that each F_i has an M -Lipschitz Hessian, and that $w_0 \in \mathcal{N}_{\varepsilon_0}(w_\star)$. Instate Assumption 1 and Assumption 2 with $\zeta = \varepsilon_0$. Run Algorithm 6 using Option I with $\mathcal{U} = \{0\}$, $m = 6$ inner-iterations, $s = 2 \log(1/\epsilon)$ outer-iterations, $\eta = 1$, and $b_g = \tilde{\mathcal{O}}\left(\tau(\mathcal{N}_{\varepsilon_0}(w_\star)) \log(\frac{1}{\delta})\right)$. Then with probability at least $1 - \delta$,*

$$F(\hat{w}^{(s)}) - F(w_\star) \leq \epsilon.$$

Hence the total number of stochastic gradient queries required to reach an ϵ -suboptimal point is bounded by

$$3 \left[n + 6 \tilde{\mathcal{O}}\left(\tau(\mathcal{N}_{\varepsilon_0}(w_\star)) \log\left(\frac{1}{\delta}\right)\right) \right] \log\left(\frac{1}{\epsilon}\right).$$

The proof is given in Appendix C.7. Theorem 26 shows that once the iterates are close enough to the optimum, SketchySVRG converges linearly with a rate independent of the condition number, provided the gradient batchsize satisfies $b_g = \tilde{\mathcal{O}}(\tau_\star^\nu(\mathcal{N}_{\varepsilon_0}(w_\star)))$. Recall $\tau_\star^\nu(\mathcal{N}_{\varepsilon_0}(w_\star))$ is always smaller than n , and significantly smaller when there are no outliers amongst the individual Hessians $\nabla^2 F_i$. As the data underlying most machine learning problems is typically i.i.d., we generally expect the Hessian dissimilarity to be small due to the statistical similarity of the data.

Previously, Dereziński (2022) established a result analogous to Theorem 26 when P is the SSN preconditioner. However, the result in Dereziński (2022) requires the gradient batchsize to satisfy $b_g = \tilde{\mathcal{O}}(\kappa)$, which can easily exceed n for ill-conditioned problems. Theorem 26 significantly improves this result by reducing the required gradient batchsize to $\tilde{\mathcal{O}}(\tau_\star^\nu(\mathcal{N}_{\varepsilon_0}(w_\star)))$. For GLMs (with some mild hypotheses), we show in Corollary 27 that the required gradient batchsize is as small as $\tilde{\mathcal{O}}(\sqrt{n})$, which is orders of magnitude smaller than n or κ . Hence Theorem 26 holds with small gradient batchsizes, which agrees with practice, as PROMISE methods provide excellent empirical performance without large gradient batchsizes. The key idea for achieving the improvements in Theorem 26 is quadratic regularity, which enables tighter control over the gradient in the inverse Hessian norm with high probability.

To better understand the implications of Theorem 26, we present the following corollary, which addresses the setting where F is a GLM.

Corollary 27 *Instate the hypotheses of Theorem 26 and let F be a bounded GLM. Moreover suppose its data matrix A has polynomially decaying singular values, the regularization*

satisfies $\nu = \mathcal{O}(1/n)$, and the ridge leverage incoherence satisfies $\chi_\star^\nu(\mathcal{N}_{\varepsilon_0}(w_\star)) = \mathcal{O}(1)$.* Run Algorithm 6 with $b_g = \tilde{\mathcal{O}}(\sqrt{n} \log(\frac{1}{\delta}))$. Then with probability at least $1 - \delta$,

$$F(\hat{w}^{(s)}) - F(w_\star) \leq \epsilon$$

after at most

$$3 \left[n + 6\tilde{\mathcal{O}} \left(\sqrt{n} \log \left(\frac{1}{\delta} \right) \right) \right] \log \left(\frac{1}{\epsilon} \right)$$

stochastic gradient queries.

Corollary 27 shows that under mild hypotheses on A and the Hessian, SketchySVRG achieves fast local convergence with a small gradient batchsize of $\tilde{\mathcal{O}}(\sqrt{n})$, for common values of the regularization parameter ν . Hence large gradient batchsizes are unnecessary to see the benefits of preconditioning for solving GLM problems—this is fortunate, since large gradient batchsizes can be prohibitively expensive for large-scale datasets. The prescription of Corollary 27, that the gradient batchsize should satisfy $b_g = \tilde{\mathcal{O}}(\sqrt{n})$, is in harmony with practice, as Table 23 shows the median value of b_g used in our experiments is around \sqrt{n} .

5.6 SketchySAGA

We now turn to the convergence of SketchySAGA. Similar to the analysis in Defazio et al. (2014), we set $b_g = 1$ and use a Lyapunov function argument. The Lyapunov function is

$$T_k := B_k \left(\frac{1}{n} \sum_{i=1}^n F_i(\psi_k^i) - F(w_\star) - \frac{1}{n} \sum_{i=1}^n \langle \nabla F_i(w_\star), \psi_k^i - w_\star \rangle + c \|w_k - w_\star\|_{P_{k-1}}^2 \right), \quad (22)$$

where

$$B_k := \begin{cases} \prod_{i=0}^{k-1} \beta_i & k \geq 1 \\ 1 & k = 0 \end{cases}.$$

The Lyapunov function in (22) is identical to that of Defazio et al. (2014), except $w_k - w_\star$ is measured in the P_{k-1} -norm, and there is a factor of B_k that arises from the changing metric.

To establish linear convergence, we must show that for appropriate learning rate, η , and constant, c , the Lyapunov function contracts in expectation. This is shown in Lemma 57: if we set $\eta = \frac{1}{2(n(1-\zeta)\gamma_\ell^{\min} + \mathcal{L}_P)}$ and $c = \frac{1}{2\eta(1-\eta(1-\zeta)\gamma_\ell^{\min})n}$, then conditioned on the first k iterations,

$$\mathbb{E}_k[T_{k+1}] \leq \left(1 - \frac{1}{\kappa_P} \right) \beta_k T_k.$$

Using the preceding result, we can easily establish the following theorem.

Theorem 28 *Instate the hypotheses of Assumption 1–Assumption 3. Run SketchySAGA with fixed learning rate $\eta = \frac{1}{2(\mathcal{L}_P + n(1-\zeta)\gamma_\ell^{\min})}$ and let $\kappa_P = \frac{\mathcal{L}_P}{(1-\zeta)\gamma_\ell^{\min}}$. Then*

$$\mathbb{E} \|w_k - w_\star\|_{P_k}^2 \leq \left(1 - \frac{1}{2(n + \kappa_P)} \right)^k \frac{nB_P}{\mathcal{L}_P + (1-\zeta)n\gamma_\ell^{\min}} T_0.$$

*. It is not hard to see, that this is equivalent to $\Phi''(Aw_\star)^{1/2}A$ being ridge-leverage incoherent.

Hence,

$$\mathbb{E}\|w_k - w_\star\|_{P_k}^2 \leq \epsilon$$

after $k = 2 \left(n + \tau_\star^\nu \frac{1+\zeta}{1-\zeta} \mathbf{q}_{\max} \right) \log \left(\frac{nB_P T_0}{(\mathcal{L}_P + n(1-\zeta)\gamma_{\ell_{\min}})\epsilon} \right)$ iterations.

The proof is given in Appendix C.8. Theorem 28 proves the linear convergence of SketchySAGA, which allows it to attain high accuracy solutions of (1). Since SketchySAGA does not require full gradient computations, it can achieve linear convergence in a streaming setting, where computing full gradients is prohibitively expensive. This is a unique advantage of SketchySAGA over SketchySVRG and SketchyKatyusha, which require periodic full gradient computations. We also note the dependence upon $\bar{\mathbf{q}}$ is identical to that of SketchySVRG up to constant factors, with the only difference being $\bar{\mathbf{q}} = \mathbf{q}_{\max}$, as we have assumed $b_g = 1$.

As an immediate corollary of Theorem 28, SketchySAGA converges linearly to the optimum, with a condition-number free rate, for ridge regression problems.

Corollary 29 (SketchySAGA: Fast ridge regression) *Instate the hypotheses of Theorem 28 and suppose F is quadratic. Then*

$$\mathbb{E}\|w_k - w_\star\|_{P_k}^2 \leq \epsilon$$

after $k = 2 \left(n + \frac{1+\zeta}{1-\zeta} [1 + \chi^\nu(A)d_{\text{eff}}^\nu(A)] \right) \log \left(\frac{nT_0}{(\tau_\star^\nu + (1-\zeta)n)\epsilon} \right)$ iterations.

5.7 SketchyKatyusha

Last, we come to the convergence of the SketchyKatyusha algorithm. Similar to Allen-Zhu (2018); Kovalev et al. (2020)* and SketchySAGA, the convergence proof for the proof is based on showing the contraction of a Lyapunov function. The Lyapunov function is

$$\Psi_k := \mathcal{W}_k + \mathcal{Y}_k + \mathcal{Z}_k, \quad (23)$$

where

$$\mathcal{W}_k = \frac{1}{\theta_1} (F(w_k) - F(w_\star)), \quad \mathcal{Y}_k = \frac{\theta_2(1 + \theta_1)}{\pi\theta_1} (F(y_k) - F(w_\star)), \quad \mathcal{Z}_k = \frac{\mathcal{L}_P(1 + \eta\sigma)}{2\eta} \|z_k - w_\star\|_{P_k}^2.$$

The definition of the Lyapunov function in (23) differs from that of Kovalev et al. (2020). The difference arises as we work in a preconditioned metric, so $\|\cdot\|$ in Kovalev et al. (2020) is replaced by $\|\cdot\|_{P_k}$. For the same reason, L is replaced by \mathcal{L}_P . Similar to SketchySAGA, the proof establishes that (23) contracts in expectation (at each iteration) for appropriately chosen values of $\pi, \sigma, \theta_1, \theta_2$, and η .

Theorem 30 (SketchyKatyusha convergence) *Instate the hypotheses of Assumption 1-Assumption 3. Run SketchyKatyusha with $\pi = b_g/n$, $\sigma = (1-\zeta)/\bar{\mathbf{q}}$, $\theta_1 = \min \left\{ \sqrt{\frac{(1-\zeta)n}{b_g\bar{\mathbf{q}}}} \theta_2, 1/2 \right\}$, $\theta_2 = 1/2$, and fixed learning rate $\eta = \frac{\theta_2}{(1+\theta_2)\theta_1}$. Then*

$$\mathbb{E}[\Psi_k] \leq \epsilon\Psi_0$$

after $k = \max \{3n/b_g, n/b_g + 2\sqrt{n\bar{\mathbf{q}}/[(1-\zeta)b_g]}\} \log \left(\frac{\epsilon_P}{\epsilon} \right)$ iterations.

*. Although Allen-Zhu (2018) does not explicitly introduce a Lyapunov function, it is implicit in their analysis.

The proof is given in Appendix C.9. Theorem 30 shows SketchyKatyusha converges linearly, just like the other variance-reduced PROMISE methods. The main difference is the convergence rate depends upon $\sqrt{\bar{q}}$ instead of \bar{q} , due to the use of acceleration in the algorithm. When \bar{q} is moderate, (i.e., $\bar{q} = \mathcal{O}(1)$ for ridge regression) it is unclear whether SketchyKatyusha offers any benefit over SketchySVRG and SketchySAGA. Indeed, comparing their respective convergence bounds is insufficient, as they all essentially require $\mathcal{O}(n \log(\frac{1}{\epsilon}))$ gradient computations in this setting. However, our numerical simulations show that acceleration provides an advantage, particularly for ridge regression problems, which tend to be more ill-conditioned than logistic regression problems. This observation motivates our recommendation that SketchyKatyusha be the default PROMISE method for ridge regression when full gradient computations are feasible. Last, we note if F is quadratic, then SketchyKatyusha also enjoys fast global linear convergence; we omit writing down the explicit corollary, as it yields nothing new relative to the ones for SketchySVRG and SketchyKatyusha.

5.8 Convergence proof of SketchySVRG

In this section we prove Theorem 24, which establishes linear convergence of SketchySVRG. The proof is divided into a sequence of helper lemmas; taken together these lemmas allow us to easily establish the theorem.

5.8.1 NOTATION

For clarity in the proof, we shall explicitly keep track of the outer iteration various quantities belong to. Specifically, we write $w_k^{(s)}$ for the k th iterate in outer iteration s , and do the same for other quantities. So, under this convention: $v_k^{(s)}$ denotes the variance reduced gradient at the k th iteration of outer iteration s , and $P_k^{(s)}$ is the current preconditioner at the k th iteration of outer iteration s .

5.8.2 PRELIMINARY LEMMAS

Here we establish the helper lemmas needed to prove Theorem 24. We start by bounding the second moment of the preconditioned variance-reduced stochastic gradients.

Lemma 31 (Variance bound) *Let $v_k^{(s)} = \widehat{\nabla}F(w_k^{(s)}) - \widehat{\nabla}F(\hat{w}^{(s)}) + \nabla F(\hat{w}^{(s)})$ be the variance-reduced stochastic gradient at inner-iteration k in outer-iteration s . Then*

$$\mathbb{E} \|v_k^{(s)}\|_{(P_k^{(s)})^{-1}}^2 \leq 4\mathcal{L}_P [F(w_k^{(s)}) - F(w_\star) + F(\hat{w}^{(s)}) - F(w_\star)].$$

Proof We have

$$\begin{aligned}
 \mathbb{E}\|v_k^{(s)}\|_{(P_k^{(s)})^{-1}}^2 &\stackrel{(1)}{\leq} 2\mathbb{E}\|\widehat{\nabla}F(w_k^{(s)}) - \widehat{\nabla}F(w_\star)\|_{(P_k^{(s)})^{-1}}^2 + 2\mathbb{E}\|[\widehat{\nabla}F(\hat{w}^{(s)}) - \widehat{\nabla}F(w_\star)] - \nabla F(\hat{w}^{(s)})\|_{(P_k^{(s)})^{-1}}^2 \\
 &= 2\mathbb{E}\|\widehat{\nabla}F(w_k^{(s)}) - \widehat{\nabla}F(w_\star)\|_{(P_k^{(s)})^{-1}}^2 \\
 &\quad + 2\mathbb{E}\|[\widehat{\nabla}F(\hat{w}^{(s)}) - \widehat{\nabla}F(w_\star)] - \mathbb{E}[\widehat{\nabla}F(\hat{w}^{(s)}) - \widehat{\nabla}F(w_\star)]\|_{(P_k^{(s)})^{-1}}^2 \\
 &\stackrel{(2)}{\leq} 2\mathbb{E}\|\widehat{\nabla}F(w_k^{(s)}) - \widehat{\nabla}F(w_\star)\|_{(P_k^{(s)})^{-1}}^2 + 2\mathbb{E}\|\widehat{\nabla}F(\hat{w}^{(s)}) - \widehat{\nabla}F(w_\star)\|_{(P_k^{(s)})^{-1}}^2 \\
 &\stackrel{(3)}{\leq} 4\mathcal{L}_P[F(w_k^{(s)}) - F(w_\star) + F(\hat{w}^{(s)}) - F(w_\star)].
 \end{aligned}$$

Here (1) invokes Lemma 35, (2) uses Lemma 34, and (3) applies Proposition 22 with $w' = w_\star$ twice. \blacksquare

Next, we have the following one-step relation.

Lemma 32 (One-step bound) *Suppose we are in outer-iteration s at inner-iteration k and $w_{k+1}^{(s)} = w_k^{(s)} - \eta(P_k^{(s)})^{-1}v_k^{(s)}$. Then*

$$\mathbb{E}_k\|w_{k+1}^{(s)} - w_\star\|_{P_k^{(s)}}^2 \leq \|w_k^{(s)} - w_\star\|_{P_k^{(s)}}^2 + 2\eta(2\eta\mathcal{L}_P - 1)[F(w_k^{(s)}) - F(w_\star)] + 4\eta^2\mathcal{L}_P[F(\hat{w}^{(s-1)}) - F(w_\star)].$$

Proof Simply use the definition of the update, expand the square, and invoke Lemma 31. \blacksquare

We now come to the key lemma for establishing convergence, which shows a contraction of suboptimality between consecutive outer-iterations.

Lemma 33 (Outer-iteration contraction) *Suppose we are in outer-iteration $s+1$. Then*

$$\mathbb{E}_{0:s}[F(\hat{w}^{(s+1)})] - F(w_\star) \leq \left[\frac{1}{(1-\zeta)\gamma\eta(1-2\eta\mathcal{L}_P)m} + \frac{2\eta\mathcal{L}_P}{1-2\eta\mathcal{L}_P} \right] \left(F(\hat{w}^{(s)}) - F(w_\star) \right), \tag{24}$$

where $\mathbb{E}_{0:s}$ denotes the expectation conditioned on outer-iterations 0 through s .

Proof Summing the bound in Lemma 32 over $k = 0, \dots, m-1$, we reach

$$\begin{aligned}
 \sum_{k=0}^{m-1} \mathbb{E}_k\|w_{k+1}^{(s)} - w_\star\|_{P_k^{(s)}}^2 &\leq \sum_{k=0}^{m-1} \|w_k^{(s)} - w_\star\|_{P_k^{(s)}}^2 + 2\eta m(2\eta\mathcal{L}_P - 1) \frac{1}{m} \sum_{k=0}^{m-1} [F(w_k^{(s)}) - F(w_\star)] \\
 &\quad + 4m\eta^2\mathcal{L}_P[F(\hat{w}^{(s)}) - F(w_\star)].
 \end{aligned}$$

Now, taking the expectation over all the inner-iterations conditioned on outer-iterations 0 through s , we find

$$\begin{aligned}
 \mathbb{E}_{0:s}\|w_m^{(s)} - w_\star\|_{P_k^{(s)}}^2 &\leq \|\hat{w}^{(s)} - w_\star\|_{P_0^{(s)}}^2 + 2\eta m(2\eta\mathcal{L}_P - 1) \left(\mathbb{E}_{0:s} [F(\hat{w}^{(s+1)})] - F(w_\star) \right) \\
 &\quad + 4m\eta^2\mathcal{L}_P[F(\hat{w}^{(s)}) - F(w_\star)].
 \end{aligned}$$

Rearranging and invoking quadratic regularity of f , we reach

$$\begin{aligned} \mathbb{E}_{0:s} \|w_m^{(s)} - w_\star\|_{P_k^{(s)}}^2 + 2\eta m (1 - 2\eta\mathcal{L}_P) \left(\mathbb{E}_{0:s} [F(\hat{w}^{(s+1)})] - F(w_\star) \right) \\ \leq 2 \left(\frac{1}{(1-\zeta)\gamma_\ell} + 2m\eta^2\mathcal{L}_P \right) [F(\hat{w}^{(s)}) - F(w_\star)]. \end{aligned}$$

Hence we conclude

$$\mathbb{E}_{0:s} [F(\hat{w}^{(s+1)})] - F(w_\star) \leq \left[\frac{1}{(1-\zeta)\gamma_\ell\eta(1-2\eta\mathcal{L}_P)m} + \frac{2\eta\mathcal{L}_P}{1-2\eta\mathcal{L}_P} \right] (F(\hat{w}^{(s)}) - F(w_\star)),$$

as desired. \blacksquare

5.8.3 SKETCHYSVRG CONVERGENCE: PROOF OF THEOREM 24

Proof From Lemma 33 we have,

$$\mathbb{E}_{0:s-1} [F(\hat{w}^{(s)})] - F(w_\star) \leq \left[\frac{1}{(1-\zeta)\gamma_\ell\eta(1-2\eta\mathcal{L}_P)m} + \frac{2\eta\mathcal{L}_P}{1-2\eta\mathcal{L}_P} \right] (F(\hat{w}^{(s-1)}) - F(w_\star)).$$

Setting $\eta = \frac{1}{8\mathcal{L}_P}$ and $m = \frac{19}{1-\zeta}\bar{q}$, we obtain

$$\mathbb{E}_{0:s-1} [F(\hat{w}^{(s)})] - F(w_\star) \leq \frac{9}{10} (F(\hat{w}^{(s-1)}) - F(w_\star)).$$

Taking the total expectation over all outer-iterations, and recursing, we reach

$$\mathbb{E}[F(\hat{w}^{(s)})] - F(w_\star) \leq \left(\frac{9}{10} \right)^s (F(w_0) - F(w_\star)).$$

Hence after $s = 10 \log \left(\frac{F(w_0) - F(w_\star)}{\varepsilon} \right)$ outer-iterations we have

$$\mathbb{E}[F(\hat{w}^{(s)})] - F(w_\star) \leq \varepsilon. \quad \blacksquare$$

6. Numerical experiments

In this section, we provide four sets of experiments that demonstrate the effectiveness of the PROMISE methods in solving l^2 -regularized least squares (i.e., ridge) and logistic regression problems. We also provide studies that examine the sensitivity of our methods to hyperparameters and investigate the quadratic regularity ratio. The results are presented as follows:

- Performance experiments (Section 6.1): We compare PROMISE methods to SVRG, b-nice SAGA (henceforth referred to as SAGA), Loopless Katyusha (L-Katyusha), and stochastic L-BFGS (SLBFGS), whose learning rates are tuned. We find that our methods outperform the competition on a testbed of 51 medium-sized least squares and logistic regression problems.

- Suboptimality experiments (Section 6.2): We show that PROMISE methods achieve global linear convergence on several least squares and logistic regression problems, which matches the global linear convergence guarantees in Section 5. Furthermore, our methods converge faster than the competition.
- Showcase experiments (Section 6.3): We evaluate PROMISE methods against the competition on the url, yelp, and acsincome datasets, which originate in real-world applications and lead to large-scale problems. We again find that our methods outperform the competition.
- Streaming experiments (Section 6.4): We test PROMISE methods on performing logistic regression with large-scale transformations of the HIGGS and SUSY datasets. These transformed datasets are so large that they do not fit in the memory of most computers, putting these experiments in a streaming setting where the computation of full gradients is prohibitive. Our methods continue to outperform the competition.
- Sensitivity study (Section 6.5): We investigate how the choice of rank r and update frequency u impacts the performance of PROMISE methods. We find that the impact of these hyperparameters depends on the spectral properties of the data.
- Regularity study (Section 6.6): We demonstrate that the quadratic regularity ratio, γ_u/γ_ℓ , is well-behaved over the optimization trajectory, which provides empirical support for our claims in Section 6.6.

The experiments in Sections 6.1 to 6.4 and 6.6 run PROMISE methods with the default hyperparameters given in Section 3. Throughout the experiments, we set the l^2 -regularization parameter $\nu = 10^{-2}/n_{\text{tr}}$, where n_{tr} is the number of samples in the training set. Setting ν in this way typically leads to an ill-conditioned problem, which can be challenging to solve for existing stochastic gradient methods. The results are qualitatively similar for larger values of ν ; when $\nu = 10^{-1}/n_{\text{tr}}$, PROMISE methods still outperform the competition on the performance experiments (Appendix D.3.2). All preconditioners use the default values of r and ρ in Table 6, unless stated otherwise. Additional details can be found in Appendix D and the code used to run our experiments can be found at <https://github.com/udellgroup/PROMISE>.

6.1 Performance experiments

Our first set of experiments compares the performance of SketchySVRG, SketchySAGA, and SketchyKatyusha, with their *default* hyperparameters, to SVRG, SAGA, L-Katyusha, and SLBFGS, with *tuned* hyperparameters, on solving ridge and l^2 -regularized logistic regression problems. These experiments therefore *understate* the performance improvement that can be expected by using PROMISE methods. Moreover, we modify SLBFGS to compute the preconditioner once per epoch rather than at every iteration for a fair comparison.

SAGA/SketchySAGA require one full pass through the data per epoch, while SVRG/L-Katyusha/SLBFGS/SketchySVRG/SketchyKatyusha use two full passes through the data per epoch since they compute full gradients^{*}. By using the number of full data passes

^{*}. L-Katyusha and SketchyKatyusha compute full gradients with random probability, and our hyperparameter settings result in one full gradient computation per epoch, in expectation.

we (roughly) equate the computation required for computing gradients, making for a fair comparison. We compute the minimum $F(w^*)$ for all ridge and logistic regression problems via scikit-learn (Pedregosa et al., 2011). We run neither SketchySGD nor SGD because these algorithms do not converge linearly and hence underperform the others (Appendix D.4.1).

Our primary metrics for comparing the performance of these methods are the wall-clock time and number of full data passes to reach suboptimality within 10^{-4} of the minimum, $F(w^*)$. We consider a problem to have been “solved” if this suboptimality condition is met over the course of optimization. Each optimizer is run until either this suboptimality condition is met, or 200 full data passes (100 epochs for SVRG, L-Katyusha, SLBFGS, SketchySVRG, and SketchyKatyusha, 200 epochs for SAGA and SketchySAGA) are completed.

6.1.1 RIDGE REGRESSION

We solve ridge regression problems of the form

$$\text{minimize}_{w \in \mathbb{R}^p} \frac{1}{n_{\text{tr}}} \sum_{i=1}^{n_{\text{tr}}} \frac{1}{2} (a_i^T w - b_i)^2 + \frac{\nu}{2} \|w\|_2^2,$$

where $a_i \in \mathbb{R}^p$ is a datapoint, $b_i \in \mathbb{R}$ is a label, and $\nu > 0$ is the regularization parameter.

Our experiments in this setting are performed on a testbed of 17 datasets from OpenML (Vanschoren et al., 2013) and LIBSVM (Chang and Lin, 2011). We apply random features (Rahimi and Recht, 2007; Mei and Montanari, 2022) to most, but not all, datasets; further details regarding preprocessing are provided in Appendix D.3.1.

The results of these experiments appear in Figs. 2 and 3. Fig. 2 shows the proportion of problems solved by both our methods and the competitor methods as a function of wall-clock time and full data passes. When combined with any one of the SSN, NYSSN, SASSN-C, and SASSN-R preconditioners, SketchySVRG, SketchySAGA, and SketchyKatyusha uniformly outperform all of the competitor methods. Furthermore, the performance of SketchySVRG, SketchySAGA, and SketchyKatyusha degrades considerably when combined with the DIAGSSN preconditioner (Fig. 24 in Appendix D.3.4), demonstrating the value of a low-rank approximation to the subsampled Hessian over a diagonal approximation.

Fig. 3 shows the average ranking of all the optimization methods over the course of optimization. To compute these rankings, we rank each optimizer by the number of problems solved at every 10 timesteps (either 10 seconds or 10 full data passes), and then compute the mean of these ranks over the entire optimization trajectory. We observe that the SSN and NYSSN preconditioners tend to outperform the other preconditioners.

Overall, SketchyKatyusha and SketchySVRG perform slightly better than SketchySAGA in this setting; this finding is in line with our recommendation in Section 3.6 of using SketchyKatyusha for ridge regression.

6.1.2 l^2 -REGULARIZED LOGISTIC REGRESSION

We solve l^2 -regularized logistic regression problems of the form

$$\text{minimize}_{w \in \mathbb{R}^p} \frac{1}{n_{\text{tr}}} \sum_{i=1}^{n_{\text{tr}}} \log(1 + \exp(b_i a_i^T w)) + \frac{\nu}{2} \|w\|_2^2,$$

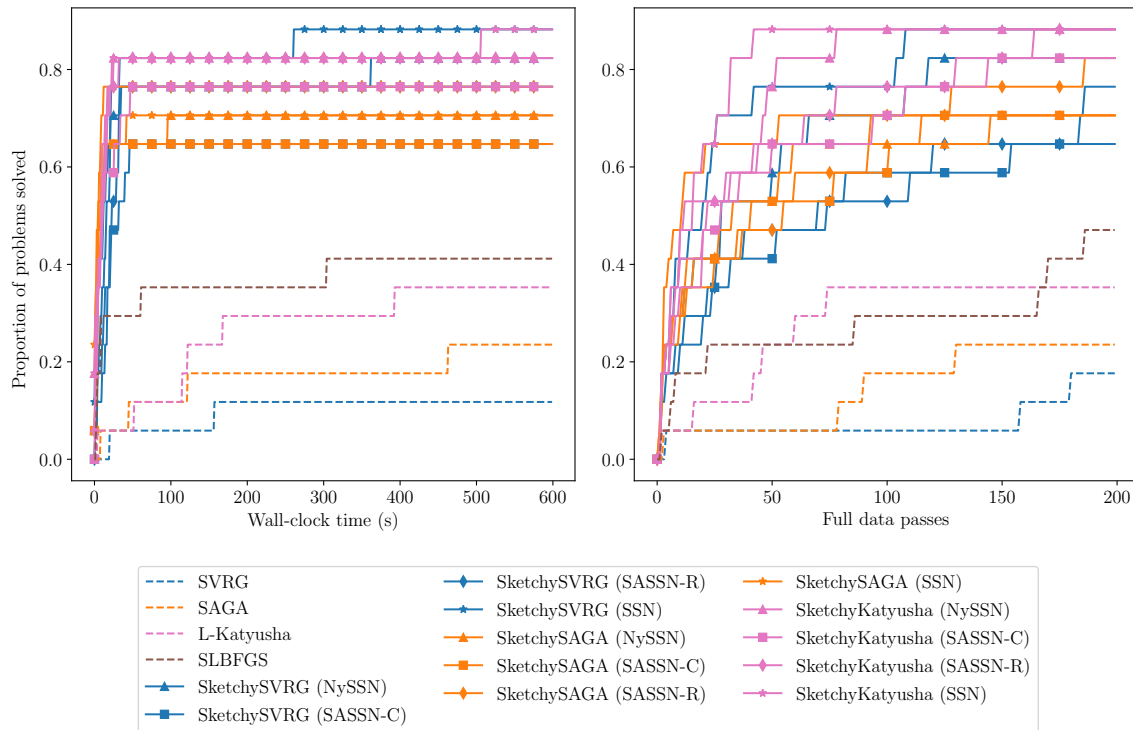


Figure 2: Proportion of ridge regression problems solved by our proposed methods and competitor methods.

where $a_i \in \mathbb{R}^p$ is a datapoint, $b_i \in \{-1, 1\}$ is a label, and $\nu > 0$ is the regularization parameter.

Our experiments in this setting are performed on a testbed of 34 datasets from LIBSVM. We apply random features to a few of the datasets; further details regarding preprocessing are provided in Appendix D.3.1.

The results of these experiments appear in Figs. 4 and 5. Fig. 4 shows the proportion of problems solved by both our methods and the competitor methods as a function of wall-clock time and full data passes. When combined with any one of the SSN, NySSN, SASSN-C, and SASSN-R preconditioners, SketchySVRG, SketchySAGA, and SketchyKatyusha uniformly outperform SVRG, SAGA and L-Katyusha. In addition, SketchySAGA and SketchyKatyusha outperform SLBFGS, which also employs preconditioning. Just like in ridge regression, the DIAGSSN preconditioner leads to degraded performance (Fig. 25 in Appendix D.3.4), which further demonstrates the value of low-rank approximations to the subsampled Hessian.

Fig. 5 shows the average ranking of all the optimization methods over the course of optimization. We calculate these rankings using the same approach as in ridge regression. The SSN preconditioner outperforms all other preconditioners, while NySSN, SASSN-C, and SASSN-R display similar performance to one another.

We compare SSN and NySSN on both sparse and dense datasets in Appendix D.3.3; we find that SSN tends to outperform NySSN on sparse problems while NySSN slightly out-

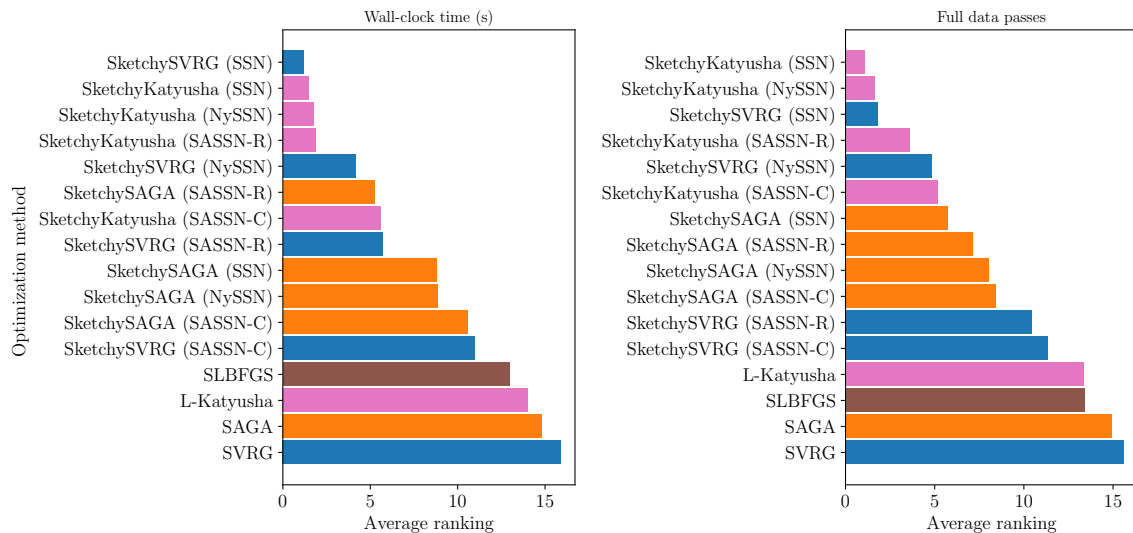


Figure 3: Average ranking of each method by number of ridge regression problems solved with respect to wall-clock time (left) and full gradient computations (right).

performs SSN on dense problems, which is in line with the preconditioner recommendations in Table 7.

Overall, SketchySAGA and SketchyKatyusha perform much better than SketchySVRG in this setting; this finding is in line with our recommendation in Section 3.6 of using SketchyKatyusha (assuming we can compute full gradients) or SketchySAGA for logistic regression.

6.2 Suboptimality experiments

We examine the objective suboptimality (with respect to the lowest attained training loss for all methods) for SketchySVRG, SketchySAGA, and SketchyKatyusha, with their *default* hyperparameters, and the competitor methods, with *tuned* hyperparameters. For simplicity, we only show PROMISE methods with the NySSN and SSN preconditioner. Each optimizer is run until 200 full data passes (100 epochs for SVRG, L-Katyusha, SLBFGS, SketchySVRG, and SketchyKatyusha, 200 epochs for SAGA and SketchySAGA) are completed. We provide additional details and a comparison with SketchySGD in Appendix D.4.

Figs. 6 and 7 display objective suboptimality (with respect to the lowest attained training loss) for selected datasets on ridge and l^2 -regularized logistic regression. The objective suboptimality for PROMISE methods decreases at a linear rate for both ridge and logistic regression, which matches the theoretical convergence guarantees in Section 5. On ridge regression, PROMISE methods uniformly outperform the competition—excitingly, PROMISE methods reach machine precision on yolanda! On logistic regression, PROMISE methods generally outperform SVRG, SAGA, and L-Katyusha. Interestingly, SLBFGS outperforms PROMISE methods on ijcnn1. However, SLBFGS can be unstable; for example, SLBFGS initially outperforms PROMISE methods on SUSY, but the training loss suddenly spikes and then diverges.

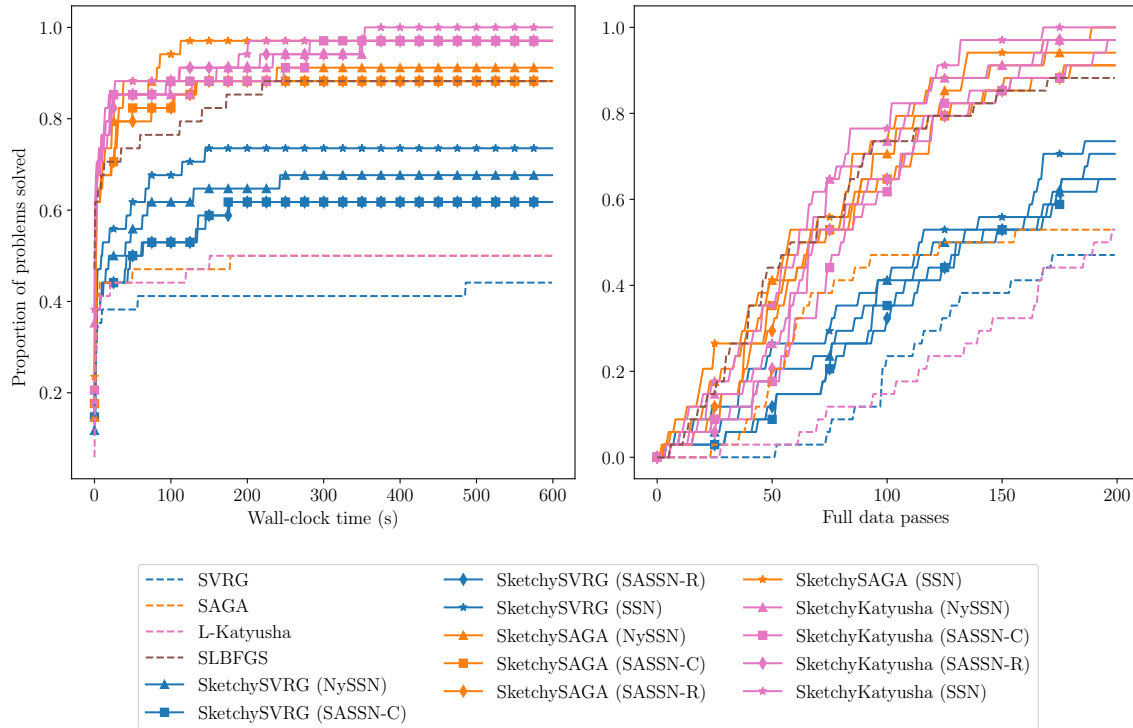


Figure 4: Proportion of l^2 -regularized logistic regression problems solved by our proposed methods and competitor methods.

6.3 Showcase experiments

Our second set of experiments compares the performance of SketchySVRG, SketchySAGA, and SketchyKatyusha, with their *default* hyperparameters, to SVRG, SAGA, L-Katyusha, and SLBFGS with both default and tuned hyperparameters on the url, yelp, and acsincome datasets. All three datasets originate in real-world applications: the url dataset is used to train a l^2 -regularized logistic regression classifier that detects malicious websites using features derived from URLs, the yelp dataset is used to train a l^2 -regularized logistic regression classifier that predicts sentiment from user reviews, and the acsincome dataset is used to train a ridge regression classifier that predicts income given demographic information such as age, employment, and education. After preprocessing, all three of these datasets have $n_{\text{tr}} > 10^6$ training examples, while url and yelp have $p > 10^6$ features, putting all three of these datasets in the big-data regime. Additional information regarding these datasets is provided in Appendix D.5.

We provide two sets of comparisons: the first set compares our methods to SVRG, SAGA, and L-Katyusha with their *default* hyperparameters, while the second set compares our methods to SVRG, SAGA, L-Katyusha, and SLBFGS with their *tuned* hyperparameters. We run each optimizer with a fixed time budget: 1 hour for url and yelp, and 2 hours for acsincome.

The first set of comparisons is presented in Figs. 8 and 9. Fig. 8 shows the training loss for our methods and the competitor methods (with default hyperparameters) as a function

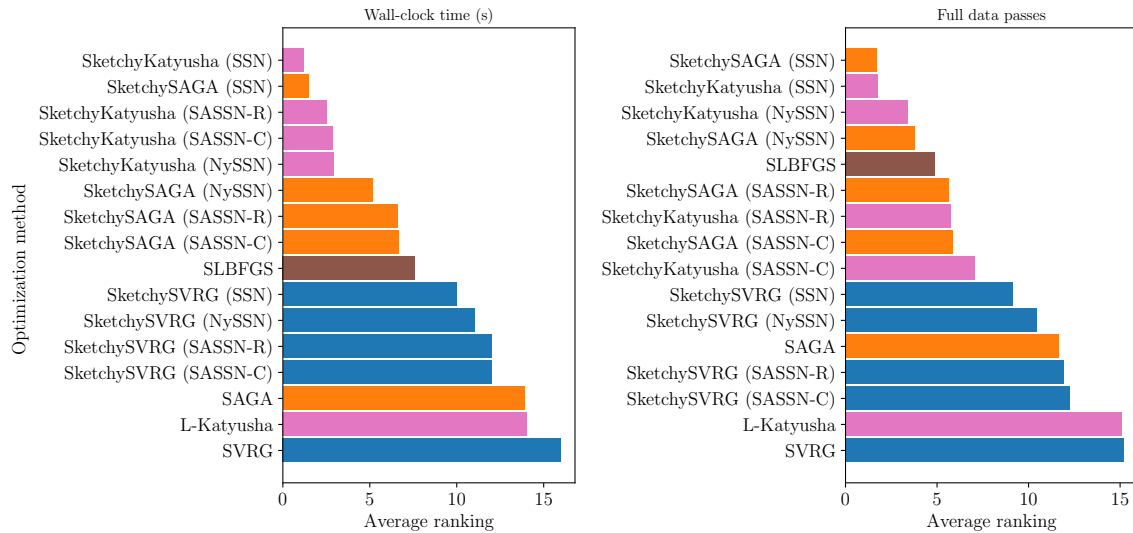


Figure 5: Average ranking of each method by number of l^2 -regularized logistic regression problems solved with respect to wall-clock time (left) and full gradient computations (right).

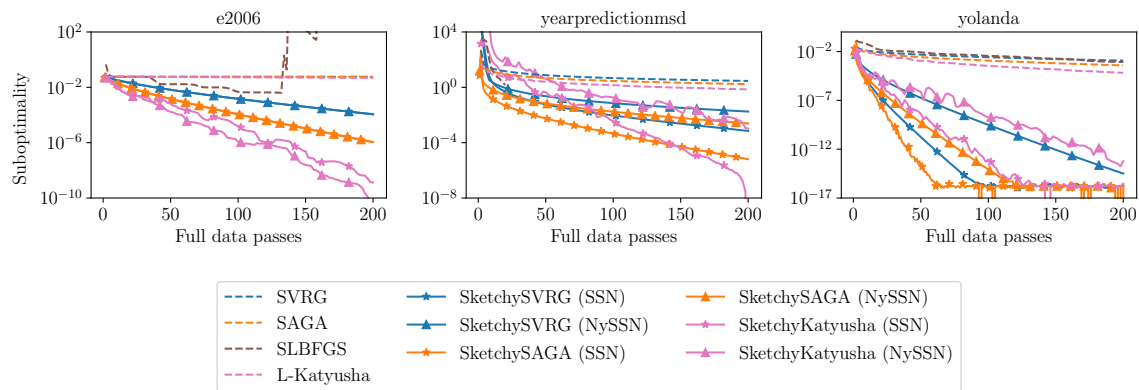


Figure 6: Suboptimality comparisons between our proposed methods and tuned competitor methods for selected datasets on ridge regression.

of wall-clock time. When combined with either of the SSN or NySSN preconditioners, SketchySVRG, SketchySAGA, and SketchyKatyusha uniformly outperform the competitor methods on their default hyperparameters. Fig. 9 compares the same optimizers, but on test classification error (url, yelp) and test loss (acsincome). We observe our methods generalize better to test data than the competitor methods while running much faster.

The second set of comparisons is presented in Figs. 10 and 11. Fig. 10 shows the training loss for our methods and the competitor methods (with tuned hyperparameters) a function of wall-clock time; Fig. 11 shows test metrics. PROMISE methods outperform the competition on url and acsincome and perform comparably on yelp. PROMISE methods are also substantially more stable along the optimization trajectory, whereas the competition often suffer sudden large increases in the loss. Moreover, recall that the performance of the

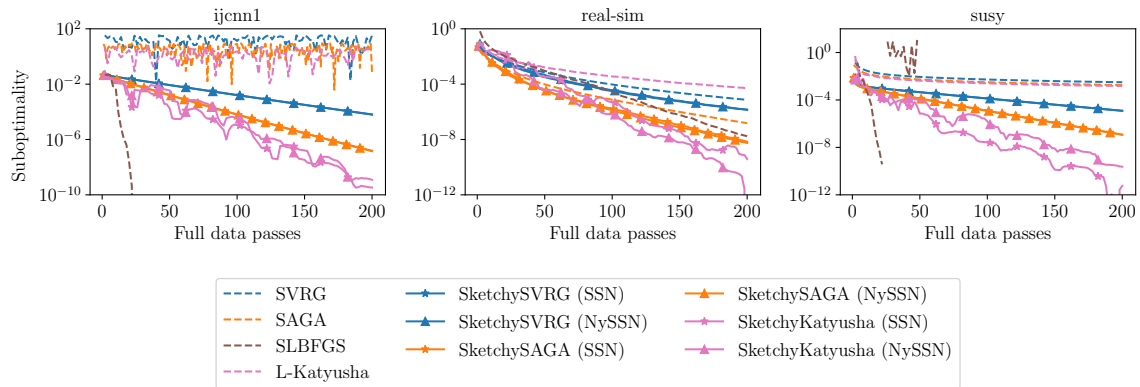


Figure 7: Suboptimality comparisons between our proposed methods and tuned competitor methods for selected datasets on l^2 -regularized logistic regression.

competitor methods is only possible after hyperparameter tuning, which is quite expensive for datasets of this size, whereas PROMISE methods still obtain good performance with default hyperparameters.

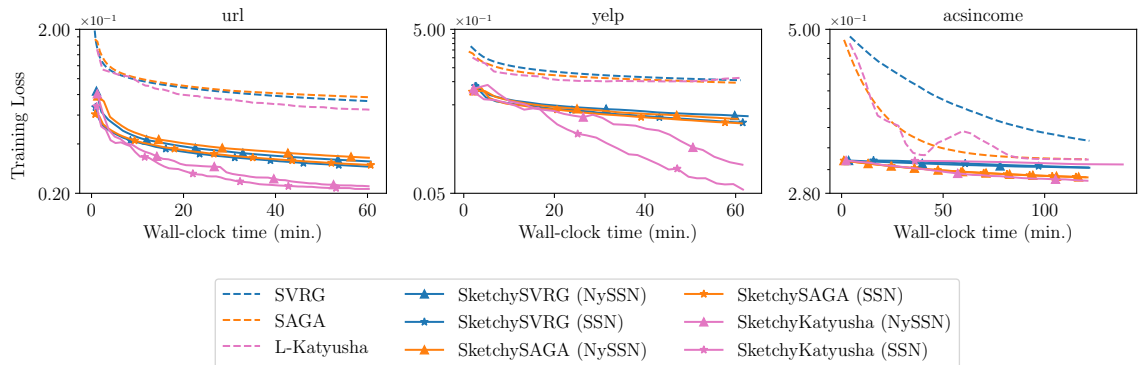


Figure 8: Comparisons to competitor methods on training loss with default learning rates (SVRG, SAGA) and smoothness parameters (L-Katyusha).

6.4 Streaming experiments

We apply random features to the HIGGS and SUSY datasets to obtain transformed datasets with sizes 840 and 720 GB respectively (see Appendix D.6.1 for more details). These transformed datasets are much larger than the hard drive and RAM capacity of most computers. We solve a l^2 -regularized logistic regression problem on each transformed dataset. To perform optimization, we load the original dataset in memory and at each iteration, form a minibatch of the transformed dataset by applying random features to a minibatch of the data. In this setting, computing a full gradient of the objective is computationally prohibitive, so we exclude SVRG, L-Katyusha, SLBFGS, SketchySVRG, and SketchyKatyusha. We compare our methods to SGD and SAGA with their *tuned* hyperparameters (a comparison

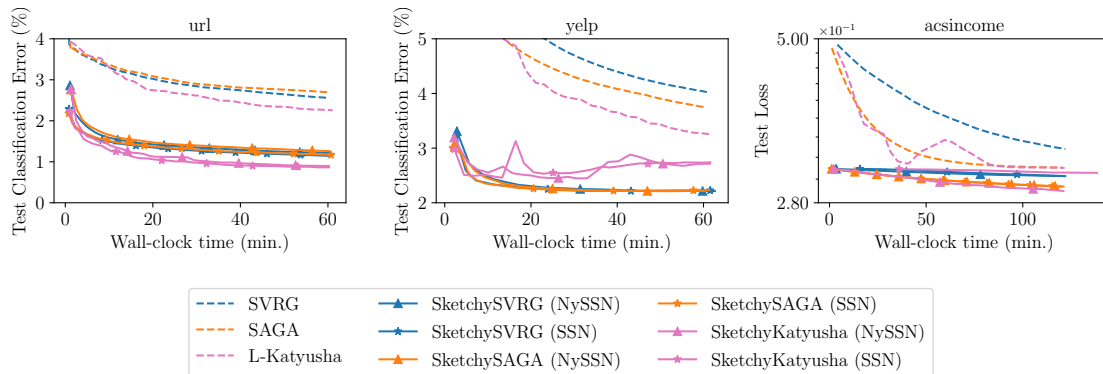


Figure 9: Comparisons to competitor methods on test metrics with default learning rates (SVRG, SAGA) and smoothness parameters (L-Katyusha).

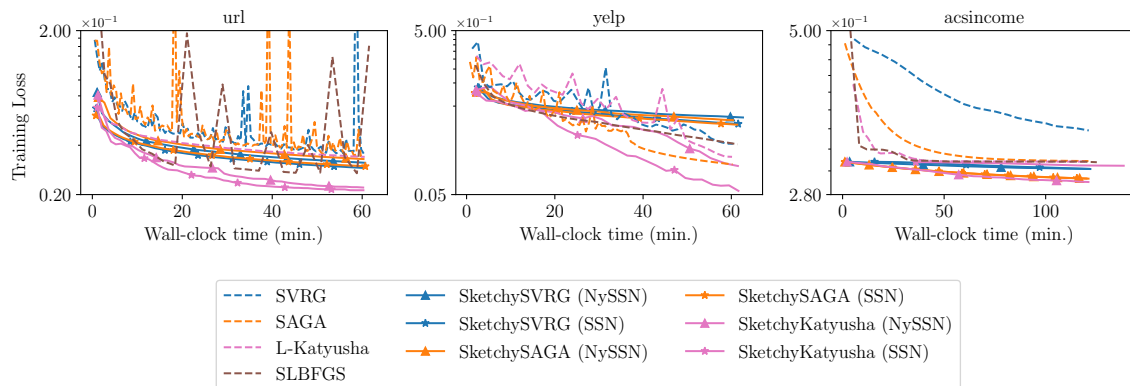


Figure 10: Comparisons to competitor methods on training loss with tuned learning rates (SGD, SVRG, SAGA, SLBFGS) and smoothness parameters (L-Katyusha).

to SAGA with its *default* hyperparameter is presented in Appendix D.6.2). All optimization methods are run for 10 epochs.

The comparison to tuned versions of SGD and SAGA is presented in Figs. 12 and 13. On these problems, PROMISE methods (SketchySGD and SketchySAGA) perform well while the competitors (SGD and SAGA) struggle to make any progress. The NYSSN preconditioner outperforms the SSN preconditioner on these large, dense problems: it achieves similar test loss at each iteration but is faster on wall-clock time. We only plot test loss, as computing the training loss suffers from the same computational issues as computing a full gradient. The plots with respect to wall-clock time only show the time taken in optimization; they do not include the time taken in repeatedly applying the random features transformation.

6.5 Sensitivity study

We investigate the sensitivity of SketchySAGA, with the NYSSN preconditioner, to the rank hyperparameter r (Section 6.5.1) and update frequency hyperparameter u (Section 6.5.2).

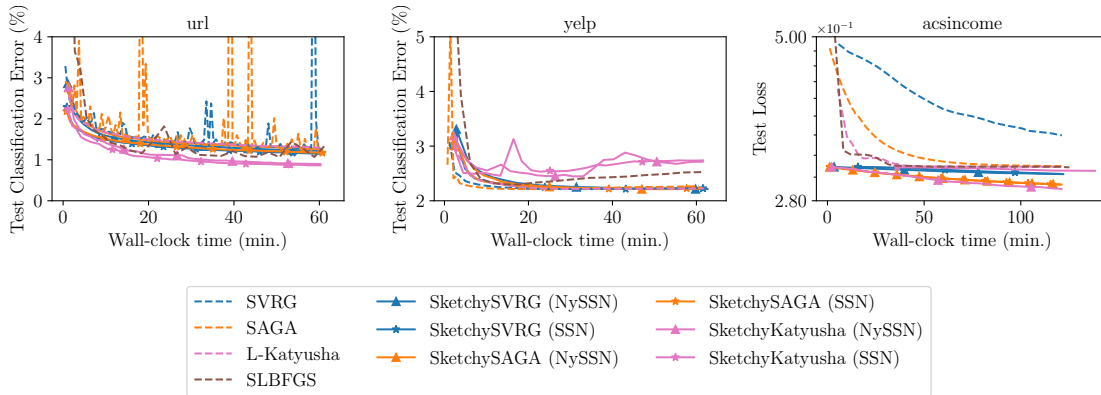


Figure 11: Comparisons to competitor methods on test metrics with tuned learning rates (SGD, SVRG, SAGA, SLBFGS) and smoothness parameters (L-Katyusha).

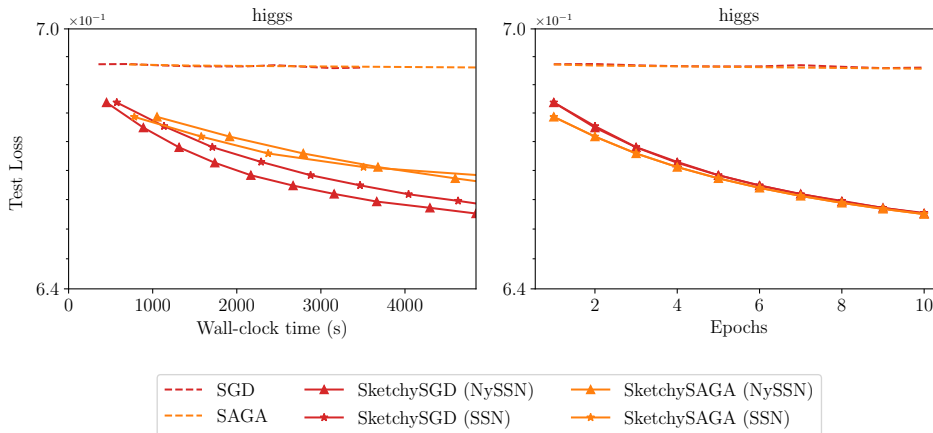


Figure 12: Comparison between SGD and SAGA with tuned learning rates, SketchySGD, and SketchySAGA on HIGGS.

In the first set of sensitivity experiments, we select ranks $r \in \{1, 2, 5, 10, 20, 50\}$ while holding the update frequency fixed at $u = \left\lceil \frac{n_{tr}}{b_g} \right\rceil$ (1 epoch)*. In the second set of sensitivity experiments, we select update frequencies $u \in \left\{ 0.5 \left\lceil \frac{n_{tr}}{b_g} \right\rceil, \left\lceil \frac{n_{tr}}{b_g} \right\rceil, 2 \left\lceil \frac{n_{tr}}{b_g} \right\rceil, 5 \left\lceil \frac{n_{tr}}{b_g} \right\rceil, \infty \right\}$, while holding the rank fixed at $r = 10$. We use the E2006-tfidf, YearPredictionMSD, yolanda, ijcnn1, real-sim, and SUSY datasets, with the same preprocessing as in Appendix D.3. Each curve is the suboptimality (measured with respect to the best attained value) of the median training loss corresponding to a given (r, u) pair across several random seeds (10 for E2006-tfidf, ijcnn1, and real-sim, 5 for YearPredictionMSD and yolanda, and 3 for SUSY). We perform 80 full data passes, which is equivalent to 80 epochs of SketchySGD/SketchySAGA or 40 epochs of SketchySVRG/SketchyKatyusha.

*. If we set $u = \infty$ in ridge regression, which fixes the preconditioner throughout the run of SketchySAGA, the potential gain from a larger rank r may not be realized due to a poor initial Hessian approximation.

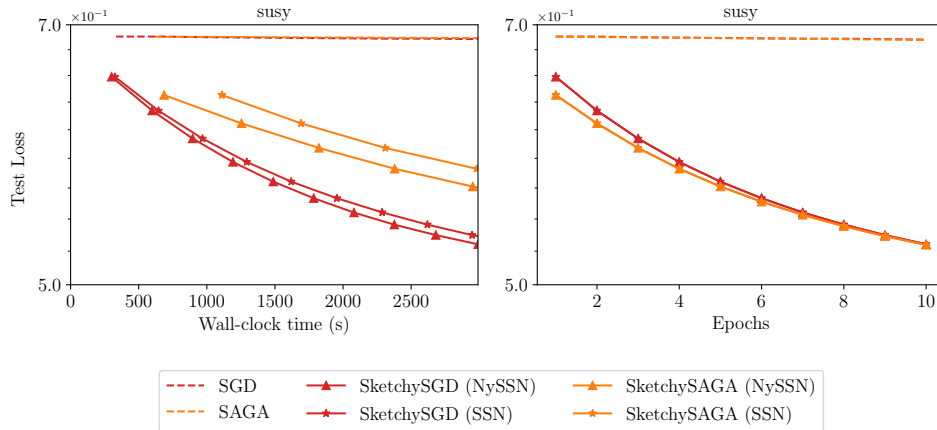


Figure 13: Comparison between SGD and SAGA with tuned learning rates, SketchySGD, and SketchySAGA on SUSY.

6.5.1 EFFECTS OF CHANGING THE RANK

Looking at Fig. 14, we see two distinct patterns: either increasing the rank has no noticeable impact on performance (E2006-tfidf, real-sim), or increasing the rank leads to faster convergence (YearPredictionMSD). We empirically observe that these patterns are related to the spectrum of each dataset (Fig. 15). For example, the spectrum of E2006-tfidf is highly concentrated in the first singular value and decays rapidly, and increasing the rank does not improve convergence. On the other hand, the spectrum of YearPredictionMSD is not as concentrated in the first singular value, but still decays rapidly, so convergence steadily improves as we increase the rank from $r = 1$ to $r = 50$. The spectrum of real-sim decays quite slowly in comparison to E2006-tfidf or YearPredictionMSD, so increasing the rank up to 50 does not capture enough of the spectrum to improve convergence. Rank sensitivity plots for yolanda, ijcnn1, and SUSY appear in Appendix D.8.1.

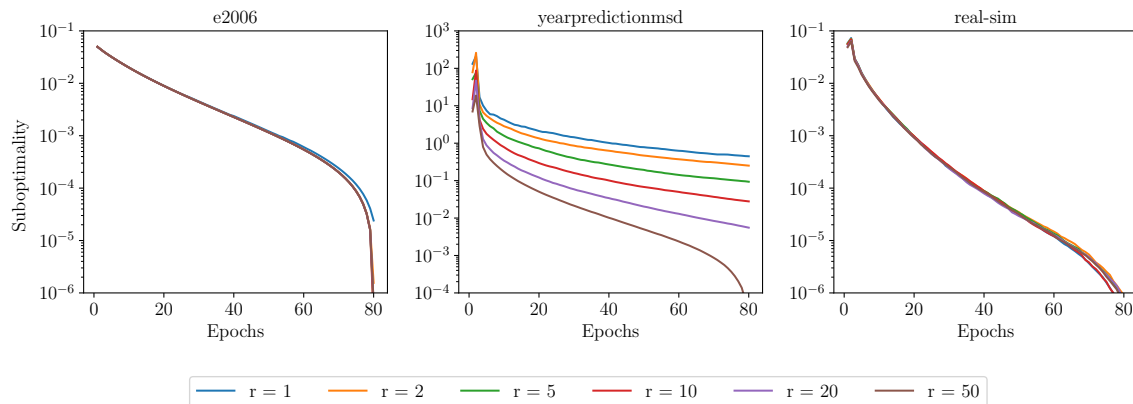


Figure 14: Sensitivity of SketchySAGA to rank r .

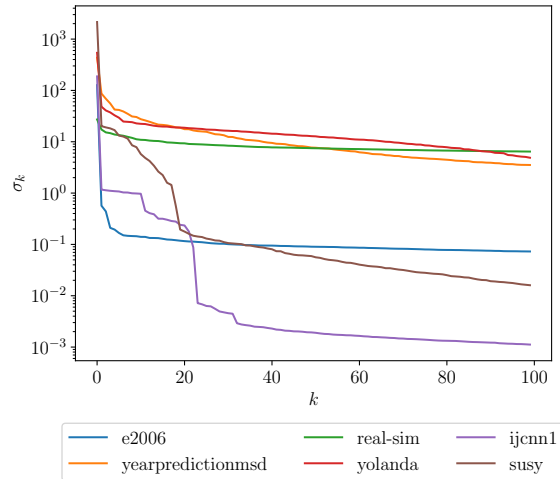
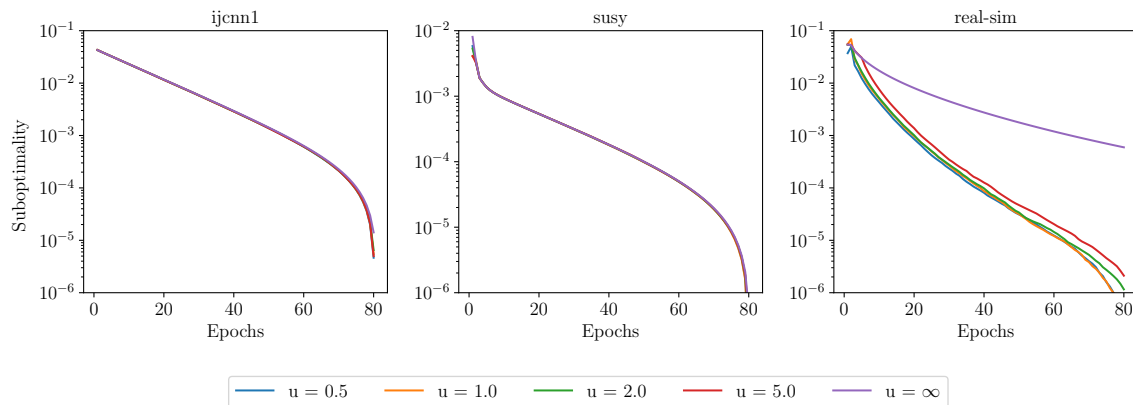


Figure 15: Top 100 singular values of datasets after preprocessing.

6.5.2 EFFECTS OF CHANGING THE UPDATE FREQUENCY

In this section, we display results only for logistic regression (Fig. 16), since there is no benefit to updating the preconditioner for a quadratic problem such as ridge regression (Appendix D.8.1): the Hessian in ridge regression is constant for all $w \in \mathbb{R}^p$. The impact of the update frequency depends on the spectrum of each dataset. The spectra of `ijcn1` and `susy` are highly concentrated in the top $r = 10$ singular values and decay rapidly (Fig. 15). Interestingly, it seems that for such problems the initial preconditioner approximates the curvature of the loss well throughout the optimization trajectory. On the other hand, the spectrum of `real-sim` decays quite slowly, so the initial preconditioner does not capture most of the curvature information in the Hessian. For `real-sim`, we find it is beneficial to update the preconditioner. These updates can be very infrequent: an update frequency of 5 epochs yields nearly identical performance to updating every 0.5 epochs.


 Figure 16: Sensitivity of SketchySAGA to update frequency u .

6.6 Regularity study: Why PROMISE methods exhibit fast global convergence

The theory in Section 5 shows that the PROMISE algorithms converge linearly, with the rate of convergence being controlled by the weighted quadratic regularity ratio \bar{q} . While it is encouraging that the convergence rate is no longer controlled by the condition number, the dependence upon \bar{q} is over all of \mathbb{R}^p , which could make this quantity quite large. Indeed, Proposition 13 implies in the worst case it may be as large as κ^2 , which is at odds with the empirical results in Sections 6.1 to 6.4. Here we provide an empirical argument that partly explains why PROMISE methods exhibit faster convergence than stochastic first-order methods. The key observation in this regard is that the optimization trajectory does not arbitrarily traverse \mathbb{R}^p —it stays in localized regions. Thus, the speed of convergence is determined by the *local* values of \bar{q} , and not its global value over all of \mathbb{R}^p . As the value of \bar{q} over a localized region may be better behaved than over the whole space, PROMISE methods can take larger step-sizes, which leads to faster convergence. Furthermore, as the iterates approach the optimum, the values of \bar{q} over these localized regions approach 1. Hence we expect the local weighted quadratic regularity ratio to be small.

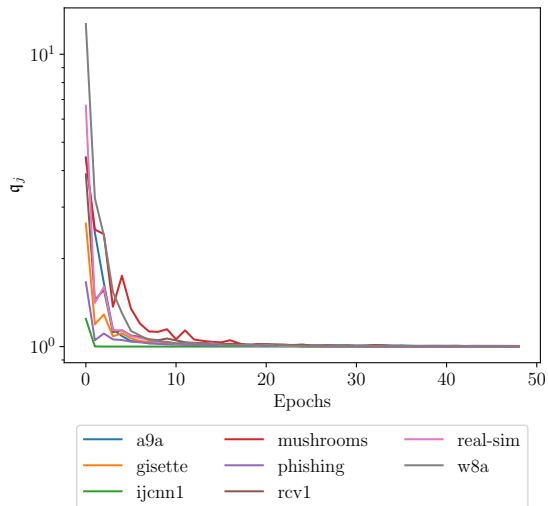
In this section we provide empirical evidence for the hypothesis of the preceding paragraph by studying a local version of the quadratic regularity ratio q along the optimization trajectory. The reason for studying q instead of its weighted version $\bar{q} = \mathcal{L}_P/\gamma_\ell$ is because \mathcal{L}_P requires knowledge of the Hessian similarity τ_\star^ν and the individual values of γ_{u_i} , which are too expensive to compute. Furthermore, $q \approx \bar{q}$ for reasonably large gradient batch-sizes, making q a reasonable proxy for \bar{q} . To this end, we start by defining appropriate local versions of the quadratic regularity constants. Close inspection of our analysis reveals that we only need quadratic regularity with w_0 equal to the iterate where we compute the preconditioner, w_1 set to be the current iterate, and w_2 set equal to the optimum. Hence appropriate definitions for the local quadratic regularity constants $\gamma_{u,j}, \gamma_{\ell,j}$ and local quadratic regularity ratio q_j are given by

$$\gamma_{u,j} := \max_{w \in S_j} \int_0^1 2(1-t) \frac{\|w_\star - w\|_{\nabla^2 F(w+t(w_\star-w))}^2}{\|w_\star - w\|_{\nabla^2 F(w_j)}^2} dt, \quad (25)$$

$$\gamma_{\ell,j} := \min_{w \in S_j} \int_0^1 2(1-t) \frac{\|w_\star - w\|_{\nabla^2 F(w+t(w_\star-w))}^2}{\|w_\star - w\|_{\nabla^2 F(w_j)}^2} dt, \quad (26)$$

$$q_j := \frac{\gamma_{u,j}}{\gamma_{\ell,j}}, \quad (27)$$

where w_j is the iterate where we compute the preconditioner, S_j is the set of iterates associated with the preconditioner P_j (i.e., iterates on the trajectory between w_j , inclusive and w_{j+1} , exclusive), and w_\star is the optimum.


 Figure 17: Plots of q_j over the optimization trajectory for selected datasets.

Dataset	# of epochs
a9a	15
gisette	86
ijcn1	94
mushrooms	20
phishing	71
rcv1	49
real-sim	39
w8a	28

Table 14: Number of epochs to solve logistic regression problems on selected datasets.

Fig. 17 shows q_j for eight datasets over 50 epochs of training using SketchySAGA with the NYSSN preconditioner. For all of these datasets, $q_j \approx 1$ after 20 epochs of training. Furthermore, this phenomenon does not arise because SketchySAGA has already converged close to the optimum; Table 14 demonstrates that $q_j \approx 1$ well before the problem has been solved (within 10^{-4} of $F(w^*)$ as in Section 6.1). For example, ijcn1 takes 94 epochs to be solved by SketchySAGA with the NYSSN preconditioner, but $q_j \approx 1$ in less than 5 epochs. See Appendix D.9 for additional details.

7. Conclusion

We introduce PROMISE, a framework for combining scalable preconditioning techniques with popular stochastic optimization methods. In particular, we present a variety of preconditioning techniques (SSN, NYSSN, SASSN-C, SASSN-R, DIAGSSN) and develop the preconditioned stochastic second-order methods: SketchySVRG, SketchySAGA, and SketchyKatyusha. Furthermore, we provide default hyperparameters for these precondition-

ers and algorithms, which enable them to work out-of-the-box, even on highly ill-conditioned data.

To analyze the PROMISE methods, we introduce quadratic regularity and the quadratic regularity ratio, which generalize the notions of smoothness, strong convexity, and condition number to the Hessian norm. We also introduce Hessian dissimilarity, which allows us to give practical requirements on the gradient batchsize, a first in the literature. We show that PROMISE methods have global linear convergence, and that this convergence is condition-number free for ridge regression.

We empirically demonstrate the superiority of PROMISE methods over popular competitor methods for ridge and logistic regression. PROMISE methods, with their default hyperparameters, consistently outperform the competition, even when they have been tuned to achieve their best performance.

8. Acknowledgements

We would like to thank John Duchi, Daniel LeJeune, Michael Mahoney, Mert Pilanci, Aaron Sidford, and Ali Teshnizi for helpful discussions regarding this work. We would also like to thank GPT-4 for inspiring the title of this work.

A. Additional preconditioner details

We present additional information related to the SASSN and DIAGSSN preconditioners that was omitted in the main text.

A.1 SASSN preconditioner

An implementation of the SASSN-C/SASSN-R preconditioners is provided in the $\mathcal{P}_{\text{sassn-c}}/\mathcal{P}_{\text{sassn-r}}$ classes (Table 15 and Algorithms 9 to 12). The attributes of the $\mathcal{P}_{\text{sassn-c}}/\mathcal{P}_{\text{sassn-r}}$ classes are given in Table 15, and pseudocode for the `update` and `direction` methods is provided in Algorithms 11 and 12, respectively. $\mathcal{P}_{\text{sassn-c}}$ and $\mathcal{P}_{\text{sassn-r}}$ have their own `generate_embedding` methods (Algorithms 9 and 10) for generating a sparse embedding.

Attribute	Description
r	Rank for constructing preconditioner
ρ	Regularization for preconditioner
Y	Sketch of subsampled Hessian
L	Lower-triangular Cholesky factor for storing preconditioner
$\lambda_{\mathcal{P}}$	Estimate of preconditioned smoothness constant

Table 15: Attributes of the $\mathcal{P}_{\text{sassn-c}}/\mathcal{P}_{\text{sassn-r}}$ classes.

The `generate_embedding` method for $\mathcal{P}_{\text{sassn-c}}/\mathcal{P}_{\text{sassn-r}}$ takes a dimension b as input and generates a column-sparse/row-sparse embedding that is used to construct the SASSN-C/SASSN-R preconditioner.

Algorithm 9 Generate column-sparse embedding for $\mathcal{P}_{\text{sassn-c}}$ preconditioner

Require: $\mathcal{P}_{\text{sassn-c}}$ object with attributes $r, \rho, Y, L, \lambda_{\mathcal{P}}$

function $\mathcal{P}_{\text{sassn-c}}.\text{generate_embedding}(b)$

```

     $r \leftarrow \mathcal{P}_{\text{sassn-c}}.r$  ▷ Get attributes
     $\zeta \leftarrow \min(r, 8)$  ▷ Sparsity parameter
     $\text{cols} \leftarrow [0, 1, \dots, b-1]^T \otimes \mathbf{1}_{\zeta}$  ▷ Column indices of nonzero entries
     $\text{rows} \leftarrow \text{rand\_choice}(\{0, 1, \dots, r-1\}, \zeta b)$  ▷ Row indices of nonzero entries
     $\Phi \leftarrow \text{sign}(\text{unif\_sample}(\zeta b) - 0.5)$  ▷ Random sign matrix
     $\Omega \leftarrow \text{csr\_matrix}\left(\sqrt{\frac{1}{\zeta}}\Phi, \text{idx} = (\text{rows}, \text{cols}), \text{shape} = (r, b)\right)$ 
    return  $\Omega$ 

```

Algorithm 10 Generate row-sparse embedding for $\mathcal{P}_{\text{sassn-r}}$ preconditioner**Require:** $\mathcal{P}_{\text{sassn-r}}$ object with attributes $r, \rho, Y, L, \lambda_{\mathcal{P}}$

```

function  $\mathcal{P}_{\text{sassn-r}}$ .generate_embedding( $b$ )
   $r \leftarrow \mathcal{P}_{\text{sassn-r}}.r$  ▷ Get attributes
   $\zeta \leftarrow \min(b, 8)$  ▷ Sparsity parameter
   $\text{cols} \leftarrow \text{rand\_choice}(\{0, 1, \dots, b-1\}, \zeta r)$  ▷ Column indices of nonzero entries
   $\text{rows} \leftarrow [0, 1, \dots, r-1]^T \otimes \mathbf{1}_{\zeta}$  ▷ Row indices of nonzero entries
   $\Phi \leftarrow \text{sign}(\text{unif\_sample}(\zeta r) - 0.5)$  ▷ Random sign matrix
   $\Omega \leftarrow \text{csr\_matrix}\left(\sqrt{\frac{b}{\zeta r}}\Phi, \text{idx} = (\text{rows}, \text{cols}), \text{shape} = (r, b)\right)$ 
  return  $\Omega$ 

```

The implementation of this method for $\mathcal{P}_{\text{sassn-c}}$ and $\mathcal{P}_{\text{sassn-r}}$ is based on Martinsson and Tropp (2020) and Derezhinski et al. (2021), respectively. We limit the sparsity parameter $\zeta \leq 8$ based on recommendations from Tropp et al. (2019).

The `update` method takes a GLM \mathcal{M} , Hessian batches $\mathcal{B}_1, \mathcal{B}_2$, and vector $w \in \mathbb{R}^p$ as input.

Algorithm 11 Update $\mathcal{P}_{\text{sassn-c}}/\mathcal{P}_{\text{sassn-r}}$ preconditioner and preconditioned smoothness constant**Require:** $\mathcal{P}_{\text{sassn-c}}/\mathcal{P}_{\text{sassn-r}}$ object with attributes $r, \rho, Y, L, \lambda_{\mathcal{P}}$

```

function  $\mathcal{P}_{\text{sassn-c}}/\mathcal{P}_{\text{sassn-r}}$ .update( $\mathcal{M}, \mathcal{B}_1, \mathcal{B}_2, w$ )
   $\rho \leftarrow \mathcal{P}_{\text{sassn-c}}/\mathcal{P}_{\text{sassn-r}}.\rho$  ▷ Get attributes

  # Phase 1: Update preconditioner
   $A_{\text{sub}} \leftarrow \mathcal{M}.\text{get\_data}(\mathcal{B}_1)$ 
   $d_{\text{sub}} \leftarrow \mathcal{M}.\text{get\_hessian\_diagonal}(\mathcal{B}_1, w)$ 
   $X \leftarrow \text{diag}(\sqrt{d_{\text{sub}}})A_{\text{sub}}$  ▷ Square root of subsampled Hessian
   $\Omega \leftarrow \mathcal{P}_{\text{sassn-c}}/\mathcal{P}_{\text{sassn-r}}.\text{generate\_embedding}(|\mathcal{B}_1|)$  ▷ Sparse embedding
   $Y \leftarrow \Omega X$  ▷ Sketched square root of subsampled Hessian
   $L \leftarrow \text{cholesky}(YY^T + \rho I)$ 

  # Phase 2: Update estimated preconditioned smoothness constant
   $A_{\text{sub}} \leftarrow \mathcal{M}.\text{get\_data}(\mathcal{B}_2)$ 
   $d_{\text{sub}} \leftarrow \mathcal{M}.\text{get\_hessian\_diagonal}(\mathcal{B}_2, w)$ 
   $Z \leftarrow A_{\text{sub}}^T \text{diag}(d_{\text{sub}})A_{\text{sub}} + \mathcal{M}.\text{get\_reg}()I$  ▷ Subsampled Hessian
   $\lambda_{\mathcal{P}} \leftarrow \text{eig}(Z(Y^T Y + \rho I)^{-1}, k=1)$  ▷ Compute largest eigenvalue

   $\mathcal{P}_{\text{sassn-c}}/\mathcal{P}_{\text{sassn-r}}.Y \leftarrow Y, \mathcal{P}_{\text{sassn-c}}/\mathcal{P}_{\text{sassn-r}}.L \leftarrow L, \mathcal{P}_{\text{sassn-c}}/\mathcal{P}_{\text{sassn-r}}.\lambda_{\mathcal{P}} \leftarrow \lambda_{\mathcal{P}}$  ▷ Set attributes

```

In the first phase, this method constructs the SASSN-C/SASSN-R preconditioner P at w by computing the square root of the subsampled Hessian, X , applying a sparse embedding to X , and computing a Cholesky factorization. The factors Y and L can be used later to

apply the preconditioner to a vector. In the second phase, this method estimates the preconditioned smoothness constant by taking a similar approach to the \mathcal{P}_{ssn} class.

The `direction` method takes a vector $g \in \mathbb{R}^p$ (typically a stochastic gradient) as input.

Algorithm 12 Compute preconditioned $\mathcal{P}_{\text{sassn-c}}/\mathcal{P}_{\text{sassn-r}}$ direction

Require: $\mathcal{P}_{\text{sassn-c}}/\mathcal{P}_{\text{sassn-r}}$ object with attributes $r, \rho, Y, L, \lambda_{\mathcal{P}}$

function $\mathcal{P}_{\text{sassn-c}}/\mathcal{P}_{\text{sassn-r}}$.`direction`(g)

$Y \leftarrow \mathcal{P}_{\text{sassn-c}}/\mathcal{P}_{\text{sassn-r}}.Y, L \leftarrow \mathcal{P}_{\text{sassn-c}}/\mathcal{P}_{\text{sassn-r}}.L, \rho \leftarrow \mathcal{P}_{\text{sassn-c}}/\mathcal{P}_{\text{sassn-r}}.\rho$ ▷ Get attributes

$v \leftarrow Yg$

$v \leftarrow L^{-1}v$ ▷ Triangular solve

$v \leftarrow L^{-T}v$ ▷ Triangular solve

$v \leftarrow Y^T v$

return $(g - v)/\rho$

The method then computes $P^{-1}g$ using the Woodbury formula with the preconditioner factors Y and L ; this computation has complexity $\mathcal{O}(rp)$ in general.

A.2 DiagSSN preconditioner

An implementation of the DIAGSSN preconditioner is provided in the $\mathcal{P}_{\text{diagssn}}$ class (Table 16 and Algorithms 13 and 14). The attributes of the $\mathcal{P}_{\text{diagssn}}$ class are given in Table 16, and pseudocode for the `update` and `direction` methods is provided in Algorithms 13 and 14, respectively.

Attribute	Description
ρ	Regularization for preconditioner
d	Vector for storing preconditioner
$\lambda_{\mathcal{P}}$	Estimate of preconditioned smoothness constant

Table 16: Attributes of the $\mathcal{P}_{\text{diagssn}}$ class.

The `update` method takes a GLM \mathcal{M} , Hessian batches $\mathcal{B}_1, \mathcal{B}_2$, and vector $w \in \mathbb{R}^p$ as input.

Algorithm 13 Update $\mathcal{P}_{\text{diagssn}}$ preconditioner and preconditioned smoothness constant

Require: $\mathcal{P}_{\text{diagssn}}$ object with attributes $\rho, d, \lambda_{\mathcal{P}}$

```

function  $\mathcal{P}_{\text{diagssn}}.\text{update}(\mathcal{M}, \mathcal{B}_1, \mathcal{B}_2, w)$ 
     $\rho \leftarrow \mathcal{P}_{\text{diagssn}}.\rho$  ▷ Get attributes

    # Phase 1: Update preconditioner
     $A_{\text{sub}} \leftarrow \mathcal{M}.\text{get\_data}(\mathcal{B}_1)$ 
     $d_{\text{sub}} \leftarrow \mathcal{M}.\text{get\_hessian\_diagonal}(\mathcal{B}_1, w)$ 
     $X \leftarrow \text{diag}(\sqrt{d_{\text{sub}}})A_{\text{sub}}$  ▷ Square root of subsampled Hessian
     $d \leftarrow \text{column\_norm}(X)^2$ 

    # Phase 2: Update estimated preconditioned smoothness constant
     $A_{\text{sub}} \leftarrow \mathcal{M}.\text{get\_data}(\mathcal{B}_2)$ 
     $d_{\text{sub}} \leftarrow \mathcal{M}.\text{get\_hessian\_diagonal}(\mathcal{B}_2, w)$ 
     $Z \leftarrow A_{\text{sub}}^T \text{diag}(d_{\text{sub}})A_{\text{sub}} + \mathcal{M}.\text{get\_reg}()I$  ▷ Subsampled Hessian
     $\lambda_{\mathcal{P}} \leftarrow \text{eig}(Z \text{diag}(d + \rho)^{-1}, k = 1)$  ▷ Compute largest eigenvalue

     $\mathcal{P}_{\text{diagssn}}.d \leftarrow d, \mathcal{P}_{\text{diagssn}}.\lambda_{\mathcal{P}} \leftarrow \lambda_{\mathcal{P}}$  ▷ Set attributes

```

In the first phase, this method constructs the DIAGSSN preconditioner P at w by computing the square root of the subsampled Hessian, X , and then using X to compute the diagonal of the subsampled Hessian, d , which is stored as a vector. In the second phase, this method estimates the preconditioned smoothness constant by taking a similar approach to the \mathcal{P}_{ssn} class.

The `direction` method takes a vector $g \in \mathbb{R}^p$ (typically a stochastic gradient) as input.

Algorithm 14 Compute preconditioned $\mathcal{P}_{\text{diagssn}}$ direction

Require: $\mathcal{P}_{\text{diagssn}}$ object with attributes $\rho, d, \lambda_{\mathcal{P}}$

```

function  $\mathcal{P}_{\text{diagssn}}.\text{direction}(g)$ 
     $d \leftarrow \mathcal{P}_{\text{diagssn}}.d, \rho \leftarrow \mathcal{P}_{\text{diagssn}}.\rho$  ▷ Get attributes
    return  $g/(d + \rho)$  ▷ Elementwise division

```

The method then computes $P^{-1}g$ by elementwise division with d ; this computation has complexity $\mathcal{O}(p)$.

B. General lemmas

Here we collect some general lemmas that will be used in our analysis. The first three lemmas follow from elementary computation.

Lemma 34 (A-norm variance decomposition) *Let A be a symmetric positive definite matrix, and $X \in \mathbb{R}^p$ a random vector. Then*

$$\mathbb{E}\|X - \mathbb{E}X\|_A^2 = \mathbb{E}\|X\|_A^2 - \|\mathbb{E}X\|_A^2,$$

and so

$$\mathbb{E}\|X - \mathbb{E}X\|_A^2 \leq \mathbb{E}\|X\|_A^2.$$

Lemma 35 (A-norm parallelogram law inequality) *Let A be a symmetric positive definite matrix, then for any vectors a, b we have*

$$\|a + b\|_A^2 \leq 2(\|a\|_A^2 + \|b\|_A^2).$$

Lemma 36 (A-norm polarization identity) *Let A be a symmetric positive definite matrix. Then for any vectors a, b, c, d , the following equality holds*

$$\langle a - b, c - d \rangle_A = \frac{1}{2}(\|a - d\|_A^2 - \|a - c\|_A^2) + \frac{1}{2}(\|c - b\|_A^2 - \|d - b\|_A^2).$$

Lemma 37 (Generalized Young Inequality) *Let A be a symmetric positive definite matrix. Then for any $a, b \in \mathbb{R}^p$ and $c_1, c_2 > 0$*

$$c_1 \langle a, b \rangle - \frac{c_2}{2} \|b\|_A^2 \leq \frac{c_1^2}{2c_2} \|a\|_{A^{-1}}^2.$$

Proof Set $a' = \frac{c_1}{\sqrt{c_2}} A^{-1} a, b' = \sqrt{c_2} b$. Then

$$c_1 \langle a, b \rangle - \frac{c_2}{2} \|b\|_A^2 = \langle a', b' \rangle_A + \frac{1}{2} \|b'\|_A^2.$$

Now, using $\|a' + b'\|_A^2 \leq 2(\|a'\|_A^2 + \|b'\|_A^2)$, expanding and rearranging, we reach

$$\langle a', b' \rangle_A \leq \frac{1}{2} (\|a'\|_A^2 + \|b'\|_A^2).$$

Hence

$$\langle a', b' \rangle_A - \frac{1}{2} \|b'\|_A^2 \leq \frac{\|a'\|_A^2}{2}.$$

Now, substituting in the values for a', b' , and using $\|A^{-1}a\|_A^2 = \|a\|_{A^{-1}}^2$, completes the proof. \blacksquare

Lemma 38 (Smoothness with respect to the A-norm) *Let $A \in \mathbb{S}_p^{++}(\mathbb{R})$, and $F(x)$ be a real-valued convex function satisfying:*

$$F(x) \leq F(y) + \langle \nabla F(y), x - y \rangle + \frac{L}{2} \|x - y\|_A^2 \quad \forall x, y \in \mathbb{R}^p.$$

Then

$$F(x) \geq F(y) + \langle \nabla F(y), x - y \rangle + \frac{1}{2L} \|\nabla F(x) - \nabla F(y)\|_{A^{-1}}^2 \quad \forall x, y \in \mathbb{R}^p.$$

Proof It is a standard fact of convex optimization (see Theorem 5.8 in Beck (2017) or Theorem 2.1.5 in Nesterov (2018)) that F satisfies the inequality

$$F(x) \leq F(y) + \langle \nabla F(y), x - y \rangle + \frac{L}{2} \|x - y\|^2 \quad \forall x, y \in \mathbb{R}^p,$$

with respect to the norm $\|\cdot\|$, if and only if it satisfies the inequality

$$F(x) \geq F(y) + \langle \nabla F(y), x - y \rangle + \frac{1}{2L} \|\nabla F(x) - \nabla F(y)\|_*^2 \quad \forall x, y \in \mathbb{R}^p,$$

where $\|\cdot\|_*$ is the dual norm of $\|\cdot\|$. The claim follows by observing that the dual norm of $\|\cdot\|_A$ is $\|\cdot\|_{A^{-1}}$. \blacksquare

C. Proofs of main results

C.1 Proof of Lemma 7

Proof The proof is by direct calculation. Indeed, for the first part of the claim, observe that

$$\begin{aligned} d_{\text{eff}}^\nu(A^T \Phi''(Aw)A) &= \sum_{j=1}^n \frac{\sigma_j^2(\Phi''(Aw)A)}{\sigma_j^2(\Phi''(Aw)A) + n\nu} \stackrel{(1)}{\leq} \sum_{j=1}^n \frac{C_1 B j^{-2\beta}}{C_1 B j^{-2\beta} + n\nu} \\ &\stackrel{(2)}{=} \sum_{j=1}^n \frac{C}{C + (n\nu)j^{2\beta}} \leq \int_0^\infty \frac{C}{C + (n\nu)x^{2\beta}} dx \stackrel{(3)}{=} C(n\nu)^{-1/(2\beta)} \int_0^\infty \frac{1}{C + u^{2\beta}} du \\ &\stackrel{(4)}{=} C(n\nu)^{-1/(2\beta)} \times C^{\frac{1}{2\beta}-1} \frac{\pi/(2\beta)}{\sin(\pi/(2\beta))} = \frac{\pi/(2\beta)}{\sin(\pi/(2\beta))} \left(\frac{C}{n\nu}\right)^{1/2\beta}. \end{aligned}$$

Here (1) uses $A^T \Phi''(Aw)A \preceq B$, our hypotheses on that $\sigma_j(A) = \mathcal{O}(j^{-2\beta})$, and that $\frac{x}{x+\nu}$ is increasing in x for $x \geq 0$, (2) sets $C = C_1 B$ and multiplies the numerator and denominator by $j^{2\beta}$, (3) uses the substitution $u = (n\nu)^{1/2\beta} x$, and (4) uses the fact that $\int_0^\infty \frac{1}{C+u^{2\beta}} du = C^{\frac{1}{2\beta}-1} \frac{\pi/(2\beta)}{\sin(\pi/(2\beta))}$ (Sutherland, 2017).

The second claim now follows from the first by plugging in $\nu = \mathcal{O}(1/n)$. \blacksquare

C.2 Proofs of sampling and low-rank approximation bounds

C.2.1 PRELIMINARIES

The following result is an immediate consequence of Theorem 1 in Cohen et al. (2016) with $A = B = D_\sigma^{1/2}$.

Proposition 39 *Let $G \in \mathbb{R}^{p \times p}$ with eigendecomposition $G = V \Lambda V^T$. Let $\sigma > 0$ and define $D_\sigma = \Lambda(\Lambda + \sigma I)^{-1}$. Assume one of the following items holds:*

1. $\frac{1}{\sqrt{r}} \Omega$, where Ω is a Gaussian random matrix with $r = \Omega \left(\frac{d_{\text{eff}}^\sigma(\widehat{\nabla}^2 f(w)) + \log(\frac{1}{\delta})}{C_0^2} \right)$ rows.

2. Ω is an SRHT matrix with $r = \Omega \left(\frac{d_{\text{eff}}^{\sigma}(\widehat{\nabla}^2 f(w)) + \log(\frac{1}{\zeta_0 \delta}) \log\left(\frac{d_{\text{eff}}^{\sigma}(\widehat{\nabla}^2 f(w))}{\delta}\right)}{\zeta_0^2} \right)$ rows.
3. Ω is an sparse sign embedding with sparsity $s = \Omega \left(\frac{\log\left(\frac{d_{\text{eff}}^{\sigma}(\widehat{\nabla}^2 f(w))}{\delta}\right)}{\zeta_0} \right)$ and $r = \Omega \left(\frac{d_{\text{eff}}^{\sigma}(\widehat{\nabla}^2 f(w)) \log\left(\frac{d_{\text{eff}}^{\sigma}(\widehat{\nabla}^2 f(w))}{\delta}\right)}{\zeta_0^2} \right)$ rows.

Then

$$\|D_{\sigma}^{1/2} V^T \Omega^T \Omega V D_{\sigma}^{1/2} - D_{\sigma}\| \leq \zeta_0, \quad (28)$$

with probability at least $1 - \delta$.

We also recall the following lemma due to Alaoui and Mahoney (2015).

Lemma 40 (Lemma 1, Alaoui and Mahoney (2015)) *Let H be a symmetric psd matrix, $\sigma > 0$ and $\hat{H} = H \langle \Omega \rangle$ be a Nyström approximation to H with test matrix Ω . Further, let the regularized Nyström approximation $H \langle \Omega \rangle_{\sigma} = (H \Omega)(\Omega^T H \Omega + \sigma I)^{-1} (H \Omega)^T$. Define $E = H - H \langle \Omega \rangle$ and $E_{\sigma} = H - H \langle \Omega \rangle_{\sigma}$. Suppose that $\|D_{\sigma}^{1/2} \Omega \Omega^T D_{\sigma}^{1/2} - D_{\sigma}\| \leq \tilde{\eta} < 1$. Then*

$$\|H - \hat{H}\| \leq \frac{\sigma}{1 - \tilde{\eta}}. \quad (29)$$

C.2.2 PROOF OF PROPOSITION 9

Proof Suppose the subsampled Hessian $\widehat{\nabla}^2 f(w)$ is constructed with batch $\mathcal{B} \subseteq [n]$ such that $|\mathcal{B}| = b_H$. Since f is a GLM,

$$\widehat{\nabla}^2 f(w) = \frac{1}{b_H} A_{\mathcal{B}}^T \Phi''(A_{\mathcal{B}} w) A_{\mathcal{B}},$$

where A is the associated data matrix. Now, as the Hessian batchsizes satisfies

$$\begin{aligned} b_H &= \Omega \left(\frac{\chi^{\rho}(\nabla^2 f(w)) d_{\text{eff}}^{\rho}(\nabla^2 f(w)) \log\left(\frac{d_{\text{eff}}^{\rho}(\nabla^2 f(w))}{\delta}\right)}{\zeta_0^2} \right) \\ &= \Omega \left(\frac{\chi^{\rho}(\Phi''(Aw)^{1/2} A) d_{\text{eff}}^{\rho}(\Phi''(Aw)^{1/2} A) \log\left(\frac{d_{\text{eff}}^{\rho}(\Phi''(Aw)^{1/2} A)}{\delta}\right)}{\zeta_0^2} \right), \end{aligned}$$

we may apply Lemma 8 to conclude

$$(1 - \zeta_0) \left(\frac{1}{b_H} A_{\mathcal{B}}^T \Phi''(A_{\mathcal{B}} w) A_{\mathcal{B}} + \rho I \right) \preceq \frac{1}{n} A^T \Phi''(Aw) A + \rho I \preceq (1 + \zeta_0) \left(\frac{1}{b_H} A_{\mathcal{B}}^T \Phi''(A_{\mathcal{B}} w) A_{\mathcal{B}} + \rho I \right)$$

holds with probability at least $1 - \delta$. The previous display is equivalent to

$$(1 - \zeta_0)(\widehat{\nabla}^2 f(w) + \rho I) \preceq \nabla^2 f(w) + \rho I \preceq (1 + \zeta_0)(\widehat{\nabla}^2 f(w) + \rho I).$$

Since $\rho \geq \nu$, a routine calculation shows that

$$\frac{\nu}{\rho}(1 - \zeta_0)(\widehat{\nabla}^2 f(w) + \rho I) \preceq \nabla^2 f(w) + \nu I \preceq (1 + \zeta_0)(\widehat{\nabla}^2 f(w) + \rho I).$$

Thus, for $\zeta = \max\{1 - \frac{\nu}{\rho}(1 - \zeta_0), \zeta_0\}$,

$$(1 - \zeta)(\widehat{\nabla}^2 f(w) + \rho I) \preceq \nabla^2 f(w) + \nu I \preceq (1 + \zeta)(\widehat{\nabla}^2 f(w) + \rho I).$$

To conclude, recall $\zeta_0 < 1$, so the max defining ζ is always attained at $1 - \frac{\nu}{\rho}(1 - \zeta_0)$. \blacksquare

C.2.3 PROOF OF PROPOSITION 10

Proof Let $E = \widehat{\nabla}^2 f(w) - \hat{H}$, and recall that it satisfies $E \succeq 0$ (Tropp et al., 2017). To control the norm of E , we may use our hypotheses on r to invoke Proposition 39 (applied to Ω^T)* and Lemma 40 to guarantee that

$$\|E\| \leq \zeta_0 \rho$$

with probability at least $1 - \delta/2$. Now, by definition of E , the regularized subsampled Hessian satisfies

$$\widehat{\nabla}^2 f(w) + \rho I = \hat{H} + \rho I + E. \quad (30)$$

Let $P = \hat{H} + \rho I$. Then combining (30) with Weyl's inequalities yields

$$\begin{aligned} \lambda_1 \left(P^{-1/2} \left(\widehat{\nabla}^2 f(w) + \rho I \right) P^{-1/2} \right) &\leq \lambda_1 \left(P^{-1/2} \left(\hat{H} + \rho I \right) P^{-1/2} \right) + \lambda_1 \left(P^{-1/2} E P^{-1/2} \right) \\ &= 1 + \|P^{-1/2} E P^{-1/2}\| \leq 1 + \|P^{-1}\| \|E\| \leq 1 + \frac{\|E\|}{\rho} \leq 1 + \zeta_0. \end{aligned}$$

To bound the smallest eigenvalue, observe that

$$\widehat{\nabla}^2 f(w) + \rho I \succeq \hat{H} + \rho I \implies \widehat{\nabla}^2 f(w) + \rho I \succeq P.$$

Thus, conjugating the preceding relation by $P^{-1/2}$ we obtain

$$P^{-1/2} \left(\widehat{\nabla}^2 f(w) + \rho I \right) P^{-1/2} \succeq I_p,$$

where I_p is the $p \times p$ identity matrix. The preceding inequality immediately yields

$$\lambda_p(P^{-1/2} \left(\widehat{\nabla}^2 f(w) + \rho I \right) P^{-1/2}) \geq 1.$$

Hence,

$$1 \leq \lambda_p(P^{-1/2} \left(\widehat{\nabla}^2 f(w) + \rho I \right) P^{-1/2}) \leq \lambda_1(P^{-1/2} \left(\widehat{\nabla}^2 f(w) + \rho I \right) P^{-1/2}) \leq 1 + \zeta_0.$$

*. If Ω is Gaussian, we apply the proposition to $\frac{1}{\sqrt{\epsilon}}\Omega^T$. We can do this, as the Nyström approximation is invariant to multiplication of Ω by scalars.

As an immediate consequence, we obtain the Loewner ordering relation

$$I_p \preceq P^{-1/2} \left(\widehat{\nabla}^2 f(w) + \rho I \right) P^{-1/2} \preceq (1 + \zeta_0) I_p$$

which we conjugate by $P^{1/2}$ to show

$$\hat{H} + \rho I \preceq \widehat{\nabla}^2 f(w) + \rho I \preceq (1 + \zeta_0) \left(\hat{H} + \rho I \right),$$

with probability at least $1 - \delta/2$.

We now relate the quality of P to the full Hessian $\nabla^2 f(w) + \nu I$. To accomplish this, we observe that by our hypothesis on b_H , Proposition 9 implies the relation

$$(1 - \zeta_0) \left(\widehat{\nabla}^2 f(w) + \nu I \right) \preceq \nabla^2 f(w) + \nu I \preceq (1 + \zeta_0) \left(\widehat{\nabla}^2 f(w) + \nu I \right),$$

holds with probability at least $1 - \delta/2$. As $\rho \geq \nu$, the preceding display yields

$$(1 - \zeta_0) \frac{\nu}{\rho} \left(\widehat{\nabla}^2 f(w) + \rho I \right) \preceq \nabla^2 f(w) + \nu I \preceq (1 + \zeta_0) \left(\widehat{\nabla}^2 f(w) + \rho I \right).$$

Hence by union bound, with probability at least $1 - \delta$, we have

$$(1 - \zeta_0) \frac{\nu}{\rho} \left(\hat{H} + \rho I \right) \preceq \nabla^2 f(w) + \nu I \preceq (1 + \zeta_0)^2 \left(\hat{H} + \rho I \right).$$

Scaling down ζ_0 by a constant factor to ζ' , so that $(1 + \zeta')^2$ is smaller than $(1 + \zeta_0)$, the previous display becomes

$$(1 - \zeta_0) \frac{\nu}{\rho} \left(\hat{H} + \rho I \right) \preceq \nabla^2 f(w) + \nu I \preceq (1 + \zeta_0) \left(\hat{H} + \rho I \right).$$

Setting $\zeta = 1 - (1 - \zeta_0) \frac{\nu}{\rho}$, we see that $\hat{H} + \rho I$ is a ζ -spectral approximation, which concludes the argument. \blacksquare

C.2.4 PROOF OF ζ -SPECTRAL APPROXIMATION FOR SASSN

Sketch-and-Solve Subsampled Newton also yields a ζ -spectral approximation under similar hypotheses as Nyström Subsampled Newton, as shown in the following proposition.

Proposition 41 *Let $w \in \mathbb{R}^p$, $\zeta_0 \in (0, 1)$, suppose F is a GLM, and that we construct the subsampled Hessian with sample size $b_H = \Omega \left(\frac{\chi^\nu(\nabla^2 f(w)) d_{\text{eff}}^\nu(\nabla^2 f(w)) \log \left(\frac{d_{\text{eff}}^\nu(\nabla^2 f(w))}{\delta} \right)}{\zeta_0^2} \right)$.*

Further assume one of the following holds:

1. $\frac{1}{\sqrt{r}} \Omega$, where Ω is a Gaussian random matrix with $r = \Omega \left(\frac{d_{\text{eff}}^\rho(\widehat{\nabla}^2 f(w)) + \log(\frac{1}{\delta})}{\zeta_0^2} \right)$ rows.
2. Ω is an SRHT matrix with $r = \Omega \left(\frac{d_{\text{eff}}^\rho(\widehat{\nabla}^2 f(w)) + \log(\frac{1}{\zeta_0}) \log \left(\frac{d_{\text{eff}}^\rho(\widehat{\nabla}^2 f(w))}{\delta} \right)}{\zeta_0^2} \right)$ rows.

3. Ω is an sparse sign embedding with sparsity $s = \Omega \left(\frac{\log \left(\frac{d_{\text{eff}}^\rho(\widehat{\nabla}^2 f(w))}{\delta} \right)}{\zeta_0} \right)$ and $r = \Omega \left(\frac{d_{\text{eff}}^\rho(\widehat{\nabla}^2 f(w)) \log \left(\frac{d_{\text{eff}}^\rho(\widehat{\nabla}^2 f(w))}{\delta} \right)}{\zeta_0^2} \right)$ rows.
4. Ω is a LESS-uniform embedding with sparsity $s = \mathcal{O} \left(\chi^\rho(\widehat{\nabla}^2 f(w)) d_{\text{eff}}^\rho(\widehat{\nabla}^2 f(w)) \right)$ and $r = \Omega \left(\frac{d_{\text{eff}}^\rho(\widehat{\nabla}^2 f(w)) \log \left(\frac{d_{\text{eff}}^\rho(\widehat{\nabla}^2 f(w))}{\delta} \right)}{\zeta_0^2} \right)$ rows.

Then with probability at least $1 - \delta$,

$$(1 - \zeta)(\hat{H} + \rho I) \preceq \nabla^2 f(w) + \nu I \preceq (1 + \zeta)(\hat{H} + \rho I), \quad (31)$$

where $\zeta = (1 - \zeta_0)\nu/\rho$.

Proof As F is a GLM, the *unregularized* portion of subsampled Hessian has the form

$$A_{\mathcal{B}}^T \Phi(A_{\mathcal{B}} w) A_{\mathcal{B}} = R^T R,$$

where $R = \Phi(A_{\mathcal{B}} w)^{1/2} A_{\mathcal{B}}$ and where \mathcal{B} corresponds to the subsampled indices. Hence

$$\widehat{\nabla}^2 f(w) + \rho I = R^T R + \rho I.$$

Now, consider the random variable

$$X := (R^T R + \rho I)^{-1/2} (R^T \Omega^T \Omega R + \rho I) (R^T R + \rho I)^{-1/2} - I_p.$$

Using the SVD, $R = U \Sigma V^T$, this may be rewritten as

$$\begin{aligned} X &= V (\Sigma^2 + \rho I)^{-1/2} V^T (V \Sigma U^T \Omega^T \Omega U \Sigma V^T + \rho I) V (\Sigma^2 + \rho I)^{-1/2} V^T - I_p \\ &= V (\Sigma^2 + \rho I)^{-1/2} V^T (V \Sigma U^T \Omega^T \Omega U \Sigma V^T + V [-\Sigma^2 + \Sigma^2 + \rho I] V^T) V (\Sigma^2 + \rho I)^{-1/2} V^T - I_p \\ &= V \Sigma (\Sigma^2 + \rho I)^{-1/2} (U^T \Omega^T \Omega U) \Sigma (\Sigma^2 + \rho I)^{-1/2} V^T - V \Sigma^2 (\Sigma^2 + \rho I)^{-1} V^T \\ &= V D_\rho^{1/2} U^T \Omega^T \Omega U D_\rho^{1/2} V^T - V D_\rho V^T. \end{aligned}$$

Hence we find

$$\|X\| = \|D_\rho^{1/2} U^T \Omega^T \Omega U D_\rho^{1/2} - D_\rho\|.$$

Now, using our hypotheses on Ω we may invoke Proposition 39* with $G = R R^T = U \Sigma^2 U^T$, to reach

$$\|X\| = \|D_\rho^{1/2} U^T \Omega^T \Omega U D_\rho^{1/2} - D_\rho\| \leq \zeta_0,$$

with probability at least $1 - \delta/2$. It now follows immediately from the preceding display that

$$(1 - \zeta_0) \left(\widehat{\nabla}^2 f(w) + \rho I \right) \preceq R^T \Omega^T \Omega R + \rho I \preceq (1 + \zeta_0) \left(\widehat{\nabla}^2 f(w) + \rho I \right),$$

*. See Lemma 7 in Dereziński et al. (2021) to understand why Proposition 39 holds for item 4.

with probability at least $1 - \delta/2$. Rearranging and scaling down ζ_0 , we reach

$$(1 - \zeta_0) (R^T \Omega^T \Omega R + \rho I) \preceq \left(\widehat{\nabla}^2 f(w) + \rho I \right) \preceq (1 + \zeta_0) (R^T \Omega^T \Omega R + \rho I).$$

Now applying the same argument as in the proof of Proposition 10, we conclude

$$(1 - \zeta_0) \frac{\nu}{\rho} (R^T \Omega^T \Omega R + \rho I) \preceq (\nabla^2 f(w) + \nu I) \preceq (1 + \zeta_0) (R^T \Omega^T \Omega R + \rho I),$$

with probability at least $1 - \delta$. Thus, setting $\zeta = 1 - \frac{\nu}{\rho}(1 - \zeta_0)$, we reach

$$(1 - \zeta)(R^T \Omega^T \Omega R + \rho I) \preceq \nabla^2 f(w) + \nu I \preceq (1 + \zeta)(R^T \Omega^T \Omega R + \rho I),$$

which concludes the argument. ■

C.3 Proofs for quadratic regularity

C.3.1 PROOF OF PROPOSITION 12

Proof For any $w_1, w_2 \in \mathcal{C}$, Taylor's theorem implies that

$$F(w_2) = F(w_1) + \langle \nabla F(w_1), w_2 - w_1 \rangle + \int_0^1 (1 - t) \|w_2 - w_1\|_{\nabla^2 F(w_t)}^2 dt,$$

where $w_t = w_1 + t(w_2 - w_1) \in \mathcal{C}$. As

$$\int_0^1 (1 - t) \|w_2 - w_1\|_{\nabla^2 F(w_t)}^2 dt = \frac{1}{2} \left(\frac{\int_0^1 2(1 - t) \|w_2 - w_1\|_{\nabla^2 F(w_t)}^2 dt}{\|w_2 - w_1\|_{\nabla^2 F(w_0)}^2} \right) \|w_2 - w_1\|_{\nabla^2 F(w_0)}^2,$$

the first two inequalities follow immediately from the definitions of γ_u and γ_ℓ .

For the last inequality, observe the first inequality implies via Lemma 38 that

$$\begin{aligned} F(w_2) &\geq F(w_1) + \langle \nabla F(w_1), w_2 - w_1 \rangle + \frac{1}{2\gamma_u(\mathcal{C})} \|\nabla F(w_2) - \nabla F(w_1)\|_{\nabla^2 F(w_0)}^2 \\ F(w_2) &\leq F(w_1) + \langle \nabla F(w_1), w_2 - w_1 \rangle + \frac{\gamma_u(\mathcal{C})}{2} \|w_2 - w_1\|_{\nabla^2 F(w_0)}^2, \end{aligned}$$

Hence combining these two inequalities, we reach

$$\frac{1}{2\gamma_u(\mathcal{C})} \|\nabla F(w_2) - \nabla F(w_1)\|_{\nabla^2 F(w_0)}^2 \leq \frac{\gamma_u(\mathcal{C})}{2} \|w_2 - w_1\|_{\nabla^2 F(w_0)}^2,$$

which yields the claim. ■

C.3.2 PROOF OF PROPOSITION 13

We first define the quadratic stability constant,

$$\Gamma(\mathcal{C}) := \sup_{w_0 \in \mathcal{C}} \left(\sup_{w_1, w_2, w_3 \in \mathcal{C}, w_2 \neq w_3} \frac{\|w_3 - w_2\|_{\nabla^2 F(w_1)}^2}{\|w_3 - w_2\|_{\nabla^2 F(w_0)}^2} \right) = \sup_{w_0 \in \mathcal{C}} \left(\sup_{w_1 \in \mathcal{C}, d \in (\mathcal{C} - \mathcal{C}) \setminus \{0\}} \frac{\|d\|_{\nabla^2 F(w_1)}^2}{\|d\|_{\nabla^2 F(w_0)}^2} \right).$$

Lemma 42 *The upper and lower quadratic regularity constants satisfy the following bound:*

$$\frac{1}{\Gamma(\mathcal{C})} \leq \gamma_\ell(\mathcal{C}) \leq \gamma_u(\mathcal{C}) \leq \Gamma(\mathcal{C}).$$

Proof Observe that,

$$\frac{\|w_2 - w_1\|_{\nabla^2 F(w_t)}^2}{\|w_2 - w_1\|_{\nabla^2 F(w_0)}^2} = \frac{\|w_t - w_1\|_{\nabla^2 F(w_t)}^2}{\|w_t - w_1\|_{\nabla^2 F(w_0)}^2},$$

where $w_t = w_1 + t(w_2 - w_1) \in \mathcal{C}$. Hence we have

$$\begin{aligned} \gamma_u(\mathcal{C}) &= \sup_{w_0 \in \mathcal{C}} \left(\sup_{w_1, w_2 \in \mathcal{C}, w_1 \neq w_2} \int_0^1 2(1-t) \frac{\|w_2 - w_1\|_{\nabla^2 F(w_1 + t(w_2 - w_1))}^2}{\|w_2 - w_1\|_{\nabla^2 F(w_0)}^2} dt \right) \\ &= \sup_{w_0 \in \mathcal{C}} \left(\sup_{w_1, w_2 \in \mathcal{C}, w_1 \neq w_2} \int_0^1 2(1-t) \frac{\|w_t - w_1\|_{\nabla^2 F(w_t)}^2}{\|w_t - w_1\|_{\nabla^2 F(w_0)}^2} dt \right) \\ &\leq \sup_{w_0 \in \mathcal{C}} \left(\int_0^1 2(1-t) \sup_{w_1, w_2 \in \mathcal{C}, w_1 \neq w_2} \frac{\|w_t - w_1\|_{\nabla^2 F(w_t)}^2}{\|w_t - w_1\|_{\nabla^2 F(w_0)}^2} dt \right) \\ &\leq \int_0^1 2(1-t) \sup_{w_0 \in \mathcal{C}} \left(\sup_{w_1 \in \mathcal{C}, d \in (\mathcal{C} - \mathcal{C}) \setminus \{0\}} \frac{\|d\|_{\nabla^2 F(w_1)}^2}{\|d\|_{\nabla^2 F(w_0)}^2} \right) dt \\ &= \Gamma(\mathcal{C}). \end{aligned}$$

By observing that

$$\inf_{w_0 \in \mathcal{C}} \left(\inf_{w_1, w_2, w_3 \in \mathcal{C}, w_2 \neq w_3} \frac{\|w_3 - w_2\|_{\nabla^2 F(w_1)}^2}{\|w_3 - w_2\|_{\nabla^2 F(w_0)}^2} \right) \geq \frac{1}{\Gamma(\mathcal{C})},$$

a nearly identical argument yields the lower bound on $\gamma_\ell(\mathcal{C})$. ■

Hence to prove Proposition 13, we just have to upper bound $\Gamma(\mathcal{C})$, and this is the strategy we shall follow.

Proof

1. If f is L -smooth and μ -strongly convex, then for any $w_0, w_1 \in \mathcal{C}$ and $d \in (\mathcal{C} - \mathcal{C}) \setminus \{0\}$, we have

$$\frac{\mu}{L} \leq \frac{\|d\|_{\nabla^2 F(w_1)}^2}{\|d\|_{\nabla^2 F(w_0)}^2} \leq \frac{L}{\mu}.$$

Hence $\Gamma(\mathcal{C}) \leq L/\mu$, and so

$$\frac{\mu}{L} \leq \gamma_\ell^* \leq \gamma_u^* \leq \frac{L}{\mu},$$

by Lemma 42.

2. Observe that for any $w_0, w_1 \in \mathcal{C}$ and $d \in (\mathcal{C} - \mathcal{C}) \setminus \{0\}$, we have

$$\frac{\|d\|_{H(w_1)}^2}{\|d\|_{H(w_0)}^2} = 1 + \frac{d^T [H(w_1) - H(w_0)] d}{\|d\|_{H(w_0)}^2} \leq 1 + \frac{MD}{\mu}.$$

Where the last inequality used that f has an M -Lipschitz Hessian and that $\|d\| \leq D$. Thus $\Gamma(\mathcal{C}) \leq 1 + \frac{MD}{\mu}$, and the claim follows immediately from Lemma 42.

3. Recall if F is generalized self-concordant, then by definition (see Definition 1 in Marteau-Ferey et al. (2019a)) the function $\phi(t) = \|d\|_{\nabla^2 F(w+td')}^2$ satisfies

$$\phi'(t) \leq k\|d'\| \|d\|_{\nabla^2 F(w+td')}^2 = k\|d'\| \phi(t) \quad \forall w \in \mathcal{C}, d, d' \in (\mathcal{C} - \mathcal{C}) \setminus \{0\}.$$

Hence,

$$\frac{\phi(1)}{\phi(0)} = \exp\left(\int_0^1 \frac{\phi'(t)}{\phi(t)} dt\right) \leq \exp\left(\int_0^1 k\|d'\| dt\right) \leq \exp(kD).$$

Setting $w = w_0$ and $d' = w_1 - w_0$, we reach

$$\frac{\|d\|_{\nabla^2 F(w_1)}^2}{\|d\|_{\nabla^2 F(w_0)}^2} \leq \exp(kD).$$

It immediately follows that $\Gamma(\mathcal{C}) \leq \exp(kD)$.

4. As F is a GLM, the Hessian has the form $\nabla^2 F(w) = \frac{1}{n} A^T \Phi''(Aw) A + \nu I$. Hence with $\hat{\Sigma} = \frac{1}{n} A^T A$, we have by definition of u and ℓ that

$$\ell \hat{\Sigma} + \nu I \preceq \nabla^2 F(w) \preceq u \hat{\Sigma} + \nu I.$$

Thus for any $w_0, w_1 \in \mathcal{C}$ and $d \in (\mathcal{C} - \mathcal{C}) \setminus \{0\}$, we have

$$\frac{\|d\|_{\nabla^2 F(w_1)}^2}{\|d\|_{\nabla^2 F(w_0)}^2} = \frac{\frac{\|d\|_{\frac{1}{n} A^T \Phi''(Aw_1) A}^2}{\|d\|^2} + \nu}{\frac{\|d\|_{\frac{1}{n} A^T \Phi''(Aw_0) A}^2}{\|d\|^2} + \nu} \leq \frac{\frac{u\|d\|_{\hat{\Sigma}}^2}{\|d\|^2} + \nu}{\frac{\ell\|d\|_{\hat{\Sigma}}^2}{\|d\|^2} + \nu} \leq \frac{u\lambda_1(\hat{\Sigma}) + \nu}{\ell\lambda_1(\hat{\Sigma}) + \nu},$$

where the last inequality follows from the variational characterization of $\lambda_1(\hat{\Sigma})$, and that the function

$$h(x) = \frac{ux + \nu}{\ell x + \nu}$$

is monotonically increasing for $x \geq 0$. Thus we conclude

$$\Gamma(\mathcal{C}) \leq \frac{u\lambda_1(\hat{\Sigma}) + \nu}{\ell\lambda_1(\hat{\Sigma}) + \nu},$$

which yields the claim via Lemma 42. ■

C.4 Proofs of Hessian dissimilarity bounds

C.4.1 PROOF OF LEMMA 19

Proof Let $H_i(w) = \nabla^2 F(w)^{-1/2} (\nabla^2 f_i(w) + \nu I) \nabla^2 F(w)^{-1/2}$. We start with the lower bound. Observe for any $w \in \mathcal{C}$ that

$$\begin{aligned} 1 &= \lambda_1 \left(\nabla^2 F(w)^{-1/2} \nabla^2 F(w) \nabla^2 F(w)^{-1/2} \right) = \lambda_1 \left(\nabla^2 F(w)^{-1/2} \left[\frac{1}{n} \sum_{i=1}^n \nabla^2 F_i(w) \right] \nabla^2 F(w)^{-1/2} \right) \\ &= \lambda_1 \left(\frac{1}{n} \sum_{i=1}^n H_i(w) \right) \leq \frac{1}{n} \sum_{i=1}^n \lambda_1(H_i(w)) \leq \max_{1 \leq i \leq n} \lambda_1(H_i(w)) \leq \tau_\star^\nu(\mathcal{C}), \end{aligned}$$

which proves the lower bound. To prove the upper bound, we note that for any $w \in \mathcal{C}$ and $i \in [n]$

$$\nabla^2 F_i(w) \preceq n \nabla^2 F(w), \quad \nabla^2 F_i(w) \preceq (L_{\max} + \nu) I_p.$$

So conjugation gives

$$H_i(w) \preceq n I_p, \quad H_i(w) \preceq (L_{\max} + \nu) \nabla^2 F(w)^{-1} \preceq \frac{(L_{\max} + \nu)}{\nu} I_p$$

which immediately implies $\tau_\star^\nu(\mathcal{C}) \leq \min\{n, 1 + \frac{L_{\max}}{\nu}\}$. ■

C.4.2 PROOF OF PROPOSITION 20

Proof Let $H_i(w) = \nabla^2 F(w)^{-1/2} (\nabla^2 f_i(w) + \nu I) \nabla^2 F(w)^{-1/2}$. As $F(w)$ is a GLM, we have that

$$\begin{aligned} H_i(w) &= \nabla^2 F(w)^{-1/2} (\nabla^2 f_i(w) + \nu I) \nabla^2 F(w)^{-1/2} \\ &= (R^T(w)R(w) + \nu I)^{-1/2} (\phi_i''(a_i^T w) a_i a_i^T + \nu I) (R^T(w)R(w) + \nu I)^{-1/2}, \end{aligned}$$

where $R(w) = \frac{1}{\sqrt{n}} \Phi''(Aw)^{1/2} A$. Hence, a direction calculation yields

$$\begin{aligned} \lambda_1(H_i(w)) &\stackrel{(1)}{\leq} \lambda_1 \left((R^T(w)R(w) + \nu I)^{-1/2} \phi_i''(a_i^T w) a_i a_i^T (R^T(w)R(w) + \nu I)^{-1/2} \right) \\ &\quad + \nu \lambda_1((R^T(w)R(w) + \nu I)^{-1}) \\ &\stackrel{(2)}{\leq} 1 + \phi_i''(a_i^T w) \lambda_1(a_i a_i^T (R^T(w)R(w) + \nu I)^{-1}) \\ &\stackrel{(3)}{\leq} 1 + \phi_i''(a_i^T w) \text{trace}(a_i a_i^T (R^T(w)R(w) + \nu I)^{-1}) \\ &\stackrel{(4)}{=} 1 + \phi_i''(a_i^T w) \text{trace}(a_i^T (R^T(w)R(w) + \nu I)^{-1} a_i) \\ &= 1 + \phi_i''(a_i^T w) a_i^T (R^T(w)R(w) + \nu I)^{-1} a_i \\ &= 1 + (\sqrt{\phi_i''(a_i^T w)} a_i)^T (R^T(w)R(w) + \nu I)^{-1} (\sqrt{\phi_i''(a_i^T w)} a_i) \\ &= 1 + n l_i^\nu(\Phi''(Aw)^{1/2} A), \end{aligned}$$

where (1) uses Weyl's inequalities, (2) uses matrix similarity, (3) uses that the trace is the sum of matrix's eigenvalues and all the eigenvalues are non-negative, and (4) uses the cyclic property of the trace. Hence we conclude

$$\begin{aligned}\tau_\star^\nu &= \sup_{w \in \mathbb{R}^p} \left(\max_{1 \leq i \leq n} \lambda_1(H_i(w)) \right) \leq \sup_{w \in \mathbb{R}^p} \left(1 + n \max_{1 \leq i \leq n} l_i^\nu(\Phi''(Aw)^{1/2}A) \right) = \sup_{w \in \mathbb{R}^p} \left(1 + nl_\infty^\nu(\Phi''(Aw)^{1/2}A) \right) \\ &= 1 + \sup_{w \in \mathbb{R}^p} (\chi^\nu(\Phi''(Aw)^{1/2}A) d_{\text{eff}}^\nu(\Phi''(Aw)^{1/2}A)) \leq 1 + \chi_\star^\nu \sup_{w \in \mathbb{R}^p} d_{\text{eff}}^\nu(\Phi''(Aw)^{1/2}A).\end{aligned}$$

Now, to conclude the desired inequality, observe that

$$\begin{aligned}d_{\text{eff}}^\nu(\Phi''(Aw)^{1/2}A) &= \sum_{j=1}^p \frac{\lambda_j(A^T \Phi''(Aw)A)}{\lambda_j(A^T \Phi''(Aw)A) + n\nu} \leq \sum_{j=1}^p \frac{B\lambda_j(A^T A)}{B\lambda_j(A^T A) + n\nu} \\ &= \sum_{j=1}^p \frac{\lambda_j(A^T A)}{\lambda_j(A^T A) + \frac{n\nu}{B}} = d_{\text{eff}}^{\nu/B}(A),\end{aligned}$$

where the first inequality follows as $A^T \Phi''(Aw)A \preceq BA^T A$ and $\frac{x}{x+\nu}$ is increasing in x for $x \geq 0$. The claim regarding logistic regression and least squares immediately follows by observing that $B = 1$ in both cases. \blacksquare

C.5 Proof of Proposition 21

Proof We only prove the result for the X_j 's, as the argument for the Y_j 's is identical. To this end, observe that

$$\frac{\|w_j - w_\star\|_{P_{j+1}}^2}{\|w_j - w_\star\|_{P_j}^2} \leq \frac{1 + \zeta}{\rho} \frac{\|w_j - w_\star\|_{\nabla^2 F(w_j)}^2}{\|w_j - w_\star\|^2} \leq (1 + \zeta) \frac{L}{\rho}.$$

Hence for any j , with probability 1

$$X_j \leq \max \left\{ 1, (1 + \zeta) \frac{L}{\rho} \right\}.$$

The desired claim now follows immediately for some ξ_j satisfying

$$\xi_j \leq \max \left\{ 1, (1 + \zeta) \frac{L}{\rho} \right\}.$$

\blacksquare

C.6 Proof of Proposition 22

We begin by recalling the following fundamental result from Gower et al. (2019b).

Theorem 43 (Theorem 3.6 and Proposition 3.8, Gower et al. (2019b)) *Suppose $F = \frac{1}{n} \sum_{i=1}^n F_i(w)$, where $F_i : \mathbb{R}^p \mapsto \mathbb{R}$. Let the following conditions hold:*

1. F_i is convex, for every $i \in [n]$.
2. For each $i \in [n]$, there exists a matrix $M_i \in \mathbb{S}_p^{++}(\mathbb{R})$, such that for all $x, h \in \mathbb{R}^p$

$$F_i(w+h) \leq F_i(w) + \langle \nabla F_i(w), h \rangle + \frac{1}{2} \|h\|_{M_i}^2.$$

3. There exists a matrix $M \in \mathbb{S}_p^{++}(\mathbb{R})$, such that for all $x, h \in \mathbb{R}^p$

$$F(w+h) \leq F(w) + \langle \nabla F(w), h \rangle + \frac{1}{2} \|h\|_M^2.$$

Then for any $w, w' \in \mathbb{R}^p$, it holds that

$$\mathbb{E} \|\widehat{\nabla} F(w) - \widehat{\nabla} F(w')\|^2 \leq 2\mathcal{L} (F(w) - F(w') - \langle \nabla F(w'), w - w' \rangle),$$

where

$$\mathcal{L} = \frac{n(b_g - 1)}{b_g(n-1)} \lambda_1(M) + \frac{n - b_g}{b_g(n-1)} \max_{i \in [n]} \lambda_1(M_i).$$

With these preliminaries out of the way, we commence the proof of Proposition 22.

Proof Observe that each F_i satisfies:

$$F_i(w+h) \leq F_i(w) + \langle \nabla F_i(w), h \rangle + \frac{1}{2} \|h\|_{M_i}^2,$$

with $M_i = \gamma_{u_i} \nabla^2 F_i(w_0)$, where w_0 is the point where the preconditioner P is constructed. Hence performing the change of variable $w = P^{-1/2}z$ and defining $F_{P_i}(z) = F_i(P^{-1/2}z)$, $F_P(z) = F(P^{-1/2}z)$, we reach

$$F_{P_i}(z + \tilde{h}) \leq F_{P_i}(z) + \langle \nabla F_{P_i}(z), \tilde{h} \rangle + \frac{\gamma_{u_i}}{2} \|\tilde{h}\|_{\nabla^2 F_{P_i}(z_0)}^2,$$

$$F_P(z + \tilde{h}) \leq F_P(z) + \langle \nabla F_P(z), \tilde{h} \rangle + \frac{\gamma_u}{2} \|\tilde{h}\|_{\nabla^2 F_P(z_0)}^2.$$

Hence the conditions of Theorem 43 are satisfied with $M_i = \gamma_{u_i} \nabla^2 F_{P_i}(z_0)$, $M = \gamma_u \nabla^2 F_P(z_0)$, and so we reach

$$\mathbb{E} \|\widehat{\nabla} F_{P_i}(z) - \widehat{\nabla} F_{P_i}(z')\|^2 \leq 2\mathcal{L} (F_{P_i}(z) - F_{P_i}(z') - \langle \nabla F_{P_i}(z'), z - z' \rangle),$$

with \mathcal{L} as in Theorem 43. Thus, we obtain

$$\mathbb{E} \|\widehat{\nabla} F(w) - \widehat{\nabla} F(w')\|_{P^{-1}}^2 \leq 2\mathcal{L} (F(w) - F(w') - \langle \nabla F(w'), w - w' \rangle).$$

Now,

$$\begin{aligned} \mathcal{L} &= \frac{n(b_g - 1)}{b_g(n-1)} \lambda_1(M) + \frac{n - b_g}{b_g(n-1)} \max_{i \in [n]} \lambda_1(M_i) \\ &= \frac{n(b_g - 1)}{b_g(n-1)} \gamma_u \lambda_1 \left(\frac{1}{n} \sum_{i=1}^n \nabla^2 F_{P_i}(z_0) \right) + \frac{n - b_g}{b_g(n-1)} \max_{i \in [n]} \lambda_1(\gamma_{u_i} \nabla^2 F_{P_i}(z_0)) \\ &\stackrel{(1)}{\leq} \frac{n(b_g - 1)}{b_g(n-1)} \gamma_u (1 + \zeta) + \frac{n - b_g}{b_g(n-1)} \gamma_u^{\max} \lambda_1(\nabla^2 F_{P_i}(z_0)) \\ &\stackrel{(2)}{\leq} \left(\frac{n(b_g - 1)}{b_g(n-1)} \gamma_u + \tau_\star^\nu \frac{n - b_g}{b_g(n-1)} \gamma_u^{\max} \right) (1 + \zeta) = \mathcal{L}_P, \end{aligned}$$

where (1), (2) both use that P is a ζ -spectral approximation, and (2) uses $\nabla^2 F_i(w) \preceq \tau_\nu^* \nabla^2 F(w)$, which follows by definition of τ_ν^* . Hence for all $w, w' \in \mathbb{R}^p$

$$\mathbb{E} \|\widehat{\nabla} F(w) - \widehat{\nabla} F(w')\|_{P^{-1}}^2 \leq 2\mathcal{L}_P (F(w) - F(w') - \langle \nabla F(w'), w - w' \rangle),$$

as desired. ■

C.7 SketchySVRG: Fast local convergence

In this section, we prove Theorem 26, which shows local condition number-free convergence of SketchySVRG in the neighborhood

$$\mathcal{N}_{\varepsilon_0}(w_\star) = \left\{ w \in \mathbb{R}^p : \|w - w_\star\|_{\nabla^2 F(w_\star)} \leq \frac{\varepsilon_0 \nu^{3/2}}{2M} \right\}.$$

The result proven here, substantially improves upon the local convergence result of Dereziński (2022), which requires a gradient batch size of $\tilde{\mathcal{O}}(\kappa)$ to obtain fast local convergence. In contrast, Theorem 26 only requires the gradient batchsize to satisfy $b_g = \tilde{\mathcal{O}}(\tau_\nu^*(\mathcal{N}_{\varepsilon_0}(w_\star)))$, which is often orders of magnitude smaller than κ in the ill-conditioned setting (see Corollary 27).

The overarching idea of the proof is similar to other local analyses of stochastic Newton methods (Li et al., 2020; Dereziński et al., 2021; Dereziński, 2022). Namely, we seek to show the iterates belong to progressively smaller neighborhoods of the optimum, with a rate of contraction that is independent of the condition number. Once this has been done, we convert from convergence in terms of distance to the optimum, to convergence in terms of suboptimality. The key to achieving these objectives, is that the Hessian always provides a good quadratic model in the sense of Lemma 14, when the iterates are close to the optimum.

We start with some standard notation, that will be used throughout the proof.

C.7.1 NOTATION

We define the following quantities:

$$\Delta_k^{(s)} := w_k^{(s)} - w_\star, \quad p_k^{(s)} := \nabla^2 F(w_k^{(s)})^{-1} v_k^{(s)}, \quad \tilde{p}_k^{(s)} := P^{-1} v_k^{(s)}.$$

$\Delta_k^{(s)}$ is the distance of the current iterate to the optimum, $p_k^{(s)}$ is the exact Newton direction, and $\tilde{p}_k^{(s)}$ is the approximate Newton direction actually computed by the algorithm.

C.7.2 PRELIMINARY LEMMAS

We begin with the following technical lemma, which shows the following items hold in $\mathcal{N}_{\varepsilon_0}(w_\star)$: (i) the quadratic regularity constants are close to unity, (ii) the Hessians are uniformly close in the Loewner ordering, (iii) taking an exact Newton step moves the iterate closer to the optimum in the Hessian norm, and (iv) P^{-1} is uniformly good approximation to the inverse Hessian.

Lemma 44 *Let $w, w' \in \mathcal{N}_{\varepsilon_0}(w_\star)$, and suppose P is a ε_0 -spectral approximation constructed at some $w_0 \in \mathcal{N}_{\varepsilon_0}(w_\star)$, then the following items hold.*

1.

$$\frac{1}{1 + \varepsilon_0} \leq \gamma_\ell^{\min}(\mathcal{N}_{\varepsilon_0}(w_\star)) \leq \gamma_u^{\max}(\mathcal{N}_{\varepsilon_0}(w_\star)) \leq (1 + \varepsilon_0).$$

2.

$$(1 - \varepsilon_0)\nabla^2 F(w) \preceq \nabla^2 F(w') \preceq (1 + \varepsilon_0)\nabla^2 F(w).$$

3.

$$\|w - w_\star - \nabla^2 F(w)^{-1} \nabla F(w)\|_{\nabla^2 F(w)} \leq \varepsilon_0 \|w - w_\star\|_{\nabla^2 F(w)}.$$

4.

$$\left\| \nabla^2 F(w)^{1/2} (\nabla^2 F(w)^{-1} - P^{-1}) \nabla^2 F(w)^{1/2} \right\| \leq 3\varepsilon_0.$$

Proof

1. Observing that $\|w - w_\star\| \leq \nu^{-1/2} \|w - w_\star\|_{\nabla^2 F(w_\star)} \leq \varepsilon\nu/M$, and each $\nabla^2 F_i$ has M -Lipschitz Hessian, the first statement follows from item 2. of Proposition 13.
2. For the second statement, observe that F having M -Lipschitz Hessian implies

$$\nabla^2 F(w) - M\|w' - w\|I_p \preceq \nabla^2 F(w') \preceq \nabla^2 F(w) + M\|w' - w\|I_p.$$

So, using $I_p \preceq 1/\nu \nabla^2 F(w)$, we find

$$\|w' - w\| \leq \nu^{-1/2} (\|w' - w_\star\|_{\nabla^2 F(w_\star)} + \|w - w_\star\|_{\nabla^2 F(w_\star)}) \leq \varepsilon_0 \nu/M$$

Hence, we conclude

$$(1 - \varepsilon_0)\nabla^2 F(w) \preceq \nabla^2 F(w') \preceq (1 + \varepsilon_0)\nabla^2 F(w).$$

3. This item follows by direct calculation:

$$\begin{aligned} & \|w - w_\star - \nabla^2 F(w)^{-1} \nabla F(w)\|_{\nabla^2 F(w)} = \|\nabla F(w) - \nabla^2 F(w)(w - w_\star)\|_{\nabla^2 F(w)^{-1}} \\ &= \left\| \int_0^1 [\nabla^2 F(w_\star + t(w - w_\star)) - \nabla^2 F(w)](w - w_\star) dt \right\|_{\nabla^2 F(w)^{-1}} \\ &= \left\| \int_0^1 [\nabla^2 F(w)^{-1/2} \nabla^2 F(w_\star + t(w - w_\star)) \nabla^2 F(w)^{-1/2} - I_p] dt \nabla^2 F(w)^{1/2} (w - w_\star) \right\| \\ &\leq \varepsilon_0 \|w - w_\star\|_{\nabla^2 F(w)}, \end{aligned}$$

where the last inequality uses item 2. and Cauchy-Schwarz.

4. The last item follows directly from the definition of a ε_0 -spectral approximation and item 2. Indeed,

$$(1 - \varepsilon_0)P \preceq \nabla^2 F(w_0) \preceq (1 + \varepsilon_0)P$$

implies

$$(1 + \varepsilon_0)^{-1} \nabla^2 F(w_0) \preceq P \preceq (1 - \varepsilon_0)^{-1} \nabla^2 F(w_0).$$

Hence by the properties of the Loewner ordering

$$(1 - \varepsilon_0)\nabla^2 F(w_0)^{-1} \preceq P^{-1} \preceq (1 + \varepsilon_0)\nabla^2 F(w_0)^{-1}.$$

Now applying item 2., we reach

$$(1 - \varepsilon_0)^2 \nabla^2 F(w)^{-1} \preceq P^{-1} \preceq (1 + \varepsilon_0)^2 \nabla^2 F(w)^{-1}.$$

As $\varepsilon \in (0, 1/6]$, the preceding display becomes

$$(1 - 3\varepsilon_0)\nabla^2 F(w)^{-1} \preceq P^{-1} \preceq (1 + 3\varepsilon_0)\nabla^2 F(w)^{-1},$$

which immediately implies the desired statement. ■

Similar to Dereziński (2022), we will use the following version of Bernstein's inequality for vectors due to Minsker (2017).

Lemma 45 (Minsker (2017) Corollary 4.1) *Let $v_1, \dots, v_m \in \mathbb{R}^p$ be independent mean zero random vectors with $\|v_i\| \leq R$ and $\sum_{i=1}^m \mathbb{E}[\|v_i\|^2] \leq \zeta^2$ almost surely. Then for all $t^2 \geq \zeta^2 + tR/3$, we have*

$$\mathbb{P} \left\{ \left\| \sum_{i=1}^m v_i \right\| \geq t \right\} \leq 28 \exp \left(\frac{-t^2/2}{\zeta^2 + \frac{1}{3}tR} \right).$$

The following corollary, which instantiates Lemma 45 with a specific value of t , will be more convenient for our analysis.

Corollary 46 *Instate the hypotheses of Lemma 45. Let $C \geq 1$ be some constant, such that $\zeta^2 = mR^2/(2C)$. Suppose $t^2 = 2 \left(\zeta^2 + \frac{tR}{3} \right) \log \left(\frac{28}{\delta} \right)$, and that $m \geq C \log(28/\delta)$. Then*

$$\mathbb{P} \left\{ \left\| \sum_{i=1}^m v_i \right\| \geq \sqrt{2\zeta^2 \left(1 + 2\sqrt{\frac{C \log \left(\frac{28}{\delta} \right)}{m}} \right) \log \left(\frac{28}{\delta} \right)} \right\} \leq \delta.$$

Proof The equality defining t can be rearranged, to yield the quadratic equation

$$t^2 - \frac{2R}{3} \log \left(\frac{28}{\delta} \right) t - 2\zeta^2 \log \left(\frac{28}{\delta} \right) = 0.$$

Solving for t by the quadratic formula, and ignoring the spurious root, we find

$$\begin{aligned}
t &= \frac{2R/3 + \sqrt{4/9R^2 \log^2\left(\frac{28}{\delta}\right) + 4\zeta^2 \log\left(\frac{28}{\delta}\right)}}{2} \\
&= 1/3 \left(R + \sqrt{1 + \frac{9\zeta^2}{R^2 \log\left(\frac{28}{\delta}\right)} R \log\left(\frac{28}{\delta}\right)} \right) \\
&= 1/3 \left(R + \sqrt{1 + \frac{9m}{2C \log\left(\frac{28}{\delta}\right)} R \log\left(\frac{28}{\delta}\right)} \right) \\
&= 1/3 \left(R + 3\sqrt{\frac{m \log\left(\frac{28}{\delta}\right)}{C}} R \right) \\
&\leq 3\sqrt{\frac{m \log\left(\frac{28}{\delta}\right)}{C}} R.
\end{aligned}$$

Now, by our choice of t , Bernstein's inequality (Lemma 45) yields

$$\mathbb{P} \left\{ \left\| \sum_{i=1}^m v_i \right\| \geq \sqrt{\left(\zeta^2 + \frac{tR}{3} \right) 2 \log\left(\frac{28}{\delta}\right)} \right\} \leq \delta.$$

Obviously, the preceding inequality must hold for any value that is larger than t . Hence, plugging in our upper bound on t , and using $R^2 = \frac{2C}{b_g} \zeta^2$, we conclude the result. \blacksquare

Our next lemma controls the deviation of the stochastic gradient: $\widehat{\nabla}F(w) - \widehat{\nabla}F(w_\star) - \nabla F(w)$, in the norm $\|\cdot\|_{\nabla^2 F(w')^{-1}}$. This lemma is the key to improving over the local convergence analysis of Dereziński (2022), which requires a gradient batchsize of $\widetilde{\mathcal{O}}(\kappa)$. The improvement is made possible thanks to quadratic regularity and Hessian dissimilarity. Quadratic regularity enables us to directly reason in the dual norm pair $(\|\cdot\|_{\nabla^2 F(w')}, \|\cdot\|_{\nabla^2 F(w')^{-1}})$, while Hessian dissimilarity allows for the tightest control possible over the gradient batchsize.

Lemma 47 *Let $\beta_g \in (0, 1)$. Suppose $w, w' \in \mathcal{N}_{\varepsilon_0}(w_\star)$, and $b_g \geq \frac{10\tau_\star^\nu(\mathcal{N}_{\varepsilon_0}(w_\star)) \log(\frac{28}{\delta})}{\beta_g^2}$. Then with probability at least $1 - \delta$,*

$$\left\| \widehat{\nabla}F(w) - \widehat{\nabla}F(w_\star) - \nabla F(w) \right\|_{\nabla^2 F(w')^{-1}} \leq \beta_g \|w - w_\star\|_{\nabla^2 F(w')}.$$

Proof We begin by observing that

$$\left\| \widehat{\nabla}F(w) - \widehat{\nabla}F(w_\star) - \nabla F(w) \right\|_{\nabla^2 F(w')^{-1}}^2 = \left\| \frac{1}{b_g} \sum_{i \in \mathcal{B}} \tilde{v}_i \right\|^2,$$

where

$$\tilde{v}_i = \nabla^2 F(w')^{-1/2} (\nabla F_i(w) - \nabla F_i(w_\star) - \nabla F(w)).$$

Now,

$$\begin{aligned}
 \|\tilde{v}_i\|^2 &\leq 2\|\nabla F_i(w) - \nabla F_i(w_\star)\|_{\nabla^2 F(w')^{-1}}^2 + 2\|\nabla F(w)\|_{\nabla^2 F(w')^{-1}}^2 \\
 &\leq 2\tau_\star^\nu(\mathcal{N}_{\varepsilon_0}(w_\star))\|\nabla F_i(w) - \nabla F_i(w_\star)\|_{\nabla^2 F_i(w')^{-1}}^2 + 2\|\nabla F(w)\|_{\nabla^2 F(w')^{-1}}^2 \\
 &= 2\tau_\star^\nu(\mathcal{N}_{\varepsilon_0}(w_\star))\|\nabla F_i(w) - \nabla F_i(w_\star)\|_{\nabla^2 F_i(w')^{-1}}^2 + 2\|\nabla F(w) - \nabla F(w_\star)\|_{\nabla^2 F(w')^{-1}}^2,
 \end{aligned}$$

where the second inequality is due to the definition of Hessian dissimilarity. As each F_i is γ_u^{\max} -upper quadratically regular and F is γ_u -upper quadratically regular, we may invoke Proposition 12 to reach

$$\begin{aligned}
 \|\tilde{v}_i\|^2 &\leq 2\tau_\star^\nu(\mathcal{N}_{\varepsilon_0}(w_\star))(\gamma_u^{\max})^2\|w - w_\star\|_{\nabla^2 F_i(w')}^2 + 2\gamma_u^2\|w - w_\star\|_{\nabla^2 F(w')}^2 \\
 &\leq 2(\tau_\star^\nu(\mathcal{N}_{\varepsilon_0}(w_\star))^2(\gamma_u^{\max})^2 + \gamma_u^2)\|w - w_\star\|_{\nabla^2 F(w')}^2 \\
 &\leq 4(1 + \varepsilon_0)^2\tau_\star^\nu(\mathcal{N}_{\varepsilon_0}(w_\star))^2\|w - w_\star\|_{\nabla^2 F(w')}^2,
 \end{aligned}$$

where the last inequality uses item 1 of Lemma 44. So, for each $i \in \mathcal{B}$, it holds with probability 1 that

$$\|\tilde{v}_i\| \leq 2(1 + \varepsilon_0)\tau_\star^\nu(\mathcal{N}_{\varepsilon_0}(w_\star))\|w - w_\star\|_{\nabla^2 F(w')}.$$

Thus, we may set $R = 2(1 + \varepsilon_0)\tau_\star^\nu(\mathcal{N}_{\varepsilon_0}(w_\star))\|w - w_\star\|_{\nabla^2 F(w')}$.

Next, observe that

$$\begin{aligned}
 \mathbb{E}[\|\tilde{v}_i\|^2] &\leq \mathbb{E}\|\nabla F_i(w) - \nabla F_i(w_\star)\|_{\nabla^2 F(w')^{-1}}^2 \\
 &\leq \tau_\star^\nu(\mathcal{N}_{\varepsilon_0}(w_\star))\mathbb{E}\|\nabla F_i(w) - \nabla F_i(w_\star)\|_{\nabla^2 F_i(w')^{-1}}^2 \\
 &\stackrel{(1)}{\leq} \tau_\star^\nu(\mathcal{N}_{\varepsilon_0}(w_\star))\mathbb{E}[2\gamma_{u_{\max}}(F_i(w) - F_i(w_\star) - \langle \nabla F_i(w_\star), w - w_\star \rangle)] \\
 &\stackrel{(2)}{\leq} 2(1 + \varepsilon_0)\tau_\star^\nu(\mathcal{N}_{\varepsilon_0}(w_\star))(F(w) - F(w_\star)) \\
 &\stackrel{(3)}{\leq} 2(1 + \varepsilon_0)^2\tau_\star^\nu(\mathcal{N}_{\varepsilon_0}(w_\star))\|w - w_\star\|_{\nabla^2 F(w')}^2.
 \end{aligned}$$

Here (1) uses F_i is γ_u^{\max} -upper quadratically regular with Lemma 38, (2) uses item 1 of Lemma 44, and (3) uses upper quadratic regularity. Hence, almost surely, the sum of the variances is bounded by

$$\varsigma^2 = 2b_g(1 + \varepsilon_0)^2\tau_\star^\nu(\mathcal{N}_{\varepsilon_0}(w_\star))\|w - w_\star\|_{\nabla^2 F(w')}^2.$$

Now, let us choose t so that $t^2 = 2(\varsigma^2 + \frac{tR}{3})\log(\frac{28}{\delta})$, and observe that $\varsigma^2 = \frac{b_g}{2\tau_\star^\nu}R^2$. Hence, the requirements of Corollary 46 are met with $m = b_g$, $C = \tau_\star^\nu$, and we find

$$\mathbb{P}\left\{\left\|\sum_{i \in \mathcal{B}} \tilde{v}_i\right\| \geq \sqrt{2\varsigma^2 \left(1 + 2\sqrt{\frac{\tau_\star^\nu(\mathcal{N}_{\varepsilon_0}(w_\star))\log(\frac{28}{\delta})}{b_g}}\right) \log\left(\frac{28}{\delta}\right)}\right\} \leq \delta.$$

The last display immediately implies with probability at least $1 - \delta$, that

$$\begin{aligned}
& \left\| \widehat{\nabla} F(w) - \widehat{\nabla} F(w_\star) - \nabla F(w) \right\|_{\nabla^2 F(w')^{-1}}^2 \leq \left(1 + 2\sqrt{\frac{\tau_\star^\nu(\mathcal{N}_{\varepsilon_0}(w_\star)) \log\left(\frac{28}{\delta}\right)}{b_g}} \right) \frac{2\zeta^2 \log(28/\delta)}{b_g^2} \\
& \stackrel{(1)}{\leq} \left(2 + \frac{2}{5}\sqrt{10} \right) \frac{\zeta^2 \log(28/\delta)}{b_g^2} = \left(2 + \frac{2}{5}\sqrt{10} \right) \frac{(1 + \varepsilon_0)^2 \tau_\star^\nu(\mathcal{N}_{\varepsilon_0}(w_\star)) \log(28/\delta)}{b_g} \|w - w_\star\|_{\nabla^2 F(w')}^2 \\
& \stackrel{(2)}{\leq} \frac{9\tau_\star^\nu(\mathcal{N}_{\varepsilon_0}(w_\star)) \log(28/\delta)}{b_g} \|w - w_\star\|_{\nabla^2 F(w')}^2,
\end{aligned}$$

where (1) uses that $b_g \geq \frac{10\tau_\star^\nu(\mathcal{N}_{\varepsilon_0}(w_\star)) \log(\frac{28}{\delta})}{\beta_g^2}$, and (2) uses $\varepsilon_0 \leq 1/6$. The desired claim now follows by taking square roots. \blacksquare

The next lemma shows that for sufficiently b_g (with high probability) the distance to the optimum in the $\nabla^2 F(w_\star)$ -norm decreases when an *exact* Newton step based on the current iterate is taken.

Lemma 48 *Let $w_k^{(s)} \in \mathcal{N}_{\varepsilon_0}(w_\star)$, and $\beta_g \in (0, 1)$. Suppose the gradient batchsize satisfies $b_g = \mathcal{O}\left(\frac{\tau_\star^\nu(\mathcal{N}_{\varepsilon_0}(w_\star)) \log\left(\frac{k+1}{\delta}\right)}{\beta_g^2}\right)$. Then with probability at least $1 - \frac{\delta}{(k+1)^2}$,*

$$\|\Delta_k^{(s)} - p_k^{(s)}\|_{\nabla^2 F(w_\star)} \leq (1 + \varepsilon_0) \left[(\varepsilon_0 + \beta_g) \|\Delta_k^{(s)}\|_{\nabla^2 F(w_\star)} + \beta_g \|\Delta_0^{(s)}\|_{\nabla^2 F(w_\star)} \right].$$

Proof We begin by applying the triangle inequality to reach

$$\begin{aligned}
& \|\Delta_k^{(s)} - p_k^{(s)}\|_{\nabla^2 F(w_k^{(s)})} = \|\Delta_k^{(s)} - \nabla^2 F(w_k^{(s)})^{-1} v_k^{(s)}\|_{\nabla^2 F(w_k^{(s)})} \\
& = \|\nabla^2 F(w_k^{(s)}) \Delta_k^{(s)} - (\widehat{\nabla} F(w_k^{(s)}) - \widehat{\nabla} F(\hat{w}^{(s)}) + \nabla F(\hat{w}^{(s)}))\|_{\nabla^2 F(w_k^{(s)})^{-1}} \\
& \leq \|\nabla^2 F(w_k^{(s)}) \Delta_k^{(s)} - \nabla F(w_k^{(s)})\|_{\nabla^2 F(w_k^{(s)})^{-1}} \\
& + \|\nabla F(w_k^{(s)}) - \widehat{\nabla} F(w_k^{(s)}) + \widehat{\nabla} F(\hat{w}^{(s)}) - \nabla F(\hat{w}^{(s)})\|_{\nabla^2 F(w_k^{(s)})^{-1}}.
\end{aligned}$$

To bound the first term, we apply item 3. of Lemma 44, which yields

$$\|\Delta_k^{(s)} - \nabla^2 F(w_k^{(s)})^{-1} \nabla F(w_k^{(s)})\|_{\nabla^2 F(w_k^{(s)})} \leq \varepsilon_0 \|\Delta_k^{(s)}\|_{\nabla^2 F(w_k^{(s)})}.$$

For the second term, the triangle inequality yields

$$\begin{aligned}
& \|\nabla F(w_k^{(s)}) - \widehat{\nabla} F(w_k^{(s)}) + \widehat{\nabla} F(\hat{w}^{(s)}) - \nabla F(\hat{w}^{(s)})\|_{\nabla^2 F(w_k^{(s)})^{-1}} \\
& \leq \|\widehat{\nabla} F(w_k^{(s)}) - \widehat{\nabla} F(w_\star) - \nabla F(w_k^{(s)})\|_{\nabla^2 F(w_k^{(s)})^{-1}} \\
& + \|\widehat{\nabla} F(\hat{w}^{(s)}) - \widehat{\nabla} F(w_\star) - \nabla F(\hat{w}^{(s)})\|_{\nabla^2 F(w_k^{(s)})^{-1}}.
\end{aligned}$$

Now, we can apply Lemma 47, to find that

$$\begin{aligned} \|\widehat{\nabla}F(w_k^{(s)}) - \widehat{\nabla}F(w_\star) - \nabla F(w_k^{(s)})\|_{\nabla^2 F(w_k^{(s)})^{-1}} &\leq \beta_g \|\Delta_k^{(s)}\|_{\nabla^2 F(w_k^{(s)})}, \\ \|\widehat{\nabla}F(\hat{w}^{(s)}) - \widehat{\nabla}F(w_\star) - \nabla F(\hat{w}^{(s)})\|_{\nabla^2 F(w_k^{(s)})^{-1}} &\leq \beta_g \|\Delta_0^{(s)}\|_{\nabla^2 F(w_k^{(s)})}, \end{aligned}$$

with probability at least $1 - \frac{\delta}{(k+1)^2}$. So,

$$\begin{aligned} &\|\nabla F(w_k^{(s)}) - \widehat{\nabla}F(w_k^{(s)}) + \widehat{\nabla}F(\hat{w}^{(s)}) - \nabla F(\hat{w}^{(s)})\|_{\nabla^2 F(w_k^{(s)})^{-1}} \\ &\leq \beta_g \left(\|\Delta_k^{(s)}\|_{\nabla^2 F(w_k^{(s)})} + \|\Delta_0^{(s)}\|_{\nabla^2 F(w_k^{(s)})} \right), \end{aligned}$$

Combining the upper bounds on terms 1 and 2, we find

$$\|\Delta_k^{(s)} - p_k^{(s)}\|_{\nabla^2 F(w_k^{(s)})} \leq (\varepsilon_0 + \beta_g) \|\Delta_k^{(s)}\|_{\nabla^2 F(w_k^{(s)})} + \beta_g \|\Delta_0^{(s)}\|_{\nabla^2 F(w_k^{(s)})}.$$

Hence applying item 2. of Lemma 44 twice, we conclude

$$\|\Delta_k^{(s)} - p_k^{(s)}\|_{\nabla^2 F(w_\star)} \leq (1 + \varepsilon_0) \left[(\varepsilon_0 + \beta_g) \|\Delta_k^{(s)}\|_{\nabla^2 F(w_\star)} + \beta_g \|\Delta_0^{(s)}\|_{\nabla^2 F(w_\star)} \right],$$

with probability at least $1 - \frac{\delta}{(k+1)^2}$. ■

Next we have the following result, which shows (with high probability) the distance to the optimum of the iterate actually computed by Algorithm 6 is decreasing in the $\nabla^2 F(w_\star)$ -norm. In particular, this implies $w_{k+1}^{(s)}$ remains in $\mathcal{N}_{\varepsilon_0}(w_\star)$.

Lemma 49 *Instate the hypotheses of Lemma 48. Then the following items hold with probability at least $1 - \frac{\delta}{(k+1)^2}$.*

1. $\|\Delta_{k+1}^{(s)}\|_{\nabla^2 F(w_\star)} \leq \frac{7}{12} \|\Delta_k^{(s)}\|_{\nabla^2 F(w_\star)} + \frac{1}{4} \|\Delta_0^{(s)}\|_{\nabla^2 F(w_\star)}$
2. $w_{k+1}^{(s)} \in \mathcal{N}_{\varepsilon_0}(w_\star)$.

Proof To start off, we apply the triangle inequality to reach

$$\|\Delta_{k+1}^{(s)}\|_{\nabla^2 F(w_\star)} \leq \|\Delta_k^{(s)} - p_k^{(s)}\|_{\nabla^2 F(w_\star)} + \|p_k^{(s)} - \tilde{p}_k^{(s)}\|_{\nabla^2 F(w_\star)}.$$

The first term may be bounded by invoking Lemma 48, so for now we focus on bounding the second term, which represents the error from computing an approximate Newton step. To this end, observe that

$$\begin{aligned} \|p_k^{(s)} - \tilde{p}_k^{(s)}\|_{\nabla^2 F(w_\star)} &= \left\| \nabla^2 F(w_k^{(s)})^{1/2} (p_k^{(s)} - \tilde{p}_k^{(s)}) \right\|_{\nabla^2 F(w_k^{(s)})^{-1/2} \nabla^2 F(w_\star) \nabla^2 F(w_k^{(s)})^{-1/2}} \\ &\stackrel{(1)}{\leq} (1 + \varepsilon_0) \left\| \nabla^2 F(w_k^{(s)})^{1/2} (p_k^{(s)} - \tilde{p}_k^{(s)}) \right\| \\ &= (1 + \varepsilon_0) \left\| \nabla^2 F(w_k^{(s)})^{1/2} (\nabla^2 F(w_k^{(s)})^{-1} - P^{-1}) \nabla^2 F(w_k^{(s)})^{1/2} (\nabla^2 F(w_k^{(s)})^{1/2} p_k^{(s)}) \right\| \\ &\stackrel{(2)}{\leq} \frac{21}{6} \varepsilon_0 \|p_k^{(s)}\|_{\nabla^2 F(w_k^{(s)})} \leq 4\varepsilon_0 \|p_k^{(s)}\|_{\nabla^2 F(w_\star)} \\ &\leq 4\varepsilon_0 \left(\|\Delta_k^{(s)}\|_{\nabla^2 F(w_\star)} + \|\Delta_k^{(s)} - p_k^{(s)}\|_{\nabla^2 F(w_\star)} \right), \end{aligned}$$

where (1) uses item 2 of Lemma 44, and (2) uses item 4 of Lemma 44, along with $\varepsilon_0 \leq 1/6$. Combining the preceding upper bound with our initial bound, we reach

$$\|\Delta_{k+1}^{(s)}\|_{\nabla^2 F(w_\star)} \leq (1 + 4\varepsilon_0)\|\Delta_k^{(s)} - p_k^{(s)}\|_{\nabla^2 F(w_\star)} + 4\varepsilon_0\|\Delta_k^{(s)}\|_{\nabla^2 F(w_\star)}.$$

Now, invoking Lemma 48 to bound $\|\Delta_k^{(s)} - p_k^{(s)}\|_{\nabla^2 F(w_\star)}$, we find with probability at least $1 - \delta/(k+1)^2$, that

$$\|\Delta_{k+1}^{(s)}\|_{\nabla^2 F(w_\star)} \leq [(1 + \varepsilon_0)(1 + 4\varepsilon_0)(\varepsilon_0 + \beta_g) + 4\varepsilon_0]\|\Delta_k^{(s)}\|_{\nabla^2 F(w_\star)} + (1 + \varepsilon_0)(1 + 4\varepsilon_0)\beta_g\|\Delta_0^{(s)}\|_{\nabla^2 F(w_\star)}.$$

Using $\varepsilon_0 \leq \frac{1}{6}$, the preceding display becomes

$$\|\Delta_{k+1}^{(s)}\|_{\nabla^2 F(w_\star)} \leq \left(\frac{1}{3} + 2\beta_g\right)\|\Delta_k^{(s)}\|_{\nabla^2 F(w_\star)} + 2\beta_g\|\Delta_0^{(s)}\|_{\nabla^2 F(w_\star)}.$$

Now, let us set $\beta_g = \frac{1}{8}$, then the preceding display simplifies to

$$\|\Delta_{k+1}^{(s)}\|_{\nabla^2 F(w_\star)} \leq \frac{7}{12}\|\Delta_k^{(s)}\|_{\nabla^2 F(w_\star)} + \frac{1}{4}\|\Delta_0^{(s)}\|_{\nabla^2 F(w_\star)},$$

which proves the first claim. To see the second claim, note that

$$\max\{\|\Delta_k^{(s)}\|_{\nabla^2 F(w_\star)}, \|\Delta_0^{(s)}\|_{\nabla^2 F(w_\star)}\} \leq \varepsilon_0 D^{3/2}/(2M),$$

as $w_k^{(s)}, \hat{w}^{(s)} \in \mathcal{N}_{\varepsilon_0}(w_\star)$. Hence, the second claim follows immediately from the first. \blacksquare

Lemma 50 (One-stage analysis) *Let $\hat{w}^{(s)} \in \mathcal{N}_{\varepsilon_0}(w_\star)$. Suppose Algorithm 6 is with $m = 6$ inner iterations and with gradient batchsize satisfies $b_g = \mathcal{O}(\tau_\star^\nu(\mathcal{N}_{\varepsilon_0}(w_\star)) \log(\frac{m+1}{\delta}))$. Then with probability at least $1 - \delta$:*

1. $\hat{w}^{(s+1)} \in \mathcal{N}_{\frac{2}{3}\varepsilon_0}(w_\star)$
2. $F(\hat{w}^{(s+1)}) - F(w_\star) \leq \frac{3}{5}(F(\hat{w}^{(s)}) - F(w_\star))$

Proof As $\hat{w}^{(s)} \in \mathcal{N}_{\varepsilon_0}(w_\star)$, it follows by union bound that the conclusions of Lemma 49 hold for all $w_k^{(s)}$, where $k \in \{0, \dots, m-1\}$, with probability at least

$$1 - \sum_{k=0}^{m-1} \frac{\delta}{(m+1)^2} = 1 - \frac{m}{(m+1)^2}\delta \geq 1 - \delta.$$

Consequently,

$$\|\Delta_m^{(s)}\|_{\nabla^2 F(w_\star)} \leq \frac{7}{12}\|\Delta_{m-1}^{(s)}\|_{\nabla^2 F(w_\star)} + \frac{1}{16}\|\Delta_0^{(s)}\|_{\nabla^2 F(w_\star)}.$$

We now recurse on the previous display, and use $m = 6 > \frac{\log(1/15)}{\log(7/12)}$, to reach

$$\begin{aligned} \|\Delta_m^{(s)}\|_{\nabla^2 F(w_\star)} &\leq \left(\frac{7}{12}\right)^m \|\Delta_0^{(s)}\|_{\nabla^2 F(w_\star)} + \left(\sum_{k=0}^{m-1} \left(\frac{7}{12}\right)^k\right) \frac{1}{4} \|\Delta_0^{(s)}\|_{\nabla^2 F(w_\star)} \\ &\leq \frac{1}{5} \|\Delta_0^{(s)}\|_{\nabla^2 F(w_\star)} + \frac{1}{4(1 - \frac{7}{12})} \|\Delta_0^{(s)}\|_{\nabla^2 F(w_\star)} \\ &= \left(\frac{1}{15} + \frac{3}{5}\right) \|\Delta_0^{(s)}\|_{\nabla^2 F(w_\star)} \leq \frac{2}{3} \|\Delta_0^{(s)}\|_{\nabla^2 F(w_\star)}. \end{aligned}$$

Hence $\hat{w}^{(s+1)} = w_m^{(s)} \in \mathcal{N}_{\frac{2}{3}\varepsilon_0}(w_\star)$. Using this last inclusion, and applying upper quadratic regularity, followed by lower quadratic regularity, we find

$$\begin{aligned} F(\hat{w}^{(s+1)}) - F(w_\star) &\leq \frac{1 + \varepsilon_0}{2} \|\Delta_m^{(s)}\|_{\nabla^2 F(w_\star)}^2 \leq \frac{1 + \varepsilon_0}{2} \frac{4}{9} \|\Delta_0^{(s)}\|_{\nabla^2 F(w_\star)}^2 \\ &\leq (1 + \varepsilon_0)^2 \frac{4}{9} \left(F(\hat{w}^{(s)}) - F(w_\star)\right) \leq \frac{2}{3} \left(F(\hat{w}^{(s)}) - F(w_\star)\right), \end{aligned}$$

as desired. ■

C.7.3 PROOF OF THEOREM 26

We now come to the proof of Theorem 26, which is reduced to union bounding over the conclusion of Lemma 50.

Proof By hypothesis, we may invoke Lemma 50 to conclude the output of the first outer iteration satisfies

$$F(\hat{w}^{(1)}) - F(w_\star) \leq \frac{2}{3} (F(w_0) - F(w_\star)), \quad \text{and } \hat{w}^{(1)} \in \mathcal{N}_{\varepsilon_0}(w_\star)$$

with probability at least $1 - \delta$. Hence we can apply Lemma 50 again to $\hat{w}^{(s)}$, the output of the second outer iteration. Repeating this logic for all the remaining outer iterations, we find by union bound, that with probability at least $1 - s\delta$,

$$F(\hat{w}^{(s)}) - F(w_\star) \leq \left(\frac{2}{3}\right)^s (F(w_0) - F(w_\star)) \leq \epsilon.$$

The theorem now follows by scaling δ down by $3 \log((F(w_0) - F(w_\star))/\epsilon)$. ■

C.8 SketchySAGA

In this subsection, we prove convergence of SketchySAGA (Algorithm 7). The convergence analysis is based on a Lyapunov function argument, with the Lyapunov function defined in the main text. We note, that unlike the proofs of the previous theorems, the intuition behind the convergence argument is less obvious, which is often the case with Lyapunov function based arguments.

C.8.1 NOTATION

Throughout this section, we shall need the following quantities:

$$\tilde{\gamma}_\ell^{\min} = (1 - \zeta)\gamma_\ell^{\min}, \quad \kappa_P = n + \frac{\mathcal{L}_P}{\tilde{\gamma}_\ell^{\min}}.$$

C.8.2 PRELIMINARY LEMMAS

We start by observing that all the F_i 's are quadratically regular.

Lemma 51 (F_i 's are quadratically regular) *Instate the hypotheses of Assumption 1. Then F_i is quadratically regular for each $i \in [n]$.*

Proof By definition $F_i(w) = f_i(w) + \frac{\nu}{2}\|w\|^2$, hence it smooth and strongly convex. Thus, $F_i(w)$ is quadratically regular by Proposition 13. \blacksquare

For the remaining lemmas, we will always assume that Assumption 1 holds, so the F_i 's will immediately be quadratically regular by Lemma 51.

Lemma 52 *Instate the hypotheses of Assumptions 1 and 2. Then for any iteration k and for all $x, y \in \mathbb{R}^p$,*

$$F_i(y) \leq F_i(x) + \langle \nabla F_i(x), y - x \rangle + \frac{\mathcal{L}_P}{2} \|y - x\|_{P_k}^2.$$

Proof As each F_i is γ_u^{\max} -upper quadratically regular, and $\mathcal{L}_P = (1 + \zeta)\tau_\star^\nu \gamma_u^{\max}$, the claim immediately follows from Lemma 16. \blacksquare

Lemma 53 *Instate the hypotheses of Assumptions 1 and 2. Then for any iteration k and for all $x, y \in \mathbb{R}^p$,*

$$F(y) \leq F(x) + \langle \nabla F(x), y - x \rangle + \frac{1}{2(1 - \zeta)\gamma_\ell} \|\nabla F(y) - \nabla F(x)\|_{P_k^{-1}}^2.$$

Proof Define $g_x(z) = F(z) - F(x) - \langle \nabla F(x), z - x \rangle$. We have $\nabla g_x(x) = \nabla F(x) - \nabla F(x) = 0$. Since g is convex, $0 = g_x(x) = \min_v g_x(v)$. Furthermore, since F is γ_ℓ lower-quadratically regular, g_x is γ_ℓ lower-quadratically regular.

Therefore,

$$\begin{aligned} 0 &= \min_v g_x(v) \geq \min_v [g_x(y) + \langle \nabla g_x(y), v - y \rangle + \frac{\gamma_\ell}{2} \|v - y\|_{\nabla^2 F(w_k)}^2] \\ &\geq \min_v [g_x(y) + \langle \nabla g_x(y), v - y \rangle + \frac{(1 - \zeta)\gamma_\ell}{2} \|v - y\|_{P_k}^2] \\ &= g_x(y) - \frac{1}{2(1 - \zeta)\gamma_\ell} \|\nabla g_x(y)\|_{P_k^{-1}}^2 \\ &= F(y) - F(x) - \langle \nabla F(x), y - x \rangle - \frac{1}{2(1 - \zeta)\gamma_\ell} \|\nabla F(y) - \nabla F(x)\|_{P_k^{-1}}^2, \end{aligned}$$

where the first inequality follows from g_x being γ_ℓ lower-quadratically regular, and the second inequality follows from Assumption 2. Rearranging the final display yields the result. \blacksquare

Lemma 54 *Instate the hypotheses of Assumptions 1 and 2. Then for any iteration k and for all $w \in \mathbb{R}^p$,*

$$\begin{aligned} \langle \nabla F(w), w_\star - w \rangle &\leq \frac{\mathcal{L}_P - \tilde{\gamma}_\ell^{\min}}{\mathcal{L}_P} [F(w_\star) - F(w)] - \frac{\tilde{\gamma}_\ell^{\min}}{2} \|w_\star - w\|_{P_k}^2 \\ &\quad - \frac{1}{2\mathcal{L}_P n} \sum_{i=1}^n \|\nabla F_i(w_\star) - \nabla F_i(w)\|_{P_k^{-1}}^2. \end{aligned}$$

Proof Define $g_i(w) = F_i(w) - \frac{(1-\zeta)\gamma_\ell^{\min}}{2} \|w\|_{P_k}^2 = F_i(w) - \frac{\tilde{\gamma}_\ell^{\min}}{2} \|w\|_{P_k}^2$. Since F_i is γ_{ℓ_i} lower-quadratically regular and Assumption 2 holds, g_i is convex. Furthermore, since F_i is γ_{u_i} upper-quadratically regular, we use Lemma 52 to conclude g_i is $(\mathcal{L}_P - \tilde{\gamma}_\ell^{\min})$ -smooth in the P_k -norm, i.e.,

$$g_i(x) \leq g_i(y) + \langle \nabla g_i(y), x - y \rangle + \frac{\mathcal{L}_P - \tilde{\gamma}_\ell^{\min}}{2} \|x - y\|_{P_k}^2$$

for all $x, y \in \mathbb{R}^p$. Hence by Lemma 38, we have

$$g_i(x) \geq g_i(y) + \langle \nabla g_i(y), x - y \rangle + \frac{1}{2(\mathcal{L}_P - \tilde{\gamma}_\ell^{\min})} \|\nabla g_i(x) - \nabla g_i(y)\|_{P_k^{-1}}^2. \quad (32)$$

Substituting the definition of g_i into Eq. (32), we find

$$\begin{aligned} F_i(x) &\geq \frac{\tilde{\gamma}_\ell^{\min}}{2} \|x\|_{P_k}^2 + F_i(y) - \frac{\tilde{\gamma}_\ell^{\min}}{2} \|y\|_{P_k}^2 + \langle \nabla F_i(y) - \tilde{\gamma}_\ell^{\min} P_k y, x - y \rangle \\ &\quad + \frac{1}{2(\mathcal{L}_P - \tilde{\gamma}_\ell^{\min})} \|\nabla F_i(x) - \nabla F_i(y) - \tilde{\gamma}_\ell^{\min} P_k(x - y)\|_{P_k^{-1}}^2 \\ &= F_i(y) + \langle \nabla F_i(y), x - y \rangle + \frac{\tilde{\gamma}_\ell^{\min}}{2} [\|x\|_{P_k}^2 - \|y\|_{P_k}^2 - 2\langle P_k y, x - y \rangle] \\ &\quad + \frac{1}{2(\mathcal{L}_P - \tilde{\gamma}_\ell^{\min})} \|\nabla F_i(x) - \nabla F_i(y)\|_{P_k^{-1}}^2 + \frac{\tilde{\gamma}_\ell^{\min}}{\mathcal{L}_P - \tilde{\gamma}_\ell^{\min}} \langle \nabla F_i(x) - \nabla F_i(y), y - x \rangle \\ &\quad + \frac{(\tilde{\gamma}_\ell^{\min})^2}{2(\mathcal{L}_P - \tilde{\gamma}_\ell^{\min})} \|x - y\|_{P_k}^2 \\ &= F_i(y) + \langle \nabla F_i(y), x - y \rangle + \frac{1}{2(\mathcal{L}_P - \tilde{\gamma}_\ell^{\min})} \|\nabla F_i(x) - \nabla F_i(y)\|_{P_k^{-1}}^2 \\ &\quad + \frac{\tilde{\gamma}_\ell^{\min} \mathcal{L}_P}{2(\mathcal{L}_P - \tilde{\gamma}_\ell^{\min})} \|y - x\|_{P_k}^2 + \frac{\tilde{\gamma}_\ell^{\min}}{\mathcal{L}_P - \tilde{\gamma}_\ell^{\min}} \langle \nabla F_i(x) - \nabla F_i(y), y - x \rangle. \end{aligned}$$

Setting $x = w_\star$, $y = w$, averaging over the F_i 's, and using $\nabla F(w_\star) = 0$, we obtain the claimed result. \blacksquare

Lemma 55 *Instate the hypotheses of Assumptions 1 and 2. Suppose each F_i is γ_{u_i} upper-quadratically regular. Then for any iteration k , and for all $\psi^i \in \mathbb{R}^p$,*

$$\frac{1}{n} \sum_{i=1}^n \|\nabla F_i(\psi^i) - \nabla F_i(w_\star)\|_{P_k^{-1}}^2 \leq 2\mathcal{L}_P \left[\frac{1}{n} \sum_{i=1}^n F_i(\psi^i) - F(w_\star) - \frac{1}{n} \sum_{i=1}^n \langle \nabla F_i(w_\star), \psi^i - w_\star \rangle \right].$$

Proof Using Lemma 52 and Lemma 38, we have

$$F_i(y) \geq F_i(x) + \langle \nabla F_i(x), y - x \rangle + \frac{1}{2\mathcal{L}_P} \|\nabla F_i(y) - \nabla F_i(x)\|_{P_k^{-1}}^2$$

for all $x, y \in \mathbb{R}^p$. Rearranging this inequality and using $y = \psi^i$ and $x = w_\star$ gives

$$\|\nabla F_i(\psi^i) - \nabla F_i(w_\star)\|_{P_k^{-1}}^2 \leq 2\mathcal{L}_P [F_i(\psi^i) - F_i(w_\star) - \langle \nabla F_i(w_\star), \psi^i - w_\star \rangle].$$

Summing over $i = 1, 2, \dots, n$ and dividing by n yields

$$\frac{1}{n} \sum_{i=1}^n \|\nabla F_i(\psi^i) - \nabla F_i(w_\star)\|_{P_k^{-1}}^2 \leq 2\mathcal{L}_P \left[\frac{1}{n} \sum_{i=1}^n F_i(\psi^i) - F(w_\star) - \frac{1}{n} \sum_{i=1}^n \langle \nabla F_i(w_\star), \psi^i - w_\star \rangle \right].$$

■

Lemma 56 *For any ψ_k^i, w_\star, w_k and $\alpha > 0$, with w_{k+1} defined as in Algorithm 7, we have*

$$\begin{aligned} \mathbb{E} \|w_{k+1} - w_k\|_{P_k}^2 &\leq \eta^2 (1 + \alpha^{-1}) \mathbb{E} \|\nabla F_j(\psi_k^j) - \nabla F_j(w_\star)\|_{P_k^{-1}}^2 \\ &\quad + \eta^2 (1 + \alpha) \mathbb{E} \|\nabla F_j(w_k) - \nabla F_j(w_\star)\|_{P_k^{-1}}^2 - \eta^2 \alpha \|\nabla F(w_k)\|_{P_k^{-1}}^2. \end{aligned}$$

Proof By the definition of the SketchySAGA update,

$$\begin{aligned} &\mathbb{E} \|w_{k+1} - w_k\|_{P_k}^2 \\ &= \mathbb{E} \left\| P_k^{-1} \left(-\frac{\eta}{n} \sum_{i=1}^n \nabla F_i(\psi_k^i) + \eta [\nabla F_j(\psi_k^j) - \nabla F_j(w_k)] \right) \right\|_{P_k}^2 \\ &= \mathbb{E} \left\| -\frac{\eta}{n} \sum_{i=1}^n \nabla F_i(\psi_k^i) + \eta [\nabla F_j(\psi_k^j) - \nabla F_j(w_k)] \right\|_{P_k^{-1}}^2 \\ &= \eta^2 \mathbb{E} \left\| \left(\nabla F_j(\psi_k^j) - \nabla F_j(w_\star) - \frac{1}{n} \sum_{i=1}^n \nabla F_i(\psi_k^i) \right) - (\nabla F_j(w_k) - \nabla F_j(w_\star) - \nabla F(w_k)) \right\|_{P_k^{-1}}^2 \\ &\quad + \eta^2 \|\nabla F(w_k)\|_{P_k^{-1}}^2, \end{aligned}$$

where the final equality follows from using $\mathbb{E}[\nabla F_j(\psi_k^j) - \frac{1}{n} \sum_{i=1}^n \nabla F_i(\psi_k^i) - \nabla F_j(w_k)] = -\nabla F(w_k)$ and the identity $\mathbb{E} \|X\|_A^2 = \mathbb{E} \|X - \mathbb{E}X\|_A^2 + \|\mathbb{E}X\|_A^2$. Using the facts (1) $\|x + y\|_A^2 \leq$

$(1 + \alpha^{-1})\|x\|_A^2 + (1 + \alpha)\|y\|_A^2$, (2) $\mathbb{E}\|X - \mathbb{E}X\|_A^2 \leq \mathbb{E}\|X\|_A^2$, and (3) $\mathbb{E}\|X\|_A^2 = \mathbb{E}\|X - \mathbb{E}X\|_A^2 + \|\mathbb{E}X\|_A^2$, we find

$$\begin{aligned}
 & \eta^2 \mathbb{E} \left\| \left(\nabla F_j(\psi_k^j) - \nabla F_j(w_\star) - \frac{1}{n} \sum_{i=1}^n \nabla F_i(\psi_k^i) \right) - (\nabla F_j(w_k) - \nabla F_j(w_\star) - \nabla F(w_k)) \right\|_{P_k^{-1}}^2 \\
 & + \eta^2 \|\nabla F(w_k)\|_{P_k^{-1}} \\
 \stackrel{(1)}{\leq} & \eta^2 (1 + \alpha^{-1}) \mathbb{E} \left\| \nabla F_j(\psi_k^j) - \nabla F_j(w_\star) - \frac{1}{n} \sum_{i=1}^n \nabla F_i(\psi_k^i) \right\|_{P_k^{-1}}^2 \\
 & + \eta^2 (1 + \alpha) \mathbb{E} \|\nabla F_j(w_k) - \nabla F_j(w_\star) - \nabla F(w_k)\|_{P_k^{-1}}^2 + \eta^2 \|\nabla F(w_k)\|_{P_k^{-1}} \\
 \stackrel{(2)}{\leq} & \eta^2 (1 + \alpha^{-1}) \mathbb{E} \left\| \nabla F_j(\psi_k^j) - \nabla F_j(w_\star) \right\|_{P_k^{-1}}^2 \\
 & + \eta^2 (1 + \alpha) \mathbb{E} \|\nabla F_j(w_k) - \nabla F_j(w_\star) - \nabla F(w_k)\|_{P_k^{-1}}^2 + \eta^2 \|\nabla F(w_k)\|_{P_k^{-1}} \\
 \stackrel{(3)}{=} & \eta^2 (1 + \alpha^{-1}) \mathbb{E} \|\nabla F_j(\psi_k^j) - \nabla F_j(w_\star)\|_{P_k^{-1}}^2 \\
 & + \eta^2 (1 + \alpha) \mathbb{E} \|\nabla F_j(w_k) - \nabla F_j(w_\star)\|_{P_k^{-1}}^2 - \eta^2 \alpha \|\nabla F(w_k)\|_{P_k^{-1}}^2.
 \end{aligned}$$

■

Lemma 57 (Contraction lemma) *Instate the hypotheses of Assumptions 1 and 2. Then*

$$\mathbb{E}_k[T_{k+1}] \leq \left(1 - \frac{1}{2(n + \kappa_P)}\right) \beta_k T_k,$$

where $\kappa_P = \frac{\mathcal{L}_P}{\tilde{\gamma}_\ell^{\min}} = \frac{\mathcal{L}_P}{(1-\zeta)\gamma_\ell^{\min}}$ and β_k is defined as in Proposition 21.

Proof By the definition of T_j for general j , we can write T_{k+1} as

$$T_{k+1} = B_{k+1} \left(\frac{1}{n} \sum_{i=1}^n F_i(\psi_{k+1}^i) - F(w_\star) - \frac{1}{n} \sum_{i=1}^n \langle \nabla F_i(w_\star), \psi_{k+1}^i - w_\star \rangle + c \|w_{k+1} - w_\star\|_{P_k}^2 \right).$$

The expectations of the first and third terms of T_{k+1} simplify as follows:

$$\begin{aligned}
 \mathbb{E} \left[\frac{1}{n} \sum_{i=1}^n F_i(\psi_{k+1}^i) \right] &= \frac{1}{n} F(w_k) + \left(1 - \frac{1}{n}\right) \frac{1}{n} \sum_{i=1}^n F_i(\psi_k^i) \\
 \mathbb{E} \left[\frac{1}{n} \sum_{i=1}^n \langle \nabla F_i(w_\star), \psi_{k+1}^i - w_\star \rangle \right] &= \left(1 - \frac{1}{n}\right) \frac{1}{n} \sum_{i=1}^n \langle \nabla F_i(w_\star), \psi_k^i - w_\star \rangle.
 \end{aligned}$$

We now bound the expectation of the final term in T_{k+1} ,

$$\begin{aligned}
& c\mathbb{E}\|w_{k+1} - w_\star\|_{P_k}^2 \\
&= c\mathbb{E}\|w_k - w_\star + w_{k+1} - w_k\|_{P_k}^2 \\
&= c\|w_k - w_\star\|_{P_k}^2 + 2c\mathbb{E}\langle w_{k+1} - w_k, w_k - w_\star \rangle_{P_k} + c\mathbb{E}\|w_{k+1} - w_k\|_{P_k}^2 \\
&= c\|w_k - w_\star\|_{P_k}^2 + 2c\langle -\eta P_k^{-1} \nabla F(w_k), w_k - w_\star \rangle_{P_k} + c\mathbb{E}\|w_{k+1} - w_k\|_{P_k}^2 \\
&= c\|w_k - w_\star\|_{P_k}^2 - 2c\eta \langle \nabla F(w_k), w_k - w_\star \rangle + c\mathbb{E}\|w_{k+1} - w_k\|_{P_k}^2 \\
&\leq c\|w_k - w_\star\|_{P_k}^2 - 2c\eta \langle \nabla F(w_k), w_k - w_\star \rangle - c\eta^2 \alpha \|\nabla F(w_k)\|_{P_k^{-1}}^2 \\
&\quad + c\eta^2(1 + \alpha^{-1})\mathbb{E}\|\nabla F_j(\psi_k^j) - \nabla F_j(w_\star)\|_{P_k^{-1}}^2 + c\eta^2(1 + \alpha)\mathbb{E}\|\nabla F_j(w_k) - \nabla F_j(w_\star)\|_{P_k^{-1}}^2,
\end{aligned}$$

where the third equality follows from the definition of the SketchySAGA update, and the inequality follows from applying Lemma 56. We will set the value of α later in the proof to reach the claimed result. Using Lemma 54 to bound $-2c\eta \langle \nabla F(w_k), w_k - w_\star \rangle$ and Lemma 55 to bound $\mathbb{E}\|\nabla F_j(\psi_k^j) - \nabla F_j(w_\star)\|_{P_k^{-1}}^2$, we obtain

$$\begin{aligned}
c\mathbb{E}\|w_{k+1} - w_\star\|_{P_k}^2 &\leq c(1 - \eta\tilde{\gamma}_\ell^{\min})\|w_k - w_\star\|_{P_k}^2 + \left((1 + \alpha)c\eta^2 - \frac{c\eta}{\mathcal{L}_P} \right) \mathbb{E}\|\nabla F_j(w_k) - \nabla F_j(w_\star)\|_{P_k^{-1}}^2 \\
&\quad - \frac{2c\eta(\mathcal{L}_P - \tilde{\gamma}_\ell^{\min})}{\mathcal{L}_P} [F(w_k) - F(w_\star)] - c\eta^2 \alpha \|\nabla F(w_k)\|_{P_k^{-1}}^2 \\
&\quad + 2c\eta^2(1 + \alpha^{-1})\mathcal{L}_P \text{Breg}_k
\end{aligned}$$

where we have defined $\text{Breg}_k := \frac{1}{n} \sum_{i=1}^n F_i(\psi_k^i) - F(w_\star) - \frac{1}{n} \sum_{i=1}^n \langle \nabla F_i(w_\star), \psi_k^i - w_\star \rangle$ for notational convenience. We now apply backwards stable evolution (Proposition 21) and Lemma 53 with $x = w_\star, y = w_k, \gamma = \gamma_{\ell_{\min}}$, from which we find

$$\begin{aligned}
c\mathbb{E}\|w_{k+1} - w_\star\|_{P_k}^2 &\leq \frac{c(1 - \eta\tilde{\gamma}_\ell^{\min})}{\beta_k} \|w_k - w_\star\|_{P_{k-1}}^2 \\
&\quad + \left((1 + \alpha)c\eta^2 - \frac{c\eta}{\mathcal{L}_P} \right) \mathbb{E}\|\nabla F_j(w_k) - \nabla F_j(w_\star)\|_{P_k^{-1}}^2 \\
&\quad + \left(-\frac{2c\eta(\mathcal{L}_P - \tilde{\gamma}_\ell^{\min})}{\mathcal{L}_P} - 2c\eta^2 \tilde{\gamma}_\ell^{\min} \alpha \right) [F(w_k) - F(w_\star)] \\
&\quad + 2c\eta^2(1 + \alpha^{-1})\mathcal{L}_P \text{Breg}_k.
\end{aligned}$$

Now we combine the bounds we have computed for the terms in $\mathbb{E}T_{k+1}$:

$$\begin{aligned}
\mathbb{E}T_{k+1} &\leq B_{k+1} \left(\frac{1}{n} F(w_k) + \left(1 - \frac{1}{n}\right) \frac{1}{n} \sum_{i=1}^n F_i(\psi_k^i) - F(w_\star) - \left(1 - \frac{1}{n}\right) \frac{1}{n} \sum_{i=1}^n \langle \nabla F_i(w_\star), \psi_k^i - w_\star \rangle \right) \\
&\quad + B_{k+1} \frac{c(1 - \eta\tilde{\gamma}_\ell^{\min})}{\beta_k} \|w_k - w_\star\|_{P_{k-1}}^2 + B_{k+1} \left((1 + \alpha)c\eta^2 - \frac{c\eta}{\mathcal{L}_P} \right) \mathbb{E}\|\nabla F_j(w_k) - \nabla F_j(w_\star)\|_{P_k^{-1}}^2 \\
&\quad + B_{k+1} \left(-\frac{2c\eta(\mathcal{L}_P - \tilde{\gamma}_\ell^{\min})}{\mathcal{L}_P} - 2c\eta^2 \tilde{\gamma}_\ell^{\min} \alpha \right) [F(w_k) - F(w_\star)] \\
&\quad + 2B_{k+1}c\eta^2(1 + \alpha^{-1})\mathcal{L}_P \text{Breg}_k.
\end{aligned}$$

Applying the definitions of T_k and B_k in the previous display, we obtain

$$\begin{aligned}
 \mathbb{E}T_{k+1} &\leq \frac{B_{k+1}}{n}F(w_k) - \frac{B_{k+1}}{n}F(w_\star) + \frac{B_{k+1}}{B_k}T_k \\
 &\quad - \frac{B_{k+1}}{n} \left(\frac{1}{n} \sum_{i=1}^n F_i(\psi_k^i) - F(w_\star) - \frac{1}{n} \sum_{i=1}^n \langle \nabla F_i(w_\star), \psi_k^i - w_\star \rangle \right) \\
 &\quad + c \left((1 - \eta \tilde{\gamma}_\ell^{\min}) \frac{B_{k+1}}{\beta_k} - B_{k+1} \right) \|w_k - w_\star\|_{P_{k-1}}^2 \\
 &\quad + B_{k+1} \left((1 + \alpha)c\eta^2 - \frac{c\eta}{\mathcal{L}_P} \right) \mathbb{E}\|\nabla F_j(w_k) - \nabla F_j(w_\star)\|_{P_k}^2 \\
 &\quad + B_{k+1} \left(-\frac{2c\eta(\mathcal{L}_P - \tilde{\gamma}_\ell^{\min})}{\mathcal{L}_P} - 2c\eta^2\tilde{\gamma}_\ell^{\min}\alpha \right) [F(w_k) - F(w_\star)] \\
 &\quad + 2B_{k+1}c\eta^2(1 + \alpha^{-1})\mathcal{L}_P \mathbf{Breg}_k \\
 &= \frac{B_{k+1}}{B_k}T_k + c \left((1 - \eta \tilde{\gamma}_\ell^{\min}) \frac{B_{k+1}}{\beta_k} - B_{k+1} \right) \|w_k - w_\star\|_{P_{k-1}}^2 \\
 &\quad + B_{k+1} \left((1 + \alpha)c\eta^2 - \frac{c\eta}{\mathcal{L}_P} \right) \mathbb{E}\|\nabla F_j(w_k) - \nabla F_j(w_\star)\|_{P_k}^2 \\
 &\quad + B_{k+1} \left(\frac{1}{n} - \frac{2c\eta(\mathcal{L}_P - \tilde{\gamma}_\ell^{\min})}{\mathcal{L}_P} - 2c\eta^2\tilde{\gamma}_\ell^{\min}\alpha \right) [F(w_k) - F(w_\star)] \\
 &\quad + B_{k+1} \left(2c\eta^2(1 + \alpha^{-1})\mathcal{L}_P - \frac{1}{n} \right) \mathbf{Breg}_k \\
 &= \beta_k T_k + c(1 - \eta \tilde{\gamma}_\ell^{\min} - \beta_k)B_k \|w_k - w_\star\|_{P_{k-1}}^2 \\
 &\quad + B_{k+1} \left((1 + \alpha)c\eta^2 - \frac{c\eta}{\mathcal{L}_P} \right) \mathbb{E}\|\nabla F_j(w_k) - \nabla F_j(w_\star)\|_{P_k}^2 \\
 &\quad + B_{k+1} \left(\frac{1}{n} - \frac{2c\eta(\mathcal{L}_P - \tilde{\gamma}_\ell^{\min})}{\mathcal{L}_P} - 2c\eta^2\tilde{\gamma}_\ell^{\min}\alpha \right) [F(w_k) - F(w_\star)] \\
 &\quad + B_{k+1} \left(2c\eta^2(1 + \alpha^{-1})\mathcal{L}_P - \frac{1}{n} \right) \mathbf{Breg}_k \\
 &= \left(1 - \frac{1}{\kappa} \right) \beta_k T_k + c(1 - \eta \tilde{\gamma}_\ell^{\min} - \beta_k + \frac{1}{\kappa}\beta_k)B_k \|w_k - w_\star\|_{P_{k-1}}^2 \\
 &\quad + B_{k+1} \left((1 + \alpha)c\eta^2 - \frac{c\eta}{\mathcal{L}_P} \right) \mathbb{E}\|\nabla F_j(w_k) - \nabla F_j(w_\star)\|_{P_k}^2 \\
 &\quad + B_{k+1} \left(\frac{1}{n} - \frac{2c\eta(\mathcal{L}_P - \tilde{\gamma}_\ell^{\min})}{\mathcal{L}_P} - 2c\eta^2\tilde{\gamma}_\ell^{\min}\alpha \right) [F(w_k) - F(w_\star)] \\
 &\quad + B_{k+1} \left(2c\eta^2(1 + \alpha^{-1})\mathcal{L}_P - \frac{1}{n} + \frac{1}{\kappa} \right) \mathbf{Breg}_k
 \end{aligned}$$

Notice that the four quantities $\|w_k - w_\star\|_{P_{k-1}}^2$, $\mathbb{E}\|\nabla F_j(w_k) - \nabla F_j(w_\star)\|_{P_k}^2$, $F(w_k) - F(w_\star)$, and \mathbf{Breg}_k in the preceding set of inequalities are all non-negative. By setting $\eta = \frac{1}{2(\tilde{\gamma}_\ell^{\min}n + \mathcal{L}_P)}$, $c = \frac{1}{2\eta(1 - \eta \tilde{\gamma}_\ell^{\min})n}$, $\kappa = \frac{1}{\eta \tilde{\gamma}_\ell^{\min}}$, and $\alpha = \frac{2\tilde{\gamma}_\ell^{\min}n + \mathcal{L}_P}{\mathcal{L}_P}$, we guarantee that the coefficients corre-

sponding to these four quantities are all ≤ 0 . Therefore,

$$\mathbb{E}_k T_{k+1} \leq \left(1 - \frac{1}{\kappa}\right) \beta_k T_k = \left(1 - \frac{1}{2(n + \kappa_P)}\right) \beta_k T_k,$$

where $\kappa_P = \frac{\mathcal{L}_P}{\tilde{\gamma}_\ell^{\min}} = \frac{\mathcal{L}_P}{(1-\zeta)\tilde{\gamma}_\ell^{\min}}$. ■

C.8.3 SKETCHYSAGA CONVERGENCE: PROOF OF THEOREM 28

Proof By the contraction lemma, we have

$$\mathbb{E}_k [T_k] \leq \left(1 - \frac{1}{2(n + \kappa_P)}\right) \beta_{k-1} T_{k-1}.$$

Hence taking the total expectation over all iterations and recursing, we reach

$$\mathbb{E}[T_k] \leq \left(1 - \frac{1}{2(n + \kappa_P)}\right)^k \left(\prod_{j=0}^{k-1} \beta_j\right) T_0 \leq \left(1 - \frac{1}{2(n + \kappa_P)}\right)^k B_P T_0. ■$$

Now, by definition $T_k \geq c \|w_k - w_\star\|_{P_k}^2$ for all k , so we obtain

$$\mathbb{E} \|w_k - w_\star\|_{P_k}^2 \leq \left(1 - \frac{1}{2(n + \kappa_P)}\right)^k \frac{B_P}{c} T_0.$$

Now using $c = \frac{1}{2\eta(1-\eta\tilde{\gamma}_\ell^{\min})n}$ and $\eta = \frac{1}{2(n\tilde{\gamma}_\ell^{\min} + \mathcal{L}_P)}$, we find

$$\frac{1}{c} = 2\eta(1-\eta\tilde{\gamma}_\ell^{\min})n = \frac{n}{n\tilde{\gamma}_\ell^{\min} + \mathcal{L}_P} \left(1 - \frac{\tilde{\gamma}_\ell^{\min}}{2(n\tilde{\gamma}_\ell^{\min} + \mathcal{L}_P)}\right) = \frac{(2n-1)\tilde{\gamma}_\ell^{\min} + \mathcal{L}_P}{2(n\tilde{\gamma}_\ell^{\min} + \mathcal{L}_P)^2} n \leq \frac{n}{n\tilde{\gamma}_\ell^{\min} + \mathcal{L}_P}$$

Therefore

$$\mathbb{E} \|w_k - w_\star\|_{P_k}^2 \leq \left(1 - \frac{1}{2(n + \kappa_P)}\right)^k B_P \left(\|w_0 - w_\star\|^2 - \frac{n}{n\tilde{\gamma}_\ell^{\min} + \mathcal{L}_P} [F(w_0) - F(w_\star)]\right).$$

Hence it immediately follows that

$$\mathbb{E} \|w_k - w_\star\|_{P_k}^2 \leq \epsilon,$$

after $k = \mathcal{O}((n + \kappa_P) \log(\frac{1}{\epsilon}))$ iterations.

C.9 SketchyKatyusha

In this subsection, we prove Theorem 30, which shows linear convergence of SketchyKatyusha (Algorithm 8). The argument is based on the Lyapunov function introduced in the main text. Similar to the previous theorems, we break down the proof of Theorem 30 into a series of lemmas, which together lead to an easy proof of the theorem. Unfortunately, similar to the analysis of classical accelerated gradient descent, the intuition behind the overall proof is somewhat opaque.

C.9.1 NOTATION

Throughout the analysis, we shall make use of the following quantities:

$$\begin{aligned}\tilde{\gamma}_\ell &:= (1 - \zeta)\gamma_\ell, \\ \kappa_P &:= \frac{\mathcal{L}_P}{\tilde{\gamma}_\ell} = \frac{\bar{q}}{1 - \zeta}, \quad \sigma := \frac{1}{\kappa_P}.\end{aligned}$$

C.9.2 PRELIMINARY LEMMAS

Lemma 58 (Variance bound) *Let $v_k = \widehat{\nabla}F(x_k) - \widehat{\nabla}F(y_k) + \nabla F(y_k)$ be the variance-reduced stochastic gradient at iteration k . Then*

$$\mathbb{E}\|v_k - \nabla F(x_k)\|_{P_k^{-1}}^2 \leq 2\mathcal{L}_P[F(y_k) - F(x_k) - \langle \nabla F(x_k), y_k - x_k \rangle].$$

Proof The proof is via direct calculation:

$$\begin{aligned}\mathbb{E}\|v_k - \nabla F(x_k)\|_{P_k^{-1}}^2 &\stackrel{(1)}{=} \mathbb{E}\left\|\widehat{\nabla}F(y_k) - \widehat{\nabla}F(x_k) - \mathbb{E}\left[\widehat{\nabla}F(y_k) - \widehat{\nabla}F(x_k)\right]\right\|_{P_k^{-1}}^2 \stackrel{(2)}{\leq} \\ &\mathbb{E}\|\widehat{\nabla}F(y_k) - \widehat{\nabla}F(x_k)\|_{P_k^{-1}}^2 \stackrel{(3)}{\leq} 2\mathcal{L}_P[F(y_k) - F(x_k) - \langle \nabla F(x_k), y_k - x_k \rangle],\end{aligned}$$

where (1) simply substitutes in the value of v_k , (2) uses $\mathbb{E}\|X - \mathbb{E}[X]\|_A^2 \leq \mathbb{E}\|X\|_A^2$, and (3) invokes Proposition 22. \blacksquare

The next two lemmas are somewhat mysterious in their content. However, they serve a concrete purpose, which is to couple various quantities involved with the Lyapunov function together in a way that will be useful for establishing contraction in Lemma 61. Given that this is the role they play, we adopt the language of Allen-Zhu (2018) (for whom two similar lemmas appear), and refer to Lemma 59 and Lemma 60 as coupling lemmas.

Lemma 59 (Coupling Lemma 1) *Let $\sigma = \frac{\tilde{\gamma}_\ell}{\mathcal{L}_P}$. Then for any iteration k , the following inequality holds*

$$\langle v_k, w_\star - x_k \rangle + \frac{\tilde{\gamma}_\ell}{2}\|x_k - w_\star\|_{P_k}^2 \geq \frac{\mathcal{L}_P}{2\eta}\|z_k - z_{k+1}\|_{P_k}^2 + \frac{1}{\xi_k}Z_{k+1} - \frac{1}{(1 + \eta\sigma)}Z_k.$$

Proof Observe the following equality

$$\begin{aligned}\langle v_k, x_k - w_\star \rangle &= \langle P_k^{-1}v_k, x_k - w_\star \rangle_{P_k} = \mathcal{L}_P\sigma\langle x_k - z_{k+1}, x_k - w_\star \rangle_{P_k} + \frac{\mathcal{L}_P}{\eta}\langle z_k - z_{k+1}, z_{k+1} - w_\star \rangle_{P_k} \\ &= \tilde{\gamma}_\ell\langle x_k - z_{k+1}, x_k - w_\star \rangle_{P_k} + \frac{\mathcal{L}_P}{\eta}\langle z_k - z_{k+1}, z_{k+1} - w_\star \rangle_{P_k},\end{aligned}$$

where the third equality uses

$$\frac{\eta}{\mathcal{L}_P}P_k^{-1}v_k = \eta\sigma(x_k - z_{k+1}) + z_k - z_{k+1}.$$

Invoking Lemma 36 twice with $A = P_k$, we reach

$$\begin{aligned} \langle v_k, x_k - w_\star \rangle &= \frac{\tilde{\gamma}_\ell}{2} (\|x_k - w_\star\|_{P_k}^2 - \|x_k - z_{k+1}\|_{P_k}^2 - \|z_{k+1} - w_\star\|_{P_k}^2) \\ &+ \frac{\mathcal{L}_P}{2\eta} (\|z_k - w_\star\|_{P_k}^2 - \|z_k - z_{k+1}\|_{P_k}^2 - \|z_{k+1} - w_\star\|_{P_k}^2) \\ &\leq \frac{\tilde{\gamma}_\ell}{2} \|x_k - w_\star\|_{P_k}^2 + \frac{\mathcal{L}_P}{2\eta} (\|z_k - w_\star\|_{P_k}^2 - (1 + \eta\sigma)\|z_{k+1} - w_\star\|_{P_k}^2) - \frac{\mathcal{L}_P}{2\eta} \|z_k - z_{k+1}\|_{P_k}^2. \end{aligned}$$

Using $\mathcal{Z}_k = \frac{\mathcal{L}_P(1+\eta\sigma)}{2\eta} \|z_k - w_\star\|_{P_k}^2$, $\|z_{k+1} - w_\star\|_{P_{k+1}}^2 \leq \xi_k \|z_{k+1} - w_\star\|_{P_k}^2$ rearranging, we find

$$\langle v_k, w_\star - x_k \rangle + \frac{\tilde{\gamma}_\ell}{2} \|x_k - w_\star\|_{P_k}^2 \geq \frac{\mathcal{L}_P}{2\eta} \|z_k - z_{k+1}\|_{P_k}^2 + \frac{1}{\xi_k} \mathcal{Z}_{k+1} - \frac{1}{1 + \eta\sigma} \mathcal{Z}_k.$$

■

Lemma 60 (Coupling Lemma 2) *For each iteration k , we have*

$$\frac{1}{\theta_1} (F(w_{k+1}) - F(x_k)) - \frac{\theta_2}{2\theta_1 \mathcal{L}_P} \|v_k - \nabla F(x_k)\|_{P_k^{-1}}^2 \leq \frac{\mathcal{L}_P}{2\eta} \|z_{k+1} - z_k\|_{P_k}^2 + \langle v_k, z_{k+1} - z_k \rangle.$$

Proof By construction of the algorithm, the following equality holds

$$\frac{\mathcal{L}_P}{2\eta} \|z_{k+1} - z_k\|_{P_k}^2 + \langle v_k, z_{k+1} - z_k \rangle = \frac{1}{\theta_1} \left(\frac{\mathcal{L}_P}{2\eta\theta_1} \|w_{k+1} - x_k\|_{P_k}^2 + \langle v_k, w_{k+1} - x_k \rangle \right).$$

Now, adding and subtracting zero twice, we reach

$$\begin{aligned} &\frac{\mathcal{L}_P}{2\eta} \|z_{k+1} - z_k\|_{P_k}^2 + \langle v_k, z_{k+1} - z_k \rangle = \\ &\frac{1}{\theta_1} \left(\frac{\mathcal{L}_P}{2\eta\theta_1} \|w_{k+1} - x_k\|_{P_k}^2 + \langle \nabla F(x_k), w_{k+1} - x_k \rangle + \langle v_k - \nabla F(x_k), w_{k+1} - x_k \rangle \right) \\ &= \frac{1}{\theta_1} \left(\frac{\mathcal{L}_P}{2} \|w_{k+1} - x_k\|_{P_k}^2 + \langle \nabla F(x_k), w_{k+1} - x_k \rangle \right) \\ &+ \frac{\mathcal{L}_P}{2\theta_1} \left(\frac{1}{\eta\theta_1} - 1 \right) \|w_{k+1} - x_k\|_{P_k}^2 + \frac{1}{\theta_1} \langle v_k - \nabla F(x_k), w_{k+1} - x_k \rangle. \end{aligned}$$

Now combining that P is ζ -spectral approximation with upper quadratic regularity, we have

$$F(w_{k+1}) - F(x_k) \leq \langle \nabla F(x_k), w_{k+1} - x_k \rangle + \frac{\mathcal{L}_P}{2} \|w_{k+1} - x_k\|_{P_k}^2.$$

Using the preceding relation, we find

$$\begin{aligned}
 & \frac{\mathcal{L}_P}{2\eta} \|z_{k+1} - z_k\|_{P_k}^2 + \langle v_k, z_{k+1} - z_k \rangle \geq \\
 & \frac{1}{\theta_1} (F(w_{k+1}) - F(x_k)) + \frac{\mathcal{L}_P}{2\theta_1} \left(\frac{1}{\eta\theta_1} - 1 \right) \|w_{k+1} - x_k\|_{P_k}^2 + \frac{1}{\theta_1} \langle v_k - \nabla F(x_k), w_{k+1} - x_k \rangle \\
 & \stackrel{(1)}{\geq} \frac{1}{\theta_1} (F(w_{k+1}) - F(x_k)) - \frac{\eta\theta_1}{2\mathcal{L}_P(1-\eta\theta_1)} \|v_k - \nabla F(x_k)\|_{P_k}^2 \\
 & \stackrel{(2)}{=} \frac{1}{\theta_1} (F(w_{k+1}) - F(x_k)) - \frac{\theta_2}{2\theta_1\mathcal{L}_P} \|v_k - \nabla F(x_k)\|_{P_k}^2.
 \end{aligned}$$

Where (1) uses Lemma 37 with $c_1 = \frac{1}{\theta_1}$, $c_2 = \frac{\mathcal{L}_P(1-\eta\theta_1)}{\eta\theta_1^2}$, and (2) uses $\theta_2 = \frac{\eta\theta_1}{1-\eta\theta_1}$. \blacksquare

With the coupling lemmas in hand, we now establish that conditioned on the k th iterate, the Lyapunov function contracts in expectation.

Lemma 61 (Contraction Lemma)

$$\mathbb{E}_k \left[\mathcal{W}_{k+1} + \mathcal{Y}_{k+1} + \frac{1}{\xi_k} \mathcal{Z}_{k+1} \right] \leq \left(1 - \frac{\pi\theta_1}{1+\theta_1} \right) \mathcal{W}_k + (1 - \theta_1(1 - \theta_2)) \mathcal{Y}_k + \frac{1}{1 + \eta\sigma} \mathcal{Z}_k$$

Proof By lower quadratic regularity of F and P_k being a ζ -spectral approximation, we have

$$F(w_\star) \geq F(x_k) + \langle \nabla F(x_k), w_\star - y_k \rangle + \frac{\tilde{\gamma}_\ell}{2} \|x_k - w_\star\|_{P_k}^2.$$

Rearranging, we reach

$$\begin{aligned}
 F(w_\star) & \stackrel{(1)}{\geq} F(x_k) + \frac{\tilde{\gamma}_\ell}{2} \|x_k - w_\star\|_{P_k}^2 + \langle \nabla F(x_k), w_\star - z_k + z_k - x_k \rangle \\
 & \stackrel{(2)}{=} F(x_k) + \frac{\tilde{\gamma}_\ell}{2} \|x_k - w_\star\|_{P_k}^2 + \langle \nabla F(x_k), w_\star - z_k \rangle + \frac{\theta_2}{\theta_1} \langle \nabla F(x_k), x_k - y_k \rangle \\
 & \quad + \frac{1 - \theta_1 - \theta_2}{\theta_1} \langle \nabla F(x_k), x_k - w_k \rangle \\
 & \stackrel{(3)}{\geq} F(x_k) + \frac{\tilde{\gamma}_\ell}{2} \|x_k - w_\star\|_{P_k}^2 + \langle \nabla F(x_k), w_\star - z_k \rangle \\
 & \quad + \frac{\theta_2}{\theta_1} \langle \nabla F(x_k), x_k - y_k \rangle + \frac{1 - \theta_1 - \theta_2}{\theta_1} (F(x_k) - F(w_k)).
 \end{aligned}$$

Where (1) adds and subtracts zero, (2) uses

$$z_k - x_k = -\frac{(1 - \theta_1)}{\theta_1} x_k - \frac{\theta_2}{\theta_1} y_k - \frac{1 - \theta_1 - \theta_2}{\theta_2} w_k = -\frac{\theta_2}{\theta_1} (x_k - y_k) - \frac{(1 - \theta_1 - \theta_2)}{\theta_1} (x_k - w_k),$$

and (3) invokes convexity of F . Now, observe that

$$\frac{\tilde{\gamma}_\ell}{2} \|x_k - w_\star\|_{P_k}^2 + \langle \nabla F(x_k), w_\star - z_k \rangle = \mathbb{E}_k \left[\frac{\tilde{\gamma}_\ell}{2} \|x_k - w_\star\|_{P_k}^2 + \langle v_k, w_\star - z_{k+1} \rangle + \langle v_k, z_{k+1} - z_k \rangle \right].$$

Hence, we can use the preceding relation with Lemma 59 and Lemma 60, to reach

$$\begin{aligned}
F(w_\star) &\geq f(x_k) + \frac{\theta_2}{\theta_1} \langle \nabla F(x_k), x_k - w_k \rangle + \frac{1 - \theta_1 - \theta_2}{\theta_1} (F(x_k) - F(w_k)) + \mathbb{E}_k \left[\frac{1}{\xi_k} \mathcal{Z}_{k+1} - \frac{1}{1 + \eta\sigma} \mathcal{Z}_k \right] \\
&+ \mathbb{E}_k \left[\langle v_k, z_{k+1} - z_k \rangle + \frac{\mathcal{L}_P}{2\eta} \|z_k - z_{k+1}\|_{P_k}^2 \right] \\
&\geq F(x_k) + \frac{\theta_2}{\theta_1} \langle \nabla F(x_k), x_k - w_k \rangle + \frac{1 - \theta_1 - \theta_2}{\theta_1} (F(x_k) - F(w_k)) + \mathbb{E}_k \left[\frac{1}{\xi_k} \mathcal{Z}_{k+1} - \frac{1}{1 + \eta\sigma} \mathcal{Z}_k \right] \\
&+ \mathbb{E}_k \left[\frac{1}{\theta_1} (F(w_{k+1}) - F(x_k)) - \frac{\theta_2}{2\theta_1 \mathcal{L}_P} \|v_k - \nabla F(x_k)\|_{P_k^{-1}}^2 \right].
\end{aligned}$$

Now, invoking the variance bound in Lemma 58, we find

$$\begin{aligned}
F(w_\star) &\geq F(x_k) + \frac{\theta_2}{\theta_1} \langle \nabla F(x_k), x_k - y_k \rangle + \frac{1 - \theta_1 - \theta_2}{\theta_1} (F(x_k) - F(w_k)) + \mathbb{E}_k \left[\frac{1}{\xi_k} \mathcal{Z}_{k+1} - \frac{1}{1 + \eta\sigma} \mathcal{Z}_k \right] \\
&+ \frac{1}{\theta_1} \mathbb{E}_k [F(w_{k+1}) - F(x_k)] - \frac{\theta_2}{\theta_1} (F(y_k) - F(x_k)) - \frac{\theta_2}{\theta_1} \langle \nabla F(x_k), x_k - y_k \rangle.
\end{aligned}$$

Hence,

$$\begin{aligned}
F(w_\star) &\geq F(x_k) + \frac{1 - \theta_1 - \theta_2}{\theta_1} (F(x_k) - F(w_k)) - \frac{1}{1 + \eta\sigma} \mathcal{Z}_k - \frac{\theta_2}{\theta_1} (F(y_k) - F(x_k)) \\
&+ \mathbb{E}_k \left[\frac{1}{\theta_1} (F(w_{k+1}) - F(x_k)) + \frac{1}{\xi_k} \mathcal{Z}_{k+1} \right].
\end{aligned}$$

Rearranging, and using that w_\star is the optimum, we reach

$$\begin{aligned}
&\frac{1 - \theta_1 - \theta_2}{\theta_1} (F(w_k) - F(y_k)) + \frac{\theta_2}{\theta_1} (F(y_k) - F(x_k)) + \frac{1}{1 + \eta\sigma} \mathcal{Z}_k + \left(\frac{1}{\theta_1} - 1 \right) (F(x_k) - F(w_\star)) \\
&\geq \mathbb{E}_k \left[\frac{1}{\theta_1} (F(w_{k+1}) - F(w_\star)) + \frac{1}{\xi_k} \mathcal{Z}_{k+1} \right].
\end{aligned}$$

Adding and subtracting $F(w_\star)$ in the first two terms in parentheses on the left handside, combining the resulting terms, and recalling the definitions of $\mathcal{W}_k, \mathcal{Y}_k, \mathcal{Z}_k$, we obtain

$$\mathbb{E}_k \left[\mathcal{W}_{k+1} + \frac{1}{\xi_k} \mathcal{Z}_{k+1} \right] \leq (1 - \theta_1 - \theta_2) \mathcal{W}_k + \frac{\pi}{1 + \theta_1} \mathcal{Y}_k + \frac{1}{1 + \eta\sigma} \mathcal{Z}_k.$$

Now, using the relation $\mathbb{E}_k[\mathcal{Y}_{k+1}] = (1 - \pi) \mathcal{Y}_k + \theta_2(1 + \theta_1) \mathcal{W}_k$, which holds by construction of the algorithm, we conclude

$$\mathbb{E}_k \left[\mathcal{W}_{k+1} + \mathcal{Y}_{k+1} + \frac{1}{\xi_k} \mathcal{Z}_{k+1} \right] \leq (1 - \theta_1(1 - \theta_2)) \mathcal{W}_k + \left(1 - \frac{\pi\theta_1}{1 + \theta_1} \right) \mathcal{Y}_k + \frac{1}{1 + \eta\sigma} \mathcal{Z}_k.$$

■

C.9.3 SKETCHYKATYUSHA CONVERGENCE: PROOF OF THEOREM 30

Proof Lemma 61 shows that

$$\mathbb{E}_k [\mathcal{W}_{k+1} + \mathcal{Y}_{k+1} + \mathcal{Z}_{k+1}] \leq \xi_k \alpha (\mathcal{W}_k + \mathcal{Y}_k + \mathcal{Z}_k),$$

where $\alpha = \max \left\{ (1 - \theta_1(1 - \theta_2)), \left(1 - \frac{\pi\theta_1}{1+\theta_1}\right), \frac{1}{1+\eta\sigma} \right\}$. Hence, taking the total expectation over all iterations and recursing, we find

$$\mathbb{E}[\Psi_k] \leq \epsilon \Psi_0,$$

after $k \geq \max \left\{ \frac{1}{\theta_1(1-\theta_2)}, \pi^{-1}(1 + \theta_1^{-1}), 1 + (\eta\sigma)^{-1} \right\} \log \left(\frac{\epsilon_P}{\epsilon} \right)$. Now, recall $\sigma = 1/\kappa_P$ and $\pi = b_g/n$, so that $\theta_1 = \min \left\{ \sqrt{\frac{n}{b_g\kappa_P}}\theta_2, 1/2 \right\}$, and $\pi = b_g/n$. We see the the analysis breaks down to two cases: $\kappa_P \leq \frac{n}{b_g}$ and $\kappa_P > \frac{n}{b_g}$.

Case 1: $\left(\kappa_P \leq \frac{n}{b_g}\right)$ Let us set $\theta_2 = 1/2$. Then for Case 1, the minimum defining θ_1 is achieved by $1/2$. Using this in conjunction with $\eta = \theta_1/[(1 + \theta_2)\theta_1]$, we find

$$\max \left\{ \frac{1}{\theta_1(1 - \theta_2)}, \pi^{-1}(1 + \theta_1^{-1}), 1 + (\eta\sigma)^{-1} \right\} = \max \left\{ 4, 3\frac{n}{b_g}, 1 + 3/2\kappa_P \right\} = 3\frac{n}{b_g},$$

Hence, as $1 \leq \kappa_P \leq n/b_g$, we conclude

$$\mathbb{E}[\Psi_k] \leq \epsilon \Psi_0$$

after $k \geq \frac{3n}{b_g} \log \left(\frac{\epsilon_P}{\epsilon} \right)$ iterations.

Case 2: $\left(\kappa_P \geq \frac{n}{b_g}\right)$ Once again set $\theta_2 = 1/2$. Given the hypothesis on κ_P , we have $\theta_1 = \sqrt{n/(b_g\kappa_P)}\theta_2$. Using the value of θ_1 , and performing some straightforward computations, we find

$$\begin{aligned} & \max \left\{ \frac{1}{\theta_1(1 - \theta_2)}, \pi^{-1}(1 + \theta_1^{-1}), 1 + (\eta\sigma)^{-1} \right\} \\ &= \max \left\{ 1/2\sqrt{\kappa_P b_g/n}, n/b_g + 2\sqrt{n\kappa_P/b_g}, 1 + 3/4\sqrt{n\kappa_P/b_g} \right\} \\ &= n/b_g + 2\sqrt{n\kappa_P/b_g}. \end{aligned}$$

Combining both cases, we see that with $\pi = b_g/n$, we have

$$\mathbb{E}[\Psi_k] \leq \epsilon \Psi_0,$$

after $k = \max \left\{ 3n/b_g, n/b_g + 2\sqrt{n\kappa_P/b_g} \right\} \log \left(\frac{\epsilon_P}{\epsilon} \right)$ iterations. Plugging in $\kappa_P = \bar{q}/(1 - \zeta)$, we obtain the desired claim. \blacksquare

D. Experimental details

Here we provide additional experimental details that were omitted from the main text.

D.1 Computational resources

The experiments in this paper are run on servers with the computational resources listed in Table 17. Although these servers have 64-core CPUs, calls to BLAS are limited to 16 threads, i.e., we only use 16 cores for any given experiment.

Experiment section	CPU	Memory (RAM)
Performance experiments (Section 6.1)	64-core Xeon E5-2698 v3 @ 2.30GHz	1007.8 GB
Showcase experiments (Section 6.3)	64-core Xeon E5-2698 v3 @ 2.30GHz	755.8 GB
Streaming experiments (Section 6.4)	64-core Xeon E5-2698 v3 @ 2.30GHz	755.8 GB
Sensitivity study (Section 6.5)	64-core Xeon E5-2698 v3 @ 2.30GHz	1007.8 GB
Regularity study (Section 6.6)	64-core Xeon E5-2698 v3 @ 2.30GHz	755.8 GB

Table 17: Computational resources used for each set of experiments.

D.2 Optimizer details

Initialization All optimizers are initialized at $w_0 = 0$.

Default hyperparameters for SVRG/SAGA/L-Katyusha The theoretical analyses of SVRG, SAGA, and L-Katyusha all yield recommended learning rates that lead to linear convergence. In practical implementations such as scikit-learn (Pedregosa et al., 2011), these recommendations are used to compute the default learning rate. For SAGA, the theoretical learning rate is given by

$$\eta = \max \left\{ \frac{1}{3L_{\max}}, \frac{1}{2(L_{\max} + n_{\text{tr}}\mu)} \right\},$$

where $L_{\max} := \max_i L_i$ is the maximum smoothness constant among the f_i s and μ is the strong convexity constant.

Now, standard computations show that the smoothness constants for least-squares and logistic regression satisfy

$$L_{\text{least-squares}} \leq \frac{1}{n_{\text{tr}}} \sum_{i=1}^{n_{\text{tr}}} \|a_i\|^2 =: \hat{L}_{\text{avg}} \leq \max_i \|a_i\|^2 =: \hat{L}_{\max},$$

$$L_{\text{logistic}} \leq \frac{1}{4n_{\text{tr}}} \sum_{i=1}^{n_{\text{tr}}} \|a_i\|^2 =: \hat{L}_{\text{avg}} \leq \frac{1}{4} \max_i \|a_i\|^2 =: \hat{L}_{\text{max}}.$$

The scikit-learn software package uses the preceding upper-bound \hat{L}_{max} in place of L_{max} to set η in their implementation of SAGA. However, \hat{L}_{max} can lead to a very conservative learning rate (especially if the data is poorly scaled), so we use \hat{L}_{avg} to calculate the default learning rate instead.

The theoretical analysis of SVRG suggests a step-size of $\eta = \frac{1}{10\mathcal{L}}$, where \mathcal{L} is the expected-smoothness constant. We have found this setting to be pessimistic relative to the SAGA default, so we use the same default for SVRG as we do for SAGA. For L-Katyusha the hyperparameters θ_1 and θ_2 are controlled by how we specify L^{-1} , the reciprocal of the smoothness constant; we use \hat{L}_{avg} in place of L as the default.

Grid search parameters (Sections 6.1 to 6.3) For ridge regression, we set $[10^{-3}, 10^2]$ as the search range for the learning rate in SGD, SVRG and SAGA, and $[10^{-2}, 10^0]$ as the search range for the smoothness parameter L in L-Katyusha. For SLBFGS, we set the search range to be $[10^{-5}, 10^0]$ in order to have the same log-width as the search range for SGD, SVRG, and SAGA. In logistic regression, the search ranges for SGD/SVRG/SAGA, L-Katyusha, and SLBFGS become $[4 \cdot 10^{-3}, 4 \cdot 10^2]$, $[2.5 \cdot 10^{-3}, 2.5 \cdot 10^{-1}]$, and $[4 \cdot 10^{-5}, 4 \cdot 10^0]$, respectively. The grid corresponding to each range samples 10 equally spaced values in log space.

Grid search parameters (Section 6.4) Instead of using a search range of $[4 \cdot 10^{-3}, 4 \cdot 10^2]$ for SGD/SAGA, we narrow the range to $[4 \cdot 10^{-2}, 4 \cdot 10^1]$ and sample 4 equally spaced values in log space. The reason for reducing the search range and grid size is to reduce the total computational cost of running the experiments on the HIGGS and SUSY datasets. Furthermore, we find that $4 \cdot 10^0$ is the best learning rate for HIGGS and SUSY, while $4 \cdot 10^1$ leads to non-convergent behavior, meaning these search ranges are appropriate.

Additional hyperparameters For SVRG and SLBFGS we perform a full gradient computation at every epoch. For SLBFGS we update the inverse Hessian approximation every epoch and set the Hessian batchsize to $\sqrt{n_{\text{tr}}}$, which matches the Hessian batchsize hyperparameter in our proposed methods. In addition, we follow Moritz et al. (2016) and set the memory size of SLBFGS to 10. For L-Katyusha, we initialize the update probability $p = b_g/n_{\text{tr}}$ to ensure the average number of iterations between full gradient computations is equal to one epoch. We follow Kovalev et al. (2020) and set μ equal to the l^2 -regularization parameter, $\sigma = \frac{\mu}{L}$, $\theta_1 = \min\{\sqrt{2\sigma n_{\text{tr}}/3}, \frac{1}{2}\}$, and $\theta_2 = \frac{1}{2}$. In Sections 6.1, 6.5 and 6.6 all algorithms use a batchsize of 256 for computing stochastic gradients; in Sections 6.3 and 6.4 all algorithms use a batchsize of 4,096 for computing stochastic gradients.

D.3 Performance experiments (additional)

D.3.1 DATASETS AND PREPROCESSING

The ridge regression experiments in Section 6.1.1 use datasets from both LIBSVM and OpenML. The details regarding dimensions and random features are provided in Tables 18 and 19. All OpenML datasets that are used do not have a designated training and test set, so we use a random 80/20 split. We preprocess each dataset from LIBSVM to have

unit row norm. We standardize each dataset from OpenML, i.e., every feature has mean 0 and standard deviation 1 after preprocessing; we also standardize the labels if they are non-binary. A bandwidth of 1 is used in the cases where Gaussian random features are applied (performed after normalization/standardization). For simplicity, we remove non-numeric features from the datasets Santander and Airlines_DepDelay_1M before running experiments.

Dataset	n_{tr}	n_{tst}	p	RF type/dimension
E2006-tfidf	16,087	3,308	150,360	
YearPredictionMSD	463,715	51,630	90	ReLU/4,367

Table 18: LIBSVM datasets used in ridge regression experiments from Section 6.1.1. n_{tr} denotes the number of training samples, n_{tst} denotes the number of test samples, and p denotes the number of features.

Dataset	ID	Binary labels?	n	p	RF type/dimension
Santander	42395	✓	200,000	201	Gaussian/1,000
Jannis	44079	✓	57,580	54	Gaussian/460
Yolanda	42705	✗	400,000	100	Gaussian/1,000
MiniBoone	41150	✓	130,064	50	Gaussian/1,000
Guillermo	41159	✓	20,000	4,296	
creditcard	1597	✓	284,807	30	Gaussian/1,000
ACSIIncome	43141	✗	1,664,500	11	Gaussian/1,000
Medical-Appointment	43617	✓	61,214	18	Gaussian/489
Airlines_DepDelay_1M	42721	✗	1,000,000	9	Gaussian/1,000
Click_prediction_small	1218	✓	1,997,410	11	Gaussian/1,000
mtp	405	✗	4,450	202	
elevators	216	✗	16,599	18	Gaussian/132
aileron	296	✗	13,750	40	Gaussian/110
superconduct	44006	✗	21,263	79	Gaussian/170
sarcos	44976	✗	48,933	21	Gaussian/391

Table 19: OpenML datasets used in ridge regression experiments from Section 6.1.1. ID is a unique identifier for the dataset on OpenML, n is the number of samples before splitting into training/test sets, and p is the number of features.

All datasets used in the logistic regression experiments in Section 6.1.2 are from LIBSVM. The details regarding dimensions, splits, and random features are provided in Table 20. The covtype.binary, german.numer, mushrooms, news20.binary, phishing, real-sim, sonar, and websample-unigram datasets do not have a designated training and test set, so we use a random 80/20 split. We preprocess each dataset to have unit row norm. A bandwidth of 1 is used in the cases where Gaussian random features are applied (performed after normalization). We note that websample-unigram is listed on LIBSVM as having 16,609,143 features, but has only 254 non-zero columns.

D.3.2 PERFORMANCE PLOTS FOR $\nu = 10^{-1}/n_{\text{tr}}$

Figs. 18 and 19 compare PROMISE methods to competitor methods using the same setting as the performance experiments in Section 6.1; the only difference is that $\nu = 10^{-1}/n_{\text{tr}}$ instead of $10^{-2}/n_{\text{tr}}$. PROMISE methods still outperform the competition on both ridge and l^2 -regularized logistic regression.

Dataset	n_{tr}	n_{tst}	p	RF type/dimension
a1a	1,605	30,956	123	
a2a	2,265	30,296	123	
a3a	3,185	29,376	123	
a4a	4,781	27,780	123	
a5a	6,414	26,147	123	
a6a	11,220	21,341	123	
a7a	16,100	16,461	123	
a8a	22,696	9,865	123	
a9a	32,561	16,281	123	
covtype.binary	581,012		54	Gaussian/100
epsilon	400,000	100,000	2,000	
german.numer	1,000		24	Gaussian/100
gisette	6,000	1,000	5,000	
HIGGS	10,500,000	500,000	28	Gaussian/500
ijcnn1	49,990	91,701	22	Gaussian/2,500
madelon	2,000	600	500	
mushrooms	8,124		112	
news20.binary	19,996		1,355,191	
phishing	11,055		68	Gaussian/100
rcv1.binary	20,242	677,399	47,236	
real-sim	72,309		20,958	
splice	1,000	2,175	60	Gaussian/100
sonar	208		60	Gaussian/100
SUSY	4,500,000	500,000	18	Gaussian/1,000
svmguid3	1,243	41	21	Gaussian/100
w1a	2,477	47,272	300	
w2a	3,470	46,279	300	
w3a	4,912	44,837	300	
w4a	7,366	42,383	300	
w5a	9,888	39,861	300	
w6a	17,188	32,561	300	
w7a	24,692	25,057	300	
w8a	49,749	14,951	300	
websample-unigram	350,000		16,609,143	

Table 20: LIBSVM datasets used in logistic regression experiments from Section 6.1.2. n_{tr} denotes the number of training samples, n_{tst} denotes the number of test samples, and p denotes the number of features.

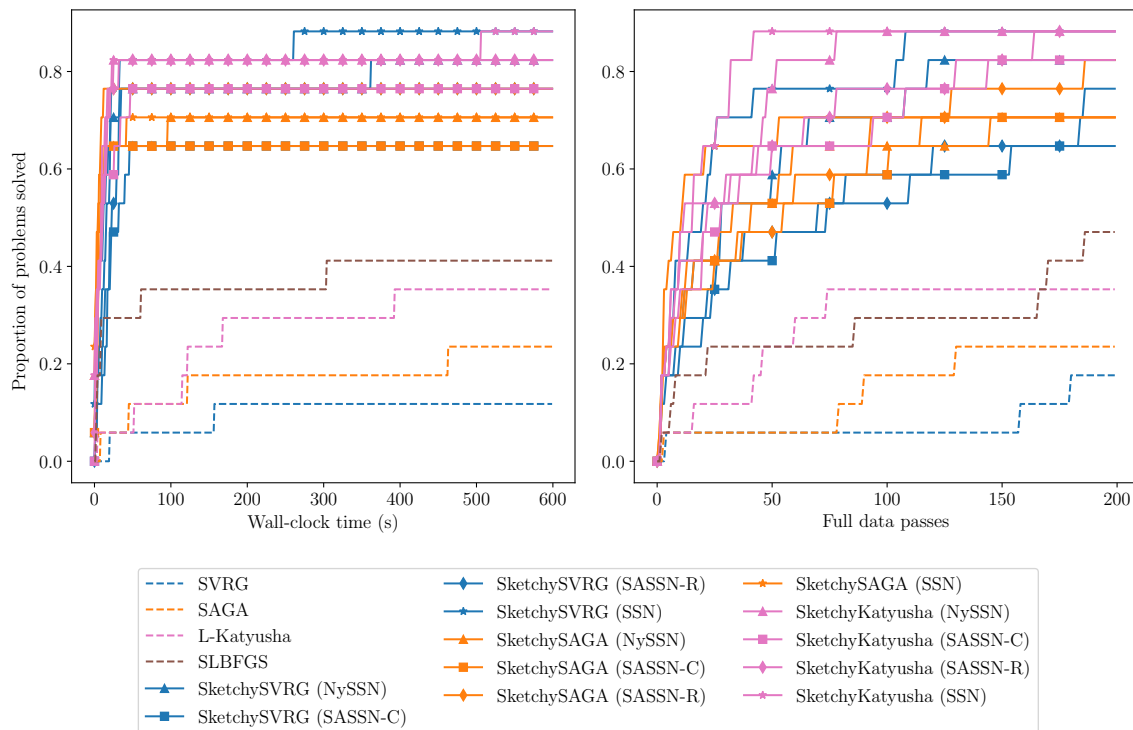


Figure 18: Proportion of ridge regression problems solved by our proposed methods and competitor methods when $\nu = 10^{-1}/n_{\text{tr}}$.

D.3.3 COMPARISON OF SSN AND NYSSN ON SPARSE/DENSE LOGISTIC REGRESSION

Here we compare the performance of the SSN and NYSSN preconditioners on both sparse and dense logistic regression problems. We consider a problem to be sparse if $< 20\%$ of the entries in the (preprocessed) data matrix are nonzero. According to this metric, the datasets a1a, a2a, a3a, a4a, a5a, a6a, a7a, a8a, a9a, mushrooms, news20, rcv1, real-sim, w1a, w2a, w3a, w4a, w5a, w6a, w7a, and w8a are sparse, while the datasets covtype, epsilon, german.numer, gisette, HIGGS, ijcnn1, madelon, phishing, splice, sonar, SUSY, svmguide3, and webspam are dense.

On sparse problems (Figs. 20 and 21), the SSN preconditioner outperforms the NYSSN preconditioner with respect to both wall-clock time and full data passes. On the other hand, the NYSSN preconditioner slightly outperforms the SSN preconditioner on dense problems (Figs. 21 and 22). These findings are in line with our preconditioner recommendations in Table 8.

D.3.4 DIAGSSN vs. SSN/NYSSN/SASSN-C/SASSN-R

Figs. 24 and 25 compare the performance of the DIAGSSN preconditioner to the other preconditioners proposed in the main text. We observe that using the DIAGSSN preconditioner significantly degrades the performance of our proposed methods.

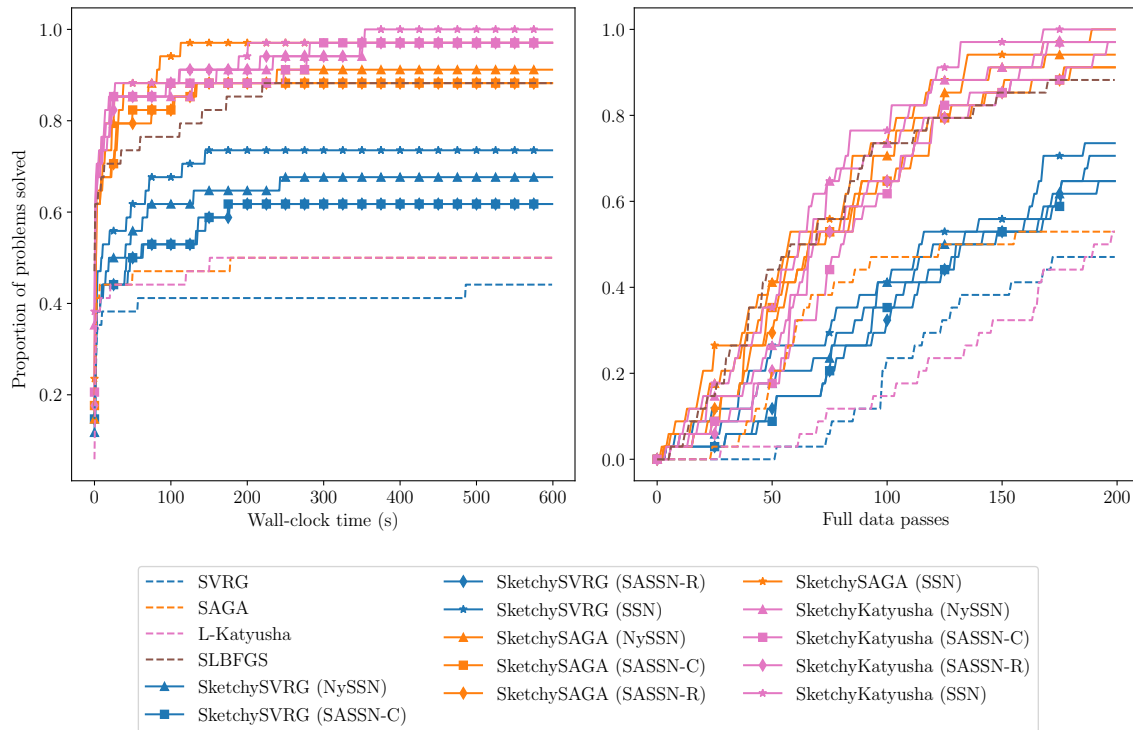


Figure 19: Proportion of l^2 -regularized logistic regression problems solved by our proposed methods and competitor methods when $\nu = 10^{-1}/n_{\text{tr}}$.

D.4 Suboptimality experiments (additional)

The suboptimality experiments in Section 6.2 use the E2006-tfidf, YearPredictionMSD, yolanda, ijcnn1, real-sim, and SUSY datasets. We preprocess these datasets in the same way as Section 6.1; see Appendix D.3.1 for details.

D.4.1 SKETCHYSGD VS. SKETCHYSVRG/SKETCHYSAGA/SKETCHYKATYUSHA

We investigate how SketchySVRG, SketchySAGA, and SketchyKatyusha, which have linear convergence guarantees, provide improved convergence in comparison to SketchySGD. We use the same datasets and run experiments using the same approach as in Section 6.2.

The results are shown in Fig. 26 and Fig. 27. SketchySGD consistently converges to a ball of noise, while SketchySVRG, SketchySAGA, and SketchyKatyusha attain lower suboptimality due to variance reduction. In the case of YearPredictionMSD, yolanda, real-sim, and SUSY, SketchySGD does not reach a suboptimality near the other three methods.

D.5 Showcase experiments (additional)

The showcase experiments in Section 6.3 use the url, yelp, and acsincome datasets. The details regarding dimensions and random features are provided in Table 21. None of the datasets have a designated training and test set, so we use a random 80/20 split. The url dataset is preprocessed to have unit row norm. The yelp dataset is created by taking the

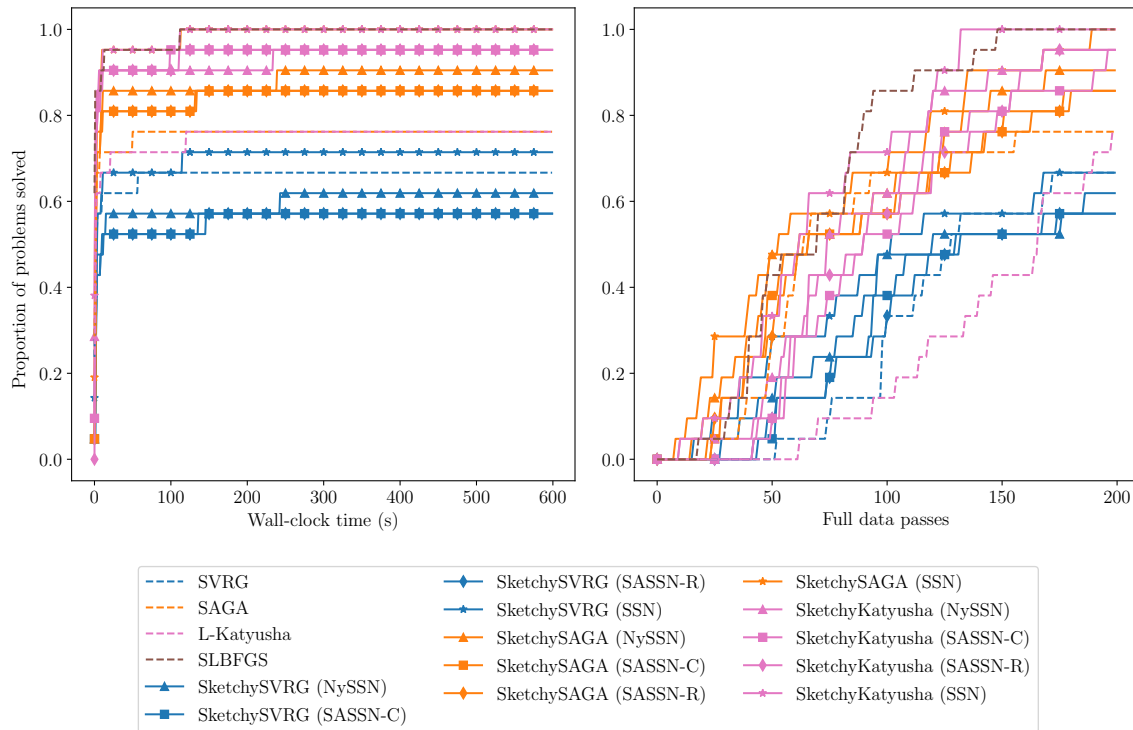


Figure 20: Proportion of l^2 -regularized logistic regression problems, with sparse data, solved by our proposed methods and competitor methods.

file `yelp_academic_dataset_review.json` (accessed on May 20, 2023), preprocessing each review into unigrams and bigrams, assigning positive (4 or 5 star) reviews a label of $+1$, assigning negative (1 or 2 star) reviews a label of -1 , and removing neutral (3 star) reviews. The `acsincome` dataset is preprocessed by first removing outliers, i.e., samples whose labels are more than 3 standard deviations from the mean. We then standardize the features and labels to have mean 0 and standard deviation 1. After standardization, we apply Gaussian random features with a bandwidth of 1.

Dataset	Source	n	p	RF type/dimension
url	LIBSVM	2,396,130	3,231,961	
yelp	(Yelp, 2023)	5,038,676	2,084,724	
ACSIIncome	OpenML (ID: 43141)	1,632,867	11	Gaussian/7,500

Table 21: Datasets used in showcase experiments from Section 6.3. n is the number of samples before splitting into training/test sets (after appropriate preprocessing) and p is the number of features.

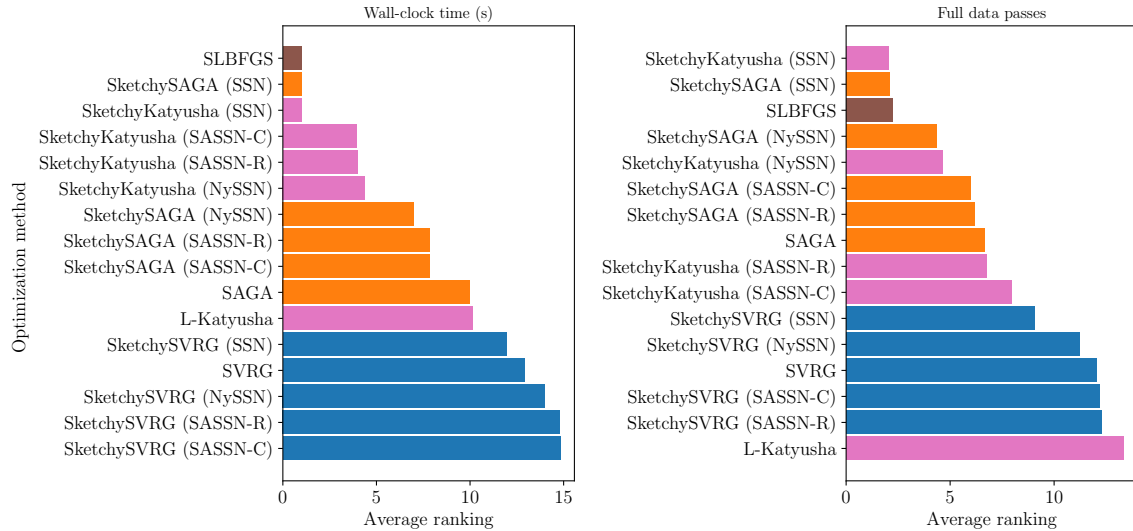


Figure 21: Average ranking of each method by number of l^2 -regularized logistic regression problems, with sparse data, solved with respect to wall-clock time (left) and full gradient computations (right).

D.6 Streaming experiments (additional)

D.6.1 DATASETS AND PREPROCESSING

We use the HIGGS and SUSY datasets from LIBSVM; details regarding dimensions, splits, and random features are provided in Table 22. We preprocess each dataset to have unit row norm, and then apply Gaussian random features with bandwidth 1 to both datasets.

Dataset	n_{tr}	n_{tst}	p	RF type/dimension
HIGGS	10,500,000	500,000	28	Gaussian/10,000
SUSY	4,500,000	500,000	18	Gaussian/20,000

Table 22: Details for HIGGS and SUSY datasets in Section 6.4. n_{tr} denotes the number of training samples, n_{tst} denotes the number of test samples, and p denotes the number of features.

D.6.2 COMPARISON TO SAGA WITH DEFAULT HYPERPARAMETERS

The comparison to SAGA with its default hyperparameter is presented in Figs. 12 and 13. The plots are constructed using the same approach as in Section 6.4. We find that SAGA makes little to no progress in decreasing the test loss, while SketchySGD and SketchySAGA, when combined with either the SSN or NYSSN preconditioner, decrease the test loss significantly.

D.7 Gradient batchsize relative to dataset size

In this subsection show how the gradient batchsize used for each experiment class compares to n , and the baseline \sqrt{n} suggested by Corollary 27. Specifically, we report the median

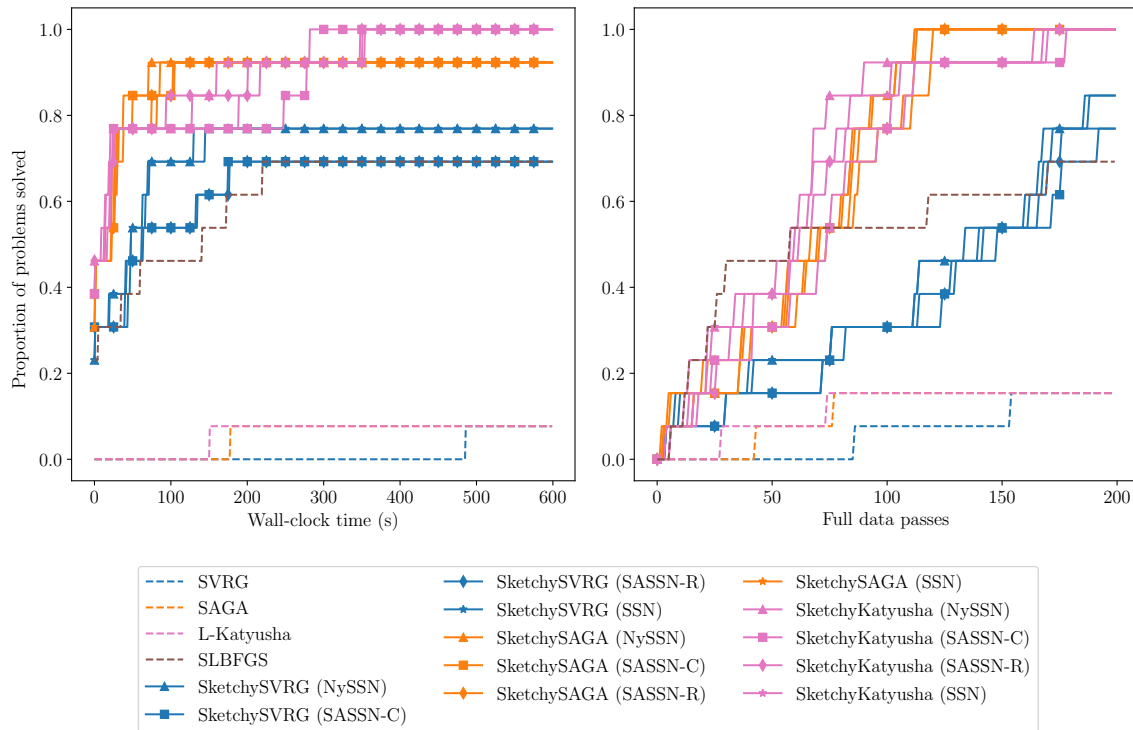


Figure 22: Proportion of l^2 -regularized logistic regression problems, with dense data, solved by our proposed methods and competitor methods.

value of b_g/n (percentage) and b_g/\sqrt{n} for all the datasets used in each class of experiment. The results are reported in Table 23.

Experiment	b_g/n (%)	b_g/\sqrt{n}
Performance (Ridge)	0.418	1.03
Performance (l^2 -Logistic)	2.31	2.43
Showcase	0.171	2.65
Streaming	0.065	1.60

Table 23: Comparison of b_g relative to n and \sqrt{n} . PROMISE does not require large gradient to achieve the excellent results observed Section 6. Moreover, the batchsizes used by PROMISE are modest multiples of \sqrt{n} , which agrees with Corollary 27, and supports setting b_g to be $\lfloor C\sqrt{n} \rfloor$, where $C \in \{1, 2, 3\}$.

D.8 Sensitivity study (additional)

D.8.1 ADDITIONAL SENSITIVITY PLOTS

We present additional plots that were omitted from the sensitivity study (Section 6.5) in the main text. Figure 30 shows how changing the rank r impacts the performance of SketchySAGA on the yolanda, ijcn1, and SUSY datasets. We again observe that the effect of increasing the rank depends on the spectrum (Fig. 15) of each dataset. Both yolanda

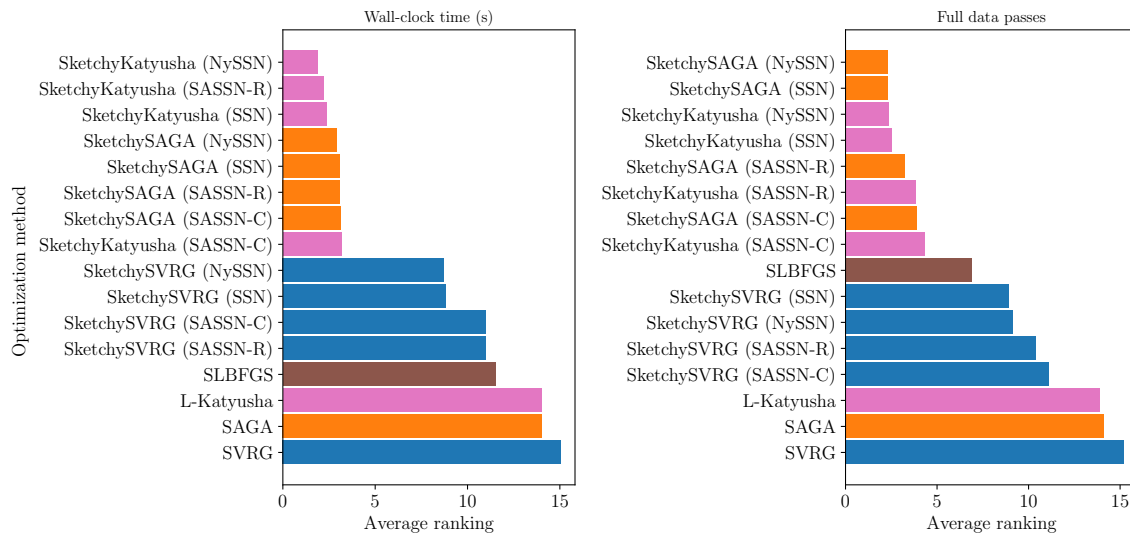


Figure 23: Average ranking of each method by number of l^2 -regularized logistic regression problems, with dense data, solved with respect to wall-clock time (left) and full gradient computations (right).

and YearPredictionMSD have similar patterns of spectral decay, and increasing the rank for yolanda leads to faster convergence. On the other hand, the spectra of ijcn1 and SUSY are highly concentrated in the first singular value, just like E2006-tfidf, and increasing the rank does not improve convergence. Fig. 31 demonstrates that adjusting the update frequency u does not impact convergence on ridge regression problems.

D.9 Regularity study (additional)

The regularity study in Section 6.6 uses the a9a, gisette, ijcn1, mushrooms, phishing, rcv1, real-sim, and w8a datasets. We preprocess these datasets in the same way as Section 6.1; see Appendix D.3.1 for details.

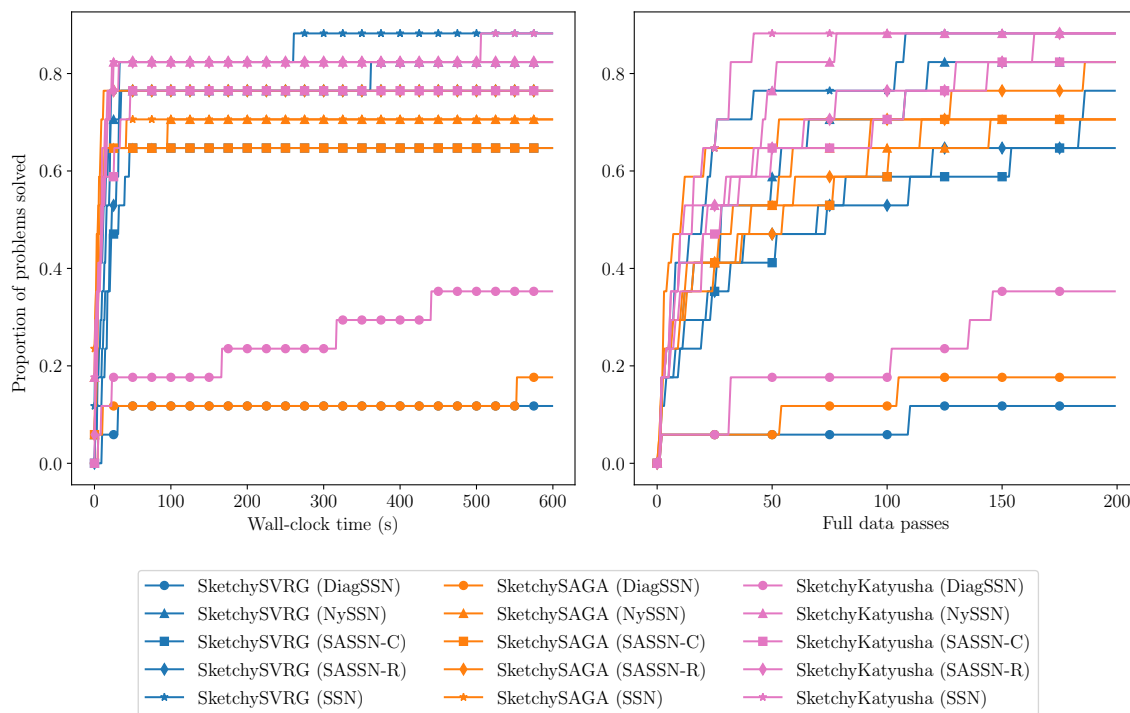


Figure 24: Proportion of ridge regression problems solved by DIAGSSN versus the other preconditioning methods.

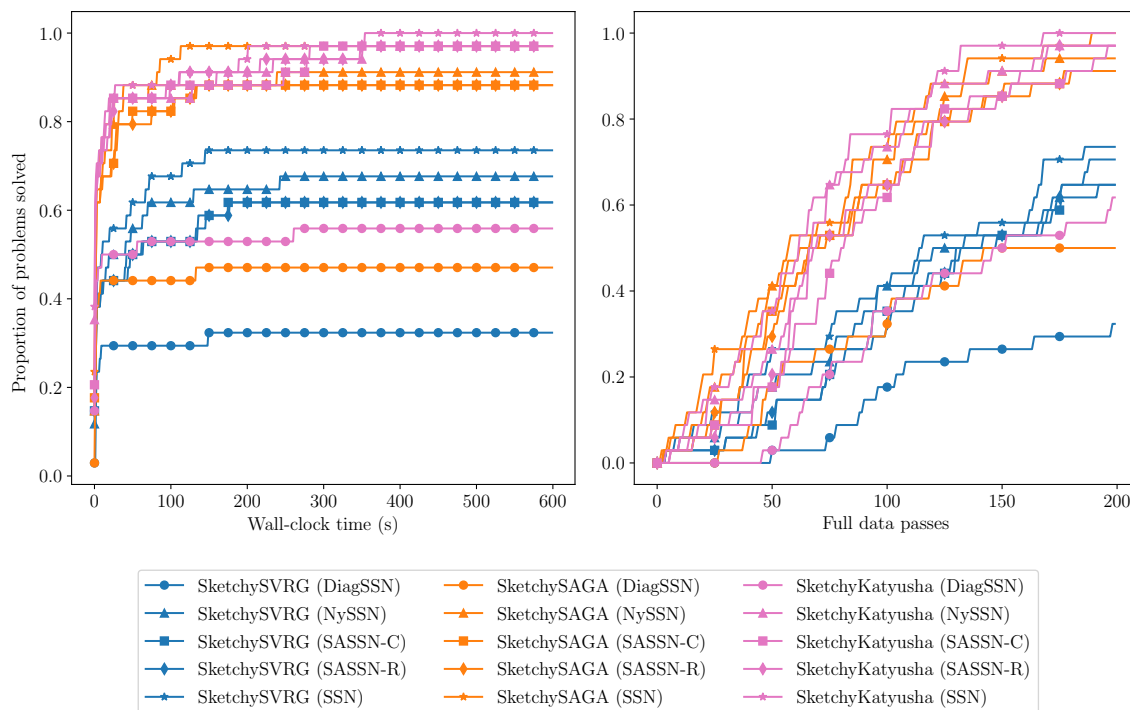


Figure 25: Proportion of l^2 -regularized logistic regression problems solved by DIAGSSN versus the other preconditioning methods.

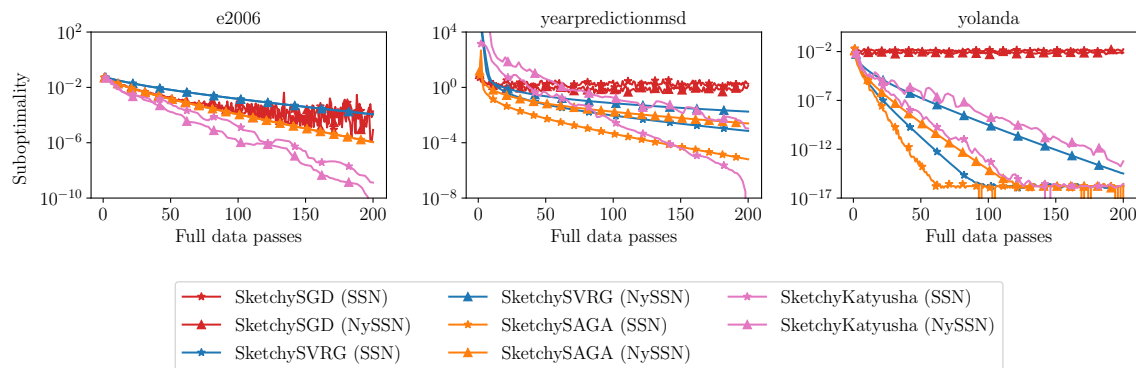


Figure 26: Comparison of SketchySGD, SketchySVRG, SketchySAGA, and SketchyKatyusha with default hyperparameters on ridge regression.

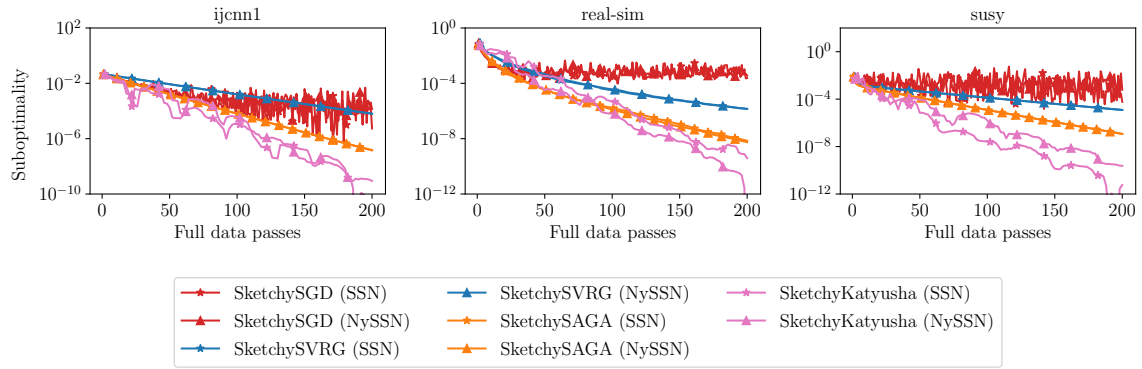


Figure 27: Comparison of SketchySGD, SketchySVRG, SketchySAGA, and SketchyKatyusha with default hyperparameters on l^2 -regularized logistic regression.

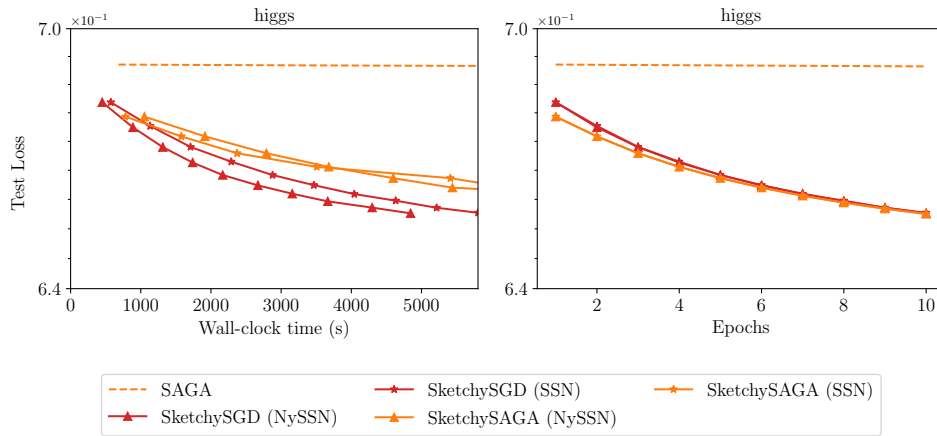


Figure 28: Comparison between SAGA with default learning rate, SketchySGD, and SketchySAGA on HIGGS.

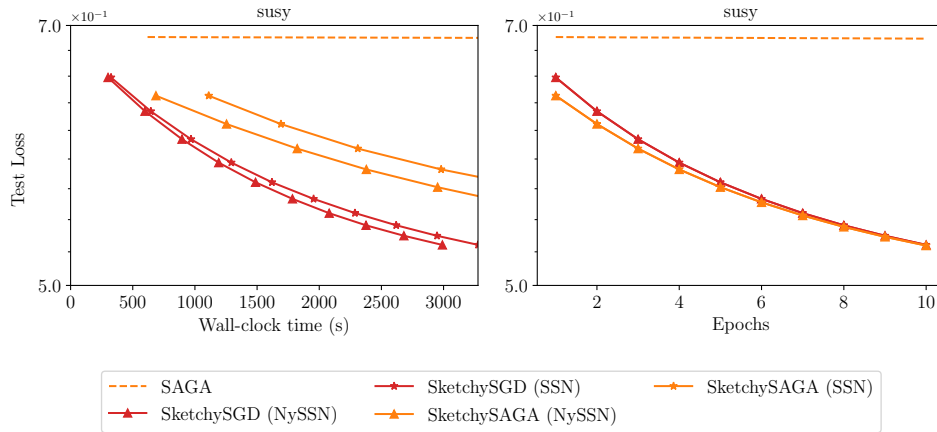


Figure 29: Comparison between SAGA with default learning rate, SketchySGD, and SketchySAGA on SUSY.

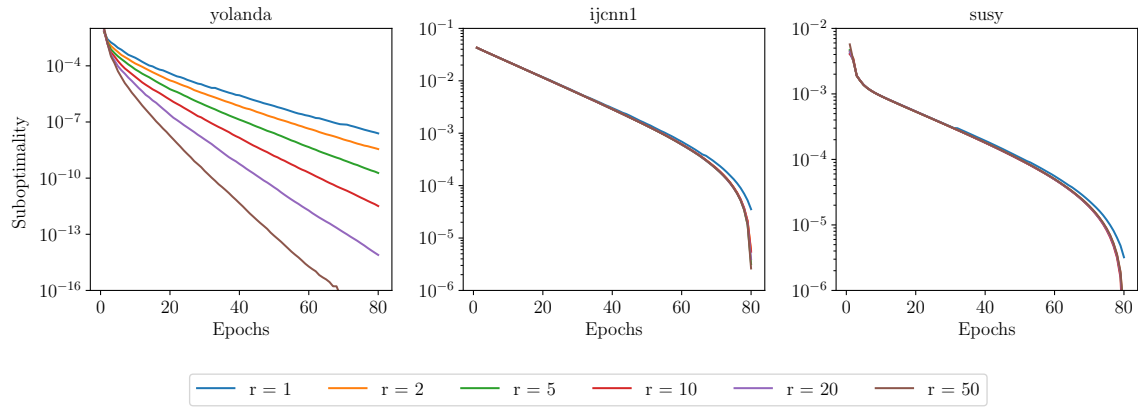


Figure 30: Sensitivity of SketchySAGA to rank r .

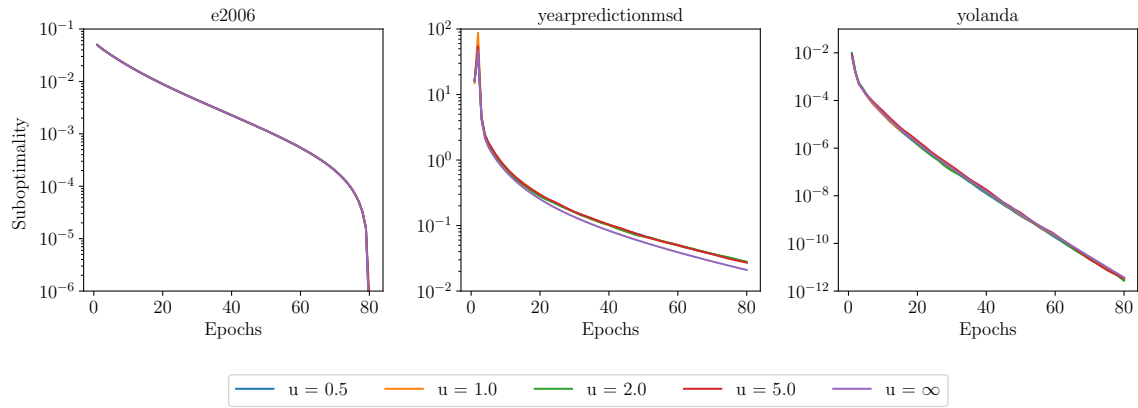


Figure 31: Sensitivity of SketchySAGA to update frequency u .

References

- Ahmed Alaoui and Michael W Mahoney. Fast Randomized Kernel Ridge Regression with Statistical Guarantees. In *Advances in Neural Information Processing Systems*, 2015.
- Zeyuan Allen-Zhu. Katyusha: The First Direct Acceleration of Stochastic Gradient Methods. *Journal of Machine Learning Research*, 18(221):1–51, 2018.
- Yossi Arjevani and Ohad Shamir. Oracle complexity of second-order methods for finite-sum problems. In *International Conference on Machine Learning*, pages 205–213. PMLR, 2017.
- Yossi Arjevani, Ohad Shamir, and Ron Shiff. Oracle complexity of second-order methods for smooth convex optimization. *Mathematical Programming*, 178:327–360, 2019.
- Francis Bach. Self-concordant analysis for logistic regression. 2010.
- Francis Bach. Sharp analysis of low-rank kernel matrix approximations. In *Conference on Learning Theory*, 2013.
- Amir Beck. *First-Order Methods in Optimization*. Society for Industrial and Applied Mathematics, Philadelphia, PA, 2017.
- Raghu Bollapragada, Jorge Nocedal, Dheevatsa Mudigere, Hao-Jun Shi, and Ping Tak Peter Tang. A progressive batching L-BFGS method for machine learning. In *International Conference on Machine Learning*, pages 620–629. PMLR, 2018.
- Raghu Bollapragada, Richard H Byrd, and Jorge Nocedal. Exact and inexact subsampled Newton methods for optimization. *IMA Journal of Numerical Analysis*, 39(2):545–578, 2019.
- Stephen P Boyd and Lieven Vandenbergh. *Convex optimization*. Cambridge University Press, 2004.
- Richard H Byrd, Gillian M Chin, Will Neveitt, and Jorge Nocedal. On the use of stochastic Hessian information in optimization methods for machine learning. *SIAM Journal on Optimization*, 21(3):977–995, 2011.
- Richard H Byrd, Samantha L Hansen, Jorge Nocedal, and Yoram Singer. A stochastic quasi-Newton method for large-scale optimization. *SIAM Journal on Optimization*, 26(2):1008–1031, 2016.
- Emmanuel Candes and Benjamin Recht. Exact matrix completion via convex optimization. *Communications of the ACM*, 55(6):111–119, 2012.
- Emmanuel Candes and Justin Romberg. Sparsity and incoherence in compressive sampling. *Inverse problems*, 23(3):969, 2007.
- Andrea Caponnetto and Ernesto De Vito. Optimal rates for the regularized least-squares algorithm. *Foundations of Computational Mathematics*, 7:331–368, 2007.

- Chih-Chung Chang and Chih-Jen Lin. LIBSVM: A library for support vector machines. *ACM Transactions on Intelligent Systems and Technology*, 2:27:1–27:27, 2011. Software available at <http://www.csie.ntu.edu.tw/~cjlin/libsvm>.
- Michael B Cohen, Jelani Nelson, and David P Woodruff. Optimal Approximate Matrix Product in Terms of Stable Rank. In *43rd International Colloquium on Automata, Languages, and Programming*, 2016.
- Michael B Cohen, Cameron Musco, and Christopher Musco. Input sparsity time low-rank approximation via ridge leverage score sampling. In *Proceedings of the Twenty-Eighth Annual ACM-SIAM Symposium on Discrete Algorithms*, pages 1758–1777. SIAM, 2017.
- Aaron Defazio, Francis Bach, and Simon Lacoste-Julien. SAGA: A fast incremental gradient method with support for non-strongly convex composite objectives. *Advances in Neural Information Processing Systems*, 27, 2014.
- Michał Dereziński. Stochastic Variance-Reduced Newton: Accelerating Finite-Sum Minimization with Large Batches. *arXiv preprint arXiv:2206.02702*, 2022.
- Michał Dereziński, Feynman T Liang, Zhenyu Liao, and Michael W Mahoney. Precise expressions for random projections: Low-rank approximation and randomized Newton. In H. Larochelle, M. Ranzato, R. Hadsell, M.F. Balcan, and H. Lin, editors, *Advances in Neural Information Processing Systems*, volume 33, pages 18272–18283. Curran Associates, Inc., 2020.
- Michał Dereziński, Jonathan Lacotte, Mert Pilanci, and Michael W Mahoney. Newton-LESS: Sparsification without Trade-offs for the Sketched Newton Update. In *Advances in Neural Information Processing Systems*, volume 34, 2021.
- Mateo Díaz, Ethan N Epperly, Zachary Frangella, Joel A Tropp, and Robert J Webber. Robust, randomized preconditioning for kernel ridge regression. *arXiv preprint arXiv:2304.12465*, 2023.
- Nikita Doikov, El Mahdi Chayti, and Martin Jaggi. Second-order optimization with lazy Hessians. In *International Conference on Machine Learning*, pages 8138–8161. PMLR, 2023.
- Murat A Erdogdu and Andrea Montanari. Convergence rates of sub-sampled Newton methods. *Advances in Neural Information Processing Systems*, 28, 2015.
- Zachary Frangella, Pratik Rathore, Shipu Zhao, and Madeleine Udell. SketchySGD: Reliable Stochastic Optimization via Randomized Curvature Estimates, 2023a.
- Zachary Frangella, Joel A. Tropp, and Madeleine Udell. Randomized Nyström Preconditioning. *SIAM Journal on Matrix Analysis and Applications*, 44(2):718–752, 2023b.
- Nidham Gazagnadou, Robert Gower, and Joseph Salmon. Optimal Mini-Batch and Step Sizes for SAGA. In *Proceedings of the 36th International Conference on Machine Learning*, Proceedings of Machine Learning Research, pages 2142–2150. PMLR, 09–15 Jun 2019.

- Alex Gittens and Michael W Mahoney. Revisiting the Nystrom method for improved large-scale machine learning. *The Journal of Machine Learning Research*, 17(1):3977–4041, 2016.
- Alon Gonen, Francesco Orabona, and Shai Shalev-Shwartz. Solving ridge regression using sketched preconditioned SVRG. In *International Conference on Machine Learning*, pages 1397–1405. PMLR, 2016.
- Robert Gower, Donald Goldfarb, and Peter Richtárik. Stochastic block BFGS: Squeezing more curvature out of data. In *International Conference on Machine Learning*, pages 1869–1878. PMLR, 2016.
- Robert Gower, Nicolas Le Roux, and Francis Bach. Tracking the gradients using the Hessian: A new look at variance reducing stochastic methods. In *International Conference on Artificial Intelligence and Statistics*, pages 707–715. PMLR, 2018.
- Robert Gower, Dmitry Kovalev, Felix Lieder, and Peter Richtárik. RSN: Randomized subspace Newton. *Advances in Neural Information Processing Systems*, 32, 2019a.
- Robert M Gower, Mark Schmidt, Francis Bach, and Peter Richtárik. Variance-reduced methods for machine learning. *Proceedings of the IEEE*, 108(11):1968–1983, 2020.
- Robert Mansel Gower, Nicolas Loizou, Xun Qian, Alibek Sailanbayev, Egor Shulgin, and Peter Richtárik. SGD: General analysis and improved rates. In *International Conference on Machine Learning*, pages 5200–5209. PMLR, 2019b.
- Nicholas J Higham. *Accuracy and stability of numerical algorithms*. SIAM, 2002.
- Daniel Hsu, Sham M Kakade, and Tong Zhang. Random Design Analysis of Ridge Regression. *Foundations of Computational Mathematics*, 3(14):569–600, 2014.
- Arun Jambulapati, Jerry Li, Christopher Musco, Aaron Sidford, and Kevin Tian. Fast and near-optimal diagonal preconditioning. *arXiv preprint arXiv:2008.01722*, 2020.
- Rie Johnson and Tong Zhang. Accelerating stochastic gradient descent using predictive variance reduction. *Advances in Neural Information Processing Systems*, 26, 2013.
- Sai Praneeth Karimireddy, Sebastian U Stich, and Martin Jaggi. Global linear convergence of Newton’s method without strong-convexity or Lipschitz gradients. *arXiv preprint arXiv:1806.00413*, 2018.
- Dmitry Kovalev, Konstantin Mishchenko, and Peter Richtárik. Stochastic Newton and cubic Newton methods with simple local linear-quadratic rates. *arXiv preprint arXiv:1912.01597*, 2019.
- Dmitry Kovalev, Samuel Horváth, and Peter Richtárik. Don’t Jump Through Hoops and Remove Those Loops: SVRG and Katyusha are Better Without the Outer Loop. In Aryeh Kontorovich and Gergely Neu, editors, *Proceedings of the 31st International Conference on Algorithmic Learning Theory*, volume 117 of *Proceedings of Machine Learning Research*, pages 451–467. PMLR, 08 Feb–11 Feb 2020.

- Jonathan Lacotte, Yifei Wang, and Mert Pilanci. Adaptive Newton sketch: linear-time optimization with quadratic convergence and effective Hessian dimensionality. In *International Conference on Machine Learning*, pages 5926–5936. PMLR, 2021.
- Xiang Li, Shusen Wang, and Zhihua Zhang. Do Subsampled Newton Methods work for High-Dimensional Data? In *Proceedings of the AAAI Conference on Artificial Intelligence*, volume 34, pages 4723–4730, 2020.
- Yanli Liu, Fei Feng, and Wotao Yin. Acceleration of SVRG and Katyusha X by inexact preconditioning. In *International Conference on Machine Learning*, pages 4003–4012. PMLR, 2019.
- Ulysse Marteau-Ferey, Francis Bach, and Alessandro Rudi. Globally convergent Newton methods for ill-conditioned generalized self-concordant losses. *Advances in Neural Information Processing Systems*, 32, 2019a.
- Ulysse Marteau-Ferey, Dmitrii Ostrovskii, Francis Bach, and Alessandro Rudi. Beyond least-squares: Fast rates for regularized empirical risk minimization through self-concordance. In *Conference on Learning Theory*, pages 2294–2340. PMLR, 2019b.
- Per-Gunnar Martinsson and Joel A Tropp. Randomized numerical linear algebra: Foundations and algorithms. *Acta Numerica*, 29:403–572, 2020.
- Song Mei and Andrea Montanari. The Generalization Error of Random Features Regression: Precise Asymptotics and the Double Descent Curve. *Communications on Pure and Applied Mathematics*, 75(4):667–766, 2022.
- Vitali D Milman and Gideon Schechtman. *Asymptotic theory of finite dimensional normed spaces: Isoperimetric inequalities in Riemannian manifolds*, volume 1200. Springer, 2009.
- Stanislav Minsker. On some extensions of Bernstein’s inequality for self-adjoint operators. *Statistics & Probability Letters*, 127:111–119, 2017.
- Philipp Moritz, Robert Nishihara, and Michael Jordan. A linearly-convergent stochastic L-BFGS algorithm. In *Artificial Intelligence and Statistics*, pages 249–258. PMLR, 2016.
- Eric Moulines and Francis Bach. Non-asymptotic analysis of stochastic approximation algorithms for machine learning. *Advances in Neural Information Processing Systems*, 24, 2011.
- Cameron Musco and Christopher Musco. Randomized block Krylov methods for stronger and faster approximate singular value decomposition. *Advances in Neural Information Processing Systems*, 28, 2015.
- Sen Na, Michał Dereziński, and Michael W Mahoney. Hessian averaging in stochastic Newton methods achieves superlinear convergence. *Mathematical Programming*, pages 1–48, 2022.
- Arkadi Nemirovski, Anatoli Juditsky, Guanghui Lan, and Alexander Shapiro. Robust stochastic approximation approach to stochastic programming. *SIAM Journal on optimization*, 19(4):1574–1609, 2009.

- Arkadi S Nemirovski and David B Yudin. *Problem complexity and method efficiency in optimization*. Wiley-Interscience, 1983.
- Yurii Nesterov. *Lectures on convex optimization*, volume 137. Springer, 2018.
- Jorge Nocedal and Stephen J Wright. *Numerical optimization*. Springer, 1999.
- Fabian Pedregosa, Gaël Varoquaux, Alexandre Gramfort, Vincent Michel, Bertrand Thirion, Olivier Grisel, Mathieu Blondel, Peter Prettenhofer, Ron Weiss, Vincent Dubourg, et al. Scikit-learn: Machine learning in Python. *the Journal of machine Learning Research*, 12:2825–2830, 2011.
- Mert Pilanci and Martin J Wainwright. Newton Sketch: A near linear-time optimization algorithm with linear-quadratic convergence. *SIAM Journal on Optimization*, 27(1):205–245, 2017.
- Zhaonan Qu, Wenzhi Gao, Oliver Hinder, Yinyu Ye, and Zhengyuan Zhou. Optimal diagonal preconditioning: Theory and practice. *arXiv preprint arXiv:2209.00809*, 2022.
- Ali Rahimi and Benjamin Recht. Random features for large-scale kernel machines. *Advances in Neural Information Processing Systems*, 20, 2007.
- Vladimir Rokhlin and Mark Tygert. A fast randomized algorithm for overdetermined linear least-squares regression. *Proceedings of the National Academy of Sciences*, 105(36):13212–13217, 2008.
- Farbod Roosta-Khorasani and Michael W Mahoney. Sub-sampled Newton methods. *Mathematical Programming*, 174(1):293–326, 2019.
- Mark Rudelson and Roman Vershynin. Hanson-Wright inequality and sub-gaussian concentration. 2013.
- Alessandro Rudi, Luigi Carratino, and Lorenzo Rosasco. Falkon: An optimal large scale kernel method. *Advances in Neural Information Processing Systems*, 30, 2017.
- Alessandro Rudi, Daniele Calandriello, Luigi Carratino, and Lorenzo Rosasco. On fast leverage score sampling and optimal learning. *Advances in Neural Information Processing Systems*, 31, 2018.
- Danica J Sutherland. Fixing an error in Caponnetto and de Vito (2007). *arXiv preprint arXiv:1702.02982*, 2017.
- Joel A Tropp, Alp Yurtsever, Madeleine Udell, and Volkan Cevher. Fixed-rank approximation of a positive-semidefinite matrix from streaming data. *Advances in Neural Information Processing Systems*, 30, 2017.
- Joel A. Tropp, Alp Yurtsever, Madeleine Udell, and Volkan Cevher. Streaming Low-Rank Matrix Approximation with an Application to Scientific Simulation. *SIAM Journal on Scientific Computing*, 41(4):A2430–A2463, 2019.

- Joaquin Vanschoren, Jan N. van Rijn, Bernd Bischl, and Luis Torgo. OpenML: Networked Science in Machine Learning. *SIGKDD Explorations*, 15(2):49–60, 2013.
- Christopher Williams and Matthias Seeger. Using the Nyström method to speed up kernel machines. *Advances in Neural Information Processing Systems*, 13, 2000.
- Blake E Woodworth and Nati Srebro. Tight complexity bounds for optimizing composite objectives. *Advances in Neural Information Processing Systems*, 29, 2016.
- Haishan Ye, Luo Luo, and Zhihua Zhang. Approximate Newton Methods. *Journal of Machine Learning Research*, 22(66):1–41, 2021. URL <http://jmlr.org/papers/v22/19-870.html>.
- Yelp. Yelp dataset, 2023. URL <https://www.yelp.com/dataset>.
- Shipu Zhao, Zachary Frangella, and Madeleine Udell. NysADMM: faster composite convex optimization via low-rank approximation. In *Proceedings of the 39th International Conference on Machine Learning*, volume 162 of *Proceedings of Machine Learning Research*, pages 26824–26840. PMLR, 17–23 Jul 2022.